Electronic supporting information

What is the Role of Acid-Acid Interactions in Asymmetric Phosphoric Acid Organocatalysis? A Detailed Mechanistic Study using Interlocked and Non-Interlocked Catalysts

Dennis Jansen,[a] Johannes Gramüller,[b] Felix Niemeyer,[a] Torsten Schaller,[a] Matthias C. Letzel[c], Stefan Grimme,[d] Hui Zhu,*[d] Ruth M. Gschwind,*[b] and Jochen Niemeyer*[a]

[a] M. Sc. D. Jansen, Dr. Felix Niemeyer, Dr. Torsten Schaller, Dr. J. Niemeyer, Faculty of Chemistry (Organic Chemistry) and Center for Nanointegration Duisburg- Essen (CENIDE), University of Duisburg-Essen, Universitätsstrasse 7, 45141 Essen (Germany).

[b] M. Sc. J. Gramüller, Prof. R. Gschwind, Organic Chemistry,University of Regensburg, 93040 Regensburg (Germany).

[c] Dr. M. C. Letzel, Institute of Organic Chemistry, University of Münster, Corrensstrasse 40, 48149 Münster (Germany).

[d] Dr. Hui Zhu, Prof. Stefan Grimme, Mulliken Center for Theoretical Chemistry, Rheinische Friedrich-Wilhelms-Universität Bonn, Beringstrasse 4, 53115 Bonn (Germany).

Table of contents

1. General information

1.1. Analytical methods

NMR spectra were recorded with a Bruker DMX 300 spectrometer [^{1}H: 300 MHz, ^{13}C: 75.5 MHz, ^{31}P: 121.5 MHz] or with a Bruker DMX 600 spectrometer [^{1}H: 600 MHz, ^{13}C: 151 MHz, ^{31}P: 243 MHz]. All measurements were performed at room temperature, using [D_1]-chloroform, [D_6]-dimethylsulfoxide, [D_6]-benzene or [D_4]-methanol as solvents. The chemical shifts are referenced relative to the residual proton signals of the solvents in the ^{1}H-NMR ([D_1]-chloroform: δ = 7.24 ppm, [D_6]-benzene: δ = 7.16 ppm, [D_4]-methanol: δ = 3.31 ppm, [D_6]-dimethylsulfoxide: δ = 2.50 ppm) or relative to the solvent signal in the ^{13}C-NMR ([D_1-chloroform: δ = 77.16 ppm, [D_6]-benzene: δ = 128.06 ppm, [D_4]-methanol: δ = 49.15 ppm, [D_6]-dimethylsulfoxide: δ = 39.51 ppm). The apparent coupling constants are given in Hertz. The description of the fine structure means: s = singlet, bs = broad singlet, d = doublet, ps d = pseudo dublet, dd = doublet of doublets, dt = doublet of triplets, t = triplet, m = multiplet.

NMR structural investigations on binary and ternary **3•4b-d** systems were performed on a Bruker Avance DRX 600 MHz spectrometer with TBI (Triple resonance broadband inverse) 5 mm CPPBBO ^{1}H/^{19}F-BB probe head with Z-gradient and BVT unit. Temperature was controlled in the VT-experiments by a BVT 3000 and BVT 3900 unit and liquid nitrogen. Additional NMR experiments were performed on Bruker Avance III HD 400 MHz spectrometer equipped with 5 mm BBO BB-1H/D probe head with Z-Gradients. Spectrometer control and spectra processing was performed with Bruker Software TopSpin (Version 3.2 PL 1). Data procession, data preparation and data presentation was performed with Microsoft Excel (Version 16.0.9126.2259 32 Bit), Corel Draw X7 and ChemBioDraw Ultra 14.0. ^{1}H and ^{13}C chemical shifts were referenced to TMS. The heteronuclei ^{15}N,^{19}F and ^{31}P were referenced, employing $\nu(X) = \nu(TMS) \cdot \Xi_{reference} / 100$ % according to Harris et al. (R. K. Harris, E. D. Becker, S. M. Cabral De Menezes, R. Goodfellow, P. Granger, *Concepts Magn. Reson. Part A Bridg. Educ. Res.* **2002**, *14*, 326–346). The following frequency ratios and reference compounds were used: $\Xi(^{15}N)$ = 10.132912 (lq. NH_3), $\Xi(^{19}F)$ = 94.094011 (CCl_3F) and $\Xi(^{31}P)$ = 40.480742 (H_3PO_4).

IR spectra were measured on a Jasco FT/IR-430 spectrometer.

Low resolution ESI mass spectra were recorded on a Bruker Amazon SL spectrometer. High resolution ESI mass spectra were recorded on a Bruker Maxis 4G spectrometer. MS/MS spectra were recorded on Thermo Fisher Scientific Orbitrap LTQ-XL mass spectrometer.

Reversed phase medium performance liquid chromatography (MPLC) was performed with the following setup: Armen Instrument Spot Liquid Chromatography Flash system (detection wavelength: 263 nm), YMC GEL ODS-AQ 12 nm, S-50 µm in Kronlab glass columns with 10 mm diameter and 500 mm length .Water for MPLC was purified with a

TKA MicroPure ultrapure water system. Chiral normal phase analytical high performance liquid chromatography (HPLC) was performed was performed with the following setup: Erma Degasser ERC-3512, Merck Hitachi Intelligent Pump L-6200A, Chiralcel OD-H column (0.46 x 25 cm), Knauer Smartline UV-Detector 2600 (detection wavelength 225 nm). Reversed phase analytical high performance liquid chromatography (RP-HPLC) was performed with the following setup: Dionex HPLC system: P680 pump, ASI-100 automated sample injector, UVD-340U UV detector (detection wavelength: 263 nm), UltiMate 3000 Column Compartment; YMC-Pack ODS-Acolumn (3.0 x 150 mm, 5 µm, 12 nm; type: AA12S05-1503QT)

Elemental analyses were performed on Euro EA – CHNSO Elemental Analyser from HEKAtech GmbH

1.2. Materials and Methods

Materials

Polygram® SOL G/UV254 TLC plates (silica gel, 0.2 mm x 40 mm x 80 mm) were used for thin layer chromatography (TLC). A UV lamp was used to visualize spots at either 254 nm or 365 nm wavelength. The products were purified by flash column chromatography on silica gel 60M (particle size: 40-63 µm) which was purchased from MACHERY-NAGEL GmbH & Co. KG.

Solvents

Dichloromethane and toluene were distilled over calcium hydride and stored over molecular sieves under argon. Deuterated dichloromethane was freshly distilled over calcium hydride and deuterated toluene over sodium prior to use. Dry tetrahydrofuran was distilled freshly from Na/benzophenone prior to use. Phosphoryl chloride ($POCl_3$) was distilled under vacuum and stored under argon. Pyridine was distilled over potassium hydroxide under vacuum and stored over molecular sieves under argon. Dimethoxyethane (DME) and aqueous sodium carbonate solution (2 M) were degassed with argon for 15 minutes and were then stored under argon.

Chemicals

p-Toluenesulfonyl chloride, 2-phenylquinoline, 2-bromoquinoline, 4-fluorophenyl boronic acid, 4-methoxyphenyl boronic acid and diethyl 2,6-dimethylpyridine-3,5-dicarboxylate were purchased from Tokyo Chemical Industry (TCI). Pentaethylene glycol, heptaethylene glycol, and diethyl 1,4-dihydro-2,6-dimethyl-pyridine-3,5-dicarboxylate (Hantzsch ester) were purchased from Fluorochem. [D_8]-toluene and [D_5]-chlorobenzene were purchased from Deutero. Amberlyst® 15 hydrogen form and

Grubb's 2nd generation catalyst were purchased from Sigma-Aldrich. Allyl bromide and potassium *tert*-butoxide were purchased from Acros Organics. All commercially available compounds were used without any further purification.

BINOL-derivative (*S*)-**9** was synthesized according to literature procedure.[1] Macrocycle (*S*)-**2b** and catenane (*S*,*S*)-**1b** were synthesized according to literature procedures.[2] Yields obtained in this work were slightly lower than previously reported and are reported in the main paper.[2]

2-(4-Methoxyphenyl)quinoline was synthesized according to literature procedure.[3]

The same conditions were used for the preparation of 2-(4-fluorophenyl)quinoline. Analytical data can be found in the literature.[4]

2. Synthesis of the catenanes 1a/b/c and macrocycles 2a/b/c

2.1. Overview

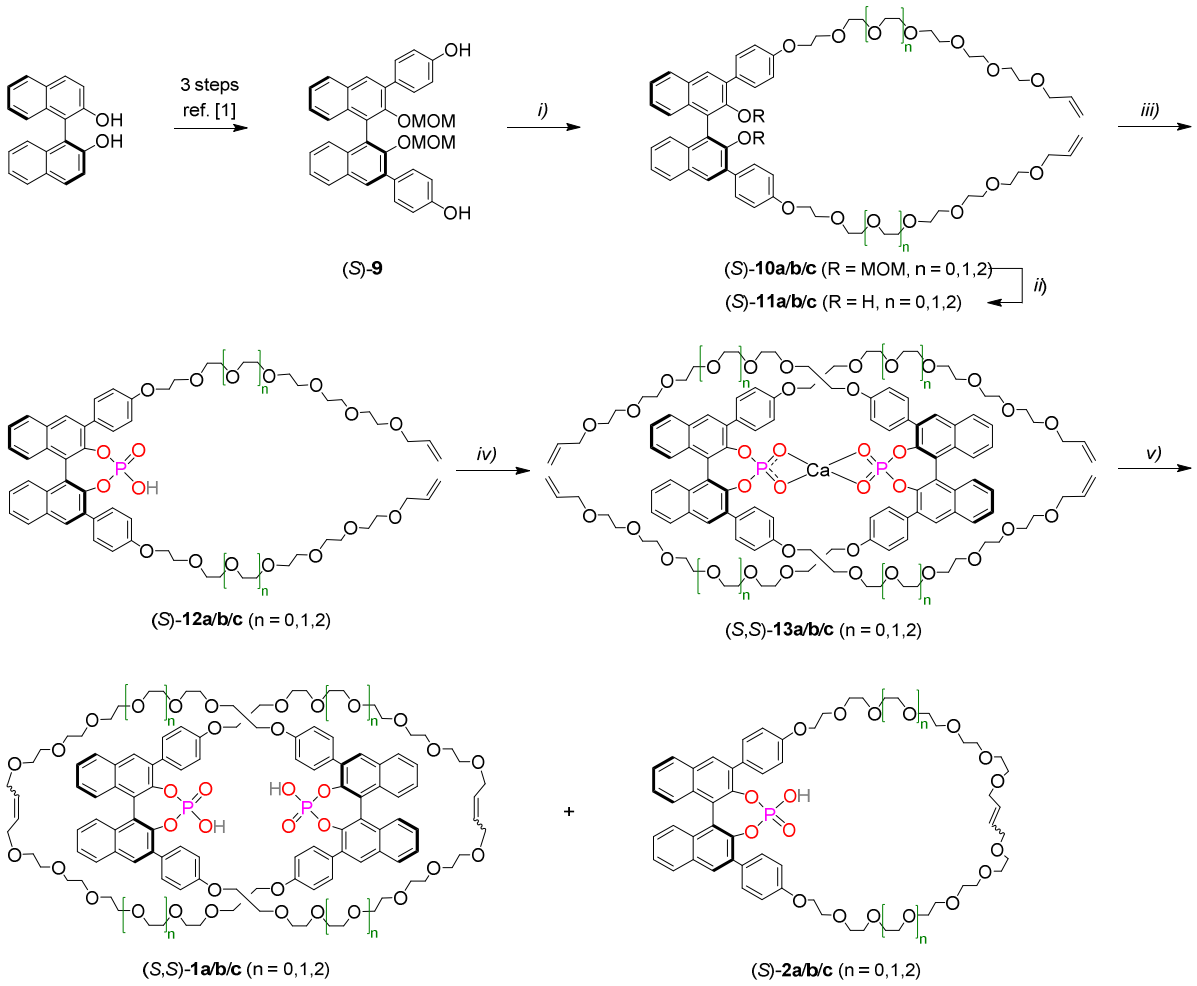

Figure S1: Synthesis of catenanes (*S*,*S*)-**1a/b/c** and macrocycles (*S*)-**2-a/b/c**. Reagents and conditions: *i*) 2.5 equiv. of *O*-allyl-pentaethylene glycol tosylate (for (*S*)-**10a)**, *O*-allyl-hexaethylene glycol tosylate (for (*S*)-**10b)** or *O*-allyl-heptaethylene glycol tosylate (for (*S*)-**10c)**, 5 equiv. K_2CO_3, 80 °C, acetonitrile 64/51/61%; *ii*) Amberlyst 15, reflux, tetrahydrofuran/methanol, 94/99/95%; *iii*) $POCl_3$, pyridine, 60 °C, then H_2O, 51/96/64%; *iv*) 0.5 equiv. $Ca(OMe)_2$, toluene 84/81/96%; *v*) Grubbs-II catalyst, dichloromethane, purification on RP-18, then washing with HCl (2M) (5%/7%/10% for **1a/b/c** and 8%/11%/15% for **2a/b/c**).

2.2. Synthesis of macrocycle (*S*)-2a and catenane (*S*,*S*)-1a

2.2.1. *Synthesis of O-(allyl)pentaethylene glycol* 14a[5]

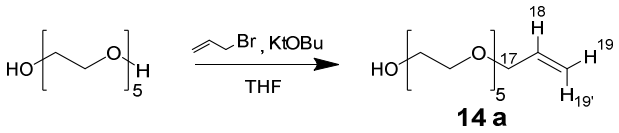

14 a

Potassium *tert*-butoxide (0.998 g, 8.90 mmol, 0.53 eq.) was dried at high vacuum in a Schlenk flask for three hours. After addition of dry tetrahydrofuran (100 ml), a solution of pentaethylene glycol (4.00 g, 16.8 mmol, 1 eq.) in dry tetrahydrofuran (50 ml) was added to the suspension. The mixture was stirred for 40 minutes before a solution of allylbromide (769 µL, 1.08 g, 8.90 mmol, 0.53 eq.) in dry tetrahydrofuran (50 ml) was added dropwise. The reaction mixture was allowed to stir for 20 hours. The resulting suspension was filtered and the solvent was evaporated to give a light yellow oil. After silica gel chromatography (22 x 5 cm, ethyl acetate/methanol 15:1) the product **14a** was obtained as a light yellow oil (1.75 g, 6.29 mmol, 71%).

$C_{13}H_{26}O_6$ 278.35 g/mol

^{1}H-NMR (600 MHz, [D$_1$]-Chloroform, 298 K) δ [in ppm] = 5.91 (ddt, ^3J(H-18,19') = 17.2 Hz, ^3J(H-18,19) = 10.4 Hz, ^3J(H-18,17) = 5.7 Hz, 1 H, H-18), 5.27 (ddt, ^3J(H-19',18) = 17.2 Hz, ^2J(H-19',19) = 1.6 Hz, ^4J(H-19',17) = 1.4 Hz, 1 H, H-19'), 5.17 (ddt, ^3J(H-19,18) = 10.4 Hz, ^2J(H-19,19') = 1.6 Hz, ^4J(H-19,17) = 1.4 Hz, 1 H, H-19), 4.02 (dt, ^3J(H-17,18) = 5.7 Hz, ^4J(H-17,19/19') = 1.4 Hz, 2 H, H-17), 3.77-3.58 (m, 20 H, core glycol-OCH_2).

2.2.2. *Synthesis of O-(allyl)pentaethylene glycol tosylate* 15a[5]

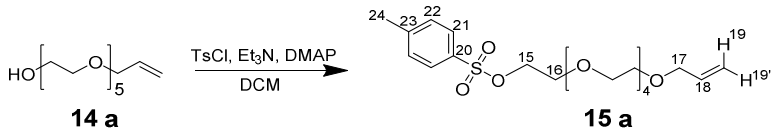

14 a **15 a**

14a (2.62 g, 7.41 mmol, 1 eq.), tosyl chloride (1.77 g, 9.28 mmol, 1.25 eq.), triethylamine (1.25 ml, 11.9 mmol, 1.6 eq.) and 4-dimethylaminopyridine (180 mg, 1.48 mmol, 0.2 eq.) were dissolved in dichloromethane (80 ml). The reaction mixture was stirred at room temperature for 20 hours. Diethyl ether (100 ml) was added and the organic phase was washed with each hydrochloric acid (2M, 100 ml), sat. sodium bicarbonate (100 ml) and brine (100 ml), respectively. The organic phase was dried over anhydrous sodium sulfate, filtered and concentrated in the rotary evaporator. The product **15a** (3.07 g, 7.10 mmol, 96%) was obtained as a light yellow oil.

$C_{20}H_{32}O_8S$ 432.53 g/mol

^{1}H-NMR (600 MHz, [D$_1$]-Chloroform, 298 K) δ [in ppm] = 7.79 (ps d, ^3J = 8.3 Hz, 2 H, H-21), 7.34 (ps d, ^3J= 7.9 Hz, 2 H, H-22), 5.90 (ddt, ^3J(H-18,19') = 17.2 Hz, ^3J(H-18,19) = 10.4 Hz, ^3J(H-18,17) = 5.7 Hz, 1 H, H-18), 5.27 (ddt, ^3J(H-19',18) = 17.2 Hz, ^2J(H-19',19) = 1.6 Hz, ^4J(H-19,17) = 1.4 Hz, 1 H, H-19'), 5.17 (ddt, ^3J(H-19,18) = 10.4 Hz, ^2J(H-19,19') = 1.6 Hz, ^4J(H-19,17) = 1.4 Hz, 1 H, H-19), 4.15 (t, ^3J(H-15,16) = 4.8 Hz, 2 H, H-15), 4.01 (dt, ^3J(H-17,18) = 5.7 Hz, ^4J(H-17,19/19') = 1.4 Hz, 2 H, H-17), 3.69-3.56 (m, 18 H, core glycol-OCH_2), 2.44 (s, 3 H, H-24).

2.2.3. *Synthesis of MOM-protected precursor* (*S*)-**10a**

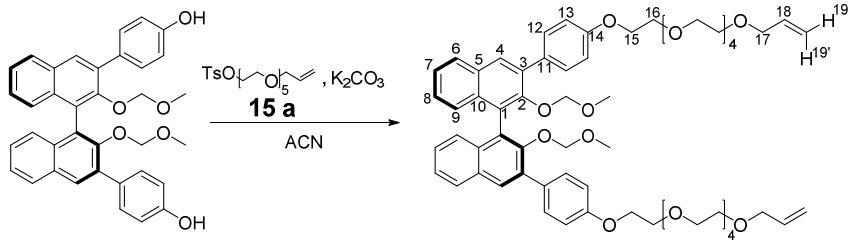

(*S*)-**9** (*S*)-**10 a**

(*S*)-**9** (1.56 g, 2.80 mmol, 1 eq.), **15a** (2.90 g, 6.70 mmol, 2.4 eq.) and potassium carbonate (1.85 g, 13.4 mmol, 4.8 eq.) were charged in a flask and acetonitrile (150 ml) was added. The resulting suspension was refluxed for 24 hours. After cooling down to room temperature the reaction mixture was filtered and the organic solvent was evaporated in the rotary evaporator. After silica gel flash column chromatography (17 x 4 cm, ethyl acetate/methanol = 40/1) the product (*S*)-**10a** (1.97 g, 1.83 mmol, 64%) was obtained as a light brown oil.

$C_{62}H_{78}O_{16}$ 1079.29 g/mol

^{1}H-NMR (600 MHz, [D$_1$]-Chloroform, 298 K) δ [in ppm] = 7.88 (s, 2 H, H-4), 7.83 (d, ^3J(H-6,7) = 8.2 Hz, 2 H, H-6), 7.66 (ps d, ^3J(H-12,13) = 8.7 Hz, 4 H, H-12), 7.35 (ddd ^3J(H-7,9) = 8.1 Hz, ^3J(H-7,8) = 6.4 Hz, ^4J(H-7,6) = 1.5 Hz, 2 H, H-7), 7.26 – 7.19 (m, 4 H, H-8, H-9 merged with $CDCl_3$ peak), 6.99 (ps d, ^3J(H-13,12) = 8.7 Hz, 4 H, H-13), 5.87 (ddt ^3J(H-18,19') = 17.2 Hz, ^3J(H-18,19) = 10.4 Hz, ^3J(H-18,17) = 5.7 Hz, 2 H, H-18), 5.25 (ddt, ^3J(H-19',18) = 17.2 Hz, ^2J(H-19',19) = 1.7 Hz, ^4J(H-19',17) = 1.7 Hz, 2 H, H-19'), 5.15 (ddt, ^3J(H-19,18) = 10.4 Hz, ^2J(H-19,19') = 1.4 Hz, ^4J(H-19,17) = 1.4 Hz, 1 H, H-19), 4.38 (d, ^2J= 5.8 Hz, 2 H, MOM-OCH_2), 4.33 (d, ^2J= 5.8 Hz, 2 H, MOM-OCH_2´), 4.13 (t, ^3J(H-15,16) = 4.9 Hz, 4 H, H-15), 3.99 (dt, ^3J(H-17,18) = 5.8 Hz, ^4J(H-17,19/19') = 1.4 Hz, 4 H, H-17), 3.86 (t, ^3J(H-16,15) = 4.9 Hz, 4 H, H-16), 3.67-3.54 (m, 32 H, core glycol-OCH_2), 2.32 (s, 6 H, MOM-OCH_3).

^{13}C-NMR (151 MHz, [D$_1$]-Chloroform, 298 K) δ [in ppm] = 158.2 (C-14), 151.3 (C-2), 134.9 (C-3), 134.8 (C-18), 133.4 (C-10), 131.5 (C-11), 130.9 (C-5), 130.6 (C-12), 130.1 (C-4), 127.7 (C-6), 126.5 (C-1), 126.4 (C-9), 126.0 (C-8), 125.0 (C-7), 117.0 (C-19), 114.4 (C-13), 98.3 (MOM-O*C*H$_2$) 72.2 (C-17), 70.8 (core glycol O*C*H$_2$), 70.6 (core glycol O*C*H$_2$), 69.7 (C-16), 69.4 (core glycol O*C*H$_2$), 67.4 (C-15), 55.8 (MOM-O*C*H$_3$).

COSY (600 MHz/600 MHz,[D$_1$]-Chloroform, 298 K) δ [in ppm] = 7.88 (H-4), 7.83/7.35 (H-6/H-7), 7.66/6.99 (H-12/H-13), 7.35/7.83 (H-7/H-6), 6.99/7.66 (H-13/H-12), 5.87/5.25, 5.15, 3.99 (H-18/H-19', H-19, H-17), 5.25/5.87, 3.99 (H-19', H-18, H-17), 5.15/5.87, 3.99 (H-19/H-18, H-17), 4.38/4.33 (MOM-OC*H$_2$*), 4.33/4.38 (MOM-OC*H$_2$*), 4.13/3.86 (H-15,H-16), 3.99/5.87 (H-17/H-18), 3.86/4.13 (H-16/H-15).

HSQC (600 MHz/151 MHz, [D$_1$]-Chloroform, 298 K) δ [in ppm] = 7.88/130.1 (H-4/C-4), 7.83/127.7 (H-6/C-6),7.66/130.6 (H-12/C-12), 7.35/125.0 (H-7/C-7), 7.26 - 7.19/126.4, 126.0 (H-9, H-8/C-9, C-8), 6.99/114.4 (H-13/C-13), 5.87/134.8 (H-18/C-18), 5.25, 5.15/117.0 (H-19´, H-19/C-19), 4.38, 4.33/98.3 (MOM-OCH$_2$) , 4.13/67.4 (H-15/C-15), 3.99/72.2 (H-17/C-17), 3.86/69.7 (H-16/C-16), 3.67 – 3.54/ 70.8, 70.6, 69.4 (core glycol OCH$_2$), 2.32/55.8 (MOM-OCH$_3$).

HMBC (600 MHz/151 MHz, [D$_1$]-Chloroform, 298 K) δ [in ppm] = 7.88/151.3,133.4, 131.5, 127.7 (H-4/C-2, C-10, C-11, C-6), 7.83/133.4, 130.1, 126.0 (H-6/C-10, C-4, C-8), 7.66/158.2, 134.9, 130.6, 114.4 (H-12/C-14, C-3, C-12, C-13), 7.35/130.9,126.4 (H-7/C-5, C-9), 7.26 – 7.19/133.4, 130.9, 127.7, 126.5, 125.0 (H-9 and H-8/C-10, C-5, C-6, C-1, C-7), 6.99/158.2, 131.5, 114.4 (H-13/C-14, C-11, C-13), 5.87/72.2 (H-18/C-17), 5.25/134.8, 72.2 (H-19´/C-18, C-17), 5.15/134.8, 72.2 (H-19/C-18, C-17), 4.38/151.3, 55.8 (MOM-OC*H$_2$*/C-2, MOM-O*C*H$_3$), 4.33/151.3, 55.8 (MOM-OC*H$_2$*/C-2, MOM-O*C*H$_3$), 4.13/158.2, 69.7 (H-15/C-14, C-16), 3.99/134.8, 117.0, 69.4 (H-17/C-18, C-19, core glycol O*C*H$_2$), 3.86/70.8, 67.4 (H-16/core glycol-OCH2, C-15), 3.67 – 3.54/ 70.8, 70.6, 69.4, 69.7 (core glycol OC*H$_2$*/core glycol O*C*H$_2$, C-16), 2.32/98.3 (MOM-OC*H$_3$*/ MOM-O*C*H$_2$).

IR (ATR) $\tilde{\upsilon}$ = 2868, 1607, 1510, 1452, 1350, 1282, 1245, 1179, 1101, 995, 969, 924, 835, 752 cm^{-1}.

MS (ESI, pos.; methanol): *m/z* = 1101.7 ([C$_{62}$H$_{78}$O$_{16}$Na]$^+$), calcd. 1101.5 for ([C$_{62}$H$_{78}$O$_{16}$Na]$^+$).

HRMS (ESI, pos.; methanol): *m/z* = 1101.5179 ([C$_{62}$H$_{78}$O$_{16}$Na]$^+$), calcd. 1101.5182 for [C$_{62}$H$_{78}$O$_{16}$Na]$^+$).

Elemental analysis calcd. for C$_{62}$H$_{78}$O$_{16}$: C, 69.00; H, 7.28. Found: C, 67.50; H, 7.34.

2.2.4. *Synthesis of the diol* (*S*)-**11a**

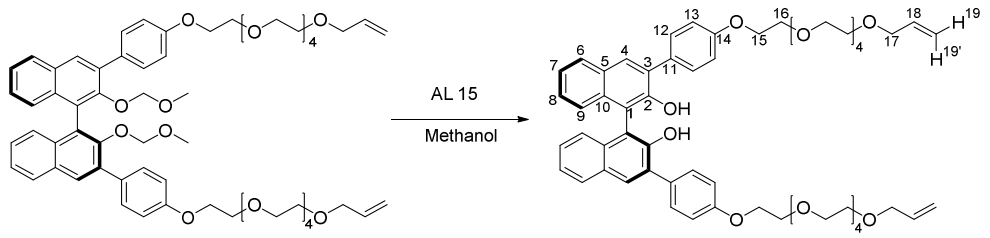

(*S*)-**10a** (*S*)-**11a**

(*S*)-**10a** (1.73 g, 1.60 mmol, 1 eq.) and Amberlyst 15 (800 mg, 1.00 g/2 mmol) were charged in a flask and methanol (50 ml) was added. The resulting mixture was refluxed for six days. After cooling down to room temperature, the mixture was filtered and the solvent was evaporated in the rotary evaporator to give the product (*S*)-**11a** (1.52 g, 1.53 mmol, 94%) as a yellow oil.

$C_{58}H_{70}O_{14}$ 991.18 g/mol

^{1}H-NMR (600 MHz, [D$_1$]-Chloroform, 298 K) δ [in ppm] = 7.96 (s, 2 H, H-4), 7.88 (d, ^3J(H-6,7) = 8.2 Hz, 2 H, H-6), 7.64 (ps d, ^3J(H-12,13) = 8.8 Hz, 4 H, H-12), 7.35 (ddd ^3J(H-7,6) = 8.1 Hz, ^3J(H-7,8) = 6.8 Hz, ^4J(H-7,9) = 1.2 Hz, 2 H, H-7), 7.27 (ddd ^3J(H-8,9) = 8.5 Hz, ^3J(H-8,7) = 6.8 Hz, ^4J(H-8,6) = 1.3 Hz, 2 H, H-8), 7.18 (d, ^3J(H-9,8) = 8.6 Hz, 2 H, H-9), 7.01 (ps d, ^3J(H-13,12) = 8.7 Hz, 4 H, H-13), 5.89 (ddt ^3J(H-18,19') = 17.2 Hz, ^3J(H-18,19) = 10.4 Hz, ^3J(H-18,17) = 5.7 Hz, 2 H, H-18), 5.40 (br s, 2 H, O*H*), 5.24 (ddt, ^3J(H-19',18) = 17.2 Hz, ^2J(H-19',19) = 1.7 Hz, ^4J(H-19',17) = 1.7 Hz, 2 H, H-19'), 5.14 (ddt, ^3J(H-19,18) = 10.4 Hz, ^2J(H-19,19') = 1.4 Hz, ^4J(H-19,17) = 1.4 Hz, 1 H, H-19), 4.17 (t, ^3J(H-15,16) = 5.0 Hz, 4 H, H-15), 3.98 (dt, ^3J(H-17,18) = 5.7 Hz, ^4J(H-17,19/19') = 1.4 Hz, 4 H, H-17), 3.86 (t, ^3J(H-16,15) = 5.0 Hz, 4 H, H-16), 3.74-3.54 (m, 32 H, core glycol-OC*H*$_2$).

^{13}C-NMR (151 MHz, [D$_1$]-Chloroform, 298 K) δ [in ppm] = 158.6 (C-14), 150.4 (C-2), 134.9 (C-18), 132.9 (C-10), 131.0 (C-4), 130.9 (C-12), 130.4 (C-3), 130.1 (C-11), 129.6 (C-5), 128.4 (C-6), 127.2 (C-8), 124.4 (C-9), 124.3 (C-7), 117.2 (C-19), 114.8 (C-13), 112.6 (C-1), 72.3 (C-17), 71.0 (core glycol O*C*H$_2$), 70.8 (core glycol O*C*H$_2$), 69.9 (C-16), 69.5 (core glycol O*C*H$_2$), 67.6 (C-15).

COSY (600 MHz/600 MHz,[D$_1$]-Chloroform, 298 K) δ [in ppm] = 7.88/7.35 (H-6/H-7), 7.64/7.01 (H-12/H-13), 7.35/7.88, 7.27 (H-7/H-6,H-8), 7.27/7.35, 7.18 (H-8/H-7, H-9), 7.18/7.27 (H-9/H-8), 7.01/7.64 (H-13/H-12), 5.87/5.24, 5.14, 3.98 (H-18/H-19', H-19, H-17), 5.24/5.87 (H-19', H-18), 5.14/5.87 (H-19/H-18), 4.17/3.86 (H-15,H-16), 3.98/5.87 (H-17/H-18), 3.86/4.17 (H-16/H-15).

HSQC (600 MHz/151 MHz, [D$_1$]-Chloroform, 298 K) δ [in ppm] =7.95/131.0 (H-4/C-4), 7.88/128.4 (H-6/C-6), 7.64/130.9 (H-12/C-12), 7.35/124.3 (H-7/C-7), 7.27/127.2 (H-8/C-8), 7.18/124.4 (H-9/C-9), 7.01/114.8 (H-13/C-13), 5.87/134.9 (H-18/C-18), 5.24,

5.14/117.2 (H-19', H-19/C-19), 4.17/67.6 (H-15/C-15), 3.98/72.3 (H-17,C-17), 3.86/69.9 (H-16/C-16), 3.74 - 3.53/71.0, 70.8, 69.5 (core glycol O*C*H_2).

HMBC (600 MHz/151 MHz, [D_1]-Chloroform, 298 K) δ [in ppm] = 7.95/150.4, 132.9, 130.1, 128.4, 112.6 (H-4/C-2, C-10, C-11, C-6, C-1), 7.88/132.9, 131.0, 127.2 (H-6/C-10, C-4, C-8), 7.64/158.7,130.9, 114.8 (H-12/C14, C-12, C-13), 7.35/129.6, 124.4 (H-7/C-5, C-9), 7.27/132.9, 128.4 (H-8/C-10, C-6), 7.18/132.9, 129.6, 124.3, 112.6 (H-9/C-10, C-5, C-7, C-1), 7.01/158.7, 130.1, 114.8 (H-13/C-14, C-11, C-13), 5.88/72.3 (H-18/C-17), 5.41/150.4, 130.4, 112.6 (O*H*/C-2, C-3, C-1), 5.24/72.4 (H-19´/C-17), 5.24/134.9, 72.3 (H-19´/C-18, C-17), 5.14/72.3(H-19/C-17), 4.17/158.6, 69.9 (H-15/C-14, C16), 3.98/134.9, 117.2, 69.5 (H-17/C-18,C-19, core glycol OCH_2), 3.86/71.0, 67.7 (H-16/core glycol-OCH2, C-15), 3.74 –3.53/71.0, 70.8, 70.7, 69.9, 69.5 (core glycol OCH_2/core glycol OCH_2, C-16).

IR (ATR) $\tilde{\upsilon}$ = 2869, 1607, 1512, 1440, 1408, 1359, 1245, 1179, 1124, 928, 832, 751 cm^{-1}.

MS (ESI, pos.; methanol): *m/z* = 1013.5 ($[C_{58}H_{70}O_{14}Na]^+$), calcd. 1013.5 for ($[C_{58}H_{70}O_{14}Na]^+$),

HRMS (ESI, pos.; methanol): *m/z* = 1013.4646 ($[C_{58}H_{70}O_{14}Na]^+$), calcd. 1013.4658 for $[C_{58}H_{70}O_{14}Na]^+$)

Elemental analysis calcd. for $C_{58}H_{70}O_{14}$: C, 70.28; H, 7.12. Found: C, 69.10; H, 6.97.

2.2.5. *Synthesis of the phosphoric acid* (*S*)-**12a**

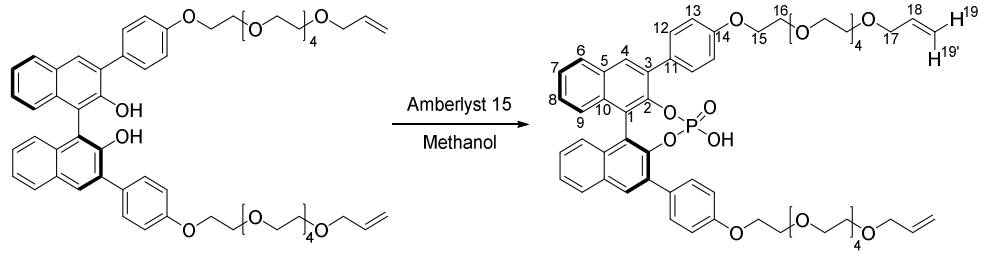

(*S*)-**11a** (*S*)-**12a**

(*S*)**-11a** (1.52 g, 1.53 mmol, 1 eq.) was charged in a Schlenk flask and dried at high vacuum for three hours. Pyridine (20 ml) and phosphoryl chloride (2.35 g, 1.40 ml, 15.3 mmol, 10 eq.) were added under argon and the resulting mixture was stirred for 16 hours at 60° C. After addition of water (10 ml) the mixture was stirred for another 3 hours at 60° C before dichloromethane (20 ml) was added and the resulting two phases were separated. The organic phase was washed with hydrochloric acid (4 x 25 ml, 2M), dried with anhydrous sodium sulfate, filtered and concentrated in the rotary evaporator. After silica gel flash column chromatography (15 x 4 cm, dichloromethane/methanol: 10/1), redissolving in dichloromethane (50 ml) and washing with hydrochloric acid (2 M, 50 ml) the product (*S*)**-12a** was obtained (816 mg, 0.775 mmol, 51%) as a brown oil.

$C_{58}H_{69}O_{16}P$ 1053.15 g/mol

^{1}H-NMR (600 MHz, [D$_1$]-Chloroform, 298 K) δ [in ppm] = 7.96 (s, 2 H, H-4), 7.92 (d, ^{3}J(H-6,7) = 8.2 Hz, 2 H, H-6), 7.59 (ps d, ^{3}J(H-12,13) = 8.8 Hz, 4 H, H-12), 7.45 (ddd ^{3}J(H-7,6) = 8.0 Hz, ^{3}J(H-7,8) = 6.7 Hz, ^{4}J(H-7,9) = 1.2 Hz, 2 H, H-7), 7.31 (d, ^{3}J(H-9,8) = 8.5 Hz, 2 H, H-9), 7.26 – 7.23 (m, 2 H, H-8 merged with $CDCl_3$ peak), 6.90 (ps d, ^{3}J(H-13,12) = 8.8 Hz, 4 H, H-13), 5.83 (ddt ^{3}J(H-18,19') = 17.2 Hz, ^{3}J(H-18,19) = 10.4 Hz, ^{3}J(H-18,17) = 5.7 Hz, 2 H, H-18), 5.20 (ddt, ^{3}J(H-19',18) = 17.2 Hz, ^{2}J(H-19',19) = 1.7 Hz, ^{4}J(H-19',17) = 1.7 Hz, 2 H, H-19'), 5.11 (ddt, ^{3}J(H-19,18) = 10.4 Hz, ^{2}J(H-19,19') = 1.6 Hz, ^{4}J(H-19,17) = 1.6 Hz, 1 H, H-19), 4.02 (t, ^{3}J(H-15,16) = 4.8 Hz, 4 H, H-15), 3.93 (dt, ^{3}J(H-17,18) = 5.7 Hz, ^{4}J(H-17,19/19') = 1.4 Hz, 4 H, H-17), 3.67 (t, ^{3}J(H-16,15) = 4.8 Hz, 4 H, H-16), 3.60-3.49 (m, 32 H, core glycol O*C*H_2).

^{13}C-NMR (151 MHz, [D$_1$]-Chloroform, 298 K) δ [in ppm] = 158.5 (C-14), 145.0 (d, $J_{C\text{-}P}$ = 9.4 Hz, C-2), 134.7 (C-18), 133.8 (d, $J_{C\text{-}P}$ = 3.0 Hz, C-3), 131.9 (C-10), 131.7 (C-5), 131.2 (C-12), 131.0 (C-4), 129.7 (C-11), 128.4 (C-6), 127.2 (C-9), 126.4 (C-8), 125.9 (C-7), 122.7 (d, $J_{C\text{-}P}$ = 2.1 Hz, C-1), 117.4 (C-19), 114.6 (C-13), 72.3 (C-17), 70.8 (core glycol O*C*H_2), 70.6 (core glycol O*C*H_2), 69.8 (C-16), 69.4 (core glycol O*C*H_2), 67.5 (C-15).

^{31}P-NMR (121.5 MHz, [D$_1$]-Chloroform, 298 K) δ [in ppm] = 1.62 (s, P(O)OH).

COSY (600 MHz/600 MHz,[D$_1$]-Chloroform, 298 K) δ [in ppm] = 7.92/7.45 (H-6/H-7), 7.59/6.90 (H-12/H-13), 7.45/7.92, 7.24 (H-7/H-6, H-8), 7.31/7.24 (H-9/H-8), 7.26 – 7.23/7.45, 7.31 (H-8/H-7, H-9), 6.90/7.59 (H-13/H-12), 5.83/5.20, 5.11, 3.93 (H-18/H-19', H-19, H-17), 5.20/5.83, 3.93 (H-19'/H-18, H-17), 5.11/5.83, 3.93 (H-19/H-18, H-17), 4.02/3.67 (H-15/H-16), 3.93/5.83, 5.20 (H-17/H-18, H19'), 3.67/4.02 (H-16/H-15).

HSQC (600 MHz/151 MHz, [D$_1$]-Chloroform, 298 K) δ [in ppm] =7.96/131.0 (H-4/C-4), 7.92/128.4 (H-6/C-6), 7.59/131.2 (H-12/C-12), 7.45/125.9 (H-7/C-7), 7.31/127.2 (H-9/C-9), 7.26 – 7.23/126.4 (H-8/C-8), 6.90/114.6 (H-13/C-13), 5.83/134.7 (H-18/C-18), 5.20, 5.11/117.4 (H-19', H-19/C-19), 4.02/67.5 (H-15/C-15), 3.93/72.3 (H-17,C-17), 3.67/69.8 (H-16/C-16), 3.60 - 3.49/70.8, 70.6, 69.4 (core glycol O*C*H_2).

HMBC (600 MHz/151 MHz, [D$_1$]-Chloroform, 298 K) δ [in ppm] = 7.96/145.0, 131.9, 129.7, 128.4, 122.4 (H-4/C-2, C-10, C-11, C-6, C-1), 7.92/131.9, 131.0, 126.4 (H-6/C-10, C-4, C-8), 7.59/158.5, 131.2, 114.6 (H-12/C-14, C-12, C-13), 7.45/131.7, 127.2 (H-7/C-5, C-9), 7.31/131.9, 131.7, 125.9, 122.7 (H-9/C-10, C-5, C-7, C-1), 7.24/131.9, 128.4 (H-8/C-10, C-6), 6.90/158.5, 129.7, 114.6 (H-13/C-14, C-11, C-13), 5.83/72.3 (H-18/C-17), 5.20/72.3 (H-19´/C-17), 5.11/134.7, 72.3 (H-19/C-18, C-17), 4.02/158.5, 69.8 (H-15/C-14, C16), 3.93/134.7, 117.4, 69.4 (H-17/C-18,C-19, core glycol OCH_2), 3.67/70.8, 67.5 (H-16/core glycol O*C*H_2, C-15), 3.60 –3.49/70.8, 70.6, 69.8, 69.4 (core glycol OCH_2/core glycol O*C*H_2, C-16).

IR (ATR) $\bar{\upsilon}$ = 2869, 1608, 1514, 1246, 1180, 1101, 957, 885, 842, 754, 615 cm^{-1}.

MS (ESI, pos.; methanol): *m/z* = 1075.5 ($[C_{58}H_{69}NaO_{16}P]^+$), calcd. 1075.4 for ($[C_{58}H_{69}NaO_{16}P]^+$).

HRMS (ESI, neg.; methanol): *m/z* = 1051.4207 ($[C_{58}H_{68}O_{16}P]^-$), calcd. 1051.4250 for $[C_{58}H_{68}O_{16}P]^-$).

Elemental analysis calcd. for $C_{58}H_{69}O_{16}P$: C, 64.48; H, 6.97. Found: C, 64.55; H, 6.39.

2.2.6. *Synthesis of the precatenane* (*S*,*S*)-13a

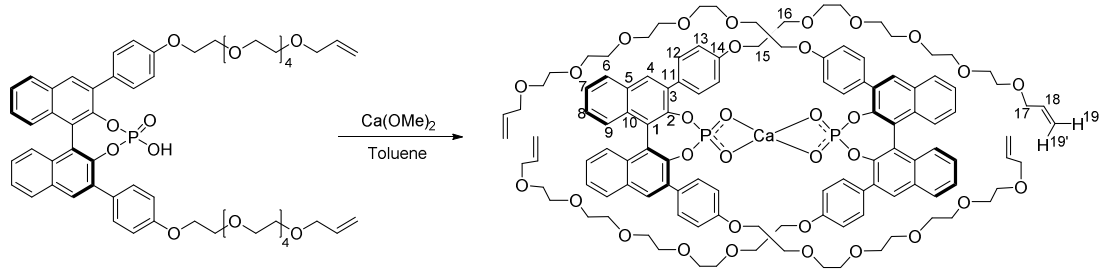

(*S*)-**12a** (*S*,*S*)-**13a**

The phosphoric acid (*S*)-**12a** (816 mg, 0.775 mmol, 1 eq.) was charged in a Schlenk flask and dried at high vacuum for three hours. Dry toluene (30 ml) and calcium methoxide (39.5 mg, 0.387 mmol, 0.5 eq.) were added and the mixture was stirred at room temperature for 16 hours. The mixture was filtered and the solvent was removed in the rotary evaporator to give the product (*S*,*S*)-**13a** (699 mg, 0.326 mmol, 84%) as a brown oil.

$C_{116}H_{138}O_{32}P_2Ca$ 2144.36 g/mol

^{1}H-NMR (600 MHz, [D$_6$]-Benzene, 298 K) δ [in ppm] = 7.94 (br s, 12 H, H-4, H-12), 7.78-7.93 (m, 4 H, H-6), 7.41 (d, ^3J(H-9,8) = 8.7, 4 H, H-9), 7.22 (t, ^3J(H-7,8,6) = 7.4 Hz, 4 H, H-7), 7.10 – 6.93 (m, 12 H, H-8, H-13), 5.77 (m, 4 H, H-18), 5.17 (d, ^3J(H-19',18) = 17.5 Hz, 4 H, H-19'), 4.99 (ddt, ^3J(H-19,18) = 10.5 Hz, 4 H, H-19), 4.04 – 3.84 (m, 8 H, H-15), 3.78 (br s, 8 H, H-17), 3.59-3.11 (m, 72 H, H16, core glycol O*CH*$_2$)

^{13}C-NMR (151 MHz, [D$_6$]-Benzene, 298 K) δ [in ppm] = 158.9 (C-14), 147.5 (C-2), 135.6 (C-18), 135.1 (C-3), 132.7 (C-10), 132.0 (C-12), 131.6 (C-5), 131.0 (C-pp4), 128.6 (C-11), 128.5 (C-6), 127.5 (C-8), 126.2 (C-9), 125.4 (C-7), 123.7 (C-1), 116.4 (C-19), 115.0 (C-13), 72.1 (C-17), 70.7 – 69.7 (C-16, core glycol O*C*H$_2$), 67.6 (C-15).

^{31}P-NMR (242.92 MHz, [D$_6$]-Benzene, 298 K) δ [in ppm] = 0.94 (s, P(O)OH).

COSY (600 MHz/600 MHz, [D$_6$]-Benzene, 298 K) δ [in ppm] =7.94/7.04 (H-12/H-13), 7.78/7.22 (H-6/H-7), 7.41/6.98 (H-9/H-8), 7.22/7.78, 6.98 (H-7/H-6, H-8), 7.04/7.94 (H-13/H-12), 6.98/7.41, 7.21 (H-8/H-9, H-7), 5.77/5.17, 4.99, 3.78 (H-18/H-19', H-19, H-17), 5.17/5.77, 3.78 (H-19'/H-18, H-17), 5.17/5.77, 3.78 (H-19/H-18, H-17), 3.78/5.77, 5.17 (H-17/H-18, H19').

HSQC (600 MHz/151 MHz, [D$_6$]-Benzene, 298 K) δ [in ppm] =7.94/132.0, 131.0 (H-4, 12/C-12, C-4), 7.78/128.5 (H-6/C-6), 7.41/127.5 (H-8/C-8), 7.22/125.4 (H-7/C-7), 7.04/115.0 (H-13/C-13), 6.98/126.2 (H-9/C-9), 5.77/135.6 (H-18/C-18), 5.17, 4.99/116.4 (H-19', H-19/C-19), 3.91/67.6 (H-15/C-15), 3.78/72.1 (H-17,C-17), 3.60 - 3.20/70.7-69.7 (core glycol O*C*H$_2$).

HMBC (600 MHz/151 MHz, [D$_6$]-Benzene, 298 K) δ [in ppm] = 7.94/147.5, 132.0, 128.6, (H-4, H-12/C-2, C-10, C-11), 7.78/126.2 (H-6/C-9), 7.41/131.6,125.4 (H-8/C5, C-7), 7.22/131.6, 127.5 (H-7/C-5, C-8), 6.98/132.7, 128.5 (H-9/C-10, C-6), 4.99/72.1 (H-19/C-17).

IR (ATR) $\bar{\upsilon}$ = 2871, 2359, 1608, 1514, 1248, 1183, 1101, 971, 832, 753, 667 cm^{-1}.

MS: Despite repeated measurements, the intact calcium complex (*S*,*S*)-**19a** could not be detected by mass spectrometry. Only the BINOL-phosphate (*S*)-**18a** was detected. This is in line with our earlier report about the synthesis of compounds **1b/2b**, where the corresponding calcium complex was only a minor peak and the free phosphate was detected as the main peak.[1]

2.2.7. *Synthesis of macrocycle* (*S*)*-2a and catenane* (*S*,*S*)*-1a*

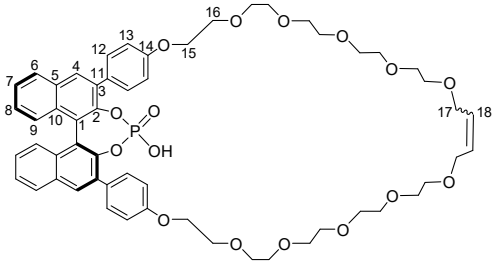

(*S*)-**2a**

(*S*,*S*)-**13a** $\xrightarrow[CH_2Cl_2]{\text{Grubbs' 2nd gen}}$ +

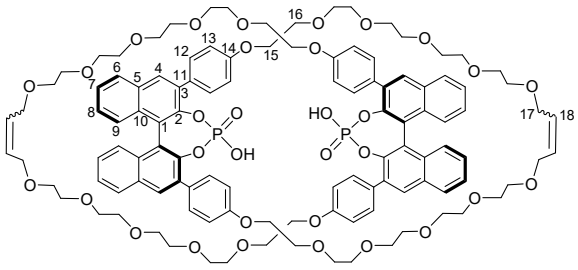

(*S*,*S*)-**1a**

(*S*,*S*)-**13a** (200 mg, 0.0933 mmol, 1 eq.) was dried in a Schlenk flask for four hours. Dry dichloromethane (80 ml) and second generation Grubb's 2nd generation catalyst (7.64 mg, 0.00933 mmol, 0.1 eq.) were added under argon and the reaction mixture was stirred at room temperature with the flask wrapped in aluminium foil to protect the catalyst from light. After five and 17 hours, 1 ml was withdrawn from the mixture to control the progress of the reaction by RP-18 HPLC.[1] After 17 hours the reaction was completed and the solvent was removed. The dark brown residue was dissolved in dichloromethane (10 ml) and methanol (40 ml) was added dropwise. The resulting suspension was filtered through a syringe filter (0.22 µm, PTFE) and the solvent was removed to give 119 mg of a brown solid. The crude product was purified by preparative MPLC (RP-18 17g Kronlab column, MeOH with 0.05% TFA : water with 0.05% TFA = 65 : 35 gradient flow firstly up to 85:15 within 48 min, secondly up to 90:10 within 22 minutes, thirdly up to 100:0 within 10 minutes, 15 ml/min). The solvent was evaporated and each of the two compounds was redissolved in dichloromethane (50 ml) and washed with hydrochloric acid (2M, 10 x 2 ml). After removing the solvent in the rotary evaporator, the 5-EG macrocycle (*S*,*S*)-**2a** (9.0 mg, 4.5%) and the 5-EG catenane (*S*,*S*)-**1a** (15 mg, 7.5%) were obtained.

Macrocycle (*S*)-2a:

$C_{56}H_{65}O_{16}P$ 1025.09 g/mol

^{1}H-NMR (600 MHz, [D$_1$]-Chloroform, 298 K) δ [in ppm] = 7.99 (s, 2 H, H-4), 7.94 (d, ^3J(H-6,7) = 8.2 Hz, 2 H, H-6), 7.71 (ps d, ^3J(H-12,13) = 8.3 Hz, 4 H, H-12), 7.45 (dd,

[1] The solvent was evaporated, the residue solved in methanol and filtered through a syringe filter (0.22 µm, PTFE). The reaction was stopped when HPLC analysis showed >95% conversion.

^{3}J(H-7,6) = 7.4 Hz, ^{3}J(H-7,8) = 7.4 Hz, 2 H, H-7), 7.33 (d, ^{3}J(H-9,8) = 8.6 Hz, 2 H, H-9), 7.29 – 7.23 (m, 2 H, H-8 merged with $CDCl_3$ peak), 7.00 (ps d, ^{3}J(H-13,12) = 8.4 Hz, 4 H, H-13), 5.70 (s, 1.85 H, H-18 (*E*-isomer)), 5.63 (s, 0.15 H, H-18 (*Z*-isomer)), 4.25 – 4.15 (m, 4 H, H-15), 3.97 – 3.82 (m, 8 H, H-1z6, H-17), 3.72 - 3.44 (m, 32 H, core glycol O*CH*$_2$).

^{13}C-NMR (151 MHz, [D$_1$]-Chloroform, 298 K) δ [in ppm] = 158.6 (C-14), 145.2 (d, $J_{C\text{-}P}$ = 8.6 Hz, C-2), 133.8 (C-3), 132.0 (C-10), 131.6 (C-5), 131.3 (C-12), 131.0 (C-4), 130.1 (C-11), 129.6 (C-18), 128.4 (C-6), 127.2 (C-9), 126.3 (C-8), 125.9 (C-7), 122.9 (C-1), 114.6 (C-13), 71.2 (C-17), 71.0 (core glycol O*C*H$_2$), 70.8 (core glycol O*C*H$_2$), 70.6 (core glycol O*C*H$_2$), 69.9 (C-15), 69.4 (core glycol O*C*H$_2$), 67.7 (C-16).

^{31}P-NMR (242.9 MHz, [D$_1$]-Chloroform, 298 K) δ [in ppm] = 1.47 (s, P(O)OH).

COSY (600 MHz/600 MHz,[D$_1$]-Chloroform, 298 K) δ [in ppm] = 7.94/7.45 (H-6/H-7), 7.71/7.00 (H-12/H-13), 7.45/7.94, 7.24 (H-7/H-6, H-8), 7.33/7.24 (H-9/H-8), 7.29 – 7.23/7.45, 7.33 (H-8/H-7, H-9), 7.00/7.71 (H-13/H-12), 5.70, 5.63/3.97 – 3.82 (H-18 /H-17), 4.25 – 4.15/3.97 – 3.82 (H-15/H-16), 3.97 – 3.82/5.70, 5.63, 4.25 – 4.15(H-16, H-17/H-18, H-15).

HSQC (600 MHz/151 MHz, [D$_1$]-Chloroform, 298 K) δ [in ppm] =7.99/131.0 (H-4/C-4), 7.94/128.4 (H-6/C-6), 7.71/131.3 (H-12/C-12), 7.45/125.9 (H-7/C-7), 7.33/127.2 (H-9/C-9), 7.29 – 7.23/126.3 (H-8/C-8), 7.00/114.6 (H-13/C-13), 5.70/129.6 (H-18/C-18), 5.63/129.6 (H-18/C-18), 4.25 – 4.15/67.7 (H-15/C-15), 3.97 – 3.82/71.2, 69.9 (H-17,H-16/C-17,C-16), 3.72 - 3.44/71.0, 70.8, 70.6, 69.4 (core glycol O*C*H$_2$).

HMBC (600 MHz/151 MHz, [D$_1$]-Chloroform, 298 K) δ [in ppm] = 7.99/145.2, 132.0, 130.1, 128.4, 122.9 (H-4/C-2, C-10, C-11, C-6, C-1), 7.94/132.0, 131.0, 126.3 (H-6/C-10, C-4, C-8), 7.71/158.6, 131.3, 114.6 (H-12/C-14, C-12, C-13), 7.33/131.6, 127.2 (H-7/C-5, C-9), 7.27/132.0, 128.4 (H-8/C-10, C-6), 7.18/132.0, 131.6, 125.9, 122.9 (H-9/C-10, C-5, C-7, C-1), 7.00/158.6,130.1, 114.6 (H-13/C-14, C-11, C-13), 5.70, 5.63/71.2 (H-18/C-18), 4.25 – 4.15/69.9, 158.6 (H-15/C-15, C-14), 3.97 – 3.82/129.6, 71.2, 69.4 (H-17, H-16/C-18,C-17, core glycol O*C*H$_2$), 3.72 –3.44/71.0, 70.8, 70.6, 69.4, 69.9 (core glycol O*CH*$_2$/core glycol O*C*H$_2$, C-16).

IR (ATR) $\tilde{\upsilon}$ = 2869, 1608, 1514, 1247, 1181, 1103, 969, 924, 840, 752 cm^{-1}.

MS (ESI, pos.; methanol): *m/z* = 1047.4 ($[C_{56}H_{65}NaO_{16}P]^+$), calcd. 1047.4 for ($[C_{56}H_{65}NaO_{16}P]^+$),

HRMS (ESI, pos.; methanol): *m/z* = 1047.3888 ($[C_{56}H_{65}NaO_{16}P]^+$), calcd. 1047.3902 for $[C_{56}H_{65}NaO_{16}P]^+$)

Catenane (*S,S*)-1a:

$C_{112}H_{130}O_{32}P_2$ 2050.18 g/mol

^{1}H-NMR (600 MHz, [D$_1$]-Chloroform, 298 K) δ [in ppm] = 7.97 (s, 4 H, H-4), 7.93 (d, ^{3}J(H-6,7) = 8.3 Hz, 4 H, H-6), 7.61 (ps d, ^{3}J(H-12,13) = 8.2 Hz, 8 H, H-12), 7.46 (dd,

^{3}J(H-7,6) = 7.5 Hz, ^{3}J(H-7,8) = 7.5 Hz, 4 H, H-7), 7.31 (d, ^{3}J(H-9,8) = 8.5 Hz, 4 H, H-9), 7.28 – 7.24 (m, 4 H, H-8 merged with $CDCl_3$ peak), 6.89 (ps d, ^{3}J(H-13,12) = 8.3 Hz, 8 H, H-13), 5.69 (s, 3.7 H, H-18 (*E*-isomer)), 5.62 (s, 0.3 H, H-18 (*Z*-isomer)), 4.27 (br s, 2H, O*H*), 4.00 (t, ^{3}J(H-15,16) = 4.7 Hz, 8 H, H-15), 3.96 – 3.92 (m, 16 H, H-16, H-17), 3.74 - 3.44 (m, 64 H, core glycol OCH_2).

^{13}C-NMR (151 MHz, [D$_1$]-Chloroform, 298 K) δ [in ppm] = 158.4 (C-14), 145.2 (d, J_{C-P} = 8.6 Hz, C-2), 133.8 (C-3), 132.0 (C-10), 131.6 (C-5), 131.2 (C-12), 131.0 (C-4), 129.8 (C-11), 129.6 (C-18), 128.4 (C-6), 127.2 (C-9), 126.3 (C-8), 125.9 (C-7), 122.9 (C-1), 114.6 (C-13), 71.2 (C-17), 71.0 (core glycol OCH_2), 70.8 (core glycol OCH_2), 70.6 (core glycol OCH_2), 69.9 (C-16), 69.4 (core glycol OCH_2), 67.4(C-15).

^{31}P-NMR (242.9 MHz, [D$_1$]-Chloroform, 298 K) δ [in ppm] = 1.58 (s, P(O)OH).

COSY (600 MHz/600 MHz,[D$_1$]-Chloroform, 298 K) δ [in ppm] = 7.93/7.46 (H-6/H-7), 7.61/6.89 (H-12/H-13), 7.46/7.93, 7.24 (H-7/H-6, H-8), 7.31/7.28 – 7.24 (H-9/H-8), 7.28 – 7.24/7.46, 7.31 (H-8/H-7, H-9), 6.89/7.61 (H-13/H-12), 5.69, 5.62/3.92 (H-18 /H-17), 4.00/3.92 (H-15/H-16), 3.96/5.69, 5.62 (H-17/H-18), 3.92/4.00 (H-16/H-15).

HSQC (600 MHz/151 MHz, [D$_1$]-Chloroform, 298 K) δ [in ppm] =7.97/131.0 (H-4/C-4), 7.93/128.4 (H-6/C-6), 7.61/131.3 (H-12/C-12), 7.46/125.9 (H-7/C-7), 7.31/127.2 (H-9/C-9), 7.28 – 7.24/126.3 (H-8/C-8), 6.89/114.6 (H-13/C-13), 5.69/129.6 (H-18/C-18), 5.62/129.6 (H-18/C-18), 4.00/67.4(H-15/C-15), 3.96 – 3.92/71.2, 69.9 (H-17,H-16/C-17,C-16), 3.74 - 3.44/71.0, 70.8, 70.6, 69.4 (core glycol OCH_2).

HMBC (600 MHz/151 MHz, [D$_1$]-Chloroform, 298 K) δ [in ppm] = 7.97/145.2, 132.0, 129.8, 128.4, 122.9 (H-4/C-2, C-10, C-11, C-6, C-1), 7.93/132.0, 131.0, 126.3 (H-6/C-10, C-4, C-8), 7.61/158.4, 131.3, 114.6 (H-12/C14, C-12, C-13), 7.46/131.6, 127.2 (H-7/C-5, C-9), 7.31/132.0, 131.6, 125.9, 122.9 (H-9/C-10, C-5, C-7, C-1), 7.27/132.0, 128.4 (H-8/C-10, C-6), 6.89/158.4,129.8, 114.6 (H-13/C-14, C-11, C-13), 5.69, 5.62/71.2 (H-18/C-17), 4.00 /69.9, 129.6 (H-15/C-16, C-18), 3.96 – 3.92/129.6, 71.2, 69.4 (H-17, H-16/C-18, C-17, core glycol OCH_2), 3.74 –3.44/71.0, 70.8, 70.6, 69.9, 69.4 (core glycol OCH_2/core glycol OCH_2, C-16).

IR (ATR) $\bar{\upsilon}$ = 2869, 1608, 1514, 1248, 1181, 1106, 971, 925, 840, 753 cm^{-1}.

MS (ESI, neg.; methanol): *m/z* = 1023.5 ($[C_{112}H_{128}O_{32}P_2]^{2-}$), calcd. 1023.4 for ($[C_{112}H_{128}O_{32}P_2]^{2-}$),

HRMS (neg.; methanol): *m/z* = 1023.3906 ($[C_{112}H_{128}O_{32}P_2]^{2-}$), calcd. 1023.3937 for $[C_{112}H_{128}O_{32}P_2]^{2-}$)

2.3. Synthesis of macrocycle (*S*)-2c and catenane (*S*,*S*)-1c

2.3.1. *Synthesis of O-(allyl)heptaethylene glycol* 14c[6]

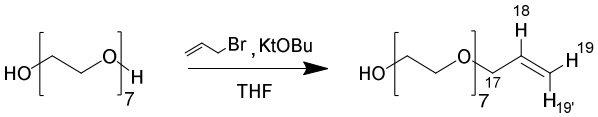

14c

Potassium *tert*-butoxide (182 mg, 1.62 mmol, 0.53 eq.) was dried at high vacuum in a Schlenk flask for three hours. After addition of dry tetrahydrofuran (40 ml), a solution of heptaethylene glycol (1.00 g, 3.06 mmol, 1 eq.) in dry tetrahydrofuran (10 ml) was added to the suspension. The mixture was stirred for 40 minutes before a solution of allylbromide (140 µL, 196 mg, 1.62 mmol, 0.53 eq.) in dry tetrahydrofuran (10 ml) was added dropwise. The reaction mixture was allowed to stir for 20 hours. The resulting suspension was filtered and the solvent was evaporated to give a light yellow oil. After silica gel chromatography (20 x 3 cm, ethyl acetate/methanol = 10:1) the product **14c** was obtained as a light yellow oil (512 mg, 1.39 mmol, 85%).

$C_{17}H_{34}O_8$ 366.45 g/mol

^{1}H-NMR (600 MHz, [D_1]-Chloroform, 298 K) δ [in ppm] = 5.89 (ddt, ^3J(H-18,19') = 17.3 Hz, ^3J(H-18,19) = 10.5 Hz, ^3J(H-18,17) = 5.7 Hz, 1 H, H-18),), 5.25 (ddt, ^3J(H-19',18) = 17.3 Hz, ^2J(H-19',19) = 1.6 Hz, ^4J(H-19',17) = 1.4 Hz, 1 H, H-19'), 5.15 (ddt, ^3J(H-19,18) = 10.5 Hz, ^2J(H-19,19') = 1.6 Hz, ^4J(H-19,17) = 1.4 Hz, 1 H, H-19), 4.00 (dt, ^3J(H-17,18) = 5.7 Hz, ^4J(H-17,19/19') = 1.4 Hz, 2 H, H-17), 3.75-3.55 (m, 28 H, core glycol-OCH_2).

2.3.2. *Synthesis of O-(allyl)heptaethylene glycol tosylate* 15c[6]

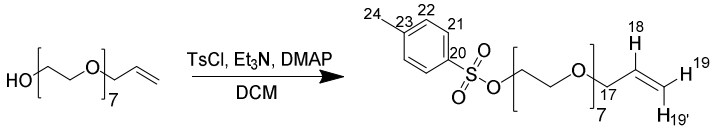

14c **15c**

14c (776 mg, 2.09 mmol, 1 eq.), tosyl chloride (498 mg, 2.06 mmol, 1.25 eq.), triethylamine (463 µl, 3.34 mmol, 1.6 eq.) and 4-dimethylaminopyridine (51.1 mg, 0.42 mmol, 0.2 eq.) were dissolved in dichloromethane (30 ml). The reaction mixture was stirred at room temperature for 20 hours. Diethyl ether (100 ml) was added and the organic phase was washed with each hydrochloric acid (2M, 100 ml), sat. sodium bicarbonate (100 ml) and brine (100 ml), respectively. The organic phase was dried over anhydrous sodium sulfate, filtered and concentrated in the rotary evaporator. The product **15c** was obtained as a light brown oil (995 mg, 1.91 mmol, 91%).

$C_{24}H_{40}O_{10}S$ 520.63 g/mol

^{1}H-NMR (600 MHz, [D$_1$]-Chloroform, 298 K) δ [in ppm] = 7.79 (ps d, ^3J = 8.3 Hz, 2 H, H-21), 7.35 (ps d, ^3J= 7.9 Hz, 2 H, H-22), 5.90 (ddt, ^3J(H-18,19') = 17.2 Hz, ^3J(H-18,19) = 10.4 Hz, ^3J(H-18,17) = 5.7 Hz, 1 H, H-18), 5.26 (ddt, ^3J(H-19',18) = 17.2 Hz, ^2J(H-19',19) = 1.6 Hz, ^4J(H-19',17) = 1.4 Hz, 1 H, H-19'), 5.17 (ddt, ^3J(H-19,18) = 10.4 Hz, ^2J(H-19,19') = 1.6 Hz, ^4J(H-19,17) = 1.4 Hz, 1 H, H-19), 4.01 (dt, ^3J(H-17,18) = 5.7 Hz, ^4J(H-17,19/19) = 1.4 Hz, 2 H, H-17), 3.69-3.56 (m, 28 H, core glycol-OC*H₂*), 2.44 (s, 3 H, H-24).

2.3.3. *Synthesis of MOM-protected precursor* (S)-**10c**

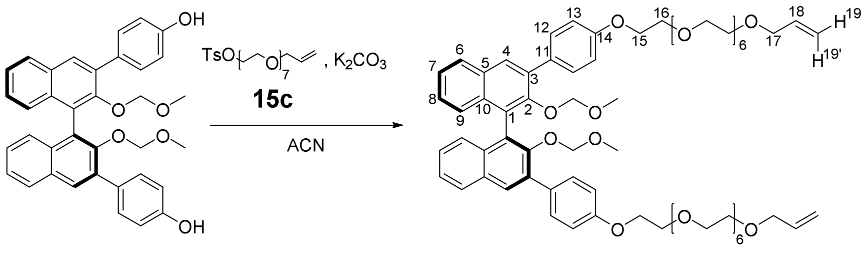

(*S*)-**9** (397 mg, 0.710 mmol, 1 eq.), **15c** (890 mg, 1.71 mmol, 2.4 eq) and potassium carbonate (469 mg, 3.41 mmol, 4.8 eq.) were charged in a flask (100 ml) and acetonitrile (50 ml) was added. The resulting suspension was refluxed for 24 hours. After cooling down to room temperature the reaction mixture was filtered and the organic solvent was evaporated in the rotary evaporator. After silica gel flash column chromatography (15 x 3 cm, ethyl acetate/methanol = 40/1) the product (*S*)-**10c** was obtained as a brown oil (546 mg, 0.43 mmol, 61%).

$C_{70}H_{94}O_{20}$ 1255.50 g/mol

^{1}H-NMR (600 MHz, [D$_1$]-Chloroform, 298 K) δ [in ppm] = 7.88 (s, 2 H, H-4), 7.84 (d, ^3J(H-6,7) = 8.4 Hz, 2 H, H-6), 7.66 (ps d, ^3J(H-12,13) = 8.7 Hz, 4 H, H-12), 7.37 (ddd ^3J(H-7,9) = 8.1 Hz, ^3J(H-7,8) = 5.8 Hz, ^4J(H-7,6) = 2.1 Hz, 2 H, H-7), 7.28– 7.23 (m, 4 H, H-8, H-9 merged with $CDCl_3$ peak), 6.99 (ps d, ^3J(H-13,12) = 8.8 Hz, 4 H, H-13), 5.88 (ddt ^3J(H-18,19') = 17.2 Hz, ^3J(H-18,19) = 10.3 Hz, ^3J(H-18,17) = 5.7 Hz, 2 H, H-18), 5.24 (ddt, ^3J(H-19',18) = 17.2 Hz, ^2J(H-19',19) = 1.6 Hz, ^4J(H-19',17) = 1.7 Hz, 2 H, H-19'), 5.15 (ddt, ^3J(H-19,18) = 10.4 Hz, ^2J(H-19,19') = 1.4 Hz, ^4J(H-19,17) = 1.4 Hz, 1 H, H-19), 4.38 (d, ^2J= 5.8 Hz, 2 H, MOM-OCH_2), 4.33 (d, ^2J= 5.8 Hz, 2 H, MOM-OCH_2'), 4.16 (t, ^3J(H-15,16) = 4.9 Hz, 4 H, H-15), 3.99 (dt, ^3J(H-17,18) = 5.7 Hz, ^4J(H-17,19/19') = 1.4 Hz, 4 H, H-17), 3.87 (t, ^3J(H-16,15) = 4.9 Hz, 4 H, H-16), 3.77-3.56 (m, 48 H, core glycol-OCH_2), 2.32(s, 6 H, MOM-OCH_3).

^{13}C-NMR (151 MHz, [D$_1$]-Chloroform, 298 K) δ [in ppm] = 158.3 (C-14), 151.4 (C-2), 135.0 (C-3), 134.9 (C-18), 133.5 (C-10), 131.6 (C-11), 131.0 (C-5), 130.7 (C-12), 130.2 (C-4), 127.8 (C-6), 126.6 (C-1), 126.5 (C-9), 126.1 (C-8), 125.1 (C-7), 117.1 (C-19), 114.5 (C-13), 98.4 (MOM-O*C*H$_2$) 72.3 (C-17), 70.9 (core glycol O*C*H$_2$), 70.7 (core glycol O*C*H$_2$), 69.8 (C-16), 69.5 (core glycol O*C*H$_2$), 67.5 (C-15), 56.0 (MOM-O*C*H$_3$).

COSY (600 MHz/600 MHz,[D$_1$]-Chloroform, 298 K) δ [in ppm] = 7.83/7.35 (H-6/H-7), 7.66/6.99 (H-12/H-13), 7.35/7.83 (H-7/H-6), 6.99/7.66 (H-13/H-12), 5.87/5.25, 5.15, 3.99 (H-18/H-19', H-19, H-17), 5.25/5.87, 3.99 (H-19'/H-18, H-17), 5.15/5.87, 3.99 (H-19/H-18, H-17), 4.38/4.33 (MOM-OC*H$_2$*), 4.33/4.38 (MOM-OC*H$_2$*), 4.13/3.86 (H-15,H-16), 3.99/5.87 (H-17/H-18), 3.86/4.13 (H-16/H-15).

HSQC (600 MHz/151 MHz, [D$_1$]-Chloroform, 298 K) δ [in ppm] = 7.88/130.2 (H-4/C-4), 7.83/127.8 (H-6/C-6),7.66/130.7 (H-12/C-12), 7.35/125.1 (H-7/C-7), 7.28 - 7.23/126.5, 126.1 (H-9, H-8/C-9, C-8), 6.99/114.5 (H-13/C-13), 5.87/134.9 (H-18/C-18), 5.25, 5.15/117.1 (H-19´, H-19/C-19), 4.38, 4.33/98.4 (MOM-OCH$_2$) , 4.13/67.5 (H-15/C-15), 3.99/72.3 (H-17/C-17), 3.86/69.8 (H-16/C-16), 3.77 – 3.56/ 70.9, 70.7, 69.5 (core glycol OCH$_2$), 2.32/56.0 (MOM-OCH$_3$).

HMBC (600 MHz/151 MHz, [D$_1$]-Chloroform, 298 K) δ [in ppm] = 7.88/151.4, 133.5, 131.6, 127.8 (H-4/C-2, C-10, C-11, C-6), 7.83/133.5, 130.2, 126.1 (H-6/C-10, C-4, C-8), 7.66/158.3, 135.0, 130.7, 114.5 (H-12/C-14, C-3, C-12, C-13), 7.35/131.0, 126.5 (H-7/C-5, C-9), 7.26 – 7.19/133.5, 131.0, 127.8, 126.6, 125.1 (H-9 and H-8/C-10, C-5, C-6, C-1, C-7), 6.99/158.3, 131.6, 114.5 (H-13/C-14, C-11, C-13), 5.87/72.3 (H-18/C-17), 5.25/134.9, 72.3 (H-19´/C-18, C-17), 5.15/134.9, 72.3 (H-19/C-18, C-17), 4.38/151.4, 56.0 (MOM-OC*H$_2$*/C-2, MOM-O*C*H$_3$), 4.33/151.4, 56.0 (MOM-OC*H$_2$*/C-2, MOM-O*C*H$_3$), 4.13/158.3, 69.8 (H-15/C-14, C-16), 3.99/134.9, 117.1, 69.5 (H-17/C-18, C-19, core glycol O*C*H$_2$), 3.86/70.9, 67.5 (H-16/core glycol-OCH2, C-15), 3.77 – 3.56/ 70.9, 70.7, 69.5, 69.8 (core glycol OC*H$_2$*/core glycol O*C*H$_2$, C-16), 2.32/98.4 (MOM-OC*H$_3$*/MOM-O*C*H$_2$).

IR (ATR) $\tilde{\upsilon}$ = 2866, 1607, 1511, 1452, 1408, 1350, 1244, 1179, 1098, 994, 924, 832, 752, 668, 617 cm^{-1}.

MS (ESI, pos.; methanol): *m/z* = 1277.7 ([C$_{70}$H$_{94}$NaO$_{20}$]$^+$), calcd. 1277.6 for ([C$_{70}$H$_{94}$NaO$_{20}$]$^+$).

HRMS (ESI, pos.; methanol): *m/z* = 1277.6218 ([C$_{70}$H$_{94}$NaO$_{20}$]$^+$), calcd. 1277.6231 for [C$_{70}$H$_{94}$NaO$_{20}$]$^+$)

2.3.4. *Synthesis of the diol* (S)-**11c**

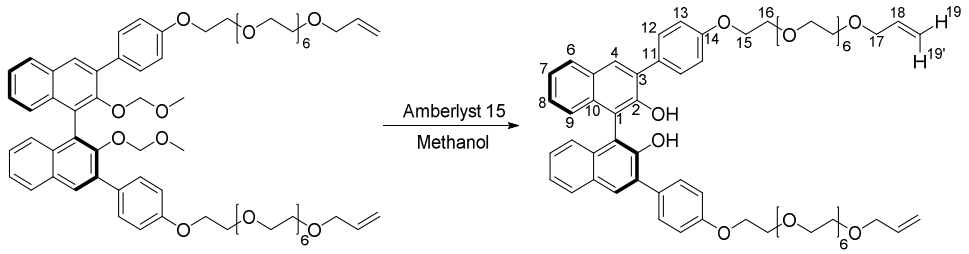

(*S*)-**10c** (*S*)-**11c**

(*S*)-**10c** (546 mg, 0.434 mmol, 1 eq.) and Amberlyst 15 (217 mg, 1.00 g/2 mmol) were charged in a flask and methanol (30 ml) was added. The resulting mixture was refluxed for six days. After cooling down to room temperature, the mixture was filtered and the solvent was evaporated in the rotary evaporator to give the product (*S*)-**11c** (481 g, 0.412 mmol, 95%) as a brown oil.

$C_{66}H_{86}O_{18}$ 1167.40 g/mol

^{1}H-NMR (600 MHz, [D$_1$]-Chloroform, 298 K) δ [in ppm] = 7.95 (s, 2 H, H-4), 7.88 (d, ^{3}J(H-6,7) = 8.1 Hz, 2 H, H-6), 7.64 (ps d, ^{3}J(H-12,13) = 8.8 Hz, 4 H, H-12), 7.35 (ddd ^{3}J(H-7,6) = 8.2 Hz, ^{3}J(H-7,8) = 6.8 Hz, ^{4}J(H-7,9) = 1.2 Hz, 2 H, H-7), 7.27 (ddd ^{3}J(H-8,9) = 8.5 Hz, ^{3}J(H-8,7) = 6.7 Hz, ^{4}J(H-8,6) = 1.3 Hz, 2 H, H-8), 7.18 (dd, ^{3}J(H-9,8) = 8.6 Hz, ^{4}J(H-9,7) = 1.1 Hz 2 H, H-9), 7.01 (ps d, ^{3}J(H-13,12) = 8.7 Hz, 4 H, H-13), 5.87 (ddt ^{3}J(H-18,19') = 17.3 Hz, ^{3}J(H-18,19) = 10.4 Hz, ^{3}J(H-18,17) = 5.7 Hz, 2 H, H-18), 5.41 (br s, 2 H, O*H*), 5.24 (ddt, ^{3}J(H-19',18) = 17.2 Hz, ^{2}J(H-19',19) = 1.7 Hz, ^{4}J(H-19',17) = 1.7 Hz, 2 H, H-19'), 5.14 (ddt, ^{3}J(H-19,18) = 10.3 Hz, ^{2}J(H-19,19') = 1.4 Hz, ^{4}J(H-19,17) = 1.4 Hz, 1 H, H-19), 4.17 (t, ^{3}J(H-15,16) = 5.0 Hz, 4 H, H-15), 3.98 (dt, ^{3}J(H-17,18) = 5.7 Hz, ^{4}J(H-17,19/19') = 1.4 Hz, 4 H, H-17), 3.86 (t, ^{3}J(H-16,15) = 5.0 Hz, 4 H, H-16), 3.74-3.53 (m, 48 H, core glycol OCH_2).

^{13}C-NMR (151 MHz, [D$_1$]-Chloroform, 298 K) δ [in ppm] = 158.6 (C-14), 150.4 (C-2), 134.9 (C-18), 132.9 (C-10), 131.0 (C-4), 130.9 (C-12), 130.4 (C-3), 130.1 (C-11), 129.6 (C-5), 128.4 (C-6), 127.2 (C-8), 124.4 (C-9), 124.3 (C-7), 117.2 (C-19), 114.8 (C-13), 112.6 (C-1), 72.3 (C-17), 71.0 (core glycol O*C*H$_2$), 70.8 (core glycol O*C*H$_2$), 69.9 (C-16), 69.5 (core glycol O*C*H$_2$), 67.6 (C-15).

COSY (600 MHz/600 MHz,[D$_1$]-Chloroform, 298 K) δ [in ppm] = 7.88/7.35 (H-6/H-7), 7.64/7.01 (H-12/H-13), 7.35/7.27, 7.88 (H-7/H-8, H-6), 7.27/7.18, 7.35 (H-8/H-9, H-7), 7.18/7.27 (H-9/H-8), 7.01/7.64 (H-13/H-12), 5.87/5.24, 5.14, 3.98 (H-18/H-19', H-19, H-17), 5.24/5.87 (H-19', H-18), 5.14/5.87 (H-19/H-18), 4.17/3.86 (H-15,H-16), 3.98/5.87 (H-17/H-18), 3.86/4.17 (H-16/H-15).

HSQC (600 MHz/151 MHz, [D$_1$]-Chloroform, 298 K) δ [in ppm] =7.95/131.0 (H-4/C-4), 7.88/128.4 (H-6/C-6), 7.64/130.9 (H-12/C-12), 7.35/124.3 (H-7/C-7), 7.27/127.2 (H-8/C-8), 7.18/124.4 (H-9/C-9), 7.01/114.8 (H-13/C-13), 5.87/134.9 (H-18/C-18), 5.24,

5.14/117.2 (H-19', H-19/C-19), 4.17/67.6 (H-15/C-15), 3.98/72.3 (H-17,C-17), 3.86/69.9 (H-16/C-16), 3.74 - 3.53/71.0, 70.8, 69.5 (core glycol O*C*H_2).

HMBC (600 MHz/151 MHz, [D_1]-Chloroform, 298 K) δ [in ppm] = 7.95/150.4, 132.9, 130.1, 128.4, 112.6 (H-4/C-2, C-10, C-11, C-6, C-1), 7.88/132.9, 131.0, 127.2 (H-6/C-10, C-4, C-8), 7.64/158.7, 130.9, 114.8 (H-12/C14, C-12, C-13), 7.35/129.6, 124.4 (H-7/C-5, C-9), 7.27/132.9, 128.4 (H-8/C-10, C-6), 7.18/132.9, 129.6, 124.3, 112.6 (H-9/C-10, C-5, C-7, C-1), 7.01/158.7, 130.1, 114.8 (H-13/C-14, C-11, C-13), 5.88/72.3 (H-18/C-17), 5.24/72.3, 134.9 (H-19´/C-17, C-18), 5.14/72.3(H-19/C-17), 4.17/158.6, 69.9 (H-15/C-14, C16), 3.98/134.9, 117.2, 69.5 (H-17/C-18, C-19, core glycol OCH_2), 3.86/71.0, 67.7 (H-16/core glycol O*C*H_2, C-15), 3.74 –3.53/71.0, 70.8, 69.9, 69.5 (core glycol OCH_2/core glycol O*C*H_2, C-16).

IR (ATR) $\tilde{\upsilon}$ = 2867, 1607, 1511, 1441, 1408, 1358, 1244, 1179, 1101, 929, 832, 751, 695, 617 cm^{-1}.

MS (ESI, pos.; methanol): *m/z* = 1189.6 ($[C_{66}H_{86}NaO_{18}]^+$), calcd. 1189.6 for ($[C_{66}H_{86}NaO_{18}]^+$).

HRMS (ESI, pos.; methanol): *m/z* = 1189.5679 ($[C_{66}H_{86}NaO_{18}]^+$), calcd. 1189.5706 for $[C_{66}H_{86}NaO_{18}]^+$).

Elemental analysis calcd. for $C_{66}H_{86}O_{18}$: C, 67.91; H, 7.43. Found: C, 67.50; H, 7.52.

2.3.5. *Synthesis of the phosphoric acid* (*S*)-**12c**

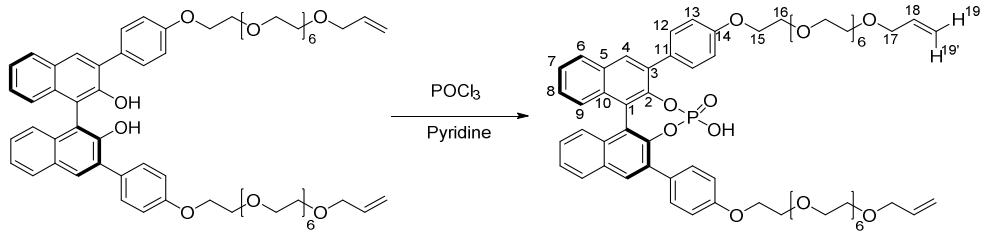

(*S*)-**11c** (*S*)-**12c**

(*S*)-**11c** (481 mg, 0.412 mmol, 1 eq.) was charged in a Schlenk flask and dried at high vacuum for three hours. Pyridine (10 ml) and phosphoryl chloride (629 mg, 375 µl, 4.12 mmol, 10 eq.) were added under argon and the resulting mixture was stirred for 16 hours at 60° C. After addition of water (5 ml) the mixture was stirred for another 3 hours at 60° C before dichloromethane (20 ml) was added and the resulting two phases were separated. The organic phase was washed with hydrochloric acid (2M, 4 x 20 ml), dried over anhydrous sodium sulfate, filtered and concentrated in the rotary evaporator. After silica gel flash column chromatography (18 x 3 cm, dichloromethane/methanol = 10/1) the product (*S*)-**12c** was obtained as a brown oil (324 mg, 0.264 mmol, 64%).

$C_{66}H_{85}O_{20}P$ 1229.36 g/mol

^{1}H-NMR (600 MHz, [D$_1$]-Chloroform, 298 K) δ [in ppm] = 7.95 (s, 2 H, H-4), 7.91 (d, ^{3}J(H-6,7) = 8.3 Hz, 2 H, H-6), 7.60 (ps d, ^{3}J(H-12,13) = 8.7 Hz, 4 H, H-12), 7.44 (ddd ^{3}J(H-7,6) = 8.1 Hz, ^{3}J(H-7,8) = 6.7 Hz, ^{4}J(H-7,9) = 1.3 Hz, 2 H, H-7), 7.30 (d, ^{3}J(H-9,8) = 8.6 Hz, 2 H, H-9), 7.27 – 7.23 (m, 2 H, H-8 merged with $CDCl_3$ peak), 6.88 (ps d, ^{3}J(H-13,12) = 8.7 Hz, 4 H, H-13), 5.85 (ddt ^{3}J(H-18,19') = 17.3 Hz, ^{3}J(H-18,19) = 10.3 Hz, ^{3}J(H-18,17) = 5.7 Hz, 2 H, H-18), 5.21 (ddt, ^{3}J(H-19',18) = 17.3 Hz, ^{2}J(H-19',19) = 1.7 Hz, ^{4}J(H-19',17) = 1.7 Hz, 2 H, H-19'), 5.12 (ddt, ^{3}J(H-19,18) = 10.4 Hz, ^{2}J(H-19,19') = 1.4 Hz, ^{4}J(H-19,17) = 1.4 Hz, 1 H, H-19), 4.01 (t, ^{3}J(H-15,16) = 4.8 Hz, 4 H, H-15), 3.94 (dt, ^{3}J(H-17,18) = 5.7 Hz, ^{4}J(H-17,19/19') = 1.4 Hz, 4 H, H-17), 3.70 (t, ^{3}J(H-16,15) = 4.8 Hz, 4 H, H-16), 3.61-3.50 (m, 48 H, core glycol OCH_2).

^{13}C-NMR (151 MHz, [D$_1$]-Chloroform, 298 K) δ [in ppm] = 158.2 (C-14), 145.0 (d, $J_{C\text{-}P}$ = 9.4 Hz, C-2), 134.6 (C-18), 133.6 (d, $J_{C\text{-}P}$ = 2.9 Hz, C-3), 131.7 (C-10), 131.4 (C-5), 131.0 (C-12), 130.7 (C-4), 129.6 (C-11), 128.2 (C-6), 127.0 (C-9), 126.1 (C-8), 125.6 (C-7), 122.6 (d, $J_{C\text{-}P}$ = 2.1 Hz, C-1), 117.1 (C-19), 114.3 (C-13), 72.1 (C-17), 70.6 (core glycol-OCH_2), 70.4 (core glycol OCH_2), 69.6 (C-16), 69.2 (core glycol OCH_2), 67.2 (C-15).

COSY (600 MHz/600 MHz,[D$_1$]-Chloroform, 298 K) δ [in ppm] = 7.91/7.44 (H-6/H-7), 7.60/6.88 (H-12/H-13), 7.44/7.91, 7.24 (H-7/H-6, H-8), 7.30/7.24 (H-9/H-8), 7.27 – 7.23/7.44, 7.30 (H-8/H-7, H-9), 6.88/7.60 (H-13/H-12), 5.85/5.21, 5.12, 3.94 (H-18/H-19', H-19, H-17), 5.21/5.87, 3.94 (H-19'/H-18, H-17), 5.14/5.87, 3.94 (H-19/H-18, H-17), 4.01/3.70 (H-15/H-16), 3.94/5.87, 5.24 (H-17/H-18, H19'), 3.70/4.01 (H-16/H-15).

^{31}P-NMR (242.9 MHz, [D$_1$]-Chloroform, 298 K) δ [in ppm] = 1.62 (s, P(O)OH).

HSQC (600 MHz/151 MHz, [D$_1$]-Chloroform, 298 K) δ [in ppm] =7.95/130.7 (H-4/C-4), 7.91/128.2 (H-6/C-6), 7.60/131.0 (H-12/C-12), 7.44/125.6 (H-7/C-7), 7.30/127.0 (H-9/C-9), 7.25/126.1 (H-8/C-8), 6.88/114.3 (H-13/C-13), 5.85/134.6 (H-18/C-18), 5.21, 5.12/117.1 (H-19', H-19/C-19), 4.01/67.2 (H-15/C-15), 3.94/72.1 (H-17,C-17), 3.70/69.6 (H-16/C-16), 3.61 - 3.50/70.6, 70.4, 69.2 (core glycol OCH_2).

HMBC (600 MHz/151 MHz, [D$_1$]-Chloroform, 298 K) δ [in ppm] = 7.95/145.0, 131.7, 129.6, 128.2, 122.6 (H-4/C-2, C-10, C-11, C-6, C-1), 7.91/131.7, 130.7, 126.1 (H-6/C-10, C-4, C-8), 7.60/158.2,131.0, 114.3 (H-12/C-14, C-12, C-13), 7.44/131.4, 127.0 (H-7/C-5, C-9), 7.30/131.7 128.2 (H-9/C-10, C-6), 7.25/131.7, 131.4, 125.6, 122.6 (H-8/C-10, C-5, C-7, C-1), 6.88/158.2, 129.6, 114.3 (H-13/C-14, C-11, C-13), 5.85/72.1 (H-18/C-17), 5.21, 5.12/72.1 (H-19', H-19/C-17), 4.01/158.2, 69.6 (H-15/C-14, C16), 3.94/134.6, 117.1, 69.2 (H-17/C-18, C-19, core glycol OCH_2), 3.70/70.6, 67.2 (H-16/core glycol OCH2, C-15), 3.74 –3.53/70.6, 70.4, 69.6, 69.2 (core glycol OCH_2/core glycol OCH_2, C-16).

IR (ATR) $\tilde{\upsilon}$ = 2868, 2359, 1608, 1514, 1455, 1247, 1181, 1102, 956, 884, 842, 754, 667 cm^{-1}.

MS (ESI, pos.; methanol): *m/z* = 1251.7 ($[C_{66}H_{85}NaO_{20}P]^+$), calcd. 1251.5 for ($[C_{66}H_{85}NaO_{20}P]^+$).

HRMS (ESI, pos.; methanol): *m/z* = 1251.5250 ($[C_{66}H_{85}NaO_{20}P]^+$), calcd. 1251.5264 for $[C_{66}H_{85}NaO_{20}P]^+$).

2.3.6. *Synthesis of the precatenane* (*S*,*S*)-**13c**

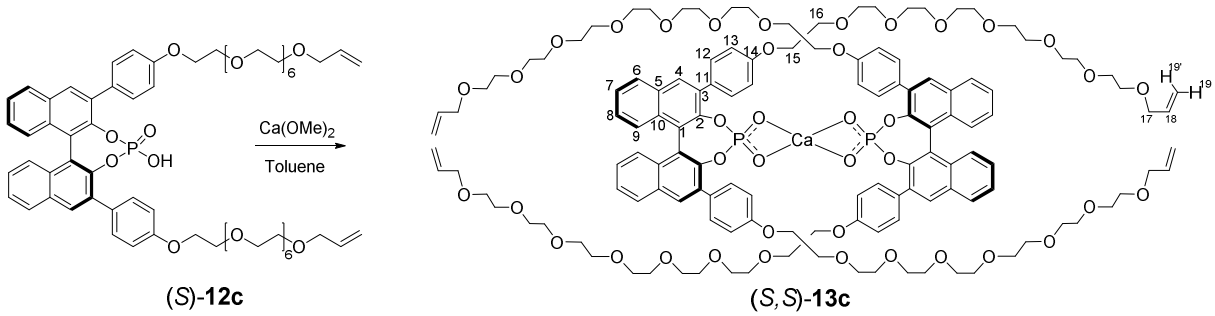

The phosphoric acid (*S*)-**12c** (324 mg, 0.264 mmol, 1 eq.) was charged in a Schlenk flask and dried at high vacuum for three hours. Dry toluene (10 ml) and calcium methoxide (13.5 mg, 0.132 mmol, 0.5 eq.) were added and the mixture was stirred at room temperature for 16 hours. The mixture was filtered and the solvent was removed in the rotary evaporator to give the product (*S*,*S*)-**13c** (316 mg, 0.127 mmol, 96%) as a brown oil.

$C_{132}H_{168}O_{40}P_2Ca$ 2496.78 g/mol

^{1}H-NMR (600 MHz, [D$_6$]-Benzene, 298 K) δ [in ppm] = 8.05 (m, 8 H, H-12), 7.93 (br s, 4 H, H-4), 7.76 (d, ^3J(H-6,7) = 8.1, 4 H, H-6), 7.40 (d, ^3J(H-9,8) = 8.6 Hz, 4 H, H-9), 7.21 (t, ^3J(H-7,6/8) = 7.5 Hz, 4 H, H-7), 7.08 - 6.87 (m, 12 H, H-8, H-12), 5.78 (m, 4 H, H-18), 5.17 (d, ^3J(H-19',18) = 17.5 Hz, 4 H, H-19'), 5.01 (d, ^3J(H-19,18) = 10.5 Hz, 4 H, H-19), 3.93 (m, 8 H, H-15), 3.79 (br s, 8 H, H-17), 3.68-3.13 (m, 104 H, H-16, core glycol OC*H*$_2$).

^{13}C-NMR (151 MHz, [D$_6$]-Benzene, 298 K) δ [in ppm] = 158.9 (C-14), 148.2 (C-2), 135.5 (C-18), 135.3 (C-3), 132.9 (C-10), 132.2 (C-12), 131.3 (C-5), 130.6 (C-4), 128.5 (C-11), 128.4 (C-6), 127.5 (C-9), 126.1 (C-8), 125.2 (C-7), 123.9 (C-1), 116.4 (C-19), 114.7 (C-13), 72.1 (C-17), 70.7 – 69.6 (C-16, core glycol O*C*H$_2$), 67.8 (C-15).

^{31}P-NMR (121.52 MHz, [D$_6$]-Benzene, 298 K) δ [in ppm] = 0.11 (s, P(O)OH).

COSY (600 MHz/600 MHz, [D$_6$]-Benzene, 298 K) δ [in ppm] = 8.05/6.98 (H-12/H-13), 7.76/7.21 (H-6/H-7), 7.41/6.98 (H-9/H-8), 7.21/6.98, 7.76 (H-7/H-8, 6), 7.08 - 6.87 /8.05, 7.41, 7.21 (H-13, H-8/H-12, H-9, H-7), 5.78/5.17, 5.01, 3.79 (H-18/H-19', H-19, H-17), 5.17/5.78, 3.79 (H-19'/H-18, H-17), 5.17/5.78, 3.79 (H-19/H-18, H-17), 3.79/5.78, 5.17 (H-17/H-18, H19').

HSQC (600 MHz/151 MHz, [D$_6$]-Benzene, 298 K) δ [in ppm] =8.05/132.1 (H-12/C-12), 7.93/130.6 (H-4/C-4), 7.76/128.4 (H-6/C-6), 7.41/127.5 (H-9/C-9), 7.21/125.2 (H-7/C-7), 7.08 – 6.87/114.7, 126.1 (H-13, H-8/C-13, C-8), 5.78/135.5 (H-18/C-18),

5.17, 5.01/116.4 (H-19', H-19/C-19), 3.93/67.8 (H-15/C-15), 3.79/72.1 (H-17,C-17), 3.68 - 3.13/70.7-69.6 (core glycol O*C*H$_2$).

HMBC (600 MHz/151 MHz, [D$_6$]-Benzene, 298 K) δ [in ppm] = 7.93/148.2, 132.2 (H-4/C-2, C-12), 7.76/126.1 (H-6/C-9), 7.41/125.2, 131.3 (H-8/C-7, C-5), 7.21/127.5, 131.3 (H-7/C-8, C-5), 7.08 – 6.87/132.8, 128.4 (H-13, H-9/C-10, C-6), 5.01/72.1 (H-19/C-17).

IR (ATR) $\bar{\upsilon}$ = 2869, 1608, 1514, 1406, 1248, 1183, 1100, 971, 830, 753 cm^{-1}.

MS: Despite repeated measurements, the intact calcium complex (*S*,*S*)-**19c** could not be detected by mass spectrometry. Only the BINOL-phosphate (*S*)-**18c** was detected. This is in line with our earlier report about the synthesis of compounds **1b/2b**, where the corresponding calcium complex was only a minor peak and the free phosphate was detected as the main peak.[1]

2.3.7. *Synthesis of macrocycle* (*S*)-**2c** *and catenane* (*S*)-**1c**

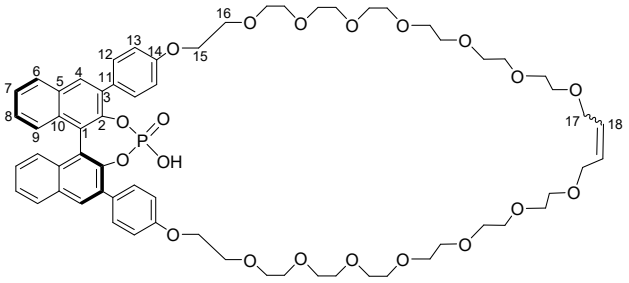

(*S*)-**2c**

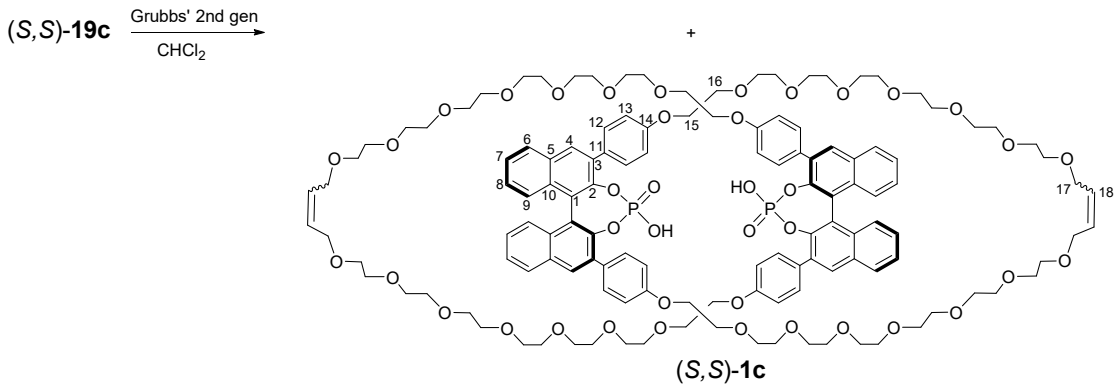

(*S*,*S*)-**1c**

(*S*,*S*)-**13c** (150 mg, 0.0601 mmol, 1 eq.) was dried in a Schlenk flask for four hours. Dry dichloromethane (50 ml) and second generation Grubb's catalyst (5.1 mg, 0.00601 mmol, 0.1 eq.) were added under argon and the reaction mixture was stirred at room temperature with the flask wrapped in aluminium foil to protect the catalyst from light.

After five and 17 hours, 1 ml was withdrawn from the mixture to control the progress of the reaction by RP-18 HPLC.[2] After 20 hours further second generation Grubb's catalyst (5.1 mg, 0.006 mmol, 0.1 eq.) was added. Additional five hours of reaction lead to full

[2] The solvent was evaporated, the residue solved in methanol and filtered through a syringe filter (0.22 µm, PTFE). The reaction was stopped when HPLC analysis showed >95% conversion.

conversion and the solvent was removed. The dark brown residue was dissolved in dichloromethane (10 ml) and methanol (40 ml) was added dropwise. The resulting suspension was filtered through a syringe filter (0.22 µm, PTFE) and the solvent was removed to give 128 mg of a brown solid. The crude product was purified by preparative MPLC (RP-18 17g Kronlab column, MeOH with 0.05% TFA : water with 0.05% TFA = 65 : 35 gradient flow firstly up to 85:15 within 48 min, secondly up to 90:10 within 22 minutes, thirdly up to 100:0 within 10 minutes, 15 ml/min). The solvent was evaporated and each of the two compounds was redissolved in dichloromethane (50 ml) and washed with hydrochloric acid (2M, 10 x 2 ml). After removing the solvent in the rotary evaporator, the 7-EG macrocycle (*S*)-**2c** (7.0 mg, 10%) and the 7-EG catenane (*S*)-**1c** (23 mg, 15%) were obtained.

Macrocycle (*S*)-**2c:**

$C_{64}H_{81}O_{20}P$ 1201.31 g/mol

^{1}H-NMR (600 MHz, [D$_1$]-Chloroform, 298 K) δ [in ppm] = 7.99 (s, 2 H, H-4), 7.93 (d, ^3J(H-6,7) = 8.2 Hz, 2 H, H-6), 7.71 (ps d, ^3J(H-12,13) = 8.3 Hz, 4 H, H-12), 7.45 (dd, ^3J(H-7,6) = 7.4 Hz, ^3J(H-7,8) = 7.4 Hz, 2 H, H-7), 7.33 (d, ^3J(H-9,8) = 8.6 Hz, 2 H, H-9), 7.29 – 7.23 (m, 2 H, H-8 merged with $CDCl_3$ peak), 7.02 (ps d, ^3J(H-13,12) = 8.4 Hz, 4 H, H-13), 5.70 (s, 1.85 H, H-18 (*E*-isomer)), 5.63 (s, 0.15 H, H-18 (*Z*-isomer)), 4.25 – 4.15 (m, 4 H, H-15), 3.97 – 3.82 (m, 8 H, H-16, H-17), 3.76-3.44 (m, 48 H, core glycol O*C*H$_2$).

^{13}C-NMR (151 MHz, [D$_1$]-Chloroform, 298 K) δ [in ppm] = 158.6 (C-14), 145.2 (d, J_{C-P} = 8.6 Hz, C-2), 133.8 (C-3), 132.0 (C-10), 131.6 (C-5), 131.3 (C-12), 131.0 (C-4), 130.1 (C-11), 129.6 (C-18), 128.4 (C-6), 127.2 (C-9), 126.3 (C-8), 125.9 (C-7), 122.9 (C-1), 114.6 (C-13), 71.2 (C-17), 71.0 (core glycol O*C*H$_2$), 70.8 (core glycol O*C*H$_2$), 70.6 (core glycol O*C*H$_2$), 69.9 (C-16), 69.4 (core glycol O*C*H$_2$), 67.7 (C-15).

^{31}P-NMR (242.9 MHz, [D$_1$]-Chloroform, 298 K) δ [in ppm] = -3.46 (s, P(O)OH).

COSY (600 MHz/600 MHz,[D$_1$]-Chloroform, 298 K) δ [in ppm] = 7.93/7.45 (H-6/H-7), 7.71/7.02 (H-12/H-13), 7.45/7.93, 7.29 – 7.23 (H-7/H-6, H-8), 7.33/7.29 – 7.23 (H-9/H-8), 7.29 – 7.23/7.45, 7.33 (H-8/H-7, H-9), 7.02/7.71 (H-13/H-12), 5.70, 5.63/3.91 (H-18/H-17), 4.20/3.91 (H-15/H-16), 3.91/4.20 (H-16/H-15).

HSQC (600 MHz/151 MHz, [D$_1$]-Chloroform, 298 K) δ [in ppm] = 7.99/131.0 (H-4/C-4), 7.93/128.4 (H-6/C-6), 7.71/131.3 (H-12/C-12), 7.45/125.9 (H-7/C-7), 7.33/127.2 (H-9/C-9), 7.29 – 7.23/126.3 (H-8/C-8), 7.02/114.6 (H-13/C-13), 5.70, 5.63/129.6 (H-18/C-18), 4.25 – 4.15/67.7 (H-15/C-15), 3.97 – 3.82/71.2, 69.9 (H-17,H-16/C-17,C-16), 3.76 - 3.44/71.0, 70.8, 70.6, 69.4 (core glycol O*C*H$_2$).

HMBC (600 MHz/151 MHz, [D$_1$]-Chloroform, 298 K) δ [in ppm] = 7.99/145.2, 132.0, 130.1, 128.4, 122.9 (H-4/C-2, C-10, C-11, C-6, C-1), 7.93/132.0, 131.0, 126.3 (H-6/C-10, C-4, C-8), 7.71/158.6, 131.3, 114.6 (H-12/C14, C-12, C-13), 7.33/131.6, 127.2 (H-7/C-5, C-9), 7.27/132.0, 128.4 (H-8/C-10, C-6), 7.18/132.0, 131.6, 125.9, 122.9 (H-9/C-10, C-5,

C-7, C-1), 7.02/158.6, 130.1, 114.6 (H-13/C-14, C-11, C-13), 5.70/71.2 (H-18/C-17), 3.97 – 3.82/129.6, 71.2, 69.4 (H-17, H-16/C-18,C-17, core glycol O*C*H_2), 3.76 – 3.44/71.0, 70.8, 70.6, 69.4, 69.9 (core glycol OCH_2/core glycol O*C*H_2, C-16).

IR (ATR) $\tilde{\upsilon}$ = 3648, 2869, 2159, 1976, 1683, 1514, 1246, 1095, 954, 834, 752, 648, 616 cm^{-1}.

MS (ESI, pos.; methanol): *m/z* = 1223.5 ($[C_{64}H_{81}NaO_{20}P]^+$), calcd. 1223.5 for ($[C_{64}H_{81}NaO_{20}P]^+$)

HRMS (ESI, pos.; methanol): *m/z* = 1223.4928 ($[C_{64}H_{81}NaO_{20}P]^+$), calcd. 1223.4951 for $[C_{64}H_{81}NaO_{20}P]^+$)

Catenane (*S,S*)-**1c:**

$C_{128}H_{162}O_{40}P_2$ 2402.62 g/mol

^{1}H-NMR (600 MHz, [D$_1$]-Chloroform, 298 K) δ [in ppm] = 7.97 (s, 4 H, H-4), 7.93 (d, ^3J(H-6,7) = 8.3 Hz, 4 H, H-6), 7.61 (ps d, ^3J(H-12,13) = 8.2 Hz, 8 H, H-12), 7.46 (dd, ^3J(H-7,6) = 7.5 Hz, ^3J(H-7,8) = 7.5 Hz, 4 H, H-7), 7.31 (d, ^3J(H-9,8) = 8.5 Hz, 4 H, H-9), 7.28 – 7.24 (m, 4 H, H-8 merged with $CDCl_3$ peak), 6.89 (ps d, ^3J(H-13,12) = 8.3 Hz, 8 H, H-13), 5.73 (s, 3.7 H, H-18 (*E*-isomer)), 5.65 (s, 0.3 H, H-18 (*Z*-isomer), 4.00 (t, ^3J(H-15,16) = 4.7 Hz, 8 H, H-15), 3.96 – 3.92 (m, 16 H, H-16, H-17), 3.74 - 3.44 (m, 96 H, core glycol OC*H*$_2$).

^{13}C-NMR (151 MHz, [D$_1$]-Chloroform, 298 K) δ [in ppm] = 158.4 (C-14), 145.2 (d, JC-P = 8.6 Hz, C-2), 133.8 (C-3), 132.0 (C-10), 131.6 (C-5), 131.2 (C-12), 131.0 (C-4), 129.8 (C-11), 129.6 (C-18), 128.4 (C-6), 127.2 (C-9), 126.3 (C-8), 125.9 (C-7), 122.9 (C-1), 114.6 (C-13), 71.2 (C-17), 71.0 (core glycol O*C*H_2), 70.8 (core glycol O*C*H_2), 70.6 (core glycol O*C*H_2), 69.9 (C-16), 69.4 (core glycol O*C*H_2), 67.4 (C-15).

^{31}P-NMR (242.9 MHz, [D$_1$]-Chloroform, 298 K) δ [in ppm] = 1.35 (s, P(O)OH).

COSY (600 MHz/600 MHz,[D$_1$]-Chloroform, 298 K) δ [in ppm] = 7.93/7.46 (H-6/H-7), 7.61/6.89 (H-12/H-13), 7.46/7.93, 7.24 (H-7/H-6, H-8), 7.31/7.24 (H-9/H-8), 7.28 – 7.24/7.46, 7.31 (H-8/H-7, H-9), 6.89/7.61 (H-13/H-12), 5.73, 5.65/3.92 (H-18/H-17), 4.00/3.92 (H-15/H-16), 3.96/5.76, 5.65 (H-17/H-18), 3.92/4.00 (H-16/H-15).

HSQC (600 MHz/151 MHz, [D$_1$]-Chloroform, 298 K) δ [in ppm] =7.97/131.0 (H-4/C-4), 7.93/128.4 (H-6/C-6), 7.61/131.3 (H-12/C-12), 7.46/125.9 (H-7/C-7), 7.31/127.2 (H-9/C-9), 7.28 – 7.24/126.3 (H-8/C-8), 6.89/114.6 (H-13/C-13), 5.73, 5.65/129.6 (H-18/C-18), 4.00/67.4 (H-15/C-15), 3.96 – 3.92/71.2, 69.9 (H-17, H-16/C-17, C-16), 3.74 - 3.44/71.0, 70.8, 70.6, 69.4 (core glycol O*C*H_2).

HMBC (600 MHz/151 MHz, [D$_1$]-Chloroform, 298 K) δ [in ppm] = 7.97/145.2, 132.0, 129.8, 128.4, 122.9 (H-4/C-2, C-10, C-11, C-6, C-1), 7.93/132.0, 131.0, 126.3 (H-6/C-10, C-4, C-8), 7.61/158.4, 131.3, 114.6 (H-12/C14, C-12, C-13), 7.46/131.6, 127.2 (H-7/C-5, C-9), 7.31/132.0, 131.6, 125.9, 122.9 (H-9/C-10, C-5, C-7, C-1), 7.27/132.0, 128.4 (H-8/C-10, C-6), 6.89/158.4, 129.8, 114.6 (H-13/C-14, C-11, C-13), 5.73/71.2 (H-18/C-17),

4.00 /69.9, 129.6 (H-15/C-16, C-18), 3.96 – 3.92/129.6, 71.2, 69.4 (H-17, H-16/C-18,C-17, core glycol O*C*H_2), 3.74 –3.44/71.0, 70.8, 70.6, 69.4, 69.9 (core glycol OCH_2/core glycol O*C*H_2, C-16).

IR (ATR) $\tilde{\upsilon}$ = 2868, 1684, 1608, 1514, 1456, 1248, 1181, 1107, 834, 648 cm^{-1}.

MS (ESI, pos.; methanol): *m/z* = 1199.7 ($[C_{128}H_{160}O_{40}P_2]^{2-}$), calcd. 1199.5 for ($[C_{128}H_{163}NaO_{40}P_2]^{+}$).

HRMS (ESI, neg.; methanol): *m/z* = 1199.4935 ($[C_{128}H_{160}O_{40}P_2]^{2-}$), calcd. 1199.4986 for $[C_{128}H_{160}O_{40}P_2]^{2-}$).

3. Catalytic reactions

General procedure for catalysis for determination of enantiomeric excess

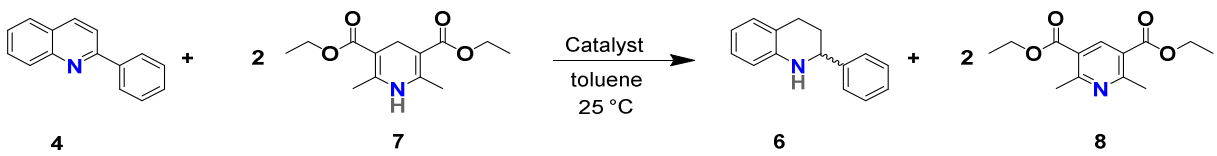

4 7 6 8

2-Phenylquinoline (4.98 µmol or 25 µmol, 1 equiv.) and diethyl 1,4-dihydro-2,6-dimethyl-3,5-pyridinedicarboxylate (11.95 µmol or 60 µmol, 2.4 equiv.) were taken in a Schlenk flask which was evacuated three times and back filled with argon. To that mixture, toluene (3 or 5 ml), followed by the catalyst (*S,S*)-**1**/(*S*)-**2**/(*S*)-**3** (stock solution in toluene, 15 mg/ml for (*S*,*S*)-**1a/b/c** and (*S*)-**2a/b/c**, 0.69 mg/ml or 1.75 mg/ml for (*S*)-**3**) were added and the reaction mixture was stirred at room temperature. The reaction was monitored by TLC with cyclohexane/ethyl acetate (10/1) mixtures. After full conversion the solvent was evaporated in the rotatory evaporator and the mixture was purified by silica gel flash column chromatography with cyclohexane/ethyl acetate (99/1) mixtures. The purified sample was used for the chiral HPLC analysis (Chiralcel OD-H column) to determine the enantiomeric excess (*ee*).

Table S1: Reaction conditions for the transfer hydrogenation of 2-phenylquinoline catalysed by catenated phosphoric acids (*S*,*S*)-**1a/b/c**, macrocyclic phosphoric acids (*S*)-**2a/b/c** or acyclic phosphoric acid (*S*)-**3.**

Entry	Catalyst	Cat. loading [mol%][(a)]	Quinoline conc [mM]	Enantiomeric excess[(b)] [%]
0	(*S*,*S*)-**1a**	2.5	5	80.9
1	(*S*,*S*)-**1b**	2.5	5	79.3
2	(*S*,*S*)-**1c**	2.5	5	81.7
3	(*S*)-**2a**	2.5	5	-16.9
4	(*S*)-**2b**	2.5	5	-12.2
5	(*S*)-**2c**	2.5	5	-16.6
6	(*S*)-**3**	0.1	1.66	-29.5
7	(*S*)-**3**	0.25	1.66	-20.9
8	(*S*)-**3**	0.5	1.66	-10.1
9	(*S*)-**3**	1	1.66	12.8
10	(*S*)-**3**	1.5	1.66	20.4
11	(*S*)-**3**	2.5	1.66	36.5
12	(*S*)-**3**	5	1.66	54.7
13	(*S*)-**3**	10	1.66	61.2
14	(*S*)-**3**	20	1.66	67.5
15	(*S*)-**3**	35	1.66	70.6
16	(*S*)-**3**	50	1.66	71.6
17	(*S*)-**3**	0.5	5	-22.8
18	(*S*)-**3**	1.5	5	14.3
19	(*S*)-**3**	2.5	5	24.5
20	(*S*)-**3**	5	5	45.0
21	(*S*)-**3**	20	5	66.1
22	(*S*)-**3**	50	5	71.1
23[(c)]	(*S*)-**3**	1	1.66	9.6

(a) Catalyst loading relative to quinoline. (b) Determined by chiral HPLC (Chiralcel OD-H column). (c) 49 mol% benzoic acid added. All values are given for the excess of (*R*)-enantiomer.

4. NMR investigations

4.1. General procedure for sample preparation and NMR-measurements

4.1.1. Sample preparation

Stock solutions of 2-phenylquinoline (16.6 mM), Hantzsch Ester (4.98 mM) and catalyst were freshly prepared and stirred in a vial with a cap until everything was dissolved. The Hantzsch Ester stock solutions were allowed to stir for 1 hour due to poor solubility in toluene. From the stock solutions the appropriate amounts (Q = 60 µL, HE = 480 µL, Cat = 60 µL; total amount: 600 µL) were transferred into a NMR tube using an Eppendorf pipette.

4.1.2. Variation of the catalyst loading

For each sample, all solutions were freshly prepared on the day of measurement.

Spectra were recorded on a Bruker DRX500 spectrometer. Before addition of catalyst solution the sample was shimmed and an initial spectrum was recorded which was used as starting point (t_0). After addition of the catalyst, spectra were recorded in defined intervals.

4.1.3. Determination of substrate orders and analysis of product inhibition

Stock solutions were freshly prepared on the day of measurement. Identical stock solutions were used for up to four measurements to enhance reproducibility between the measurements.

Spectra were recorded on a Bruker DRX600 spectrometer. Before addition of catalyst solution, each sample was shimmed and an initial spectrum was recorded which was used as starting point (t_0). After addition of the catalyst, all samples (up to 4) were recorded in an alternating fashion in defined time intervals.

4.2. Data Analysis

4.2.1. Software

All data were processed using TopSpin version 4.0.6. The obtained FIDs were fourier transformed, baseline corrected and phase corrected using the commands –efp, -absn and –apk respectively.

4.2.2. *Integral regions*

Ten different signals were followed during the reaction. The integration regions and assignments are listed in Table S2 and Table S3.

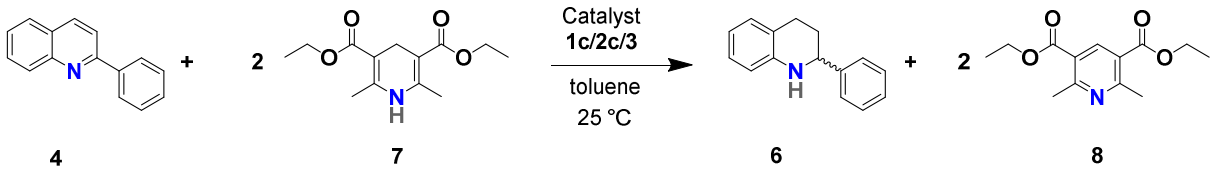

4 7 6 8

Table S2: Integration regions and assignments for macrocyclic phosphoric acid (*S*,*S*)-**2c** and catenated phosphoric acid (*S*,*S*)-**1c**

No. of Signal	Integral region	Compound	Number of protons
0	8.80 – 8.74	**8**	1H
1	8.30 – 8.14	**4**	3H
2	7.96 – 7.78	**1c/2c**	12H/6H
3	7.75 – 7.61	**4**	1H
4	3.61 – 3.56	**7**	2H
5	2.93 – 2.86	**8**	6H
6	2.66 – 2.55	**6**	1H
7	2.50 – 2.41	**6**	1H
8	2.11 – 2.04	**toluene**	9H
9	1.89 – 1.84	**7**	6H

Table S3: Integration regions and assignments for acyclic phosphoric acid (*S*)-**3**

No. of Signal	Integral region	Compound	Number of protons
0	8.80 – 8.74	**8**	1H
1	8.30 – 8.14	**4**	3H
2	7.75 – 7.61	**4**	1H
3	3.61 – 3.56	**7**	2H
4	3.42 – 3.30	**3**	6H
5	2.93 – 2.86	**8**	6H
6	2.66 – 2.55	**6**	1H
7	2.50 – 2.41	**6**	1H
8	2.11 – 2.04	**toluene**	9H
9	1.89 – 1.84	**7**	6H

The curve of conversion was created by following the decrease of signal 1. Quinoline was used as a solid and its concentration was determined directly based on weight and amount of solvent. All other concentrations were determined indirectly based on their integrals in comparison to integral 1.

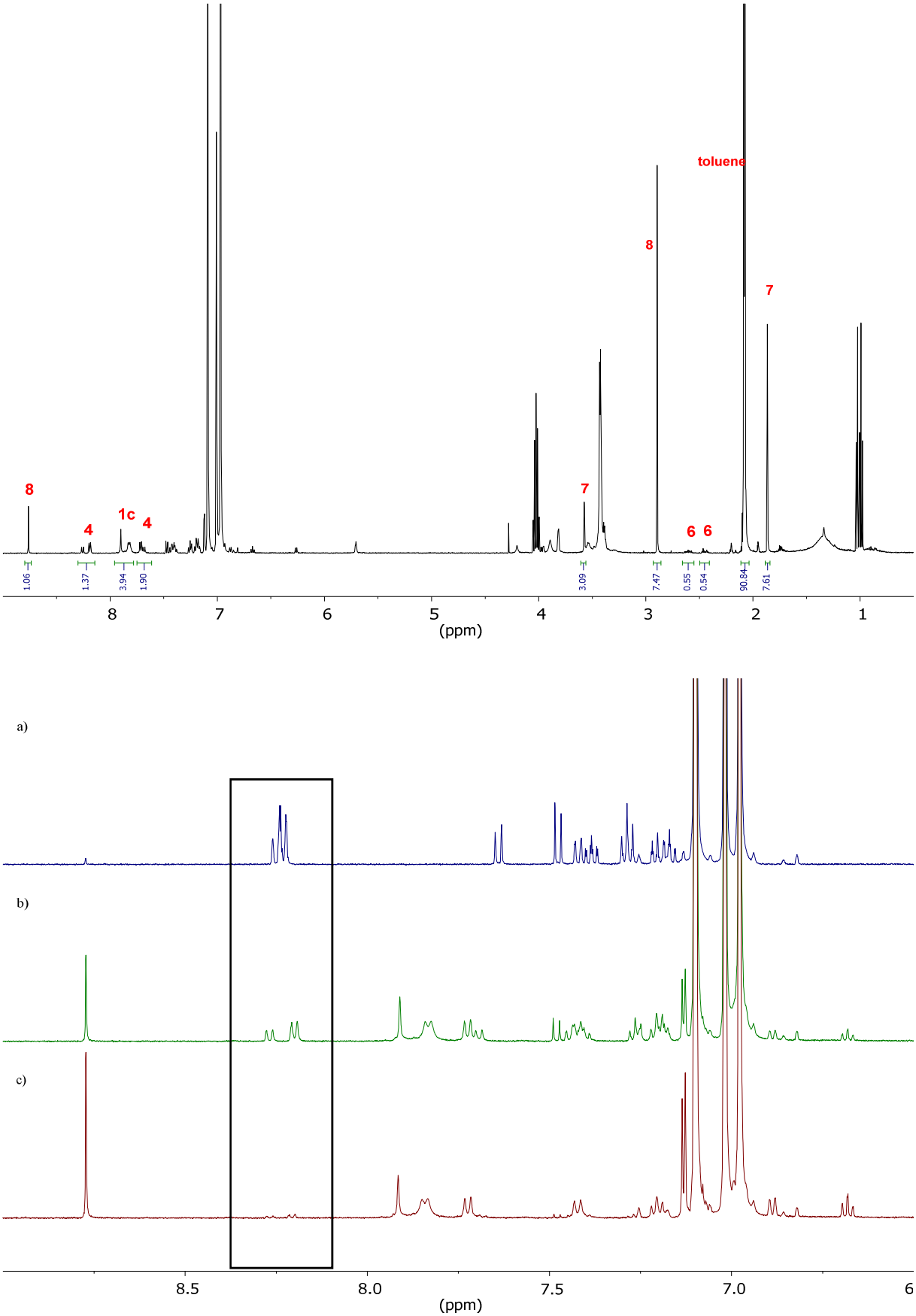

Figure S2: ^{1}H-NMR spectra of the catalytic reaction. **Top:** Overview of all signals that were followed during the reaction (with 34.65 mol % **1-c** as catalyst at 49 % conversion) **Bottom:** Aromatic region with highlighted proton signals of **4** that were used to track conversion of the reaction (with 34.65 mol % of **1-c** as catalyst: a) Before catalyst addition, b) 49 % conversion, c) 94 % conversion.

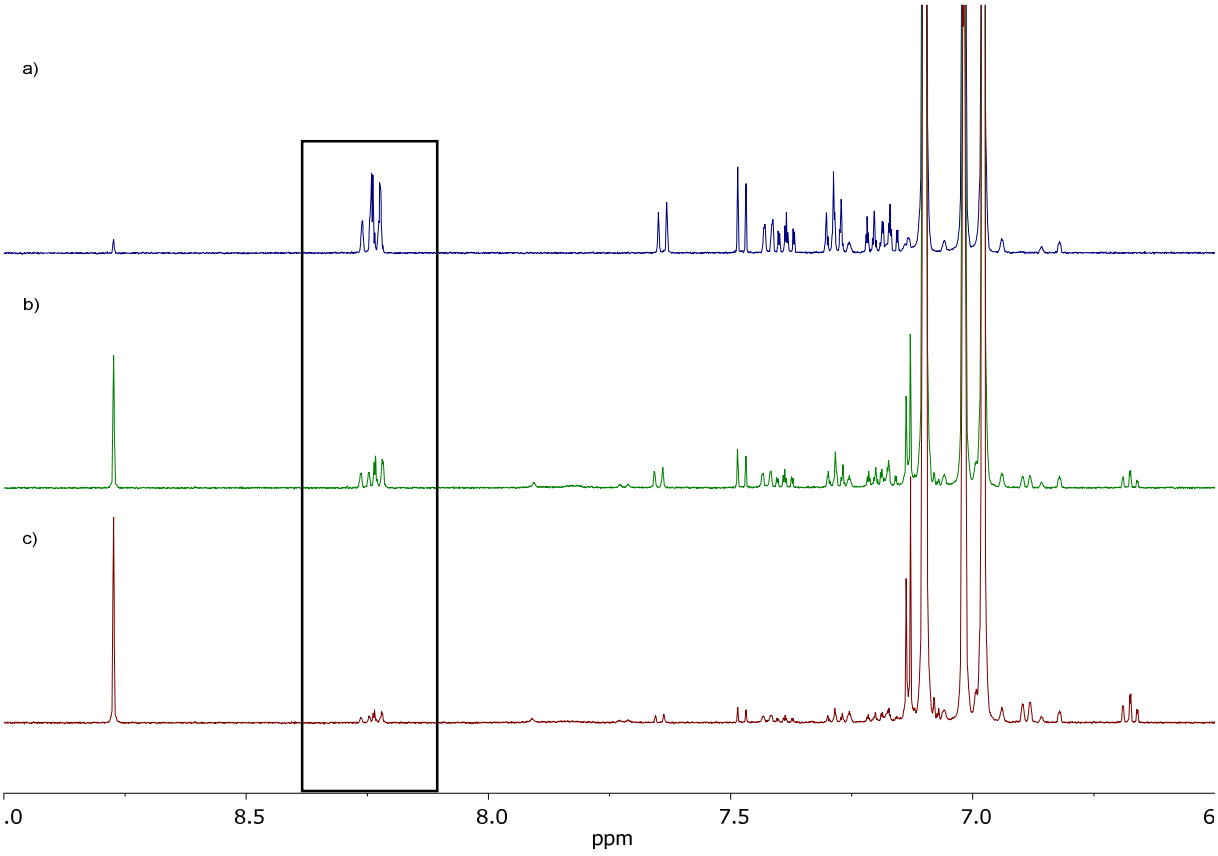

Figure S3: ^{1}H-NMR spectra of the catalytic reaction. Aromatic region with highlighted proton signals of **4** that were used to track conversion of the reaction (with 3.98 mol % of **1-c** as catalyst: a) Before catalyst addition, b) 50 % conversion, c) 80 % conversion.

4.3. Determination of k_{obs} and v_0

4.3.1. *Linear fitting*

The linearization of the data was performed based on the rate law of the reaction, assuming first order in both substrates. In all cases, this mathematical treatment gave linear plots (see Figure S71-Figure S116). Comparative analysis of the data based on different substrate orders did not give linear plots (see Figure S4), suggesting that indeed first order in both substrates can be expected.

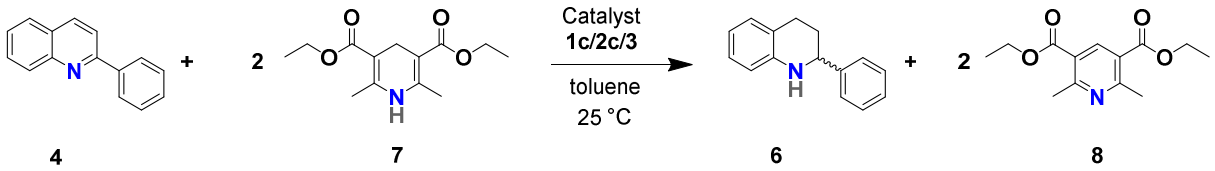

4 **7** **6** **8**

-d[**4**]/dt =	k_{Obs} * [**4**]^m * [**7**]^n = k * [**Cat**]^p * [**4**]^m * [**7**]^n
with	[**6**] = [**4**]$_0$ – [**4**]
with	[**7**] = [**7**]$_0$ – 2*[**6**] = [**7**]$_0$ – 2*[**4**]$_0$ + 2*[**4**]
and	m = n = 1
-d[**4**]/dt =	k_{Obs} * [**4**] * ([**7**]$_0$ – 2*[**4**]$_0$ + 2*[**4**])
d[**4**]/([**4**] * ([**7**]$_0$ – 2*[**4**]$_0$ + 2*[**4**])) =	-k_{Obs} * dt
with	c = [**7**]$_0$–2*[**4**]$_0$
and	x = [**4**]
Partial fraction decomposition gives:	
∫dx/(x*(2x + c)) =	1/c*(∫1/x - ∫2/(2x+c))dx = 1/c*(ln(x)-ln(2x+c))
Integration from [**4**]$_0$ to [**4**] and t$_0$ = 0 to t gives:	
1/c*(ln[**4**]-ln[**4**]$_0$-ln(2*[**4**]+c)+ln(2*[**4**]$_0$+c)) =	-k_{Obs} * t
1/c*ln(([**4**]*(2*[**4**]$_0$+c))/([**4**]$_0$*(2*[**4**]+c))) =	-k_{Obs} * t
1/c*ln(([**4**]*[**7**]$_0$))/([**4**]$_0$*(2*[**4**]+c))) =	-k_{Obs} * t

Thus, -k_{Obs} was determined as the slope in the plot of 1/c*ln(([**4**]*[**7**]$_0$))/([**4**]$_0$*(2*[**4**]+c))) vs. t

a)

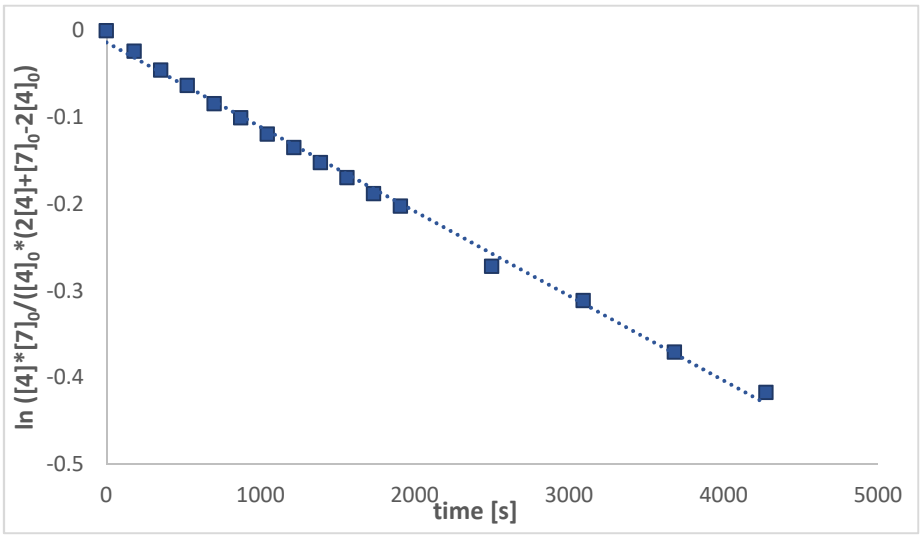

b)

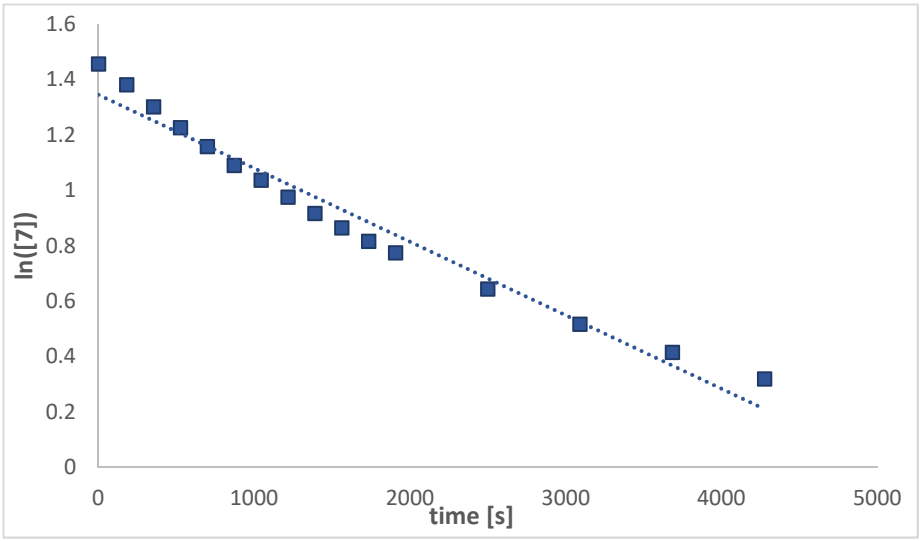

c)

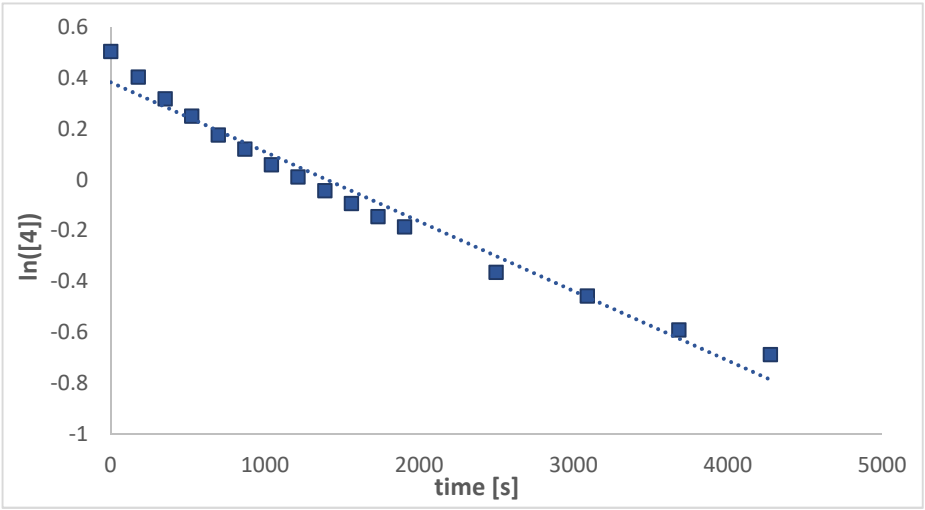

Figure S4: Comparative analysis of the concentrations vs. time data. a) for m = n = 1, b) for m = 0 and n = 1, c) for m = 1 and n = 0.

4.3.2. *Nonlinear fitting*

The nonlinear fitting data was performed based on the rate law of the reaction, assuming first order in both substrates.

$1/c*\ln(([\mathbf{4}]*[\mathbf{7}]_0))/([\mathbf{4}]_0*(2*[\mathbf{4}]+c))) =$	$-k_{Obs} * t$
$[\mathbf{4}]*[\mathbf{7}]_0/([\mathbf{4}]_0*(2*[\mathbf{4}]+c)) =$	$\exp(-c*k_{Obs}*t)$
$[\mathbf{4}]/(2*[\mathbf{4}]+c) =$	$([\mathbf{4}]_0*\exp(-c*k_{Obs}*t))/[\mathbf{7}]_0$
$1/(2+c/[\mathbf{4}]) =$	$([\mathbf{4}]_0*\exp(-c*k_{Obs}*t))/[\mathbf{7}]_0$
$2+c/[\mathbf{4}] =$	$[\mathbf{7}]_0/([\mathbf{4}]_0*\exp(-c*k_{Obs}*t))$
$c/[\mathbf{4}] =$	$[\mathbf{7}]_0/([\mathbf{4}]_0*\exp(-c*k_{Obs}*t)) - 2$
$c/[\mathbf{4}] =$	$[\mathbf{7}]_0-2*([\mathbf{4}]_0*\exp(-c*k_{Obs}*t))/([\mathbf{4}]_0*\exp(-c*k_{Obs}*t))$
$c/[\mathbf{4}] =$	$(([\mathbf{7}]_0*\exp(c*k_{Obs}*t))-2[\mathbf{4}]_0)/[\mathbf{4}]_0$
$[\mathbf{4}]/c =$	$[\mathbf{4}]_0/(([\mathbf{7}]_0*\exp(c*k_{Obs}*t))-2[\mathbf{4}]_0)$
$[\mathbf{4}] =$	$c*[\mathbf{4}]_0/(([\mathbf{7}]_0*\exp(c*k_{Obs}*t))-2[\mathbf{4}]_0)$

Fitting of k_{Obs} was performed in Microsoft Excel using the SOLVER plugin. The sum of square residues for the calculated [**4**] was minimized by changing k_{Obs}.

Due to the autooxidation of the Hantzsch-ester **7** after prolonged reaction times, the fitting was only performed for data from t = 0 until t = t_{max}, with t_{max} defined as follows:

*For catenane **1c**:*

t_{max} is defined as 10 hours for catalyst concentrations of <0.1 mM.

t_{max} is defined as the time when the reaction reaches 70% conversion (based on **4**) for catalyst concentrations of > 0.1 mM.

*For macrocycle **2c**:*

t_{max} is defined as the time when the reaction reaches 70% conversion (based on **4**). Due to the faster rate of **2c** in comparison to **1c**, this is always reached in a time <10 hours.

*For acyclic catalyst **3**:*

t_{max} is defined as the time when the reaction reaches 70% conversion (based on **4**) for catalyst concentrations of <0.2 mM.

t_{max} is defined as the time when the reaction reaches 90% conversion (based on **4**) for catalyst concentrations of between 0.2 mM and 0.8 mM.

t_{max} is defined as the time when the reaction reaches 95% conversion (based on **4**) for catalyst concentrations of >0.8 mM.

Due to the faster rate of **3** in comparison to **1c**, this is always reached in a time <10 hours.

The initial rate v_0 was determined as the slope of the first three data points of the fitted data in the [**4**] vs. t plot. The fitted data was used instead of the original data because the fitted value for k_{Obs} (and thus all fitted data points) is obtained from the whole data range. In addition, determination of v_0 from the original data gives large variations of v_0 from small variations of [**4**] (e.g. due to noise), which is not the case in the fitted data.

4.4. Variable time normalization analysis

Variable time normalization analysis (VTNA) was performed according to the protocols described by Burés.[7] Based on the stoichiometry of the reaction, the excess was calculated as follows:

excess =	$0.5*[\mathbf{7}]_0 - [\mathbf{4}]_0$

4.4.1. *Determination of substrate order for quinoline 4*

For determination of the substrate orders of quinoline **4**, the normalized substrate concentration was plotted vs. the normalized time axis as follows:

Normalized quinoline concentrations "[4] (norm)":

In a series of experiments with different starting quinoline concentrations, the largest employed quinoline concentration was used as a reference point. For all other experiments with lower quinoline concentrations, the corrected concentrations were calculated by addition of the difference between the starting concentrations to all concentration values.

Normalized time axis "t (norm)":

The normalized time axis was calculated as follows:

t_x (norm) :	Normalized time at time point x
t_{x+1} (norm) :	Normalized time at time point x+1
$[\mathbf{4}]_x$:	Concentration of **4** at time point x
$[\mathbf{4}]_{x+1}$:	Concentration of **4** at time point x+1
m:	Substrate order for quinoline
t_{x+1} (norm) =	t_x (norm) + ((0.5*($[\mathbf{4}]_x$ + $[\mathbf{4}]_{x+1}$))^m)*(t_{x+1}- t_x)

Determination of substrate order:

The substrate order *m* was varied to achieve the best overlap between all x vs. y plots of t (norm) vs. [**4**] (norm) (see Figure S7, Figure S11, Figure S15).

4.4.2. *Determination of substrate order for Hantzsch-ester 7*

For determination of the substrate orders of Hantzsch-ester **7**, the normalized substrate concentration was plotted vs. the normalized time axis as follows:

Normalized Hantzsch-ester concentrations "[7] (norm)":

In a series of experiments with different starting Hantzsch-ester concentrations, the lowest employed Hantzsch-ester concentration was used as a reference point. For all other experiments with higher Hantzsch-ester concentrations, the corrected concentrations were calculated by subtraction of the difference between the starting concentrations from all concentration values.

Normalized time axis "t (norm)":

The normalized time axis was calculated as follows:

t_x (norm) :	Normalized time at time point x
t_{x+1} (norm) :	Normalized time at time point x+1
$[\mathbf{7}]_x$:	Concentration of **7** at time point x
$[\mathbf{7}]_{x+1}$:	Concentration of **7** at time point x+1
m:	Substrate order for quinoline
t_{x+1} (norm) =	t_x (norm) + ((0.5*($[\mathbf{7}]_x$ + $[\mathbf{7}]_{x+1}$))^n)*(t_{x+1}- t_x)

Determination of substrate order:

The substrate order *n* was varied to achieve the best overlap between all x vs. y plots of t (norm) vs. [**7**] (norm) (see Figure S7, Figure S11, Figure S15).

4.4.3. *Determination of catalyst orders*

For determination of the order in catalysts **1c/2c/3**, the experimentally determined concentration of [**4**] was plotted vs. the normalized time axis as follows:

Normalized time axis "t (norm)":

The normalized time axis was calculated as follows:

t_x (norm) :	Normalized time at time point x
t_x :	Time at time point x
[**Cat**]	Catalyst concentration (time invariable)
p:	Order in catalyst
t_x (norm) =	t_x / [Cat]^p

Determination of substrate order:

The catalyst order *p* was varied to achieve the best overlap between all x vs. y plots of t (norm) vs. [**4**] (see Figure S9, Figure S13, Figure S17,

Figure **S18**).

4.4.4. *Determination of product inhibition/catalyst deactivation*

For determination of product inhibition/catalyst deactivation, the experimentally determined concentration of [**4**] was plotted vs. the normalized time axis as follows:

Normalized quinoline concentrations "[4] (norm)":

In a series of experiments with different starting quinoline concentrations, the largest employed quinoline concentration was used as a reference point. For all other experiments with lower quinoline concentrations, the corrected concentrations were calculated by addition of the difference between the starting concentrations to all concentration values.

Normalized time axis "t (norm)":

The normalized time axis was calculated as follows:

t_x (norm) :	Normalized time at time point x
t_x :	Time at time point x
Δt :	Elapsed time for reaction with higher $[\mathbf{4}]_0$ to reach concentration of **4** that is equal to $[\mathbf{4}]_0$ of reaction with lower $[\mathbf{4}]_0$
t_x (norm) =	$t_x + \Delta t$

Determination of product inhibition/catalyst deactivation:

Same-excess experiments were conducted with different starting concentrations $[\mathbf{4}]_0$. If both curves overlap in the x vs. y plots of t (norm) vs. [**4**], there is no product inhibition or catalyst deactivation. If the reaction with higher $[\mathbf{4}]_0$ shows slower conversion (indicating product inhibition or catalyst deactivation), the reaction with lower $[\mathbf{4}]_0$ is repeated with added pyridine **8**. Overlapping curves then indicate product inhibition.

4.5. Overview of kinetic results

Table S4: Experimental data and results for kinetic experiments with catenated catalysts **1a/b/c** (for stereoselectivity data for catalysts **1a/b/c** and catalysts **2a/b/c** see table S1).

Experimental setup											Analysis for k_{Obs} and v_0[c]			
		Concentrations									Linear fit	Nonlinear fit		
Exp.-No.	Catalyst	[4][a] (mM)	[4][a] (M)	[7][b] (mM)	[7][b] (M)	[8][c] (mM)	[8][c] (M)	[Cat][b] (mM)	[Cat][b] (M)	[Cat][b] (mol%)	k_{Obs} ($s^{-1} M^{-1}$)	k_{Obs} ($s^{-1} M^{-1}$)	v_0 ($M\ s^{-1}$)	v_0 / [Cat] (s^{-1})
1	**1a**	1.66	1.66E-03	3.87	3.87E-03	-	-	0.161	1.61E-04	9.68	5.67E-02	6.66E-02	3.66E-07	2.27E-03
2	**1b**	1.66	1.66E-03	4.32	4.32E-03	-	-	0.196	1.96E-04	11.79	3.94E-02	4.59E-02	3.12E-07	1.59E-03
3	**1c**	1.66	1.66E-03	4.08	4.08E-03	-	-	0.158	1.58E-04	9.53	2.68E-02	3.03E-02	1.98E-07	1.25E-03

a) Determined by weight of **4** and the volume of solvent. b) Determined by the relative integrals of **4** and **7/8/Cat**. c) Determined by linear or nonlinear fitting of the respective concentration over time data (see the SI for details).

Table S5: Experimental data and results for kinetic experiments with catenated catalyst **1c**.

Experimental setup											Analysis for k_{Obs} and v_0[c]					
		Concentrations									Linear fit	Nonlinear fit			Double ln plot	
Exp.-No.	Exp.-Type	[4][a] (mM)	[4][a] (M)	[7][b] (mM)	[7][b] (M)	[8][c] (mM)	[8][c] (M)	[Cat][b] (mM)	[Cat][b] (M)	[Cat][b] (mol%)	k_{Obs} ($s^{-1} M^{-1}$)	k_{Obs} ($s^{-1} M^{-1}$)	v_0 ($M\ s^{-1}$)	v_0 / [Cat] (s^{-1})	ln [4]	ln v_0
1	Different excess for [4]	1.66	1.66E-03	3.93	3.93E-03	-	-	0.068	6.84E-05	4.12	1.84E-02	1.88E-02	8.92E-08	1.30E-03	-6.40	-16.2
2		1.26	1.26E-03	3.93	3.93E-03	-	-	0.075	7.47E-05	5.93	1.92E-02	1.98E-02	7.35E-08	9.84E-04	-6.68	-16.4
3		0.84	8.40E-04	3.93	3.93E-03	-	-	0.080	7.98E-05	9.50	2.02E-02	1.94E-02	5.09E-08	6.38E-04	-7.08	-16.8
4		0.63	6.30E-04	3.93	3.93E-03	-	-	0.075	7.51E-05	11.93	1.95E-02	2.21E-02	4.09E-08	5.45E-04	-7.37	-17.0
5	Different excess for [7]	0.83	8.30E-04	3.93	3.93E-03	-	-	0.036	3.59E-05	4.33	1.44E-02	1.50E-02	4.23E-08	1.18E-03	-5.54	-17.0
6		0.83	8.30E-04	3.32	3.32E-03	-	-	0.036	3.58E-05	4.32	1.50E-02	1.54E-02	3.79E-08	1.06E-03	-5.70	-17.1
7		0.83	8.30E-04	2.66	2.66E-03	-	-	0.036	3.62E-05	4.37	1.59E-02	1.62E-02	3.21E-08	8.87E-04	-5.94	-17.3
8		0.83	8.30E-04	1.99	1.99E-03	-	-	0.035	3.53E-05	4.26	1.79E-02	1.86E-02	2.63E-08	7.43E-04	-6.23	-17.5
1	Same excess	1.66	1.66E-03	3.93	3.93E-03	-	-	0.068	6.84E-05	4.12	1.84E-02	1.88E-02	8.92E-08	1.30E-03	-6.40	-16.23
15		1.26	1.26E-03	3.26	3.26E-03	-	-	0.113	1.13E-04	8.94	2.70E-05	2.68E-05	9.81E-05	8.68E-04	-6.68	-9.2
16		1.26	1.26E-03	3.12	3.12E-03	0.90	9.01E-04	0.118	1.18E-04	9.33	2.65E-05	2.69E-05	9.44E-05	8.00E-04	-6.68	-9.3
9	Different excess for [Cat]	1.66	1.66E-03	4.05	4.05E-03	-	-	0.066	6.60E-05	3.98	1.33E-02	1.17E-02	8.79E-08	1.33E-03	-9.63	-16.2
10		1.66	1.66E-03	4.08	4.08E-03	-	-	0.158	1.58E-04	9.53	3.03E-02	2.68E-02	1.98E-07	1.25E-03	-8.75	-15.4
11		1.66	1.66E-03	4.21	4.21E-03	-	-	0.251	2.51E-04	15.13	3.40E-02	3.27E-02	2.28E-07	9.06E-04	-8.29	-15.3
12		1.66	1.66E-03	3.62	3.62E-03	-	-	0.352	3.52E-04	21.19	5.70E-02	4.40E-02	3.20E-07	9.10E-04	-7.95	-15.0
13		1.66	1.66E-03	4.13	4.13E-03	-	-	0.575	5.75E-04	34.65	8.32E-02	7.58E-02	5.15E-07	8.95E-04	-7.46	-14.5
14		1.66	1.66E-03	4.29	4.29E-03	-	-	0.748	7.48E-04	45.06	1.12E-01	1.01E-01	6.95E-07	9.29E-04	-7.20	-14.2

a) Determined by weight of **4** and the volume of solvent. b) Determined by the relative integrals of **4** and **7/8/Cat**. c) Determined by linear or nonlinear fitting of the respective concentration over time data (see SI for details).

Table S6: Experimental data and results for kinetic experiments with macrocyclic catalyst **2c**.

Experimental setup											Analysis for k_{Obs} and v_0[c]					
		Concentrations									Linear fit	Nonlinear fit			Double ln plot	
Exp.-No.	Exp.-Type	[**4**][a] (mM)	[**4**][a] (M)	[**7**][b] (mM)	[**7**][b] (M)	[**8**][c] (mM)	[**8**][c] (M)	[**Cat**][b] (mM)	[**Cat**][b] (M)	[**Cat**][b] (mol%)	k_{Obs} ($s^{-1} M^{-1}$)	k_{Obs} ($s^{-1} M^{-1}$)	v_0 ($M\ s^{-1}$)	v_0 / [**Cat**] (s^{-1})	ln [**Cat**]	ln v_0
2c-1	Different excess for [**4**]	1.66	1.66E-03	4.00	4.00E-03	-	-	0.077	7.67E-05	4.62	3.32E-05	3.48E-05	2.23E-07	2.90E-03	-	-
2c-3		1.26	1.26E-03	4.02	4.02E-03	-	-	0.078	7.82E-05	6.21	3.06E-05	3.19E-05	1.57E-07	2.00E-03	-	-
2c-2	Different excess for [**7**]	1.26	1.26E-03	3.24	3.24E-03	-	-	0.078	7.85E-05	6.23	3.26E-05	3.42E-05	1.35E-07	1.73E-03	-	-
2c-3		1.26	1.26E-03	4.02	4.02E-03	-	-	0.078	7.82E-05	6.21	3.06E-05	3.19E-05	1.57E-07	2.00E-03	-	-
2c-1	Same excess	1.66	1.66E-03	4.00	4.00E-03	-	-	0.077	7.67E-05	4.62	3.32E-05	3.48E-05	2.23E-07	2.90E-03	-	-
2c-2		1.26	1.26E-03	3.24	3.24E-03	-	-	0.078	7.85E-05	6.23	3.26E-05	3.42E-05	1.35E-07	1.73E-03	-	-
2c-4		1.26	1.26E-03	3.07	3.07E-03	0.71	7.10E-04	0.081	8.10E-05	6.43	3.23E-05	3.50E-05	1.32E-07	1.62E-03	-	-
2c-5	Different excess for [**Cat**]	1.66	1.66E-03	4.02	4.02E-03	-	-	0.070	7.00E-05	4.22	2.39E-02	1.17E-02	1.50E-07	2.15E-03	-9.57	-15.7
2c-6		1.66	1.66E-03	4.03	4.03E-03	-	-	0.135	1.35E-04	8.12	4.88E-02	2.68E-02	3.34E-07	2.48E-03	-8.91	-14.9
2c-7		1.66	1.66E-03	3.83	3.83E-03	-	-	0.268	2.68E-04	16.16	9.54E-02	3.27E-02	5.77E-07	2.15E-03	-8.22	-14.4
2c-8		1.66	1.66E-03	4.11	4.11E-03	-	-	0.445	4.45E-04	26.80	1.94E-01	4.40E-02	1.06E-06	2.38E-03	-7.72	-13.8
2c-9		1.66	1.66E-03	4.05	4.05E-03	-	-	0.532	5.32E-04	32.02	1.63E-01	7.58E-02	1.12E-06	2.11E-03	-7.54	-13.7
2c-10		1.66	1.66E-03	4.13	4.13E-03	-	-	0.609	6.09E-04	36.68	2.05E-01	1.01E-01	1.16E-06	1.91E-03	-7.40	-13.7
2c-11		1.66	1.66E-03	4.27	4.27E-03	-	-	0.657	6.57E-04	39.57	2.24E-01	0.00E+00	1.29E-06	1.96E-03	-7.33	-13.6
2c-12		1.66	1.66E-03	3.97	3.97E-03	-	-	0.712	7.12E-04	42.91	2.32E-01	0.00E+00	1.42E-06	1.99E-03	-7.25	-13.5
2c-13		1.66	1.66E-03	4.00	4.00E-03	-	-	0.821	8.21E-04	49.47	2.27E-01	0.00E+00	1.44E-06	1.76E-03	-7.10	-13.4
2c-14		1.66	1.66E-03	3.93	3.93E-03	-	-	0.852	8.52E-04	51.31	2.81E-01	0.00E+00	1.46E-06	1.71E-03	-7.07	-13.4

a) Determined by weight of **4** and the volume of solvent. b) Determined by the relative integrals of **4** and **7/8/Cat**. c) Determined by linear or nonlinear fitting of the respective concentration over time data (see the SI for details).

Table S7: Experimental data and results for kinetic experiments with acyclic catalyst **3**.

Experimental setup											Analysis for k_{Obs} and v_0[c]					
		Concentrations									Linear fit	Nonlinear fit			Double ln plot	
Exp.-No.	Exp.-Type	[**4**][a] (mM)	[**4**][a] (M)	[**7**][b] (mM)	[**7**][b] (M)	[**8**][c] (mM)	[**8**][c] (M)	[**Cat**][b] (mM)	[**Cat**][b] (M)	[**Cat**][b] (mol%)	k_{Obs} ($s^{-1} M^{-1}$)	k_{Obs} ($s^{-1} M^{-1}$)	v_0 ($M\ s^{-1}$)	v_0 / [**Cat**] (s^{-1})	ln [**Cat**]	ln v_0
1	Different excess for [**4**]	1.66	1.66E-03	4.1203071	4.12E-03	-	-	0.025	2.54E-05	1.53	5.51E-05	5.58E-05	2.86E-04	1.13E-02	-10.58	-8.2
2		1.26	1.26E-03	4.2359206	4.24E-03	-	-	0.021	2.14E-05	1.70	4.36E-05	4.38E-05	1.89E-04	8.81E-03	-10.75	-8.6
2	Different excess for [**7**]	1.26	1.26E-03	3.3746167	3.37E-03	-	-	0.016	1.64E-05	1.30	6.94E-05	6.94E-05	2.22E-04	1.36E-02	-11.02	-8.4
3		1.26	1.26E-03	4.2359206	4.24E-03	-	-	0.021	2.14E-05	1.70	4.36E-05	4.38E-05	1.89E-04	8.81E-03	-10.75	-8.6
1	Same excess	1.66	1.66E-03	4.1203071	4.12E-03	-	-	0.025	2.54E-05	1.53	5.51E-05	5.58E-05	2.86E-04	1.13E-02	-10.58	-8.2
2		1.26	1.26E-03	3.3746167	3.37E-03	-	-	0.016	1.64E-05	1.30	6.94E-05	6.94E-05	2.22E-04	1.36E-02	-11.02	-8.4
4		1.26	1.26E-03	4.2359206	4.24E-03	0.90	9.00E-04	0.017	1.71E-05	1.36	5.31E-05	5.42E-05	1.82E-04	1.07E-02	-10.98	-8.6
5	Different excess for [**Cat**]	1.66	1.66E-03	4.44	4.44E-03	-	-	0.041	4.12E-05	2.48	0.10	0.11	7.21E-07	1.75E-02	-10.10	-14.1
6		1.66	1.66E-03	4.03	4.03E-03	-	-	0.074	7.38E-05	4.44	0.38	0.42	1.80E-06	2.44E-02	-9.51	-13.2
7		1.66	1.66E-03	3.83	3.83E-03	-	-	0.115	1.15E-04	6.91	0.61	0.57	2.29E-06	2.00E-02	-9.07	-13.0
8		1.66	1.66E-03	4.11	4.11E-03	-	-	0.227	2.27E-04	13.65	1.28	1.08	3.95E-06	1.74E-02	-8.39	-12.4
9		1.66	1.66E-03	4.05	4.05E-03	-	-	0.402	4.02E-04	24.23	1.52	1.41	4.17E-06	1.04E-02	-7.82	-12.4
10		1.66	1.66E-03	4.13	4.13E-03	-	-	0.406	4.06E-04	24.45	1.43	1.21	3.92E-06	9.66E-03	-7.81	-12.4
11		1.66	1.66E-03	4.27	4.27E-03	-	-	0.625	6.25E-04	37.66	1.55	1.57	5.39E-06	8.62E-03	-7.38	-12.1
12		1.66	1.66E-03	3.97	3.97E-03	-	-	0.649	6.49E-04	39.10	1.50	1.65	5.43E-06	8.36E-03	-7.34	-12.1
13		1.66	1.66E-03	4.00	4.00E-03	-	-	0.783	7.83E-04	47.17	1.98	1.58	4.69E-06	5.99E-03	-7.15	-12.3
14		1.66	1.66E-03	3.93	3.93E-03	-	-	0.863	8.63E-04	51.97	2.22	2.29	5.68E-06	6.58E-03	-7.06	-12.1

a) Determined by weight of **4** and the volume of solvent. b) Determined by the relative integrals of **4** and **7/8/Cat**. c) Determined by linear or nonlinear fitting of the respective concentration over time data (see the SI for details).

4.6. Results for catenanes 1a/b/c

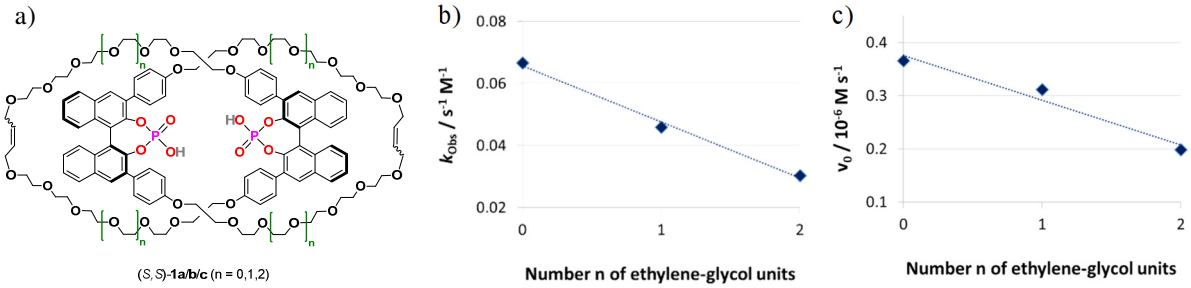

Figure S5: a) Structures of catenated catalysts **1a/b/c**, b) Dependence of k_{Obs} on ring size, c) Dependence of v_0 on ring size.

4.7. Results for catenane 1c

4.7.1. *Substrate orders based on initial rate*

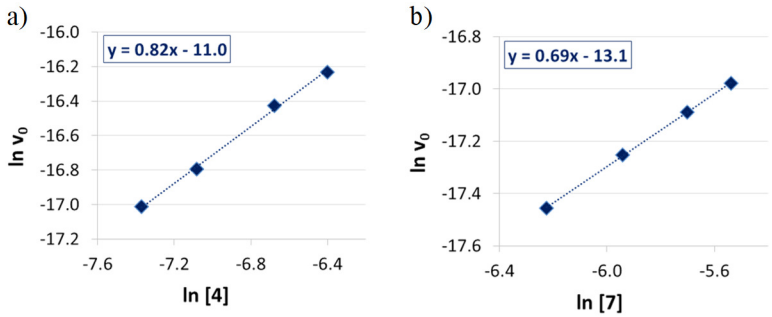

Figure S6: Different excess experiments for substrate order determination for catenane **1c** as determined in the ln v_0 / ln [Substrate] plots (v_0 in M^{-1} s^{-1}, substrate concentrations in M). a) ln v_0 / ln [Substrate] plot for quinoline **4**, b) ln v_0 / ln [Substrate] plot for Hantzsch-Ester **7**.

4.7.2. *Substrate orders based on VTNA*

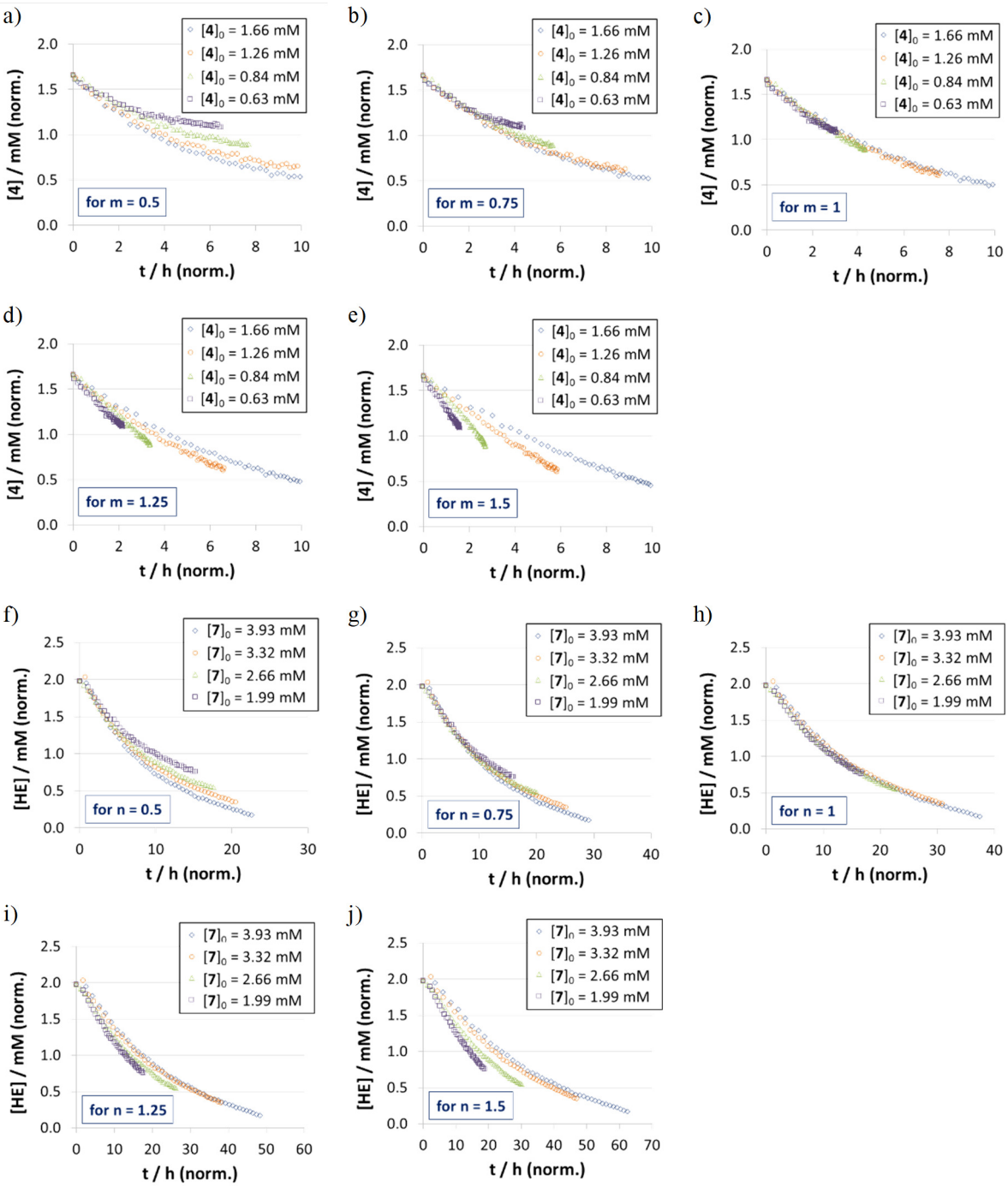

Figure S7: Different excess experiments for substrate order determination for catenane **1c** as determined by VTNA. a)-e) VTNA plots for quinoline **4** for different values of *m*, f-j) VTNA plots for for Hantzsch-Ester **7** for different values of *n*.

4.7.3. *Catalyst orders based on initial rate*

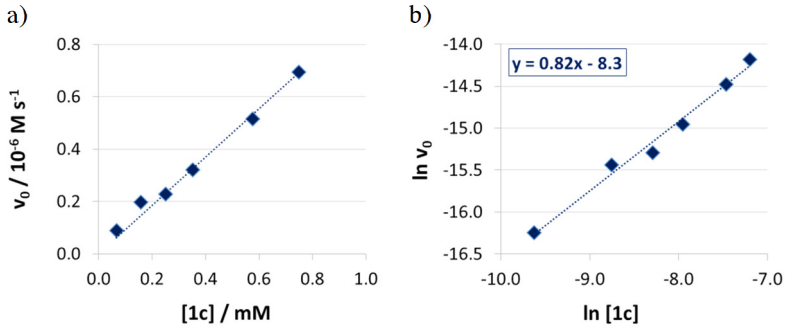

Figure S8: Influence of catalyst loading on reaction rates for catalyst **1c**. a) Initial rates at different catalyst loadings (all at 1.66 mM quinoline **4** and 3.93 mM Hantzsch-ester **7**), b) Determination of the order in catalyst order in the ln v_0 / ln [catalyst] plot (v_0 in M^{-1} s^{-1}, catalyst concentrations in M).

4.7.4. *Catalyst orders based on VTNA*

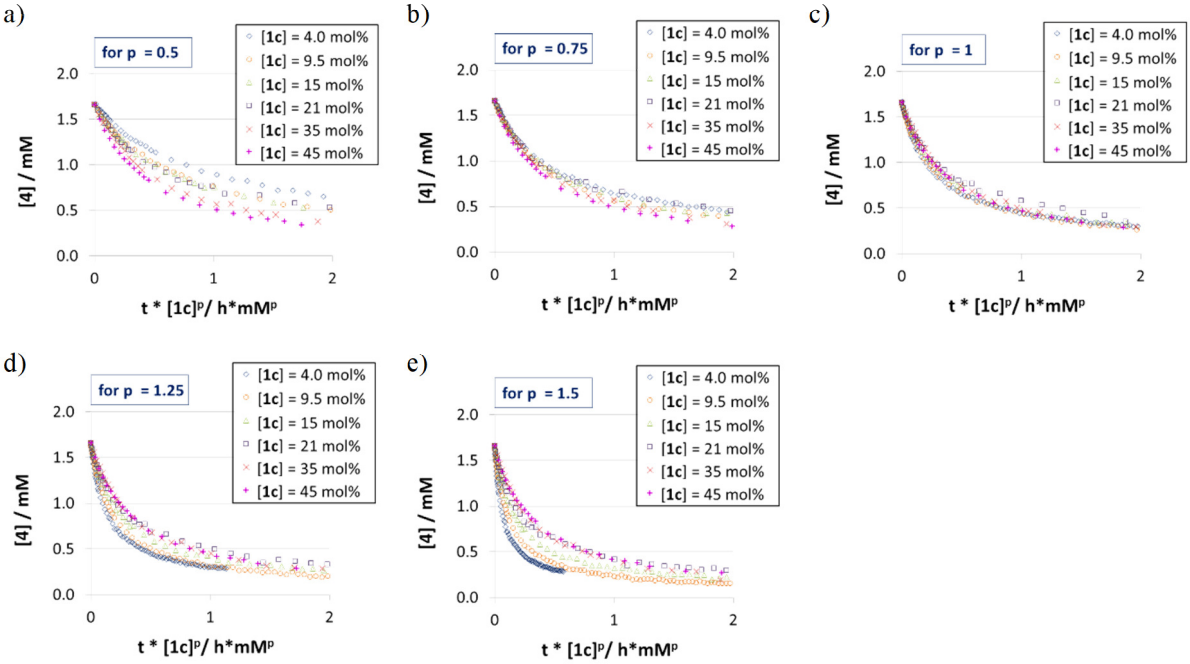

Figure S9: Determination of the order in catalyst **1c** by VTNA. a)-e) VTNA plots for different values of *p* (all at 1.66 mM quinoline **4** and 3.93 mM Hantzsch-ester **7**).

4.7.5. *Product inhibition based on VTNA*

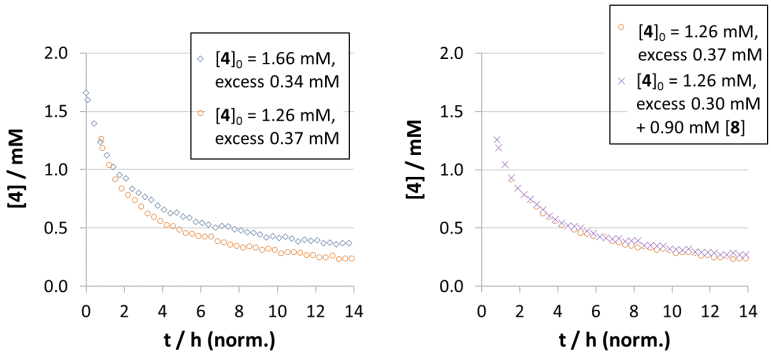

Figure S10: Investigation of product inhibition for catalyst **1c** by VTNA.

4.8. Results for macrocycle 2c

4.8.1. *Substrate orders based on VTNA*

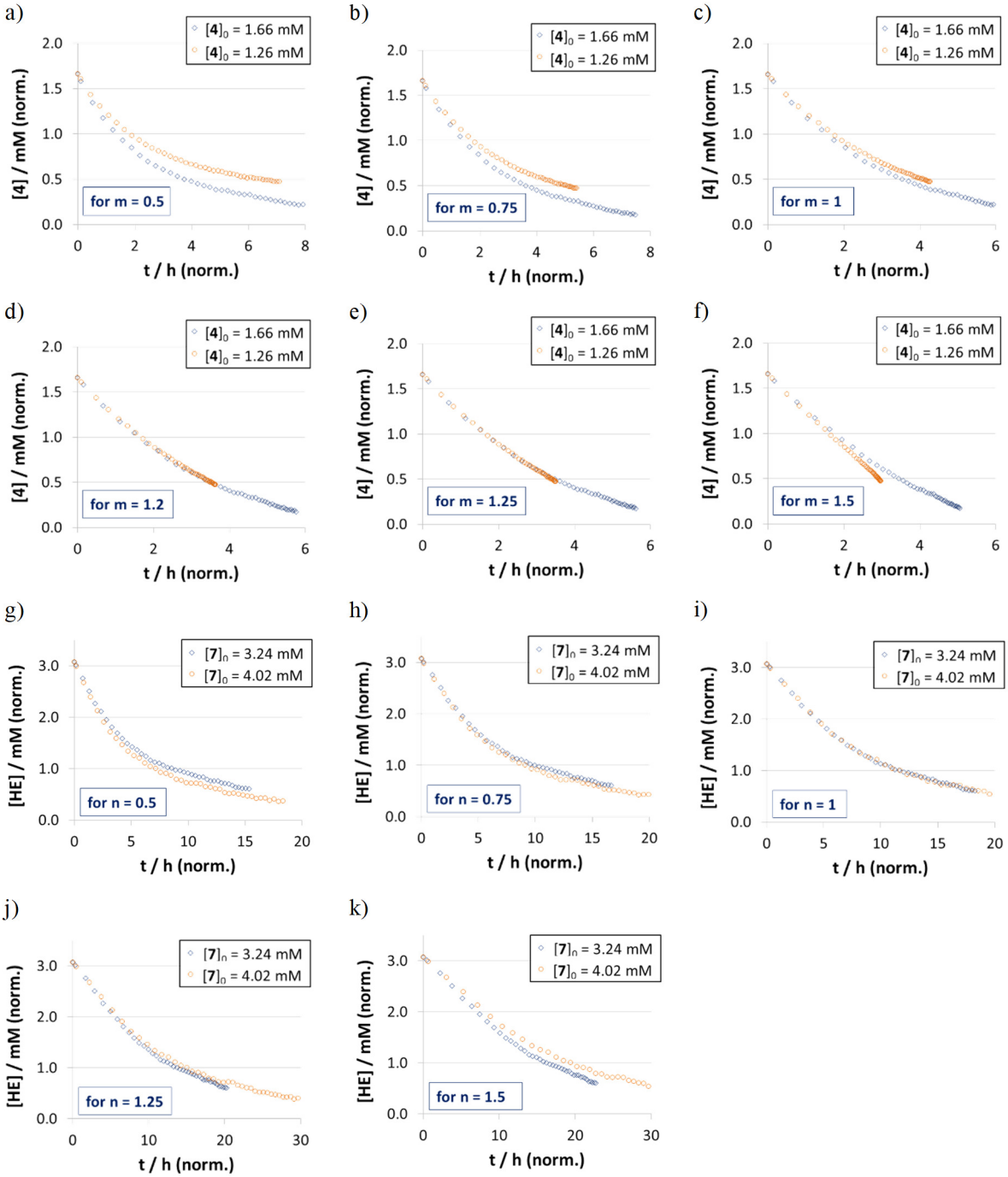

Figure S11: Different excess experiments for substrate order determination for macrocycle **2c** as determined by VTNA. a)-f) VTNA plots for quinoline **4** for different values of *m*, g-k) VTNA plots for for Hantzsch-Ester **7** for different values of *n*.

4.8.2. *Catalyst orders based on initial rate*

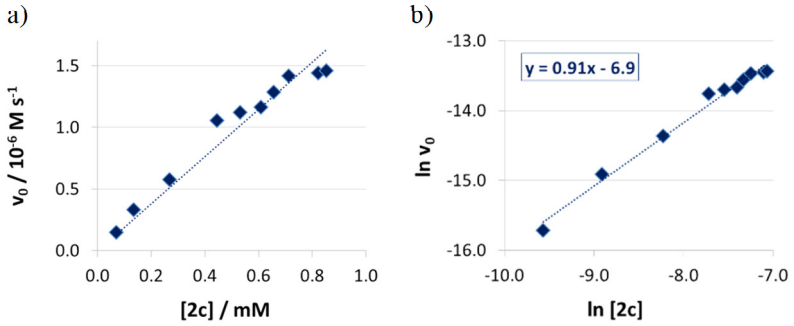

Figure S12: Influence of catalyst loading on reaction rates for catalyst **2c**. a) Initial rates at different catalyst loadings (all at 1.66 mM quinoline **4** and 3.93 mM Hantzsch-ester **7**), b) Determination of the order in catalyst order in the ln v_0 / ln [catalyst] plot (v_0 in M^{-1} s^{-1}, catalyst concentrations in M).

4.8.3. *Catalyst orders based on VTNA*

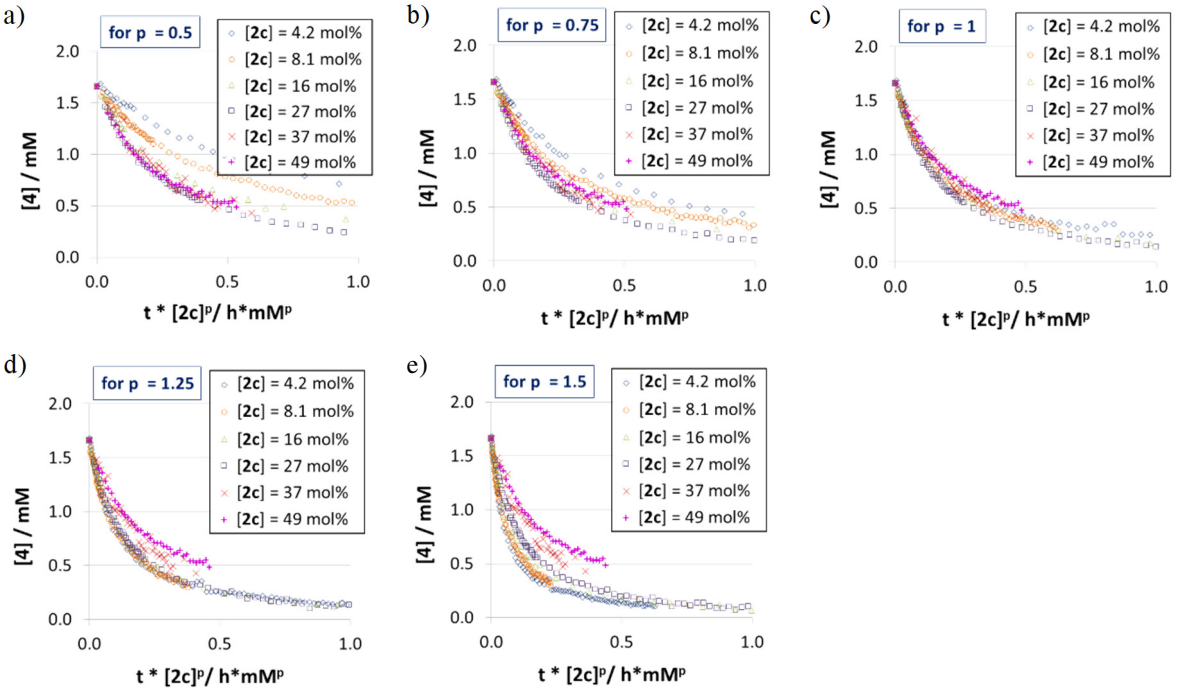

Figure S13: Determination of the order in catalyst **2c** by VTNA. a)-e) VTNA plots for different values of *p* (all at 1.66 mM quinoline **4** and 3.93 mM Hantzsch-ester **7**).

4.8.4. *Product inhibition based on VTNA*

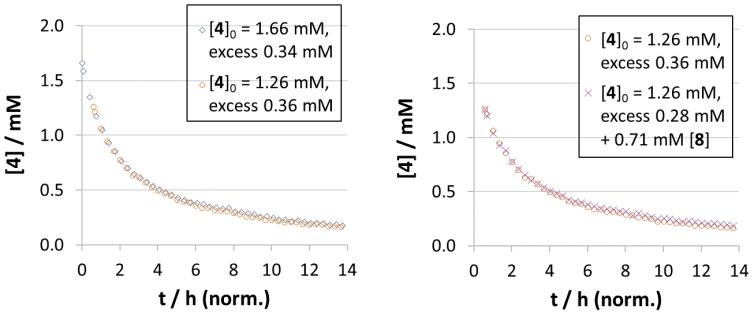

Figure S14: Investigation of product inhibition for the macrocyclic catalyst **2c** by VTNA.

4.9. Results for acyclic catalyst 3

4.9.1. *Substrate orders based on VTNA*

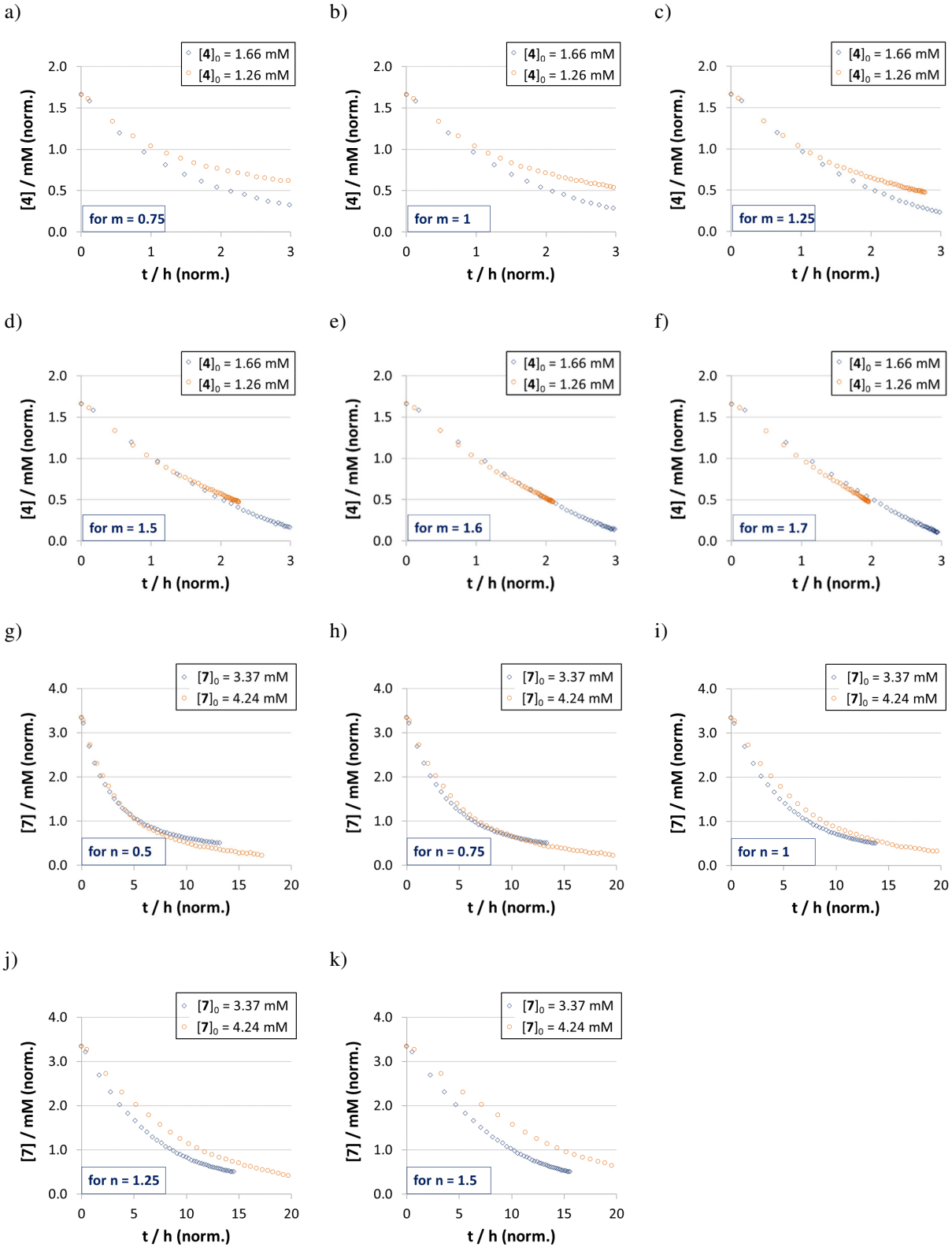

Figure S15: Different excess experiments for substrate order determination for **3** as determined by VTNA. a)-e) VTNA plots for quinoline **4** for different values of *m*, f-j) VTNA plots for for Hantzsch-Ester **7** for different values of *n*.

4.9.2. *Initial rate measurements*

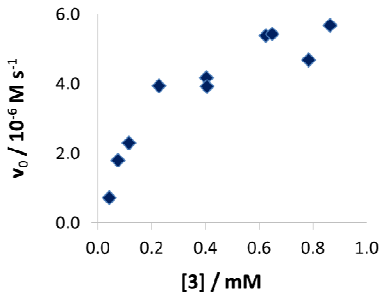

Figure S16: Influence of catalyst loading on reaction rates for catalyst **3**, depicted as initial rates at different catalyst loadings (all at 1.66 mM quinoline **4** and 3.93 mM Hantzsch-ester **7**).

Due to the nonlinear v_0 vs. [**3**] plot, the catalyst order could not be determined from the ln v_0 vs. ln [**3**] plot. Instead, the catalyst order was determined by VTNA (see below).

4.9.3. *Catalyst orders based on VTNA*

Due to the nonlinear dependence of reaction rates on the concentration of the acyclic catalyst **3**, the VTNA plots were generated independently for low catalyst loadings (<0.25 mM or 15 mol%) and high catalyst loadings (>0.6 mM or 35 mol%).

Low catalyst loadings:

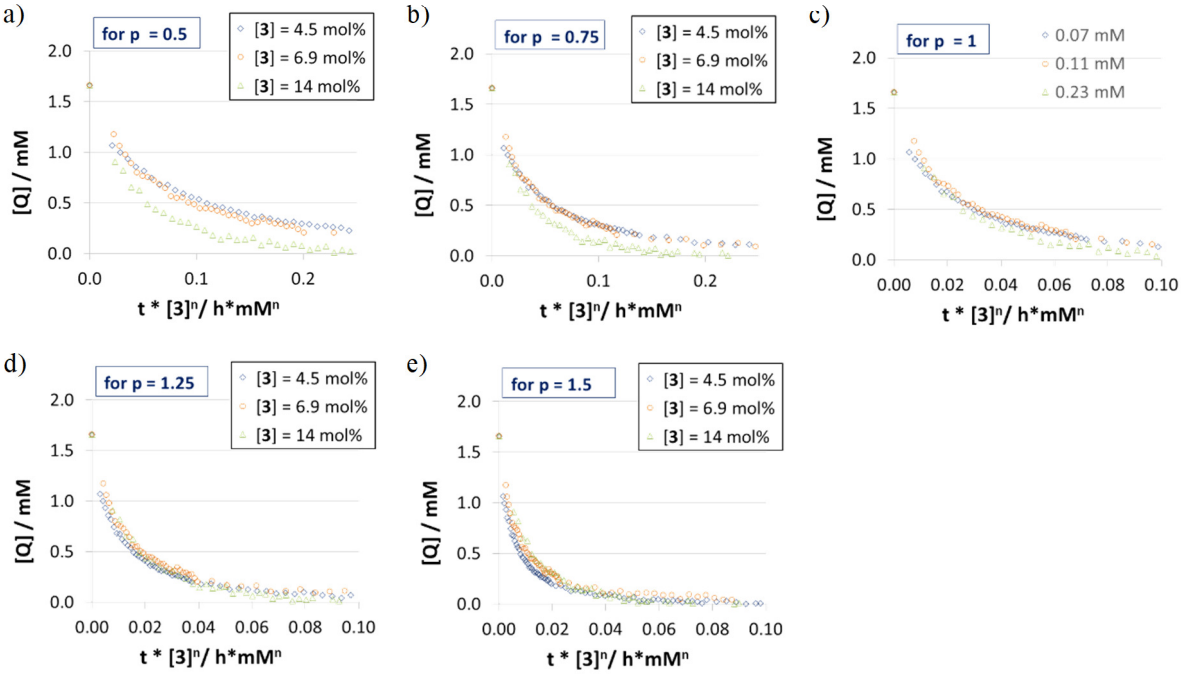

Figure S17: Determination of the order in catalyst **3** by VTNA for low catalyst loadings (<0.25 mM or 15 mol%). a)-e) VTNA plots for different values of *p* (all at 1.66 mM quinoline **4** and 3.93 mM Hantzsch-ester **7**).

High catalyst loadings:

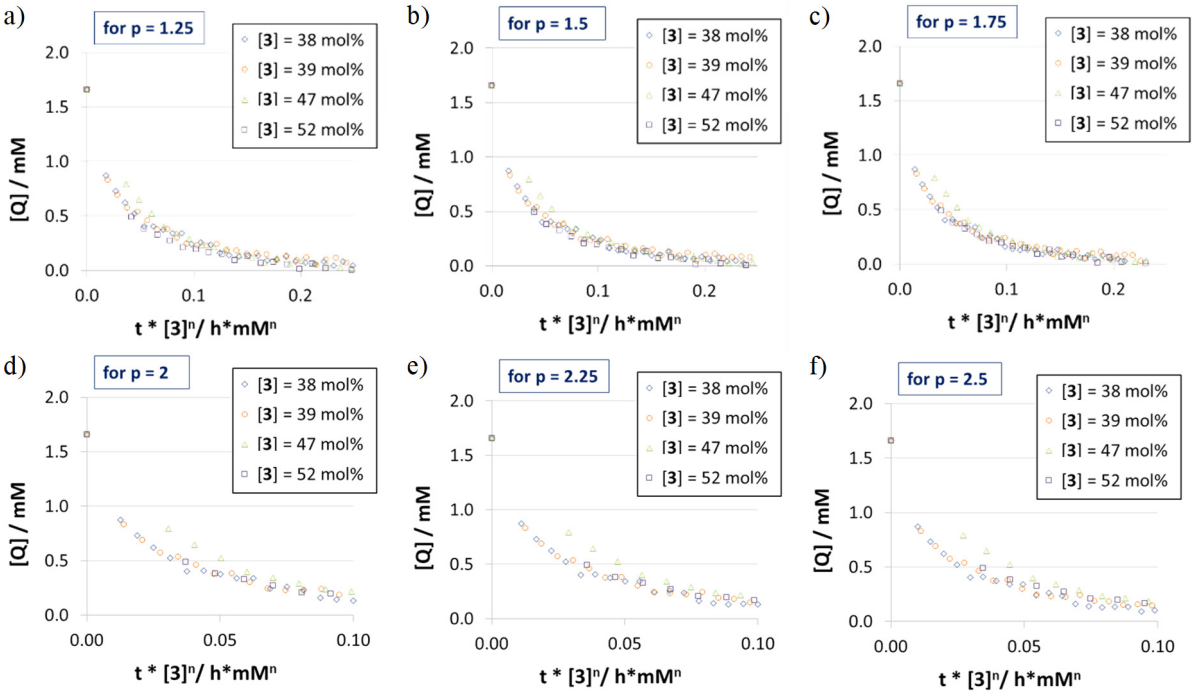

Figure S18: Determination of the order in catalyst **3** by VTNA for high catalyst loadings (>0.6 mM or 35 mol%). a)-f) VTNA plots for different values of *p* (all at 1.66 mM quinoline **4** and 3.93 mM Hantzsch-ester **7**).

4.9.4. *Product inhibition based on VTNA*

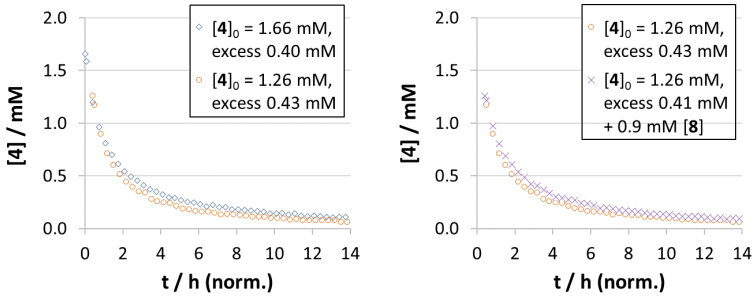

Figure S19: Investigation of product inhibition for the macrocyclic catalyst **3** by VTNA.

4.10. Normalized initial rates for catalysts 1c/2c/3

The normalized rates $v_{Norm} = v_0/[\mathbf{Cat}]$ (also see Table S5 - Table S7) are shown in Figure **S20**.

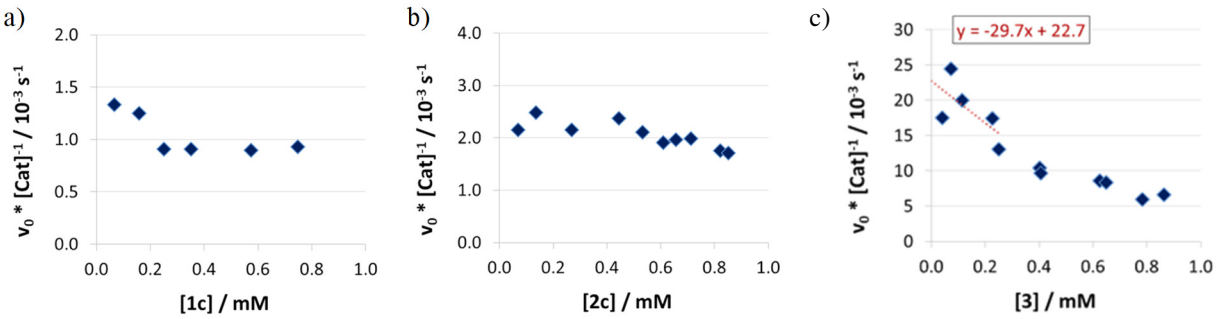

Figure S20: Reaction rates per catalyst (v_0/[Cat]) for catalysts **1c/2c/3**.

For catalysts **1c** and **2c**, the value for v_{Norm} is almost independent of the catalyst concentration. For catalyst **3**, the upper limit for v_{Norm} [i.e. $v_{norm}(\mathbf{3}_{Mono})$] was estimated by linear regression of the data points for [**3**] < 0.25 mM in the v_{Norm} vs. [**Cat**] plot (see Figure S20). The lower limit for v_{Norm} [i.e. $v_{norm}(\mathbf{3}_{Di})$] was estimated as the mean value for the two data points at highest concentration ([**3**] > 0.75 mM).

Table S8: Normalized initial rate constants for catalysts **1c/2c/3**.

Catalyst	$v_{Norm} = v_0$ / [Cat] (10^{-3} s^{-1})
1c	1.04[a]
2c	2.06[a]
$\mathbf{3}_{Di}$ (>0.6 mM)	<6.29[b]
$\mathbf{3}_{Mono}$ (<0.25 mM)	22.7[c]

[a] Mean value for all catalyst concentrations, [b] Mean value for catalyst concentrations >0.6 mM, [c] Determined as y-intercept in the k_{Obs} / [Cat] plot for concentrations <0.25 mM

5. Detailed analysis for the acyclic phosphoric acid 3

5.1. Dependence of stereoselectivity on catalyst concentration

According to the general protocol for catalytic reaction (see section 3), the reduction of quinoline **4** was performed with varying concentration of catalyst 3. In addition, the overall concentration was varied (initial quinoline concentration of 1.66 mM and 5 mM, respectively). The resulting stereoselectivities were determined by chiral HPLC (see Table S10).

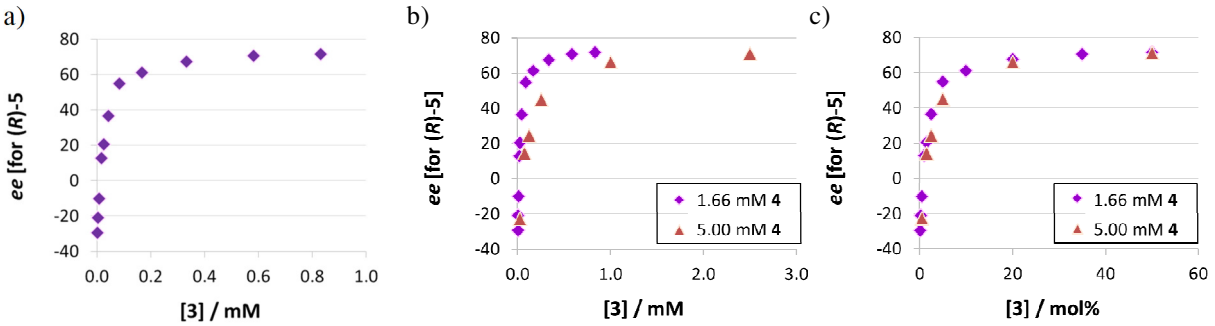

Figure S21: Influence of catalysts loading on enantioselectivities for catalyst **3** (given as enantiomeric excess for (*R*)-**6**). a) For 1.66 mM quinoline concentration. b)/c) Comparison of enantiomeric excesses for 1.66 mM and 5.0 mM quinoline concentration, plotted vs. concentration of **3** or loading of **3**, respectively.

5.2. Fitting of rate

Based on the initial rates (see Table S8) for the monomeric and the dimeric catalyst, the total rate data for different concentrations of **3** (see Figure S16) was fitted as follows:

$v_{max}(\mathbf{3}_{Mono})$	$= v_{Norm}(\mathbf{3}_{Mono}) * [\mathbf{3}_{Mono}]$
with	$v_{Norm}(\mathbf{3}_{Mono}) = 26.3 * 10^{-3}\ s^{-1}$
$v_{max}(\mathbf{3}_{Di})$	$= v_{Norm}(\mathbf{3}_{Di}) * [\mathbf{3}_{Di}]$
with	$v_{Norm}(\mathbf{3}_{Di}) = 6.29 * 10^{-3}\ s^{-1}$
v_0	$= v_0(\mathbf{3}_{Mono}) + v_0(\mathbf{3}_{Di})$
with	$v_0(\mathbf{3}_{Mono}) = v_{max}(\mathbf{3}_{Mono}) * x_{Mono}$
with	$v_0(\mathbf{3}_{Di}) = v_{max}(\mathbf{3}_{Di}) * x_{Di}$
v_0	$= v_{max}(\mathbf{3}_{Mono}) * x_{Mono} + v_{max}(\mathbf{3}_{Di}) * x_{Di}$
$v_0 / v_{max}(\mathbf{3}_{Mono})$	$= x_{Mono} + (v_{max}(\mathbf{3}_{Di})/v_{max}(\mathbf{3}_{Mono})) * x_{Di}$
with	$v_{max}(\mathbf{3}_{Di})/v_{max}(\mathbf{3}_{Mono}) =$ $v_{Norm}(\mathbf{3}_{Di})/ v_{Norm}(\mathbf{3}_{Mono}) = 6.29/26.3 = 0.239$
with	$x_{Di} = 1 - x_{Mono}$

$v_0 / v_{max}(\mathbf{3}_{Mono})$	$= x_{Mono} + 0.239*(1 - x_{Mono})$
$v_0 / v_{max}(\mathbf{3}_{Mono})$	$= x_{Mono} + 0.239 - 0.239*x_{Mono}$
$v_0 / v_{max}(\mathbf{3}_{Mono})$	$= 0.761*x_{Mono} + 0.239$
x_{Mono}	$= ((v_0 / v_{max}(\mathbf{3}_{Mono}))-0.239)/0.761$

Table S 9: Experimental data and results for rate fitting using different concentrations of acyclic catalyst **3**.

Experimental setup					Results					
	Concentrations				Calculated		Fitted			
Exp.-No.	[**4**][a] (mM)	[**7**][b] (mM)	[**Cat**][b] (mM)	[**Cat**][b] (mol%)	$v_{max}(\mathbf{3}_{Mono})$ ($M\,s^{-1}$)	$v_{max}(\mathbf{3}_{Di})$ ($M\,s^{-1}$)	x_{Mono}	x_{Di}	$v_0(\mathbf{3}_{Mono})$ ($M\,s^{-1}$)	$v_0(\mathbf{3}_{Di})$ ($M\,s^{-1}$)
1	1.66	4.03	0.074	4.44	1.94E-06	4.64E-07	0.91	0.09	1.76E-06	4.32E-08
2	1.66	3.83	0.115	6.91	3.02E-06	7.21E-07	0.69	0.31	2.07E-06	2.27E-07
3	1.66	4.11	0.227	13.65	5.96E-06	1.42E-06	0.56	0.44	3.32E-06	6.32E-07
4	1.66	4.05	0.402	24.23	1.06E-05	2.53E-06	0.20	0.80	2.16E-06	2.01E-06
5	1.66	4.27	0.625	37.66	1.64E-05	3.93E-06	0.12	0.88	1.91E-06	3.47E-06
6	1.66	3.97	0.649	39.10	1.71E-05	4.08E-06	0.10	0.90	1.77E-06	3.66E-06
7	1.66	3.93	0.863	51.97	2.27E-05	5.42E-06	0.01	0.99	3.32E-07	5.34E-06

a) Determined by weight of **4** and the volume of solvent. b) Determined by the relative integrals of **4** and **7**/**8**/**Cat**.

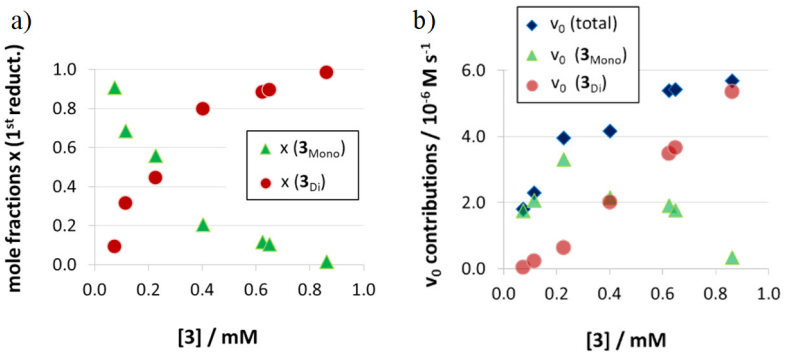

Figure S22: Mole fractions (a) and v_0 contributions (b) for the monomeric and dimeric pathway for different concentrations of catalyst **3** for the first reduction step [$x(\mathbf{3}_{Mono})$: mole fraction of monomeric catalyst, $x(\mathbf{3}_{Di})$: mole fraction of phosphoric acid **3** bound in dimeric catalyst].

5.3. Fitting of stereoselectivity data

For the fitting of the stereoselectivity data for different concentrations of **3**, the following input values were used:

- The relative rates of dimeric and monomeric pathway were calculated based on the DFT-results.[2] Based on an energy difference of 1.7 kcal, the rate difference was calculated as f = k_{Di} / k_{Mono} = 17.7.
- The enantiomeric excesses for the purely monomeric and purely dimeric pathways were estimated based on the measured *ee*-curve (see Figure S21a). Thus, we estimated the stereoselectivity of the dimeric pathway as ee_{Di} = 75% and the stereoselectivity of the monomeric pathway as ee_{Mono} = -35%.

Based on these input values, the mole fractions and relative *ee*-contributions were calculated as follows:

ee_{Tot} =	(*ee*_contr. ($\mathbf{3}_{Mono}$) + *ee*_contr. ($\mathbf{3}_{Di}$))/(x_{Mono} * k_{Mono} + x_{Di} * k_{Di})
with *ee*_contr. ($\mathbf{3}_{Mono}$) =	x_{Mono} * k_{Mono} *ee_{Mono}
with *ee*_contr. ($\mathbf{3}_{Di}$) =	x_{Di} * k_{Di} * ee_{Di}
with x_{Di} =	1 - x_{Mono}
with k_{Di} =	f*k_{Mono}
with ee_{Rel_mono} =	ee_{Mono} / ee_{tot}
with ee_{Rel_Di} =	ee_{Di} / ee_{tot}
with f =	k_{Di} / k_{Mono} = 17.7 (based on DFT)
ee_{Tot} =	(x_{Mono} * k_{Mono} *ee_{Mono} + x_{Di} * k_{Di} * ee_{Di})/(x_{Mono} * k_{Mono} + x_{Di} * k_{Di})
1 =	(x_{Mono} * k_{Mono} *ee_{rel_mono} + X_{Di} * k_{Di} * ee_{rel_Di})/(x_{Mono} * k_{Mono} + x_{Di} * k_{Di})
1 =	(x_{Mono} * k_{Mono} *ee_{rel_mono} + (1 - x_{Mono}) * f * k_{Mono} * ee_{rel_Di})/ (x_{Mono} * k_{Mono} + (1 - x_{Mono} * f * k_{Mono})
1 =	(x_{Mono}*ee_{rel_mono} + (1 - x_{Mono}) * f * ee_{rel_Di})/(x_{Mono} + (1 - x_{Mono}) * f)
x_{Mono} + (1 - x_{Mono}) * f =	x_{Mono}*ee_{rel_mono} + (1 - x_{Mono}) * f * ee_{rel_Di}
x_{Mono} * (1 - f) + f =	(x_{Mono} * (ee_{Rel_Mono} - f * ee_{Rel_Di}) + f * ee_{Rel_Di}
x_{Mono} * (1 - f) - x_{Mono}* (ee_{Rel_mono} - f * ee_{Rel_Di}) =	f * ee_{Rel_Di} - f
x_{Mono} (1 - f - ee_{Rel_mono} + f * ee_{Rel_Dit}) =	f * ee_{Rel_Di} - f
x_{Mono} =	(f * ee_{Rel_Di} - f) / (1 - f - ee_{Rel_Mono} + f * ee_{Rel_Di})

Table S10: Experimental data and results for fitting of stereoselectivity data using different concentrations of acyclic catalyst **3** (for the stereoselectivity data also see table S1).

Experimental setup						Results						
		Concentrations				*ee*	Calculated		Fitted			
Exp.-No.	Exp.-Type	[**4**][a] (mM)	[**7**][a] (mM)	[**3**][a] (mM)	[**3**][a] (mol%)	*ee*[b] (%)	*ee* / *ee* (**3**$_{Mono}$) (%)	*ee* / *ee* (**3**$_{Di}$) (%)	x_{Mono}	x_{Di}	*ee*_contr. (**3**$_{Mono}$) (%)	*ee*_contr. (**3**$_{Di}$) (%)
1	Different excess for [**3**] at 1.66 mM quinoline	1.66	3.93	0.0002	0.01	-[c]	-[c]	-[c]	-[c]	-[c]	-[c]	-[c]
2		1.66	3.93	0.0017	0.10	-29.5	1.19	-2.55	1.00	0.00	-33.2	3.8
3		1.66	3.93	0.0042	0.25	-20.9	1.67	-3.58	0.99	0.01	-30.5	9.6
4		1.66	3.93	0.0083	0.50	-10.1	3.47	-7.43	0.98	0.02	-27.1	17.0
5		1.66	3.93	0.0166	1.00	12.8	-2.72	5.84	0.96	0.04	-19.8	32.6
6		1.66	3.93	0.0249	1.50	20.4	-1.71	3.67	0.95	0.05	-17.4	37.8
7		1.66	3.93	0.0415	2.50	36.5	-0.96	2.05	0.90	0.10	-12.2	48.8
8		1.66	3.93	0.0830	5.00	54.7	-0.64	1.37	0.80	0.20	-6.5	61.2
9		1.66	3.93	0.1660	10.00	61.2	-0.57	1.23	0.72	0.28	-4.4	65.6
10		1.66	3.93	0.3320	20.00	67.5	-0.52	1.11	0.57	0.43	-2.4	69.9
12		1.66	3.93	0.5810	35.00	70.6	-0.50	1.06	0.43	0.57	-1.4	72.0
13		1.66	3.93	0.8300	50.00	71.6	-0.49	1.05	0.36	0.64	-1.1	72.7
12	Different excess for [**3**] at 5.0 mM quinoline	1.66	3.93	0.0250	0.50	-22.7	1.54	-3.30	0.99	0.01	-31.1	8.4
13		1.66	3.93	0.0750	1.50	14.3	-2.45	5.24	0.96	0.04	-19.3	33.6
14		1.66	3.93	0.1250	2.50	24.5	-1.43	3.06	0.94	0.06	-16.1	40.6
15		1.66	3.93	0.2500	5.00	45.0	-0.78	1.67	0.87	0.13	-9.6	54.5
16		1.66	3.93	1.0000	20.00	66.1	-0.53	1.14	0.61	0.39	-2.8	68.9
17		1.66	3.93	2.5000	50.00	71.1	-0.49	1.05	0.39	0.61	-1.2	72.3

a) Determined by weight of **4**/**7**/**3** and the volume of solvent. b) Determined by chiral HPLC. Enantiomeric excesses given for the (*R*)-product isomer. [c] No conversion observed.

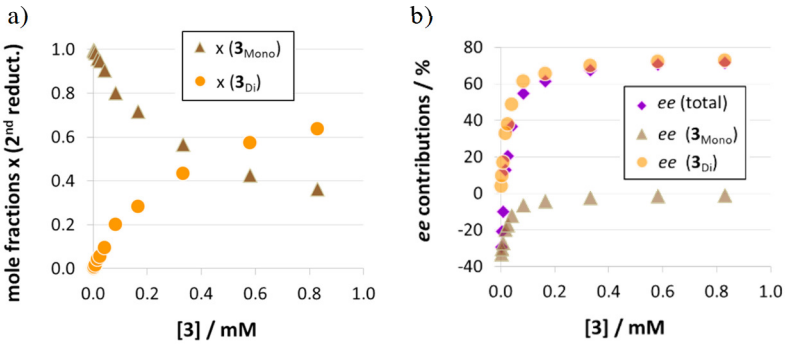

Figure S23: Mole fractions and *ee* contributions for the monomeric and dimeric pathway for different concentrations of catalyst **3** for the second reduction step [x(**3**$_{Mono}$): mole fraction of monomeric catalyst, x(**3**$_{Di}$): mole fraction of phosphoric acid **3** bound in dimeric catalyst].

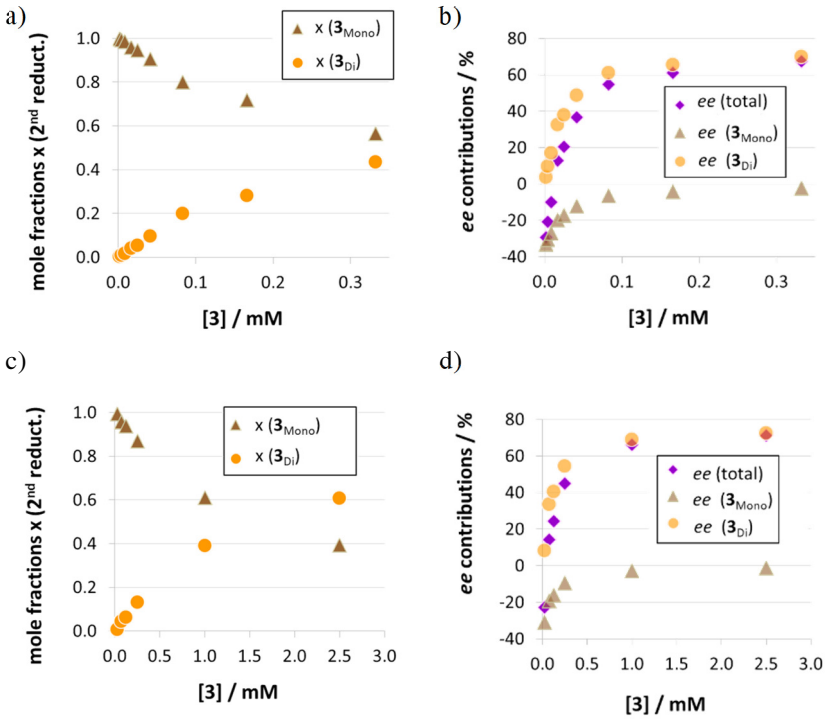

Figure S24: Mole fractions and *ee* contributions for the monomeric and dimeric pathway for different concentrations of catalyst **3** for the second reduction step, using different total concentrations. a)/b) For 1.66 mM quinoline **4**, c/d) for 5.0 mM quinoline **4** [x($\mathbf{3}_{Mono}$): mole fraction of monomeric catalyst, x($\mathbf{3}_{Di}$): mole fraction of phosphoric acid **3** bound in dimeric catalyst].

5.4. Evolution of enantiomeric excess over the course of the reaction

Table S11: Conversion vs. time and enantiomeric excess vs. time data for the catalytic reaction using 1 mol% **3** (1.6 mM **4** in toluene).

Entry	Time [h]	Conversion [%]	Enantiomeric excess[(b)] [%]
1	0.5	15.5	9.3
2	1	23.7	8.6
3	2	41.9	8.8
4	3	50.6	9.0
5	4	57.3	9.0
6	5	64.1	8.3
7	6	69.1	8.2
8	7	73.8	8.8
9	24	94.9	8.1

(a) Determined by chiral HPLC, approximated by using identical extinction coefficients for starting materials **4** and product **6**. (b) Determined by chiral HPLC (Chiralcel OD-H column). All values are given for the excess of (*R*)-enantiomer.

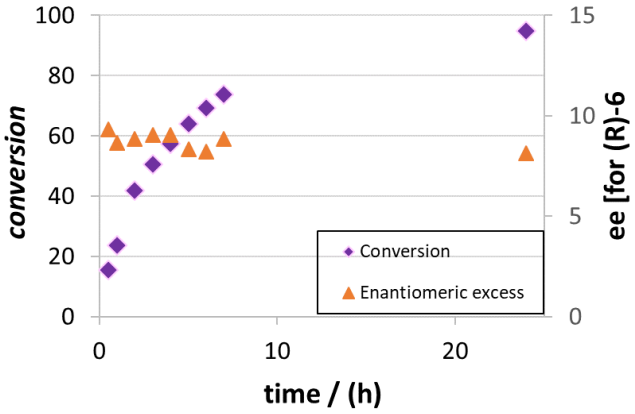

Figure S 25: Influence of conversion on enantioselectivities for catalyst **3** for reaction in toluene (givesn as enantiomeric excess for (*R*)-**6**).

6. NMR-investigation of catalyst-substrate complexes

6.1. General information

6.1.1. Sample preparation

Samples in CD_2Cl_2: The acyclic chiral phosphoric acid catalyst **3** was weighed into a 5 mm NMR tube and dried at 150 °C for at least 30 min under reduced pressure. After the tube came to room temperature, quinolines **4b-d** were weighed directly into the NMR tube. The tube was evacuated and flushed with Argon three times. Freshly distilled CD_2Cl_2 (0.6 mL) was added under Argon flow and TMS atmosphere (0.5 mL) was added. The tube was closed and sealed with parafilm. The samples were stored in the fridge at -80°C.

Samples in freonic mixtures: Acyclic chiral phosphoric acid catalyst **3** was weighed into a 5 mm heavy wall J-Young valve NMR tube and dried under reduced pressure at 150 °C and 30 min. After the tube came to room temperature, quinoline **4b** was weighed directly into the NMR tube. The tube was evacuated and flushed with Argon three times. The sample was connected to a vaccuumline and the NMR tube was frozen in a Dewar filled with liquid nitrogen and a freonic mixture was condensed through a column filled with P_2O_5 and KOH into the NMR tube. The overall concentration was judged by the filling level freonic solution at r.t. (14 cm ~ 512 µL). The samples in the freonic mixtures were stored at ~ 4°C between the measurements.

6.1.2. NMR pulse program parameters

Standard pulse sequences from the Bruker pulse sequence catalogue (zg, zg30, etc.) with the following parameters have been used.

^{1}H-NMR: Pulse program zg30, Relaxation delay = 2.00 s, Acquisition time = 2.54 s, SW = 22 ppm, TD = 66 K, ns = 1 – 256; ^{13}C NMR: Pulse program: zgpg30, Relaxation delay = 2.00 s, Acquisition time = 0.80 s, TD = 66 K; SW = 270.0 ppm, TD = 64k, NS = 1k – 2k; ^{19}F-NMR: Pulse program: zg30; Relaxation delay = 2.00 s, Acquisition time = 5.79 s, SW = 20.0 ppm, TD = 131k, NS = 64; ^{31}P-NMR: Pulse program: zgpg30; Relaxation delay = 1.00 s, Acquisition time = 2.25 s, SW = 40-60.0 ppm, TD = 65k, NS = 64 - 512; 2D-^{1}H,^{1}H NOESY: Pulse program: noesygpph; Relaxation delay = 5.00 s, NS = 8-16, mixing time (D8) = 300.00 ms; TD = 4096; increments = 256 - 1k; 2D-^{1}H,^{1}H COSY: Pulse program: cosygpqf; Relaxation delay = 5.00 s, NS = 4-16, TD = 4096; increments = 512; 2D-^{1}H,^{13}C HSQC: Pulse program: hsqcedetgpsisp2.3; Relaxation delay = 6 s, NS = 8-16, $^1J_{XH}$ = 145 Hz; TD = 4096; increments = 512; 2D-^{1}H,^{13}C HMBC: Pulse program: hmbcgplpndqf; Relaxation delay = 4.00 s, NS = 8-16, $^1J_{XH}$ = 145 Hz, J_{XH}(long range) = 10 Hz; TD = 4096; increments = 512 - 1k; 2D-^{1}H,^{31}P HMBC: Pulse program: inv4gplrndqf; Relaxation delay = 6.00 s, NS = 4-16, TD = 4096; increments = 256 - 512; ^{1}H DOSY: Pulse program: see at respective chapter, Relaxation delay = 2.00 s – 6.00 s,

NS = 64-512, TD = 58 K, increments = 20, Diffusion time delay = 45.0 ms, gradient strength 5-95% linear, gradient pulse: 0.6 – 2.0 ms.

6.2 Temperature screening

By lowering the temperature, exchange process within the system and the hydrogen bonds could be slowed and sharper line widths and a better signal dispersion was obtained. For samples with a 1:1 stoichiometry of CPA and quinoline, 180 K proved to be the optimum temperature for measurements, as it provided best line widths and signal dispersion. For samples with a 2:1 stoichiometry of CPA and quinoline (see Figure S26 for **3/4b)** 180 - 200 K was found as the optimum temperature range. For **4b**, measurements (especially determination of the integrals) were done at 200 K due to the optimum line separation of the two signals at 16.75 and 16.51 ppm. For quinolines **4c** and **4d**, 180 K was selected as measurement temperature.

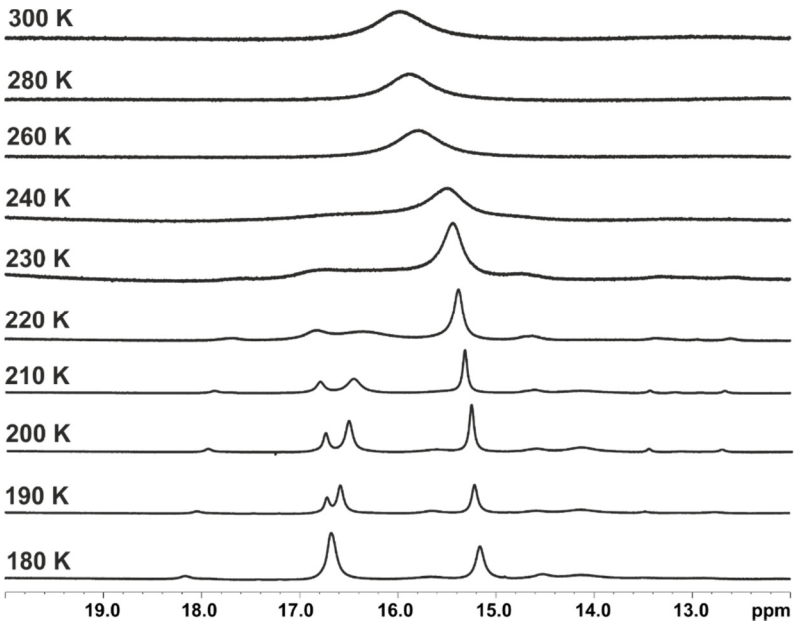

Figure S26: Excerpts of the hydrogen bond region at 600 MHz in CD_2Cl_2 at variable temperatures of a sample containing **3** and **9a** at a 2:1 stoichiometry at a catalyst concentration of 50 mM. Different scaling factors were applied to better visualize the line broadening for increased temperatures, but the spectra were recorded with identical parameters, e.g. identical number of scans (64).

6.3 Solvent screening

Deuterated toluene, chlorobenzene, dichloromethane and freonic mixture of $CDCl_2F$ and $CDClF_2$ were tested as solvents to investigate binary CPA•quinoline complexes. Toluene provided poor solubility of the catalyst at low temperatures (see Figure S27B). Chlorobenzene was not applicable due to its higher freezing point (≈ -45 °C), because at that temperature the exchange processes were not sufficiently slowed down to detect hydrogen bond signals with adequate line widths (see Figure S27C). In freonic mixture, the catalyst **3** was insoluble. Hence, CD_2Cl_2 was selected as solvent as it provided good solubility, gave narrow line widths and a good signal dispersion at 180 K.

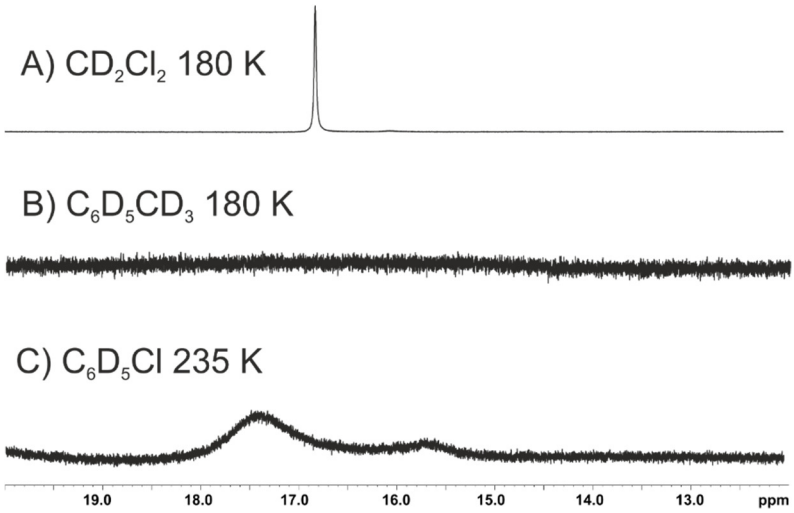

Figure S27: Excerpt of the spectra of **3**:**9a** at a 1:1 stoichiometry and a concentration of 10 mM in A) CD_2Cl_2 at 180 K, B) in deuterated toluene at 180 K and C) in C_6D_5Cl at 235 K. Only the hydrogen bond region (12-20 ppm) is showed. Different scaling factors were applied, but the spectra were measured with identical parameters, e.g. identical number of scans (64).

In the previous work, the transfer hydrogenation of **4a** with catalyst **3** in CH_2Cl_2 gave a significantly different *ee* value than in toluene[2], which can indicate a limited comparability of the NMR-structure investigations in CD_2Cl_2 compared to the reaction analysis in toluene. However, theoretical calculations showed, that in dichloromethane analogous species should be populated as in toluene (see chapter 7).

In order to obtain experimental proof that catalyst aggregation also influences the catalytic behaviour in dichloromethane-solution, we have performed the catalytic reaction in dichloromethane with catalyst loadings ranging from 1 mol% to 50 mol%. Indeed, we found that the stereoselectivity continually changes from -33% to -6% (expressed for (*R*)6, see Table S12 and Figure S 28).

Table S12: Reaction conditions for the transfer hydrogenation of 2-phenylquinoline catalysed by acyclic phosphoric acid (*S*)-**3** in dichloromethane**.**

Entry	Catalyst	Cat. loading [mol%][(a)]	Quinoline conc [mM]	Enantiomeric excess[(b)] [%]
1	(*S*)-**3**	1	1.66	-33.3
2	(*S*)-**3**	2.5	1.66	-30.3
3	(*S*)-**3**	5	1.66	-29.1
4	(*S*)-**3**	10	1.66	-23.6
5	(*S*)-**3**	20	1.66	-17.7
6	(*S*)-**3**	35	1.66	-5.3
7	(*S*)-**3**	50	1.66	-6.0

(a) Catalyst loading relative to quinoline. (b) Determined by chiral HPLC (Chiralcel OD-H column). All values are given for the excess of (*R*)-enantiomer.

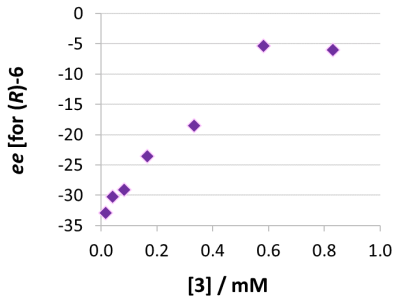

Figure S 28: Influence of catalysts loading on enantioselectivities for catalyst **3** for reaction in dichloromethane (given as enantiomeric excess for (*R*)-**6**).

6.4 Chemical shift assignments

^{1}H (black), ^{13}C (blue) and ^{31}P (green) chemical shifts of the **3•4b** complex at a 1:1 stoichiometry were assigned with standard 2D NMR experiments (^{1}H,^{1}H COSY, ^{1}H,^{1}H NOESY, ^{1}H,^{13}C HSQC, ^{1}H,^{13}C HMBC and ^{1}H,^{31}P HMBC) at 180 K. Some ^{13}C chemical shifts could not be assigned.

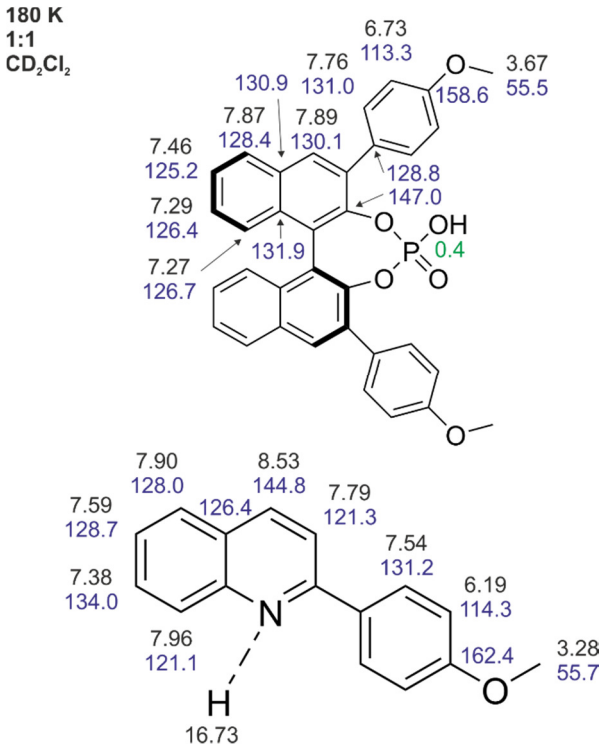

Figure S29: Chemical shift assignment of the binary **3•9a** complex at a 1:1 stoichiometry in CD_2Cl_2.

6.5 Hydrogen bond investigation

The presence of the hydrogen bond was shown by the detection of magnetization transfer between the proton in the hydrogen bond and the phosphorus atom of **3** (see Figure S30, red, $^{1}H,^{31}P$ HMBC) and one proton of **4b** (see Figure S30, blue, $^{1}H,^{1}H$ COSY). The detection of magnetization transfer between the hydrogen bonded proton and both CPA and substrate was also shown in the previous investigations in CPA•imine systems.[9a,9b]

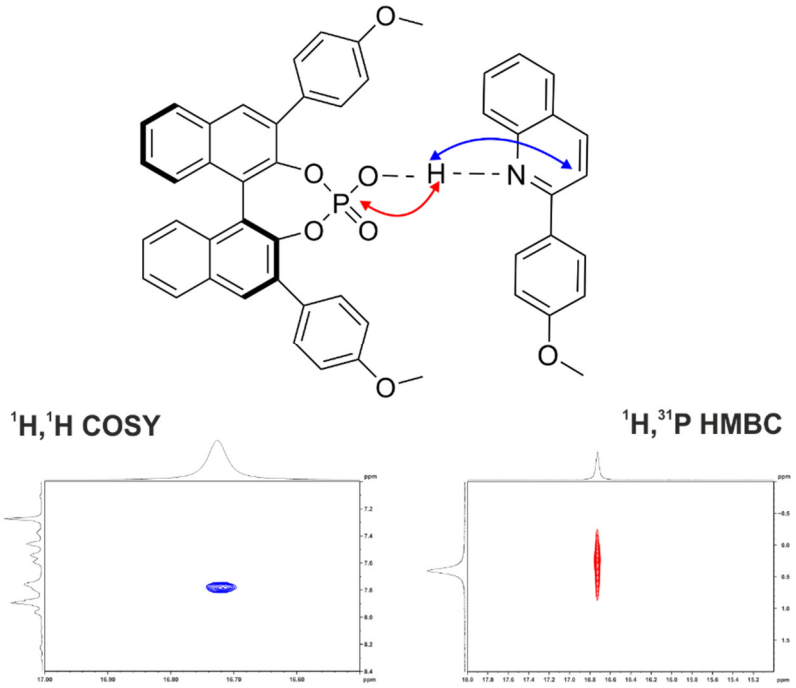

Figure S30: Excerpts of the $^{1}H,^{1}H$ COSY and $^{1}H,^{31}P$ HMBC spectra of **3**:**4a** at a 1:1 stoichiometry and a concentration of 50 mM in CD_2Cl_2 at 600 MHz. The detection of magnetization transfer between the hydrogen bonded proton and the quinoline (left, blue) and the phosphorus atom of **3** (right, red) proves the presence of a hydrogen bond.

In agreement with the previous NMR investigations on CPA•imine complexes,[9] more basic quinolines (pK_b: **4b** > **4c** > **4d**) feature weaker hydrogen bond protons (lower chemical shift of the H-bond proton) due to a stronger proton transfer onto the quinoline (stronger ion pair character). This trend is observed for the proton in the $PO^{-}\cdots H\cdot N^{+}$ hydrogen bond in the binary **3**•Qu complex at a 1:1 and 2:1 stoichiometry (Figure S31, green proton), as well as for the $PO^{-}\cdots H\cdot N^{+}$ hydrogen bond in the **3**•**3**•Qu complex (Figure S31, blue proton). For the $PO^{-}\cdots H\cdot OP$ hydrogen bond in the **3**•**3**•Qu complex (Figure S31, red proton), this trend is not observed because that hydrogen bond is not directly affected by the quinoline substituent.

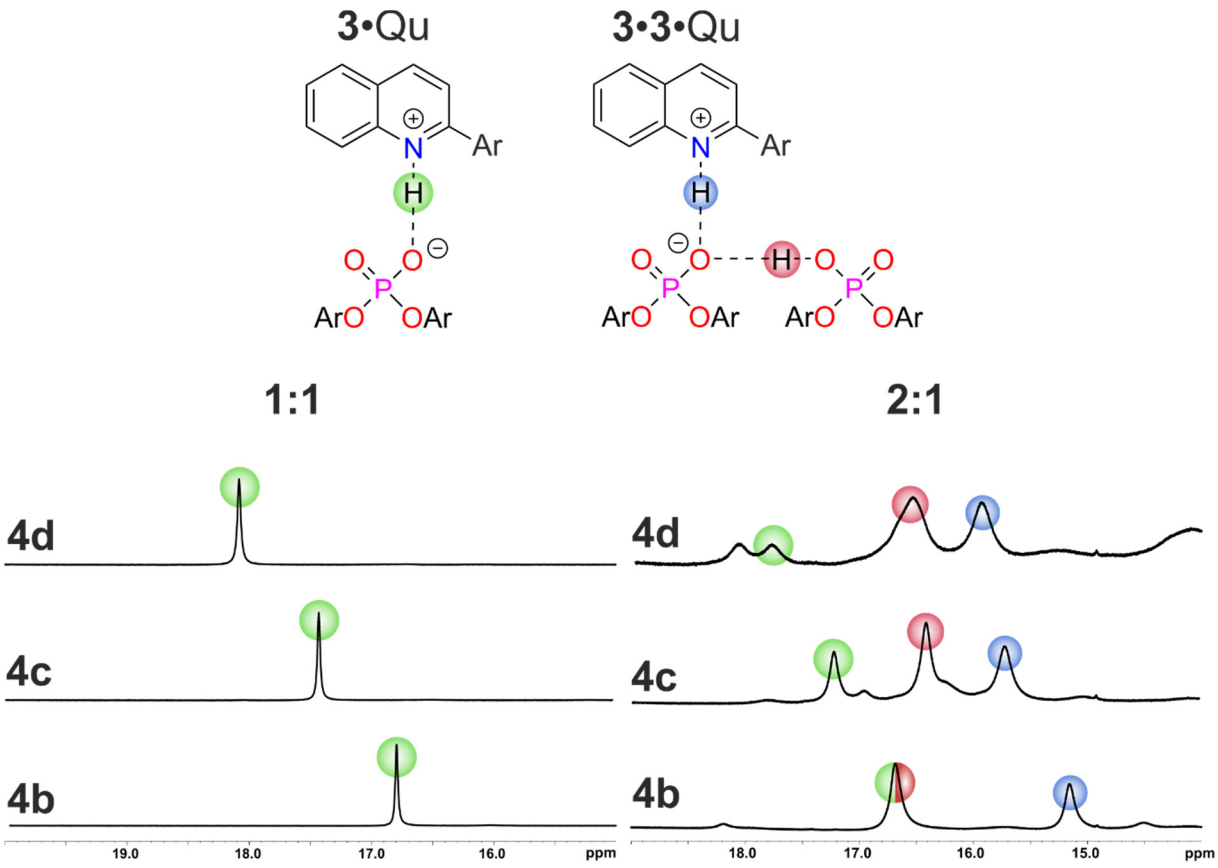

Figure S31: Excerpts of the ^{1}H spectra of **3** and **4b-d** at a 1:1 (left) or 2:1 (right) stoichiometry at 600 MHz and 180 K in CD_2Cl_2. Modulation of the basicity of the quinoline gives stronger hydrogen bonds (higher chemical shifts) for less basic quinolines, demonstrating a hydrogen bond assisted ion pair nature of the complexes.

6.6 Structural investigations of 3•4b

Based on the chemical shift assignment, a NOESY analysis was performed to reveal the structure of binary **3•4b** complex. NOE contacts of the MeO group of the catalyst (Figure S32, highlighted in orange) were detected to both sides of the quinoline (blue and red arrows). It should be noted, that in the previously computed structures[2] only one MeO group of the catalyst is in close contact to the quinoline. Hence, the detection of NOE contacts A and B, as well as C and D (Figure S32) reveals the presence of two different conformations of the binary **3•4b** complex which are in a fast exchange with each other and thus give only one set of signals. This observation is analogous to the previous studies on binary CPA•imine complexes, where also two fast exchanging conformers (Type I and Type II) were identified.[10]

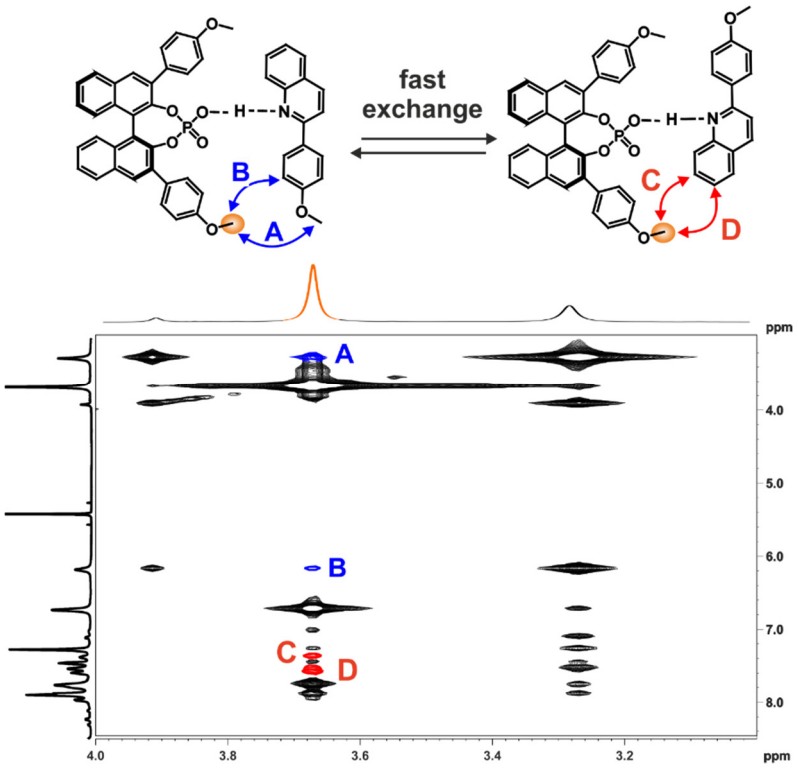

Figure S32: Identified structures and their respective characteristic NOE cross signals at 600 MHz and 180 K for a **3**:**4b** sample at a 1:1 stoichiometry and a concentration of 50 mM in CD_2Cl_2.

Both structures are on a fast exchange on the NMR time scale and thus give one averaged set of signals. In analogy with previous investigations in binary CPA•imine complexes,[10] only one set of signals for both naphthyl-fragments of the CPA BINOL-backbone was observed. This shows in combination with the strong binding of catalyst and substrate, that the exchange pathway between the two fast exchanging binary CPA•Qu structures features switching of the hydrogen bond donor oxygen atom, as well as a rotation of the quinoline (see Figure S32 for a more detailed explanation). The possible rotation of the substrate while bound to the catalyst reveals a bigger binding pocket of **3** compared to other catalysts typically used in synthesis.[11]

In summary, the NMR structural investigations for binary monomeric **3**•Qu complexes showed, that these systems are analogous in terms of structures, their dynamics and hydrogen bonding to binary monomeric CPA•imine complexes. Thus, at least in case of monomeric complexes the investigated system is a typical representative of catalyst•substrate complexes in CPA catalyzed transformations.

6.7 Diffusion Ordered Spectroscopy

The DOSY measurements were performed with the convection suppressing DSTE (double stimulated echo) pulse sequence developed by Jerschow and Müller in a pseudo 2D mode.[12] TMS was used to reference the viscosity of the solvent. The diffusion time delay was set to 45 ms. The gradient pulse lengths (p16, SMSQ10.100 smoothed square shape; 90% of rectangular gradient strength) were optimized for each species to give a sigmoidal signal decay for varying gradient strengths and range between 700 to 1500 µs at 300 K. For each species, twenty spectra with linear varying gradient strength of 5% - 95% of the maximum gradient strength (5.3400094 G/mm for rectangular gradient) have been measured. The used probe signals for the analysis are listed in the respective tables. The signal intensities of the respective groups were analyzed as a function of the gradient strength by Bruker TopSpin 3.2 software T1/T2 relaxation package by employing the Stejskal-Tanner equation.[13] No line broadening occurred for increasing gradient strength. The sigmoidal fit provided the translational self-diffusion coefficients D_i listed in the respective tables. The molecular radii were derived by the Stokes-Einstein equation[14] using Chens correction.[15]

$$D_i = \frac{k_B T}{6\pi\eta r_H} * (1 + 0.695 * \left(\frac{r_{solv}}{r_H}\right)^{2.234}$$

D_i is the self-diffusion coefficient derived by the measurement, η is the viscosity of the solvent, r_H is the hydrodynamic radius of the observed molecule and r_{solv} the radius of the solvent. No form factor correction was applied. The viscosity was determined by measuring the diffusion coefficient of the reference tetramethylsilane (TMS) and solving the equation for η with the literature value[16]of the radius of 2.96 Å. The solvent radius of CD_2Cl_2 (2.46 Å) was taken from the reference.[17]

For the error estimation, the separate diffusion coefficients for different probes belonging to the same species (e.g. all probes of the quinoline for the CPA•quinoline complex) were averaged and the standard deviation was determined. The molecular radii were determined based on the averaged diffusion coefficient, the averaged diffusion coefficient plus the standard deviation and the averaged diffusion coefficient minus the standard deviation. The resulting radii are given as the radius derived from the averaged diffusion coefficient and the error range is given by:

$$Error\ range = \frac{1}{2} * [\left(r_i^{aver} - r_i^{aver+StDev}\right) + (r_i^{aver-StDev} - r_i^{aver})]$$

Where r_i^{aver} is the radius derived from the averaged diffusion coefficient, $r_i^{aver+StDev}$ is the minimum radius derived from the averaged diffusion coefficient plus the standard deviation and $r_i^{aver-StDev}$ is the maximum radius derived from the averaged diffusion coefficient minus the standard deviation.

Table S13: Summary of the determined diffusion coefficients and derived molecular radii for samples of **3** and **4b-d** with a 1:1 or 2:1 stoichiometry at 300 K or 180 K and for **3** or **4b** alone.

Temper.	Sample	Species	D_t(averaged)	D_t(StaDev)	D_t(min)	D_t(max)	r_t(averaged)	r_t(min)	r_t(max)	Result	+/-	D_t TMS
[K]			[m^2/s] e-10	[m^2/s] e-10	[m^2/s] e-10	[m^2/s] e-10	[Å]	[Å]	[Å]	[Å]	[Å]	[m^2/s] e-10
300	3/4b 1:1	4b	1.137	0.1105	1.027	1.248	6.365	5.886	6.954	6.37	0.77	3.296
300	3/4b 1:1	3	0.872	0.0118	0.860	0.883	8.046	7.949	8.146	8.05	0.15	3.296
300	3/4b 2:1	4b	0.678	0.0223	0.656	0.701	8.531	8.283	8.796	8.53	0.38	2.736
300	3/4b 2:1	3	0.644	0.0024	0.642	0.647	8.947	8.916	8.978	8.95	0.05	2.736
300	3	3	0.786	0.0012	0.785	0.787	7.899	7.889	7.911	7.90	0.02	2.913
300	4b	4b	1.979	0.1623	1.817	2.142	3.779	3.585	4.009	3.78	0.31	2.913
180	3/4b 1:1	4b	0.0600	0.01045	0.0495	0.0704	7.206	6.268	8.561	7.21	1.62	0.200
180	3/4b 1:1	3	0.0463	0.00063	0.0456	0.0469	9.113	9.000	9.230	9.11	0.17	0.200
300	3/4c 1:1	4c	1.282	0.1762	1.106	1.458	5.098	4.615	5.744	5.10	0.81	2.836
300	3/4c 1:1	3	0.850	0.0123	0.838	0.863	7.193	7.102	7.286	7.19	0.14	2.836
300	3/4c 2:1	4c	0.679	0.0365	0.642	0.715	8.272	7.889	8.702	8.27	0.60	2.647
300	3/4c 2:1	3	0.653	0.0004	0.652	0.653	8.572	8.567	8.578	8.57	0.01	2.647
300	3/4d 1:1	4d	-	-	-	-	-	-	-	-	-	2.677
300	3/4d 1:1	3	0.641	0.0145	0.626	0.655	8.815	8.635	9.004	8.82	0.27	2.677
300	3/4d 2:1	4d	0.611	0.0180	0.593	0.629	9.823	9.561	10.102	9.82	0.40	2.871
300	3/4d 2:1	3	0.624	0.0272	0.597	0.651	9.639	9.263	10.049	9.64	0.58	2.871

In general, an increase of the determined radii of approx. 2 – 3 Å was determined for samples with a 2:1 stoichiometry compared to the respective 1:1 samples, demonstrating the population of higher aggregates of the CPA•quinoline complexes.

Table S14: Probe signal and their respective diffusion coefficients for all measured samples. The chemical shifts in the DOSY experiments were not referenced and hence the given values can deviate from the chemical shifts in the given assignments.

A) 3:4b; 1:1; 300 K; p16 = 1200 us		
Species	$\delta(^1H)$ [ppm]	D_i [m^2/s] e-9
4b	8.52	1.2880
4b	8.18	1.0260
3	7.72	0.8599
4b	7.55	1.0980
3	6.7	0.8834

B) 3:4b; 2:1; 300 K; p16 = 1500 us		
Species	$\delta(^1H)$ [ppm]	D_i [m^2/s] e-9
4b	8.36	0.7092
3	7.82	0.6444
3	7.53	0.6479
3	6.58	0.6412
4b	6.35	0.6691
3	3.47	0.6433
4b	3.34	0.6571

C) CPA 3; 300 K; p16 = 1400 us		
Species	$\delta(^1H)$ [ppm]	D_i [m^2/s] e-9
3	8.10	0.7872
3	8.05	0.7845
3	7.38	0.7855
3	6.92	0.7860
3	3.56	0.7878

D) Quinoline 4b; 300 K; p16 = 900 us		
Species	$\delta(^1H)$ [ppm]	D_i [m^2/s] e-9
4b	8.08	1.934
4b	7.88	2.194
4b	7.83	1.709
4b	7.71	1.917
4b	7.51	1.963
4b	7.05	2.160

E) 3:4b 1:1; 180 K, p16 = 5500 us		
Species	$\delta(^1H)$ [ppm]	D_i [m^2/s] e-9
3	7.46	0.045646
3	7.28	0.046673
3	7.86	0.047088
4b	6.31	0.070417
3	3.74	0.045661
4b	3.40	0.049517
TMS	0.00	0.2005

F) 3:4c; 1:1, 300 K; p16 = 1300 us		
Species	$\delta(^1H)$ [ppm]	D_i [m^2/s] e-10
4c	8.66	1.5526
4c	8.23	1.1219
3	7.73	0.8631
4c	7.65	1.1288
3	7.50	0.8600
4c	6.78	1.3254
3	6.79	0.8452
3	3.81	0.8323

G) 3:4c; 2:1, 300 K; p16 = 1500 us		
Species	$\delta(^1H)$ [ppm]	D_i [m^2/s] e-9
4c	8.45	0.71530
4c	7.85	0.64221
3	7.81	0.65340
3	7.52	0.65257
3	6.60	0.65237

H) 3:4d; 1:1, 300 K; p16 = 1500 us		
Species	$\delta(^1H)$ [ppm]	D_i [m^2/s] e-9
3	7.61	0.6483
3	7.51	0.6339
3	7.12	0.6652
3	6.73	0.6256
3	3.62	0.6296

I) 3:4d; 2:1, 300 K; p16 = 1500 us		
Species	$\delta(^1H)$ [ppm]	D_i [m^2/s] e-9
4d	8.67	0.63310
4d	8.28	0.58908
4d	8.18	0.61177
-	7.92	0.67035
-	7.62	0.62084
-	7.55	0.59940
3	6.74	0.59502
3	3.74	0.63368

Note: No signals of **4d** could be analysed due to signal overlap and too low signal intensities

6.8 Structural investigation in 2:1 complexes

The exchange between **3•4b** and **3•3•4b** can be observed in the NOESY spectrum (see S29). Exchange peaks (marked in red) between the signal at 16.75 ppm (**3•4b**) and 15.27 ppm (**3•3•4b**) show, that the $PO^{-}\cdots H\cdot N^{+}$ hydrogen bond of the **3•3•4b** complex is the signal at 15.27 ppm, as the PO··H··OP hydrogen bond signal at 16.51 ppm does not show exchange signals.

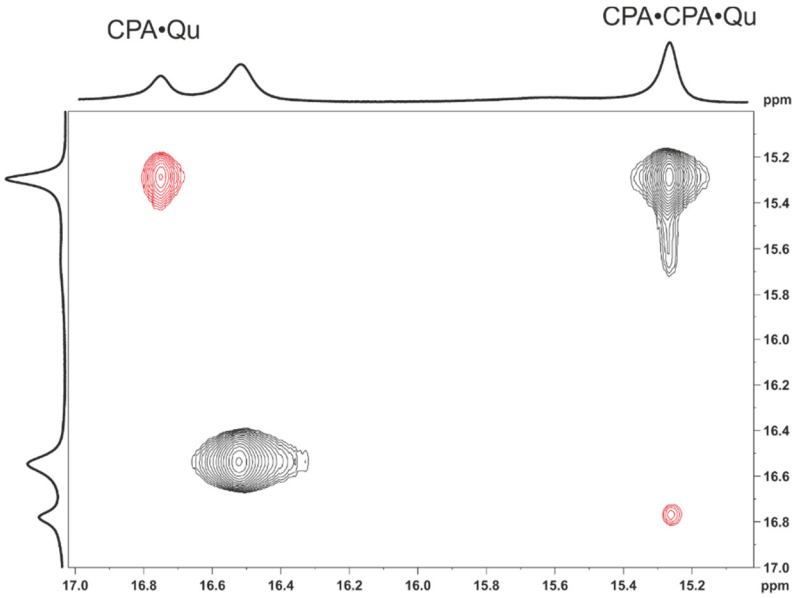

Figure S33: Excerpt of the NOESY spectrum of a 2:1 sample of **3**:**4b** at 200 K and 600 MHz in CD_2Cl_2. The exchange peaks between the different signals are marked in red.

6.9 Speciation in the ^{31}P spectrum

At a 2:1 stoichiometry of **3** and quinoline **4b**, the ^{31}P spectra shows 3 dominant signals, two of them with severe line broadening (see figure below). We assume, that the signal marked in red corresponds to the phosphorus nucleus in the monomeric complex, while the two signals marked in green correspond to the two chemically different phosphorus nuclei in the dimeric complex. We assume, that the more highfield shifted signal at 0.1 ppm corresponds to the phosphorus nucleus which forms the H-bond to the quinoline which would be in in line with studies from photoredox catalysis. In the CPA/CPA/Qu complex, the proton is stronger transferred onto Qu compared to the respective CPA/Qu complex. Therefore, the respective ^{31}P signal should be also highfield shifted.

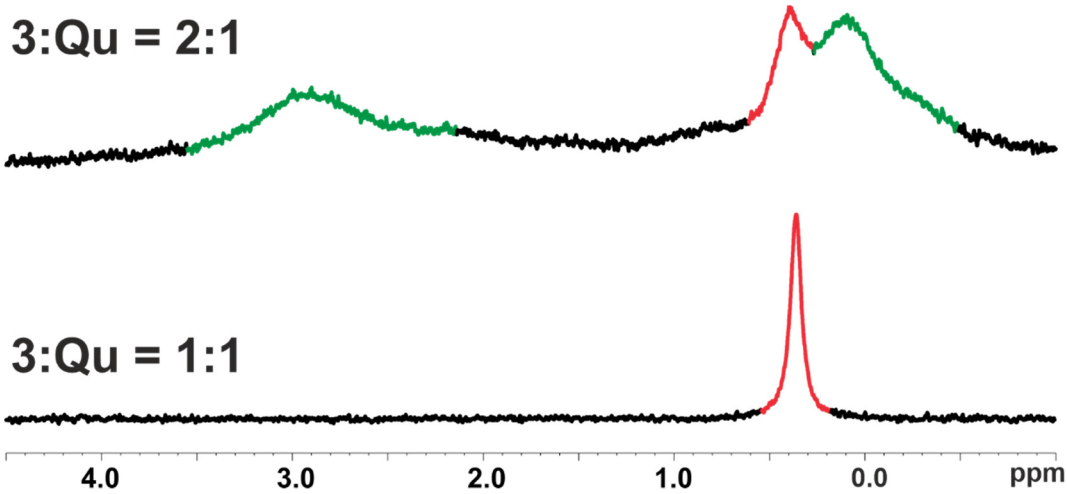

Figure S 34: ^{31}P spectra of samples with **3** and **4b** at a 1:1 (bottom) or 2:1 (top) stoichiometry at 180 K and 600 MHz in CD_2Cl_2. At a 1:1 stoichiometry, only one signal is observed, corresponding to the monomeric CPA/Qu complex. At a 2:1 stoichiometry, additionally 2 broad signals (marked in green) are observed, which are assumed to correspond to the CPA/CPA/Qu complex.

7. DFT-investigations

7.1. Computational details

The GFN-xTB method[18] as implemented in the xtb program[19] is used for initial structure optimization and conformational searching in toluene employing the GBSA solvation model[20]. The TURBOMOLE V7.0 suite of programs[21] was used for all DFT calculations. All structures are fully optimized at the TPSS-D3/def2-SVP + DCOSMO-RS (toluene) level of theory, which combines the TPSS meta-GGA density functional[22] with the BJ-damped D3 dispersion correction[23,24] and the def2-SVP basis set[25,26], together with the DCOSMO-RS (for toluene solvent ε_r=2.38 , R_{sol}= 3.48 Å) solvation model[27,28]. The density-fitting RI-J approach[29,30] is used to accelerate the geometry optimization and harmonic frequency calculations. Vibrational frequency analysis is used to identify the nature of located stationary points and to provide thermal and free-energy corrections according to the modified ideal gas–rigid rotor–harmonic oscillator model.[31] The structures are characterized as true minima (with no imaginary frequency) or transition states (with only one imaginary frequency). Improved free energies in toluene and in CH_2Cl_2 solution are obtained from the sum of TPSS-D3/def2-QZVP single-point energies,[32] COSMO-RS[33-35] solvation free energies (for toluene using the BP_TZVP_C30_1301.ctd parameter and for CH_2Cl_2 using the BP_TZVP_C30_1601.ctd parameter with the Gsolv=molar option) and TPSS-D3/def2-SVP thermal corrections at 298.15 K related to ideal gas under 1 atm (*i.e.*, 0.04 mol/L). In our discussion, the final TPSS-D3/def2-QZVP + COSMO-RS free energies (in kcal/mol) are used unless specified otherwise.

7.2 Computational results

Energetic profiles for the formation of catalyst-substrate aggregates in toluene vs. dichloromethane

In toluene solution, the double O···HO H-bonded dimer **ssh2** is 4.8 kcal/mol more stable than two separated **sh** monomers. When a base **Q** is also present in solution, one H-bond of **ssh2** may break to form the transient singly H-bonded **ssh2***, which is 14.2 kcal/mol less stable but more reactive toward base **Q** to rapidly form the contact ion pair $\mathbf{ssh^-Qh^+}$ in a −20.3 kcal/mol exergonic step. $\mathbf{ssh^-Qh^+}$ is 1.9 kcal/mol more stable than separated $\mathbf{Sh + S^-Qh^+}$.

The present experimental NMR investigations are done in CD_2Cl_2 rather than in toluene. Test DFT calculations show that there is no big effect on the reaction mechanism analysis. In CD_2Cl_2 the double O…HO H-bonded dimer **ssh2** is 5.2 and 13.2 kcal/mol more stable than two separated **sh** monomers and the singly H-bonded structure **ssh2***, respectively. **ssh2*** may react with **Q** in a −22.4 kcal/mol exergonic step to form the

contact ion pair **ssh^{-}Qh^{+}**, which is 2.9 kcal/mol more stable than **Sh + S^{-}Qh^{+}**. The reaction sequences remain qualitatively the same.

Expected stereoselectivities in toluene vs. dichloromethane

With regard to the activation barriers of the competing monomeric and dimeric pathways, we found that in toluene, the rate-limiting barriers for the monomeric (**s^{-}Qh^{+}** to **shQh2_ts**) and dimeric (**ssh^{-}Qh^{+}** to **ssh2***) pathways are 19.8 and 22.2 kcal/mol, respectively, with the monomeric pathway being kinetically 2.4 kcal/mol more favorable. The stereoselectivity of the monomeric pathway is very low (1.0 kcal/mol stereoselectivity for the (*R*)-product), so that the absolute stereoselectivity of the monomeric pathway is difficult to predict based on the DFT work. Indeed, we find a slight preference for the (*S*)-product experimentally. In contrast, the dimeric pathway shows a high (*R*)-selectivity (3.9 kcal/mol stereoselectivity), which allows for a safe prediction of the stereoselectivity of the reaction. Indeed, we find a strong (*R*)-selectivity at high catalyst concentrations.

In dichloromethane, the rate-limiting barriers for the monomeric (s-Qh+ to shQh2_ts) and dimeric (ssh-Qh+ to ssh2*) pathways are 20.2 and 24.5 kcal/mol, respectively, with the monomeric pathway being kinetically 4.3 kcal/mol more favorable. Once again, the stereoselectivity of the monomeric pathway is very low (0.8 kcal/mol (*R*)-selectivity predicted). In dichloromethane, the dimeric pathway is also significantly more stereoselective, but its stereoselectivity (3.3 kcal/mol (*R*)-selectivity) is lower than in toluene (3.9 kcal/mol (*R*)-selectivity, vide supra). Thus, the dimeric pathway is kinetically even more disfavoured than in toluene and is less stereoselective, so that significantly lower stereoselectivities are expected in CD_2Cl_2 solution, consistent with experiment.

8. Appendix A: Synthesis

8.1. NMR-spectra

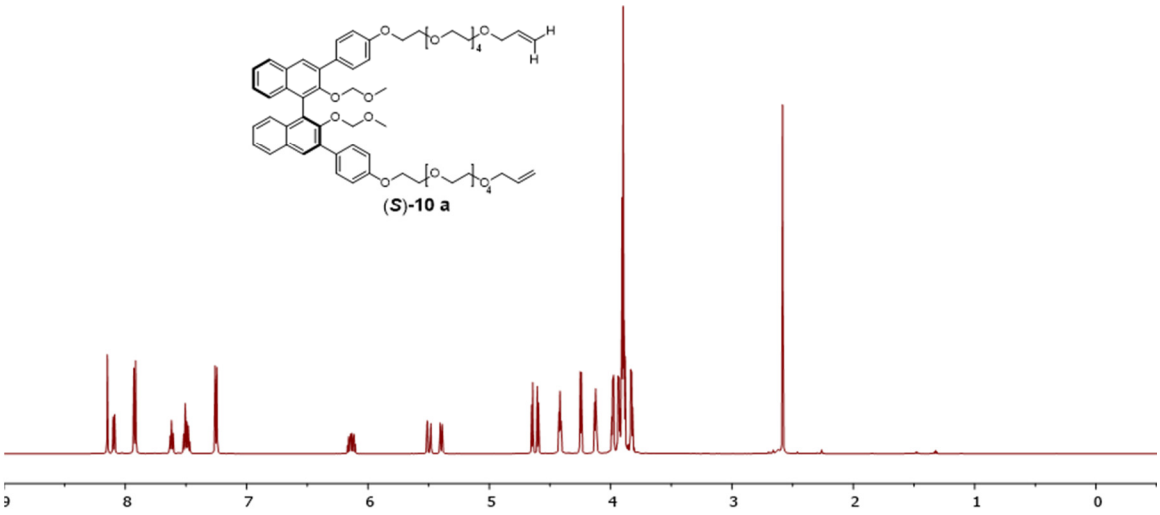

Figure S35: ^{1}H-NMR spectrum of (*S*)-**10a** (298 K, 600 MHz, [D$_1$]-chloroform).

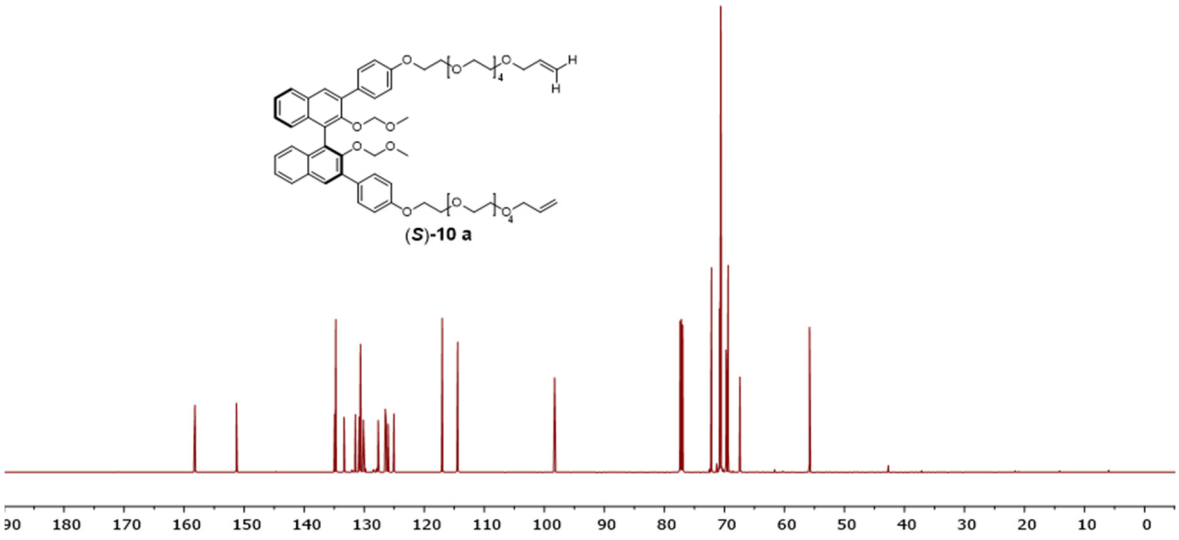

Figure S36: ^{13}C-NMR spectrum of (S)-**10a** (298 K, 150 MHz, [D$_1$]-chloroform).

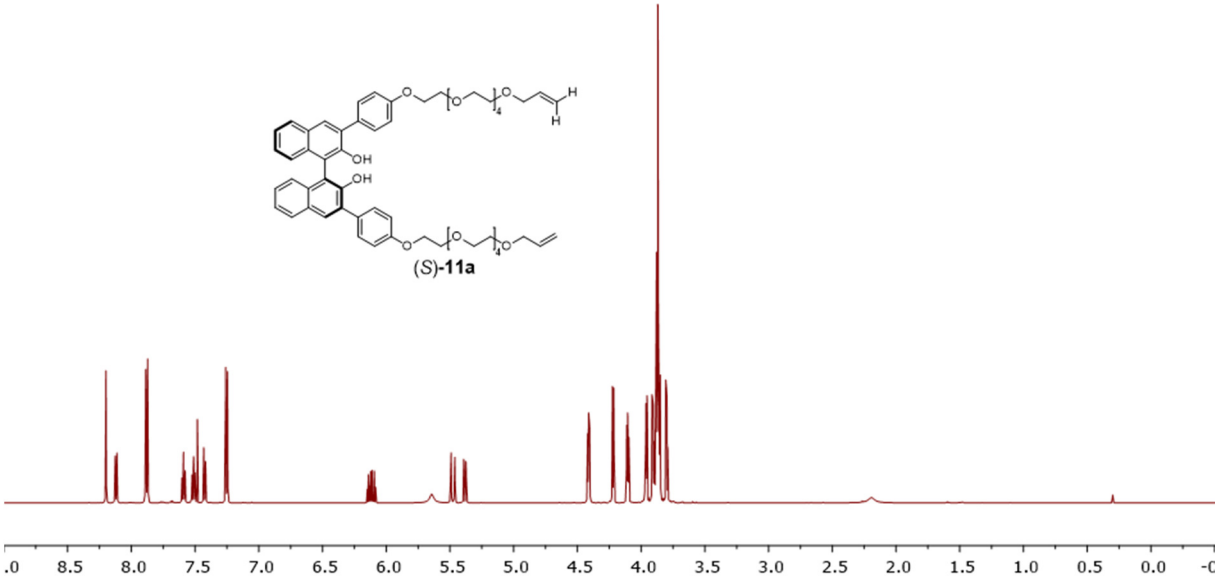

Figure S37: ^{1}H-NMR spectrum of (*S*)-**11a** (298 K, 600 MHz, [D$_1$]-chloroform).

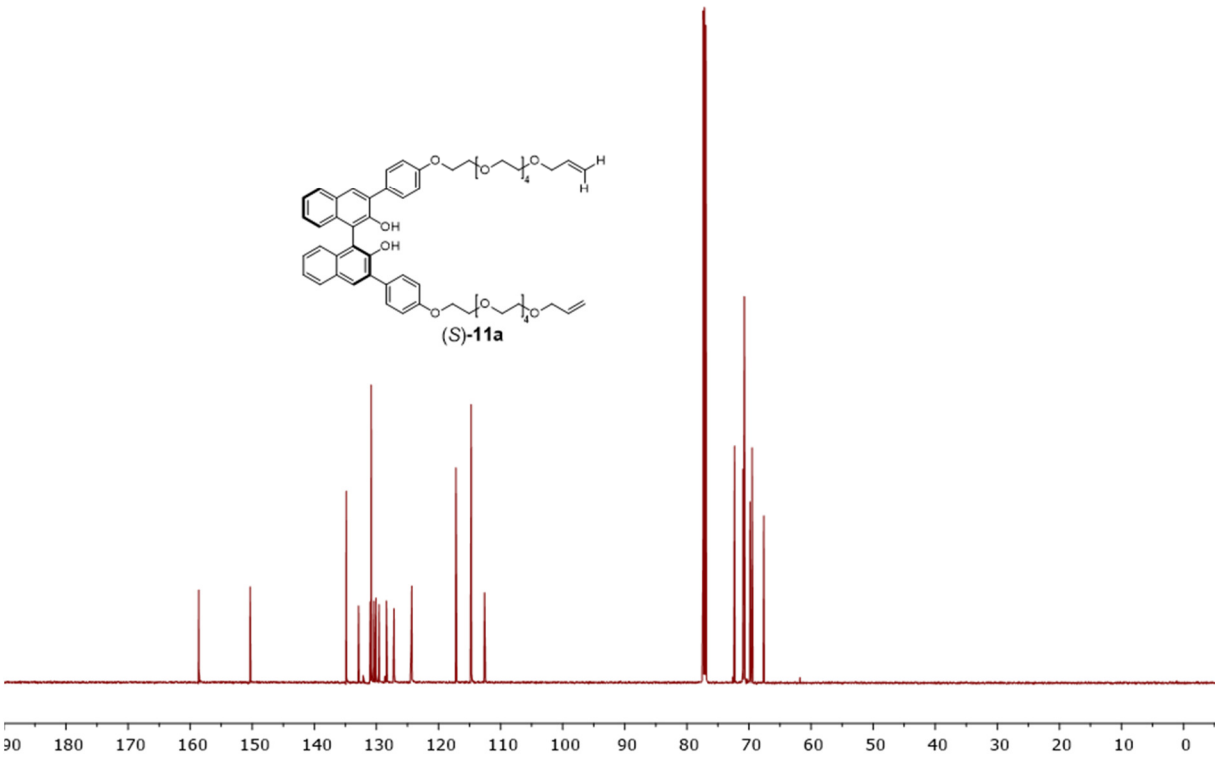

Figure S38: ^{13}C-NMR spectrum of (S)-**11a** (298 K, 150 MHz, [D$_1$]-chloroform).

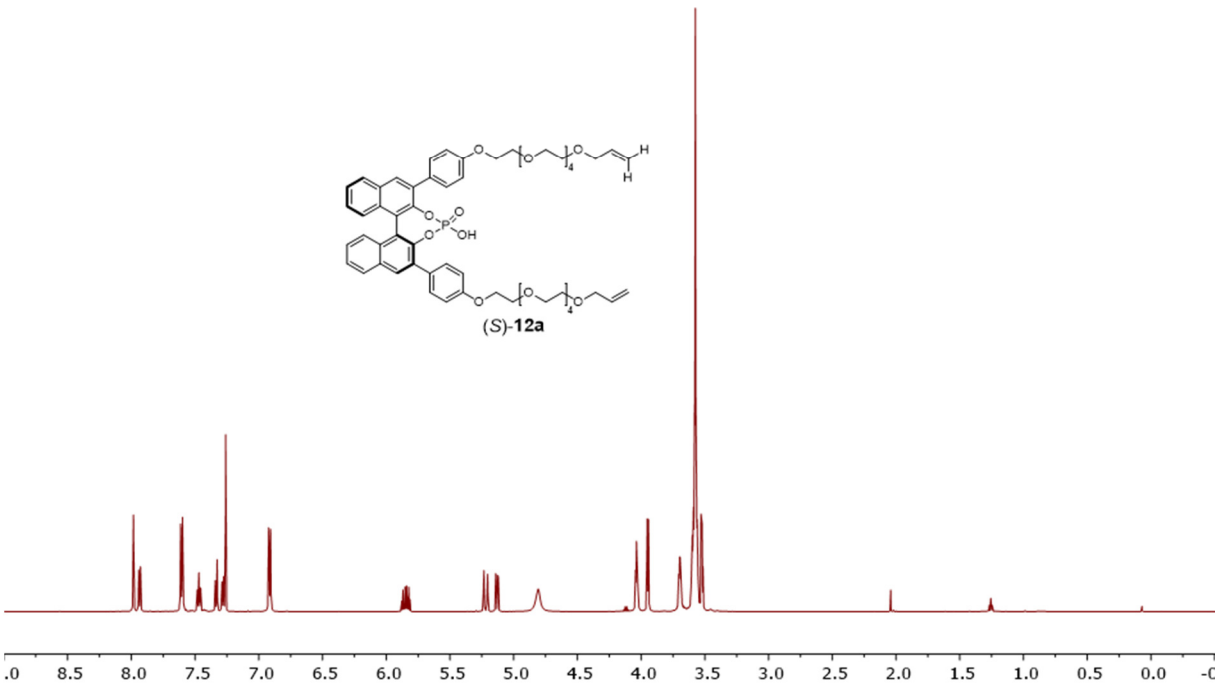

Figure S39: ^{1}H-NMR spectrum of (*S*)-**12a** (298 K, 600 MHz, [D$_1$]-chloroform).

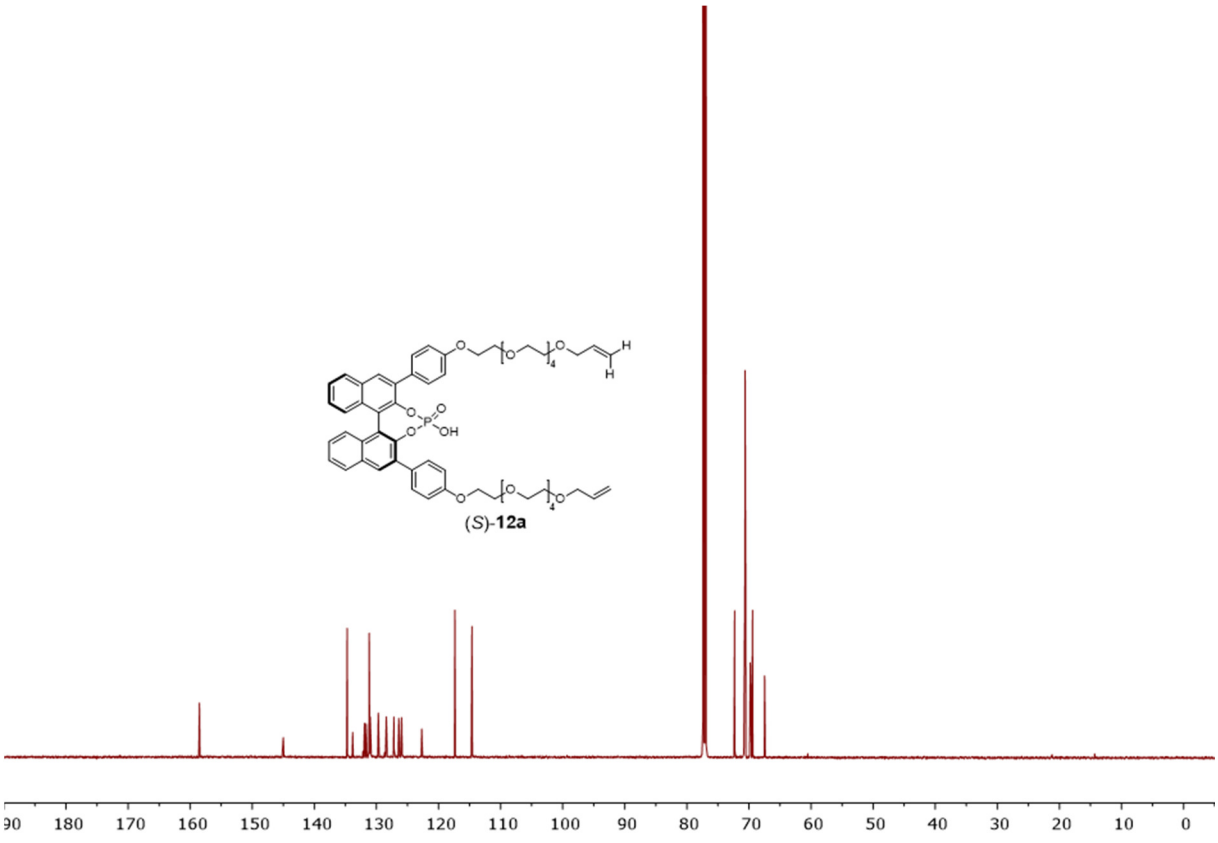

Figure S40: ^{13}C-NMR spectrum of (S)-1**2a** (298 K, 150 MHz, [D$_1$]-chloroform).

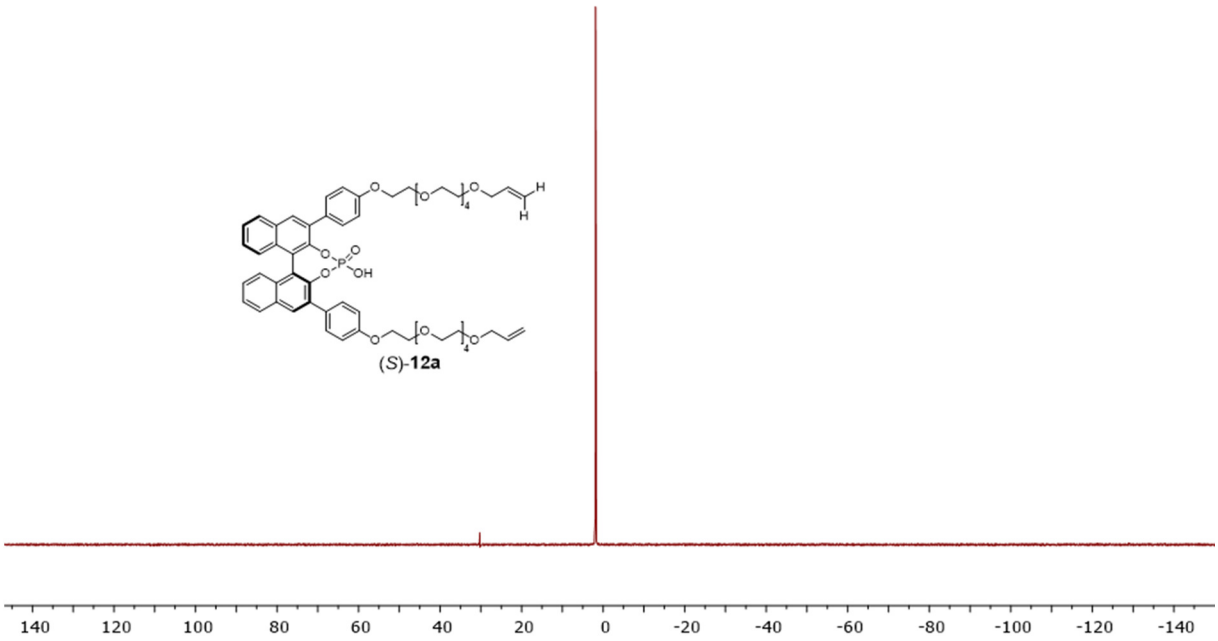

Figure S41: ^{31}P-NMR spectrum of (*S*)-**12a** (298 K, 243 MHz, [D_1]-chloroform).

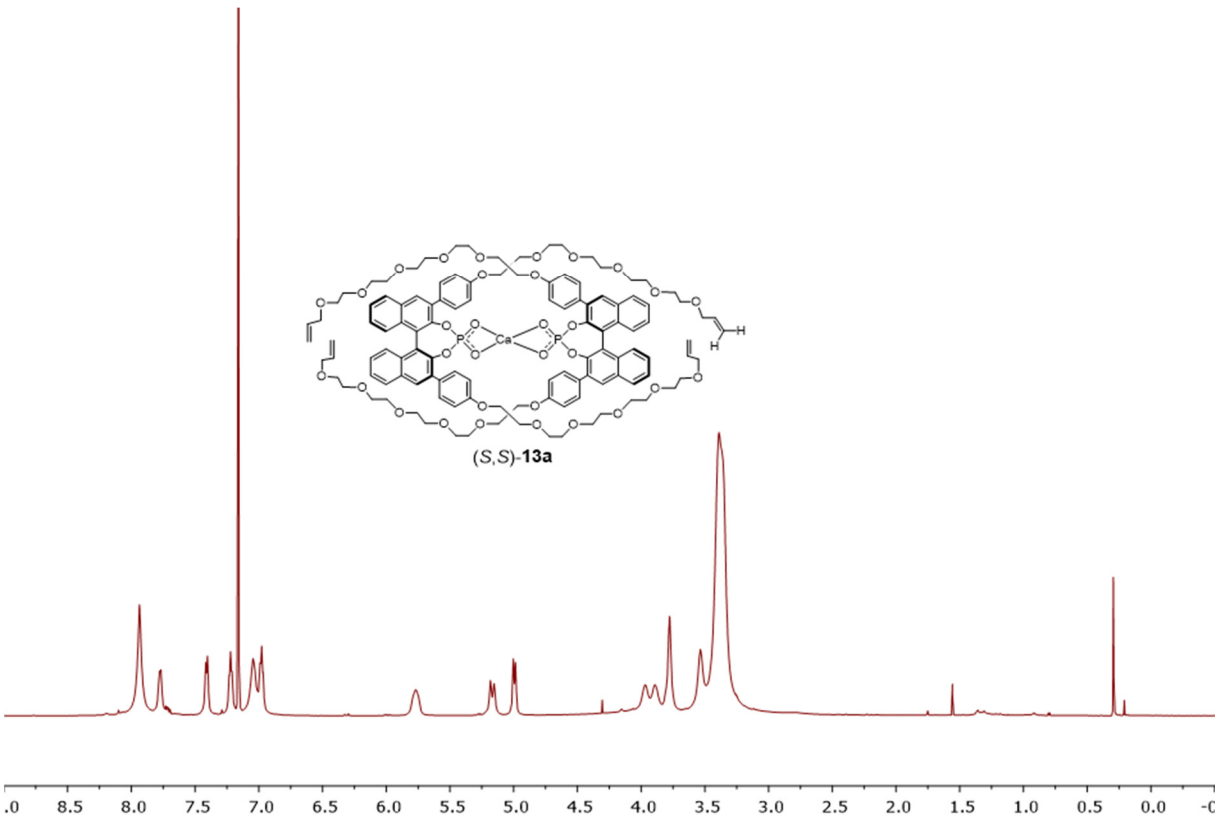

Figure S42: ^{1}H-NMR spectrum of (*S*,*S*)-**13a** (298 K, 600 MHz, [D_6]-benzene).

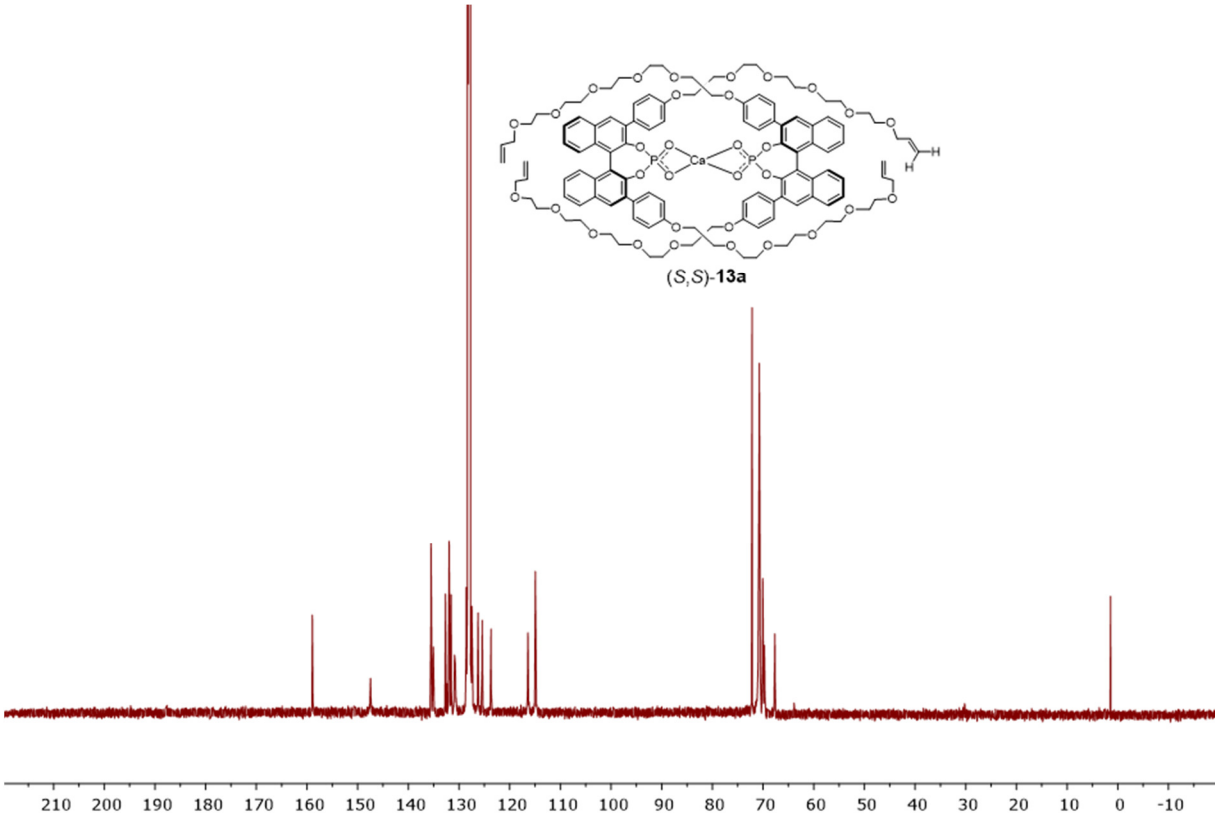

Figure S43: ^{13}C-NMR spectrum of (*S*,*S*)-**13a** (298 K, 150 MHz, [D_6]-benzene).

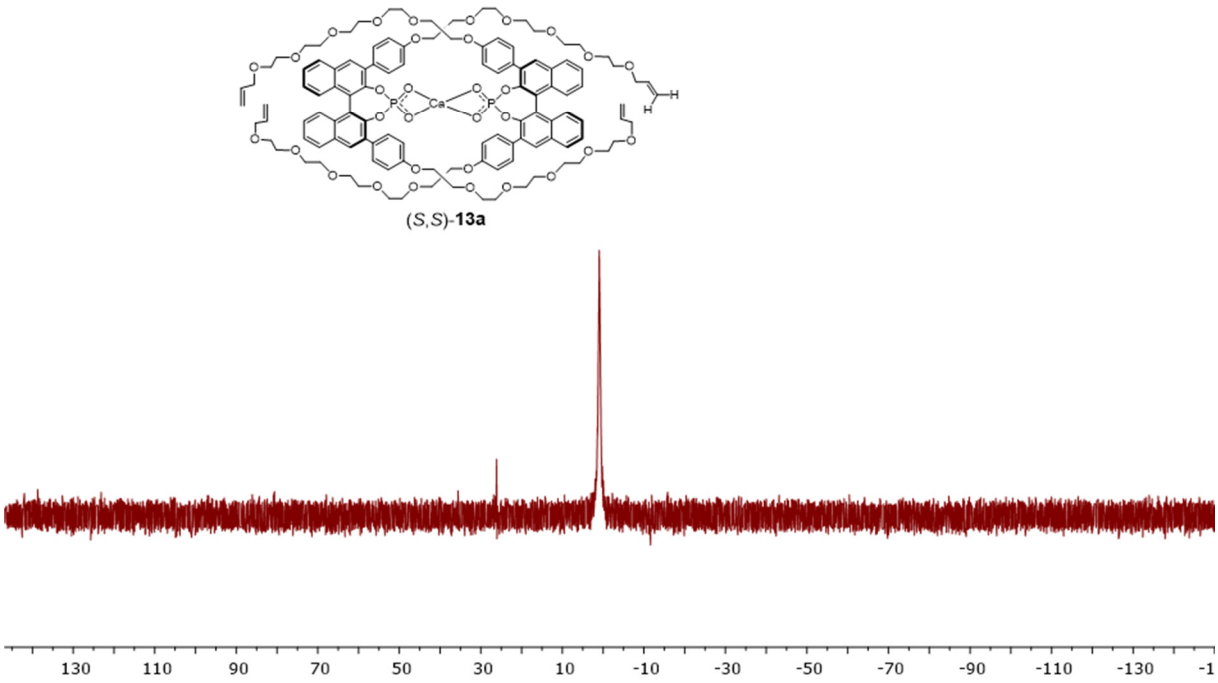

Figure S44: ^{31}P-NMR spectrum of (*S*,*S*)-**13a** (298 K, 243 MHz, [D_6]-benzene).

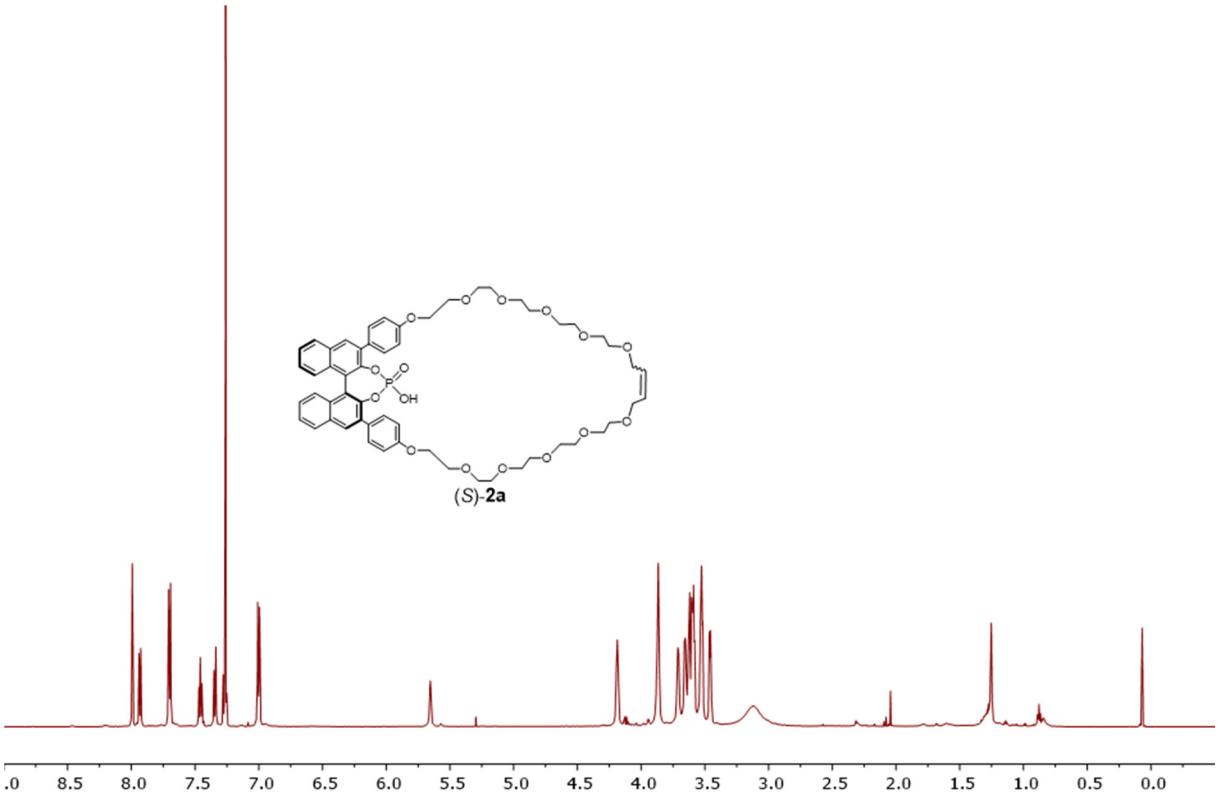

Figure S45: ^{1}H-NMR spectrum of (*S*)-**2a** (298 K, 600 MHz, [D$_1$]-chloroform).

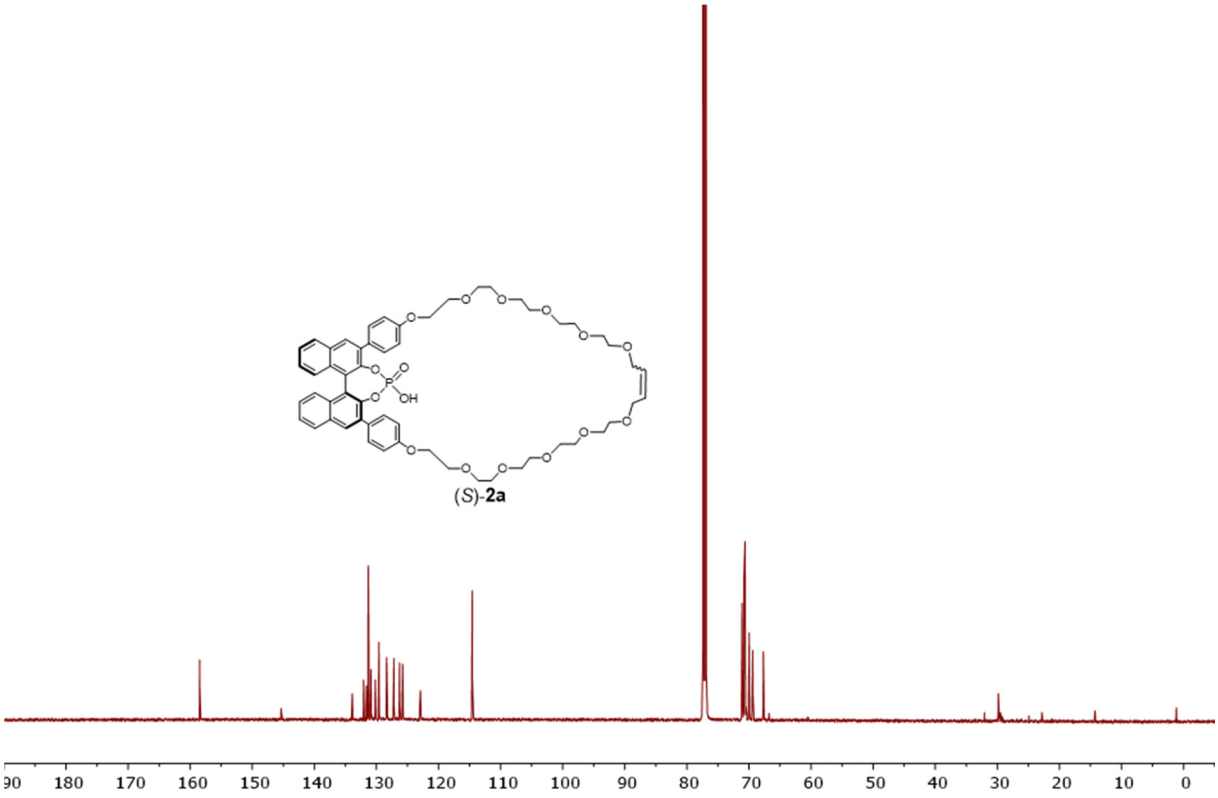

Figure S46: ^{13}C-NMR spectrum of (S)-**2a** (298 K, 150 MHz, [D$_1$]-chloroform)

.

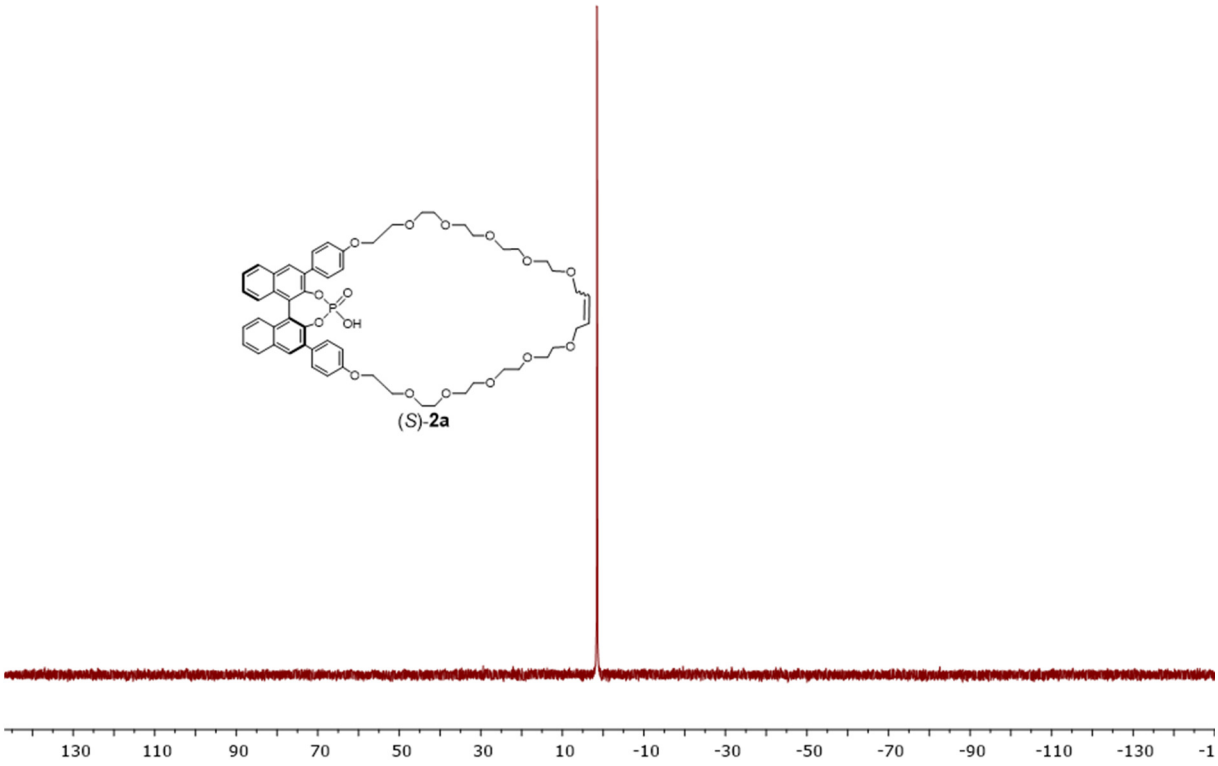

Figure S47: ^{31}P-NMR spectrum of (*S*)-**2a** (298 K, 243 MHz, [D$_1$]-chloroform).

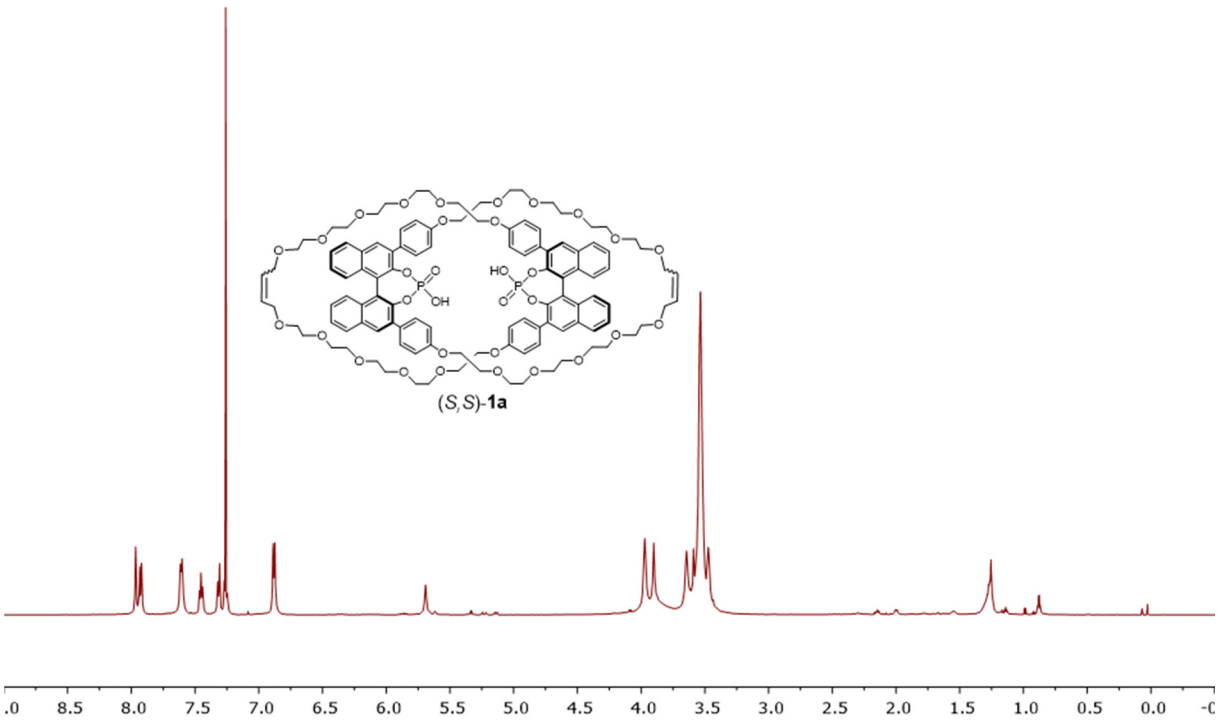

Figure S48: ^{1}H-NMR spectrum of (*S,S*)-**1a** (298 K, 600 MHz, [D$_1$]-chloroform).

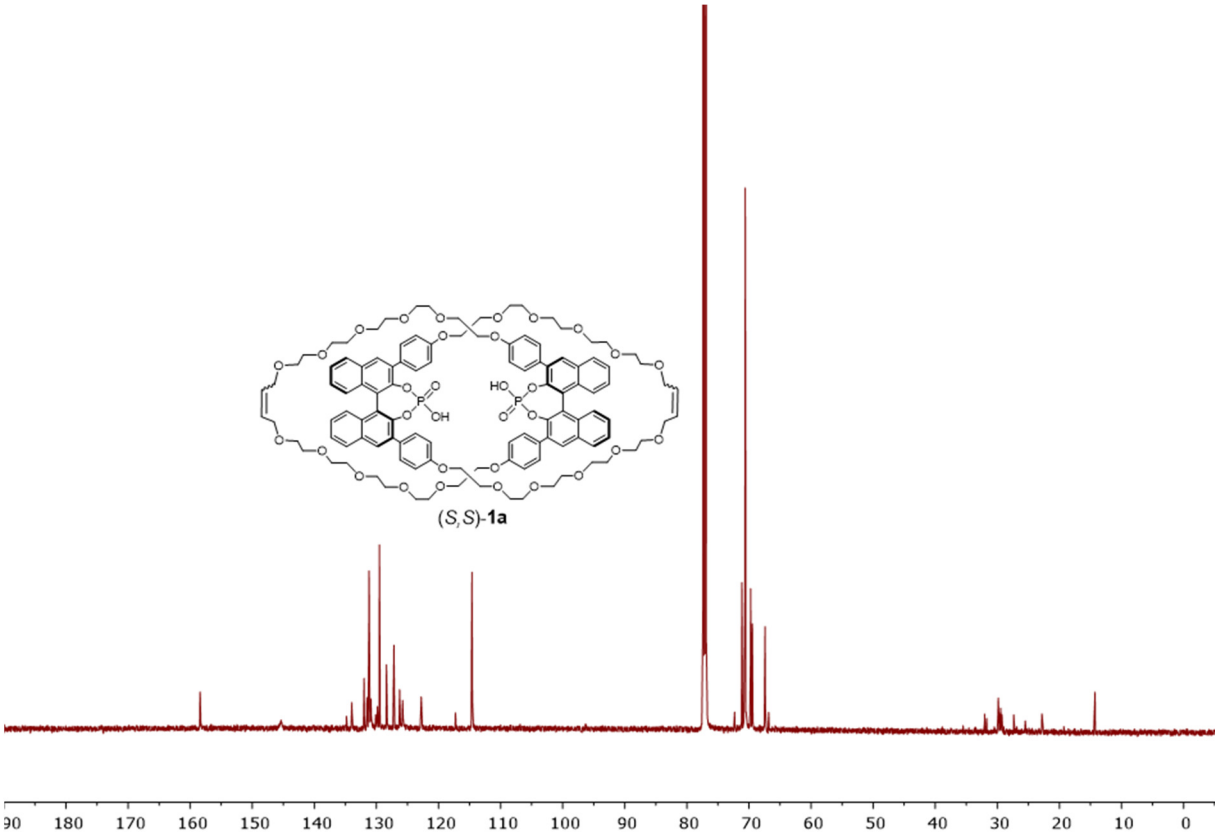

Figure S49: ^{13}C-NMR spectrum of (S,S)-**1a** (298 K, 150 MHz, [D_1]-chloroform).

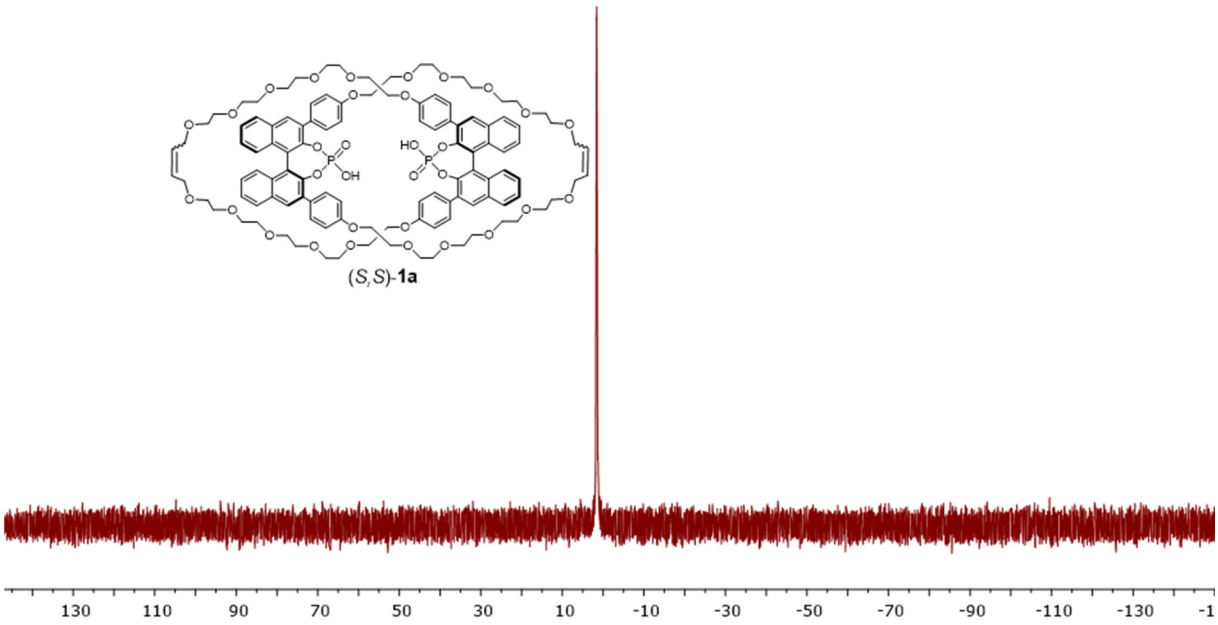

Figure S50: ^{31}P-NMR spectrum of (*S*)-**2a** (298 K, 243 MHz, [D_1]-chloroform).

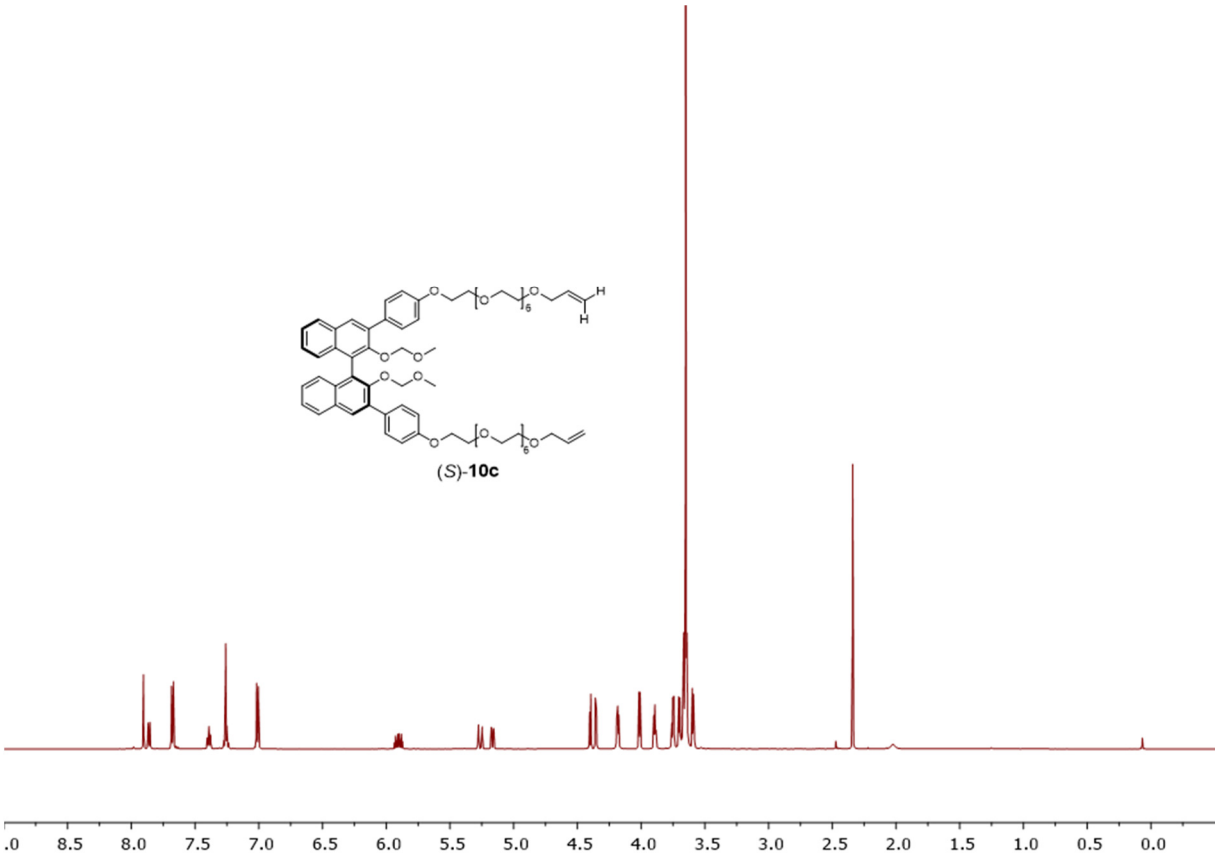

Figure S51: ^{1}H-NMR spectrum of (*S*)-**10c** (298 K, 600 MHz, [D$_1$]-chloroform).

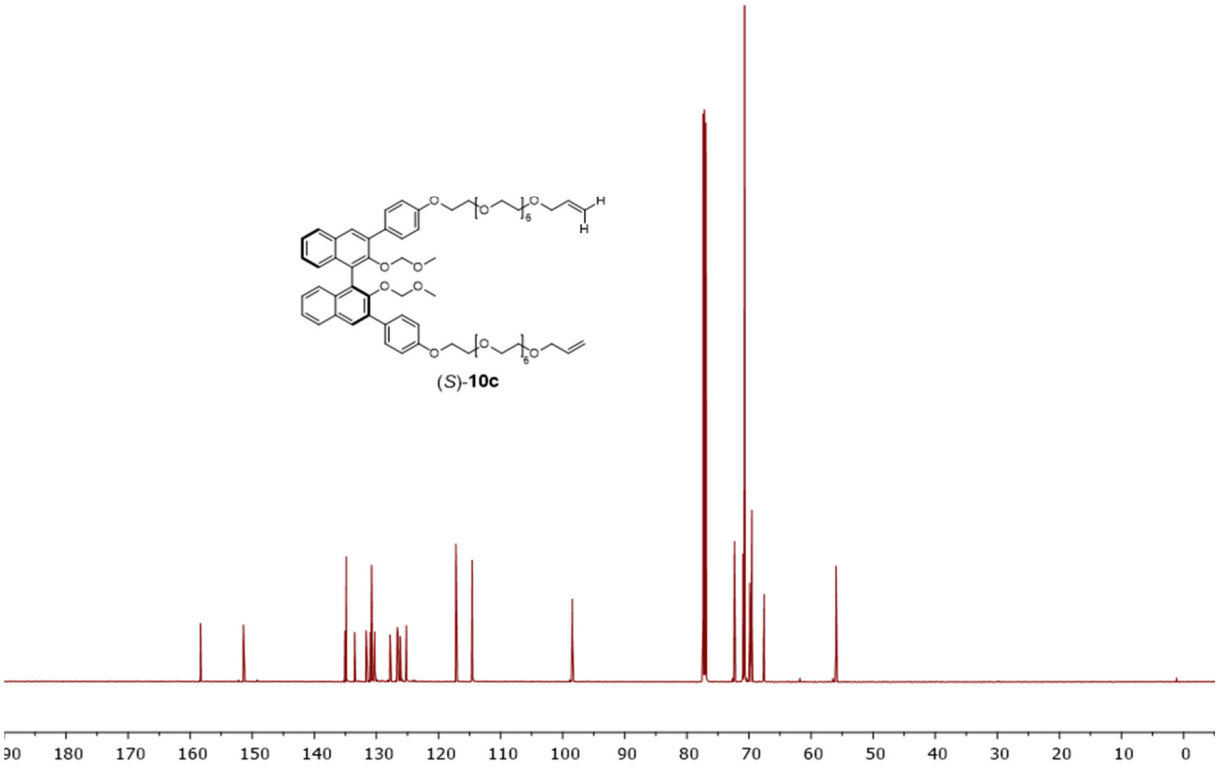

Figure S52: ^{13}C-NMR spectrum of (*S*)-**10c** (298 K, 150 MHz, [D$_1$]-chloroform).

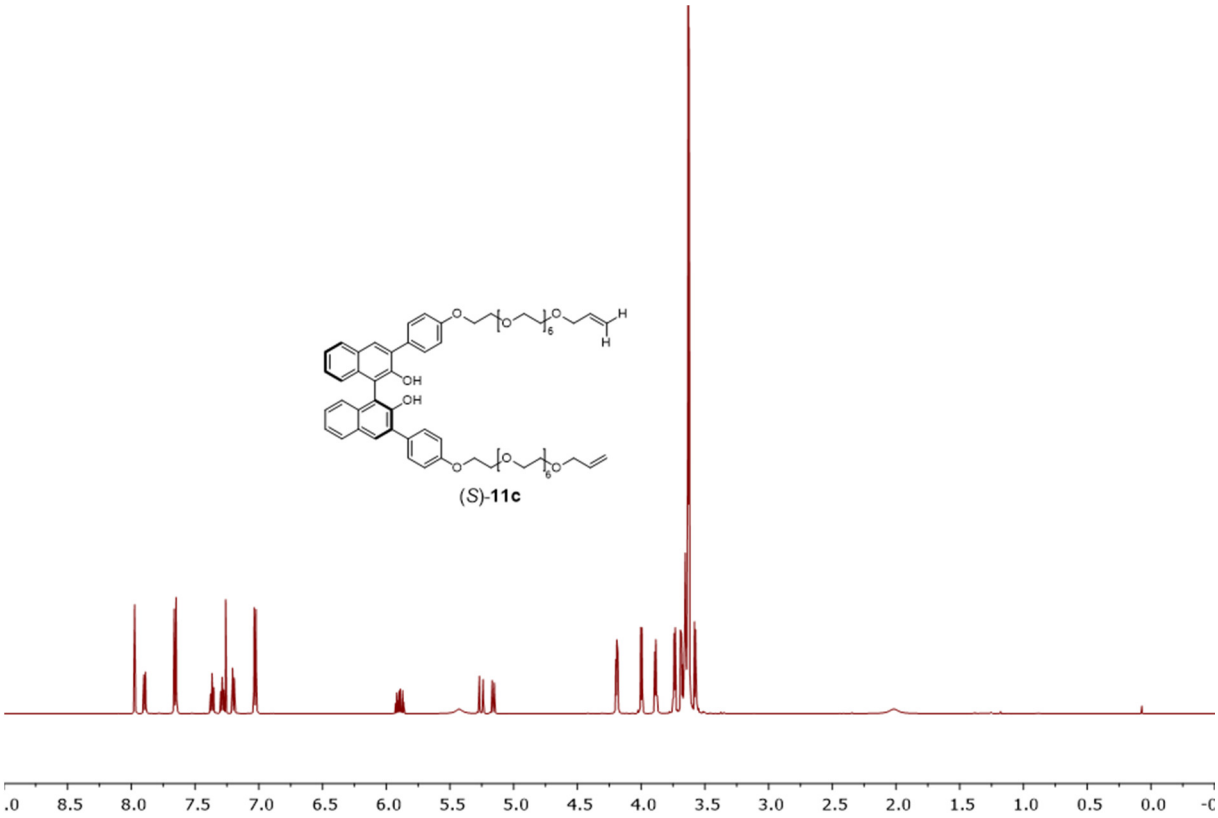

Figure S53: ^{1}H-NMR spectrum of (*S*)-**11c** (298 K, 600 MHz, [D$_1$]-chloroform).

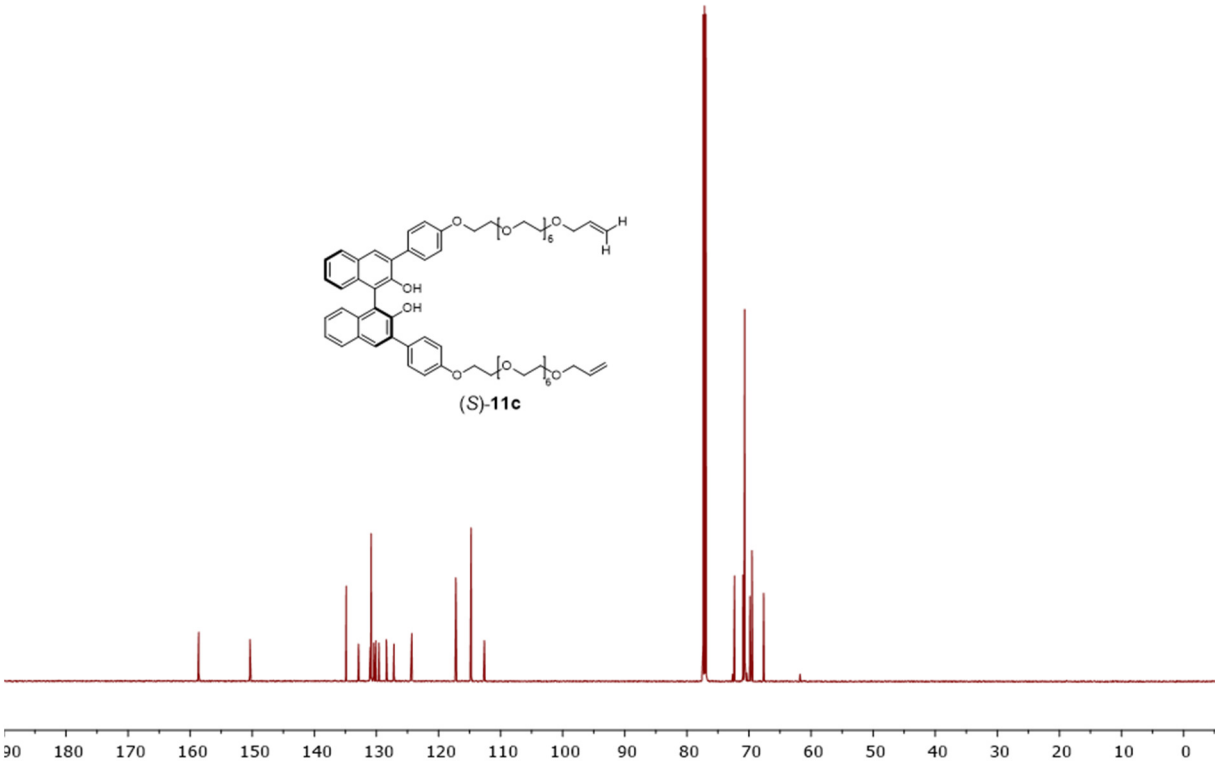

Figure S54: ^{13}C-NMR spectrum of (*S*)-**11c** (298 K, 150 MHz, [D$_1$]-chloroform).

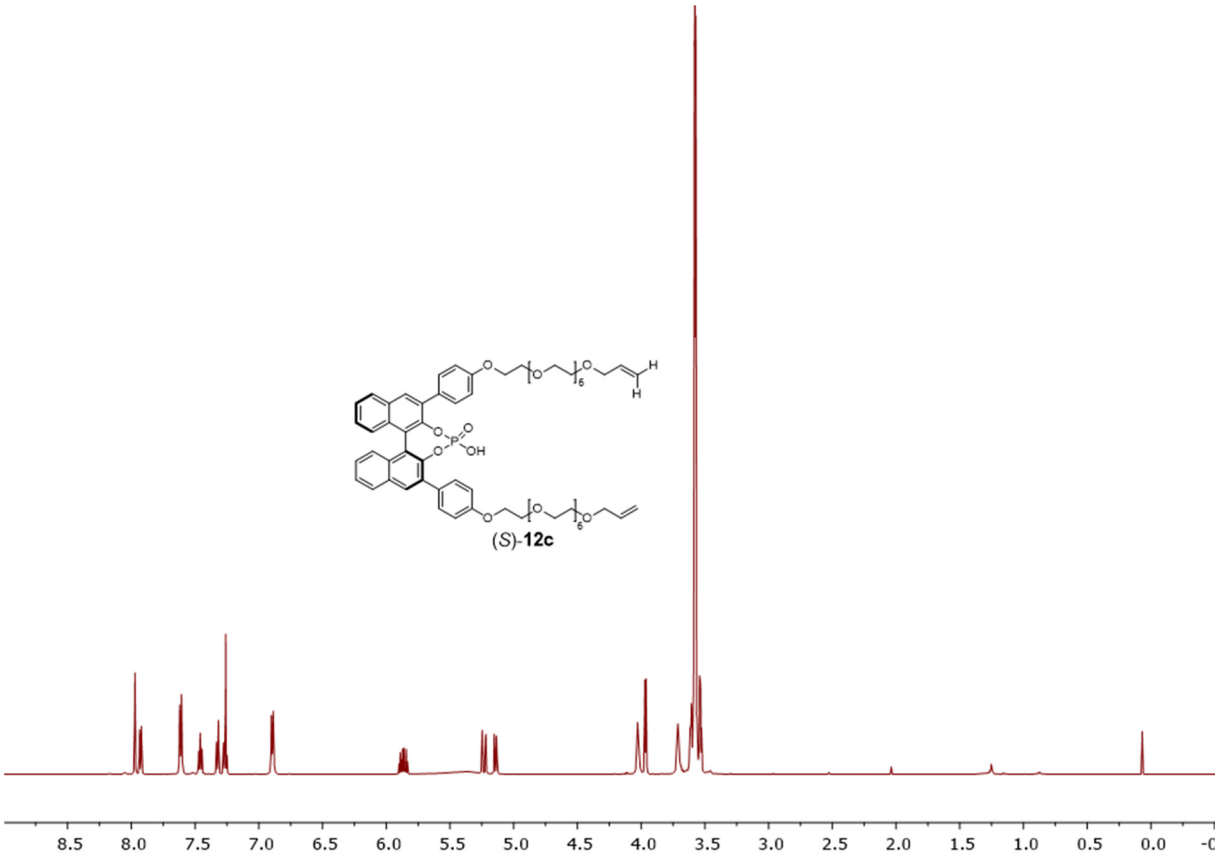

Figure S55: ^{1}H-NMR spectrum of (*S*)-**12c** (298 K, 600 MHz, [D$_1$]-chloroform).

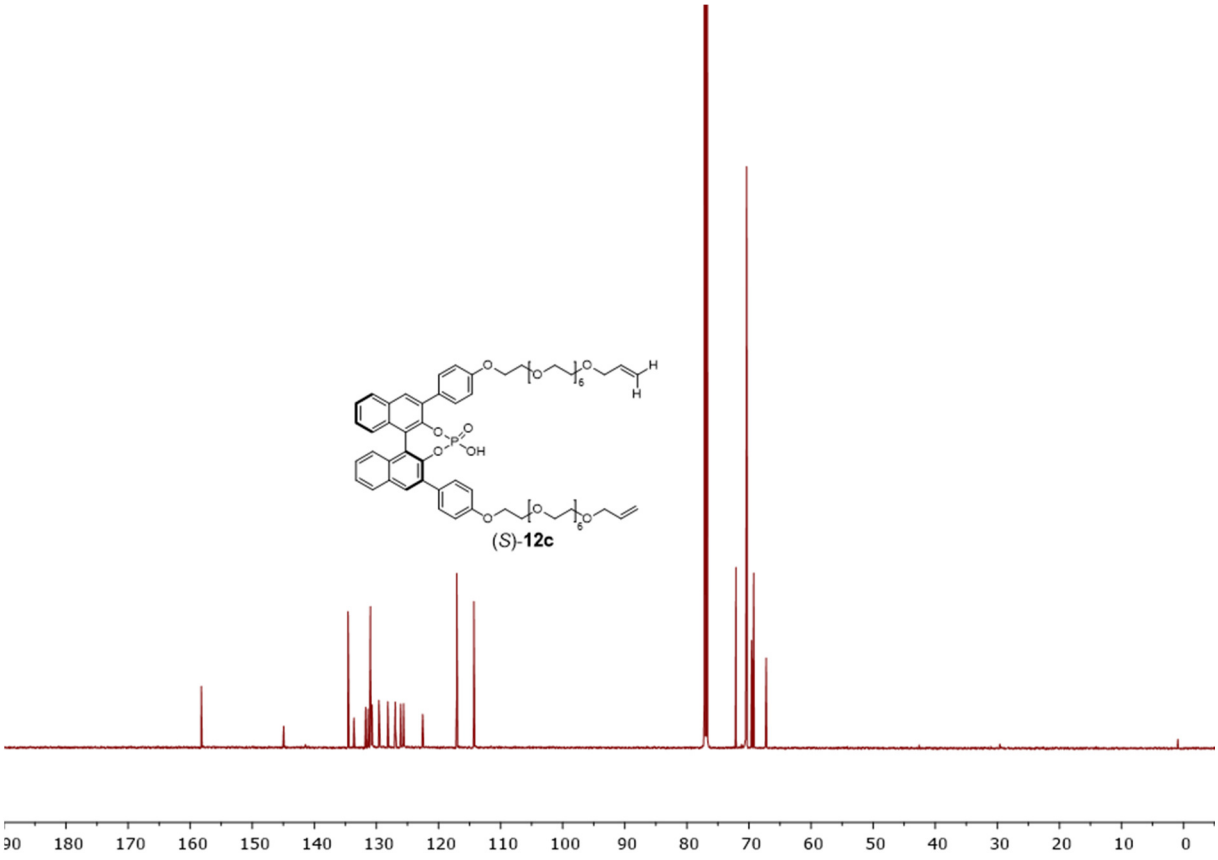

Figure S56: ^{13}C-NMR spectrum of (*S*)-**12c** (298 K, 150 MHz, [D$_1$]-chloroform).

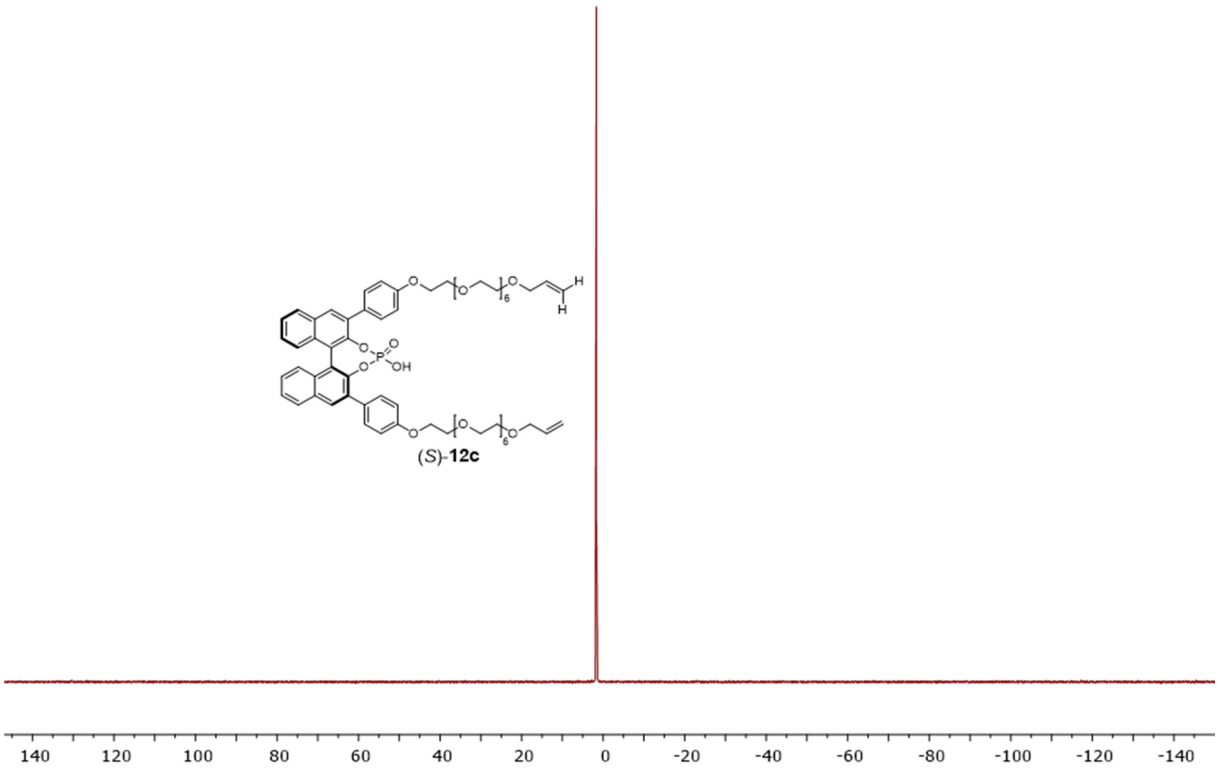

Figure S57: ^{31}P-NMR spectrum of (*S*)-1**2c** (298 K, 243 MHz, [D_1]-chloroform).

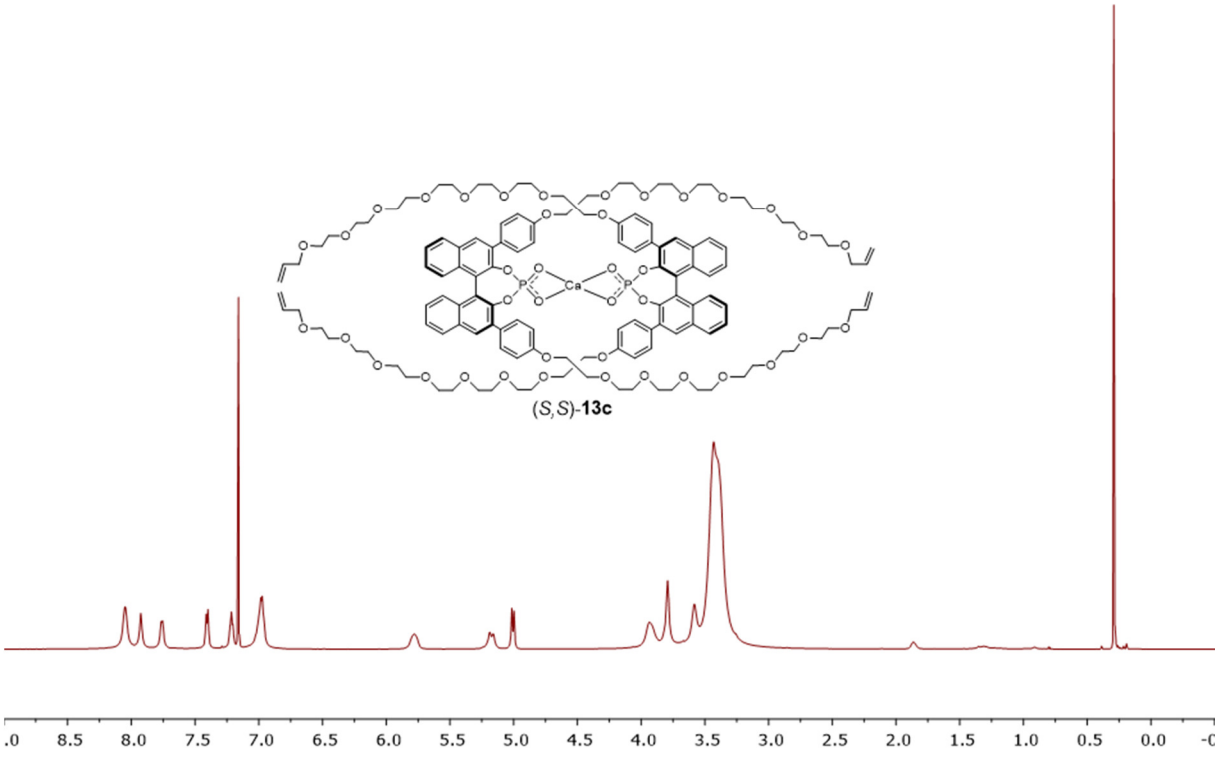

Figure S58: ^{1}H-NMR spectrum of (*S,S*)-**13c** (298 K, 600 MHz, [D_6]-benzene).

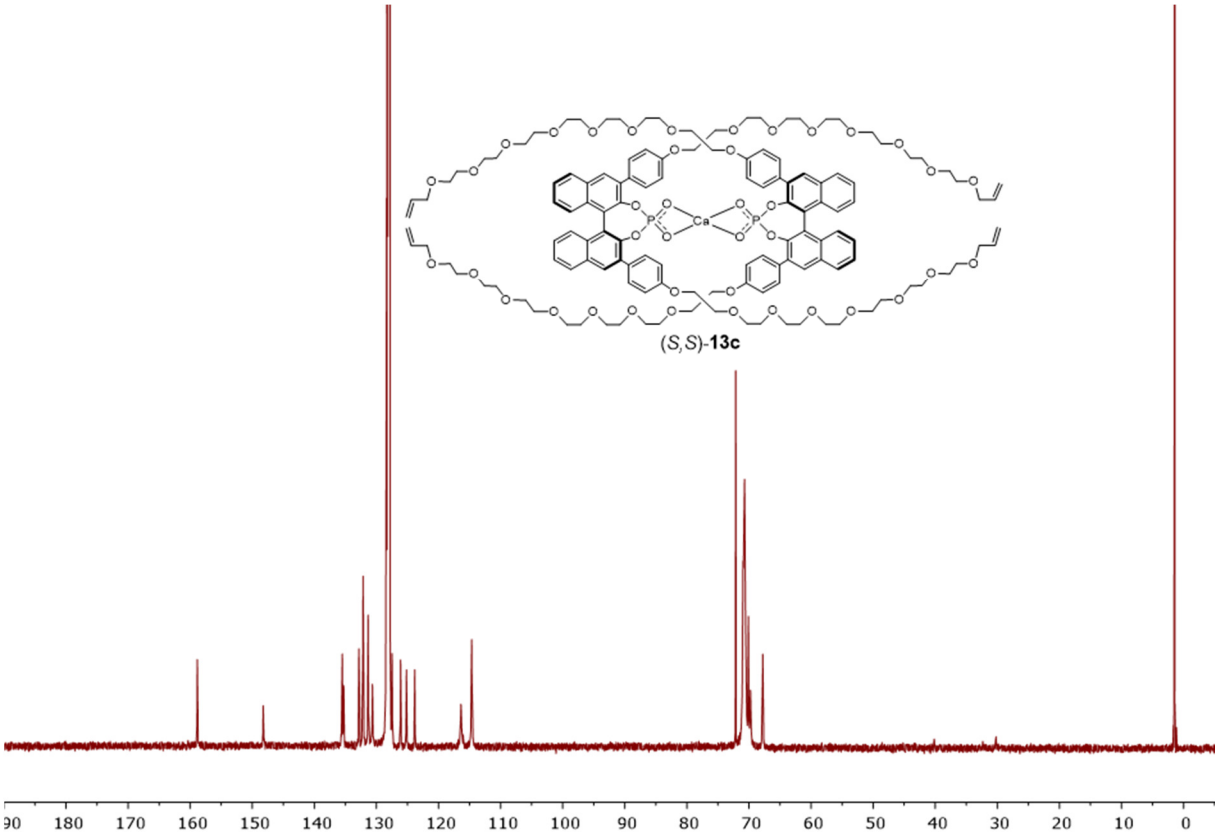

Figure S59: ^{13}C-NMR spectrum of (S,S)-**13c** (298 K, 150 MHz, [D_6]-benzene).

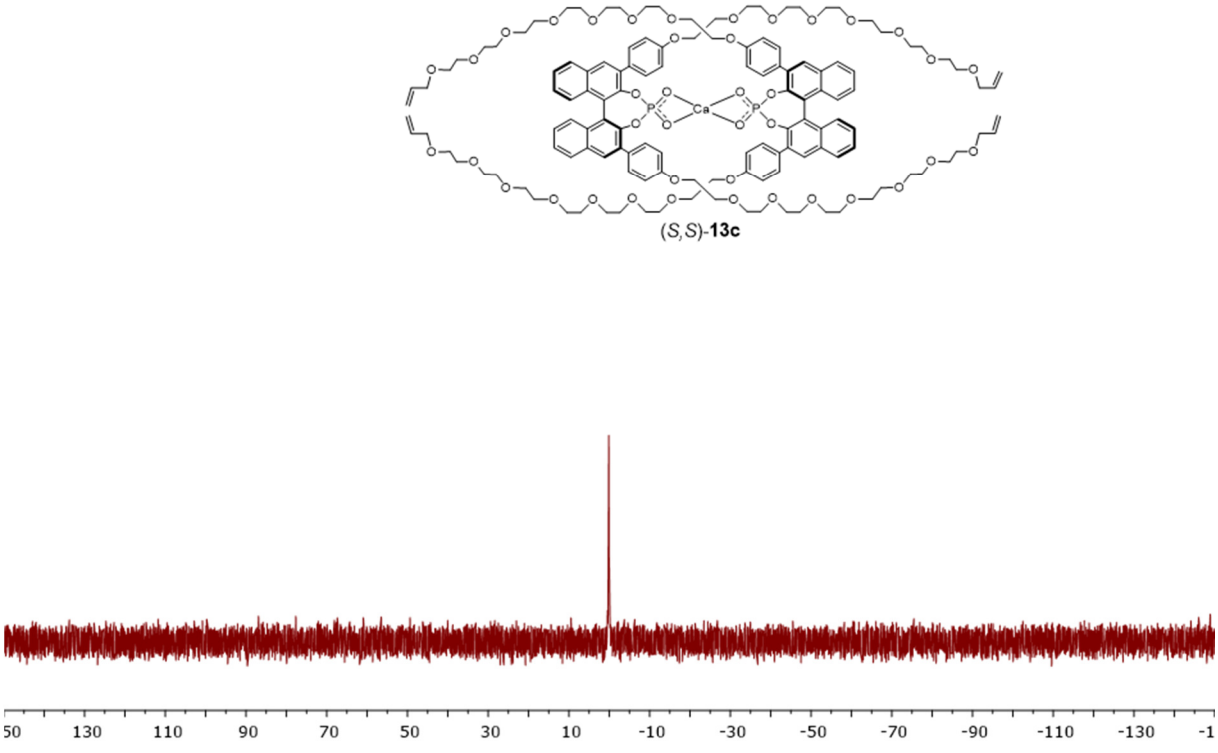

Figure S60: ^{31}P-NMR spectrum of (*S,S*)-1**3c** (298 K, 122 MHz, [D_6]-benzene).

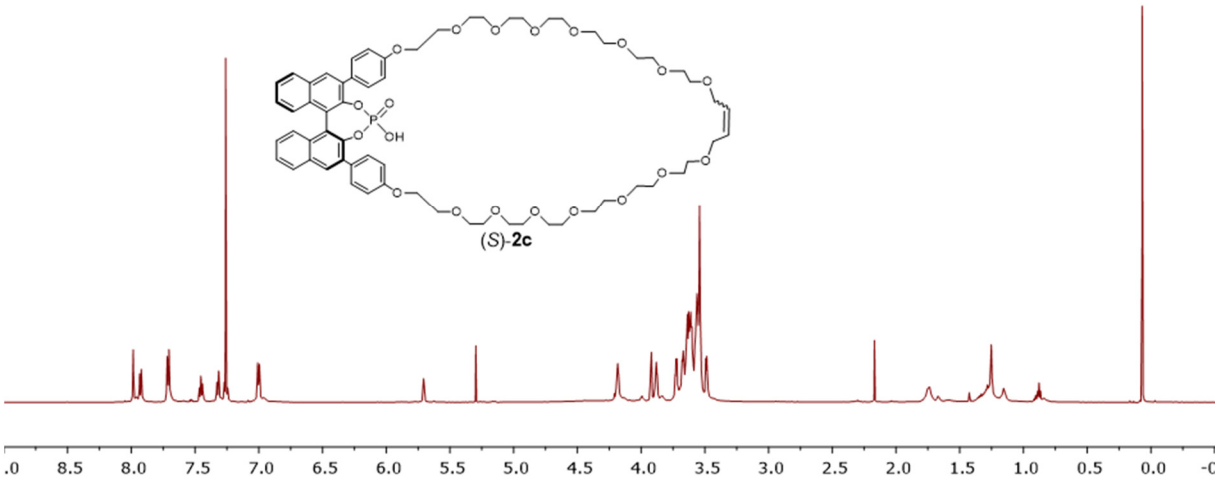

Figure S61*:* ^{1}H-NMR spectrum of (*S*)-**2c** (298 K, 600 MHz, [D_1]-chloroform).

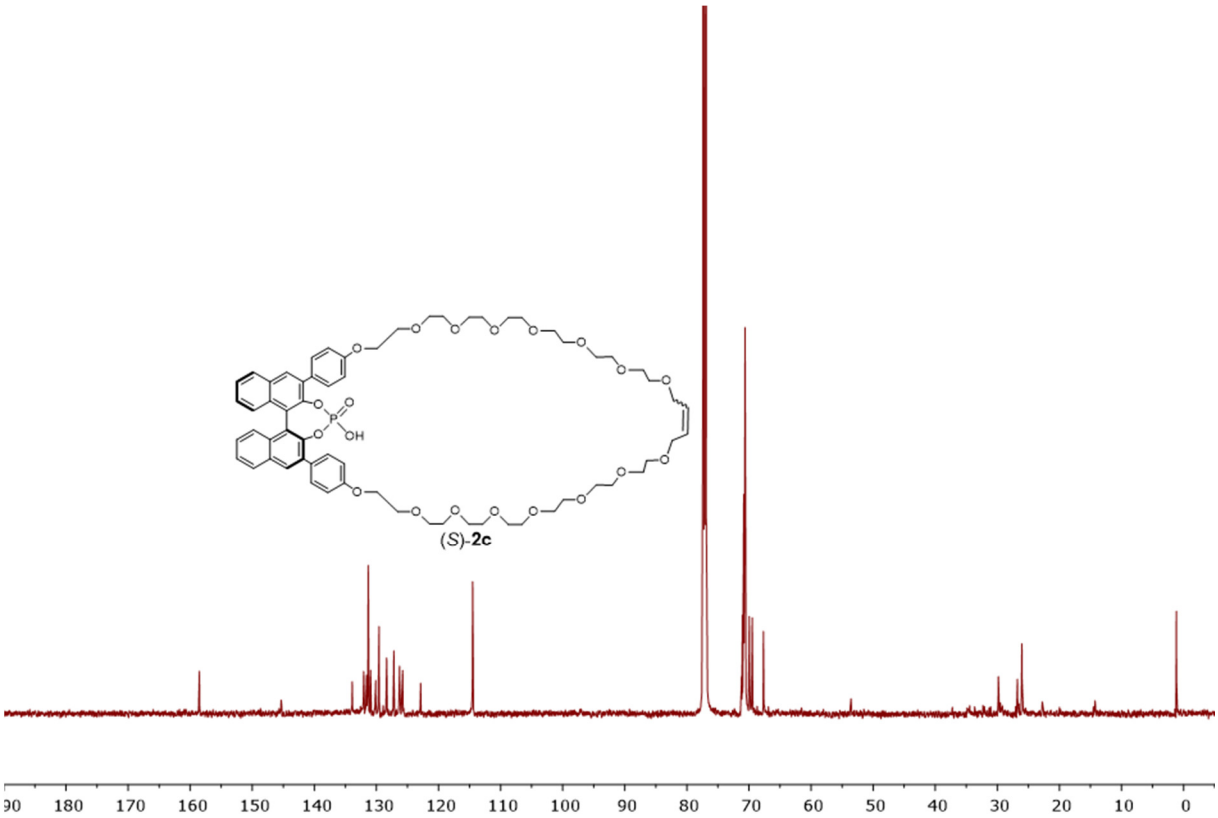

Figure S62: ^{13}C-NMR spectrum of (*S*)-**2c** (298 K, 150 MHz, [D_1]-chloroform).

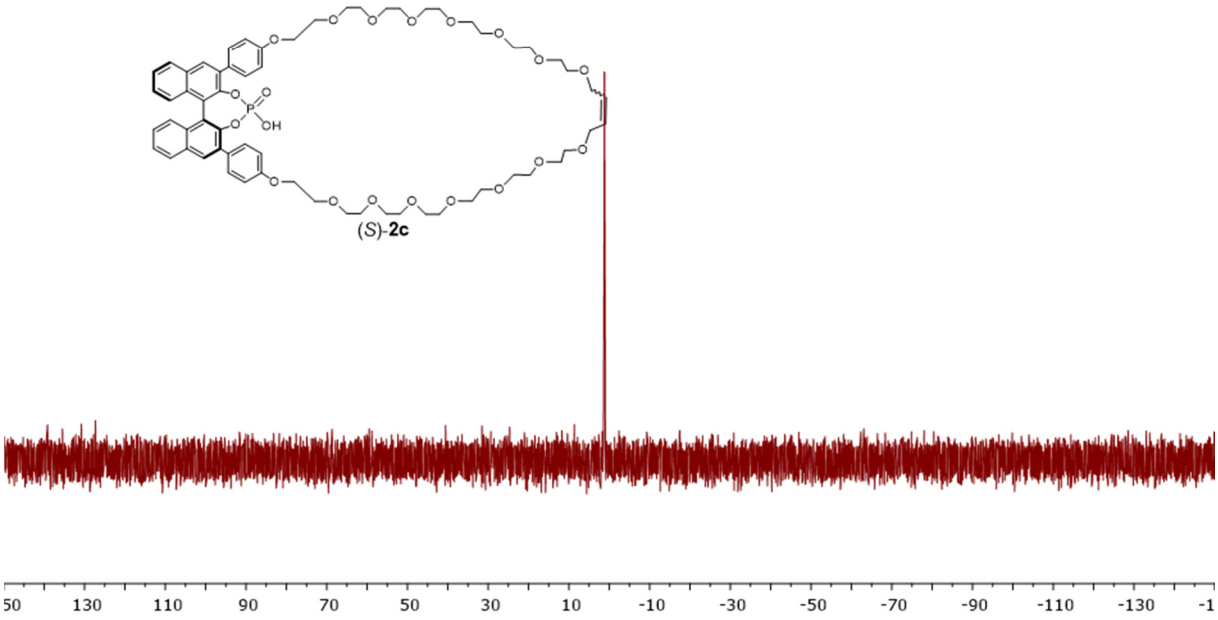

Figure S63: ^{31}P-NMR spectrum of (*S*)-**2c** (298 K, 122 MHz, [D$_1$]-chloroform).

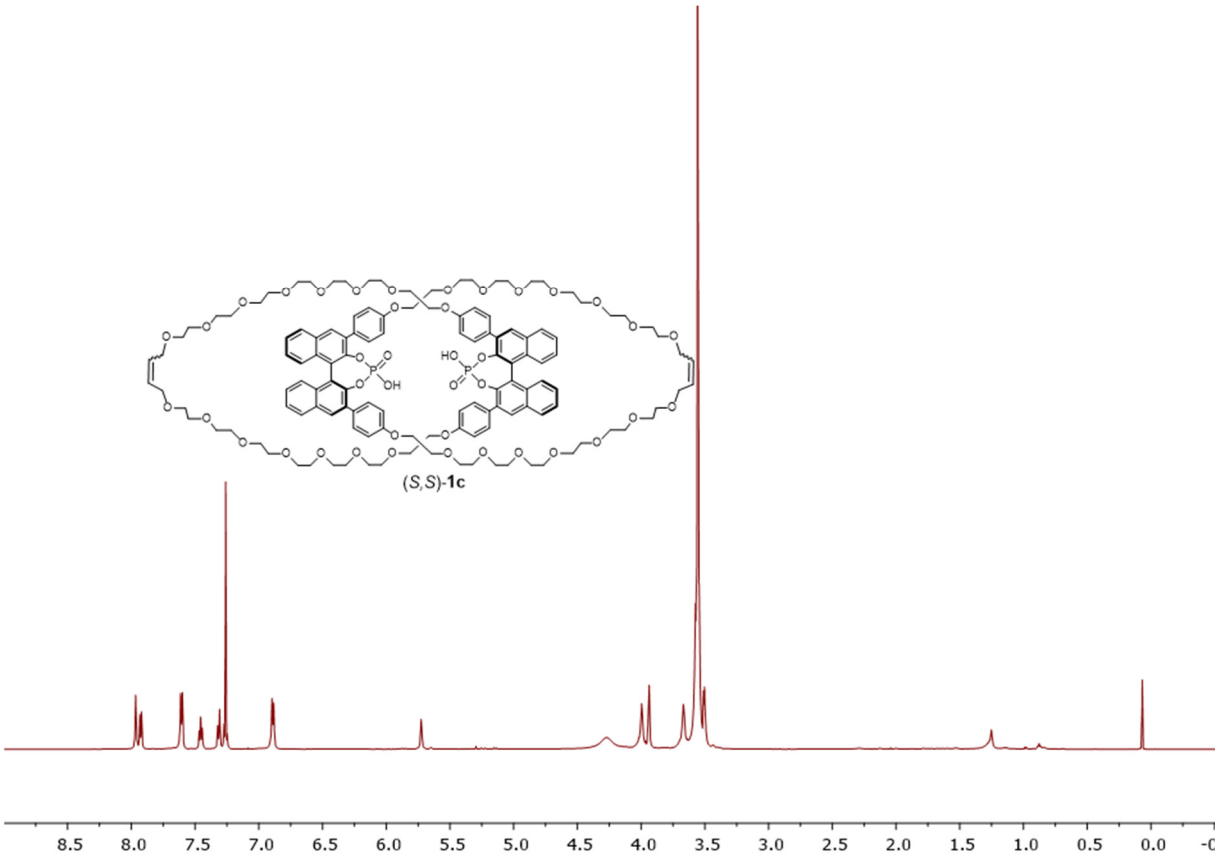

Figure S64: ^{1}H-NMR spectrum of (*S,S*)-**1c** (298 K, 600 MHz, [D$_1$]-chloroform).

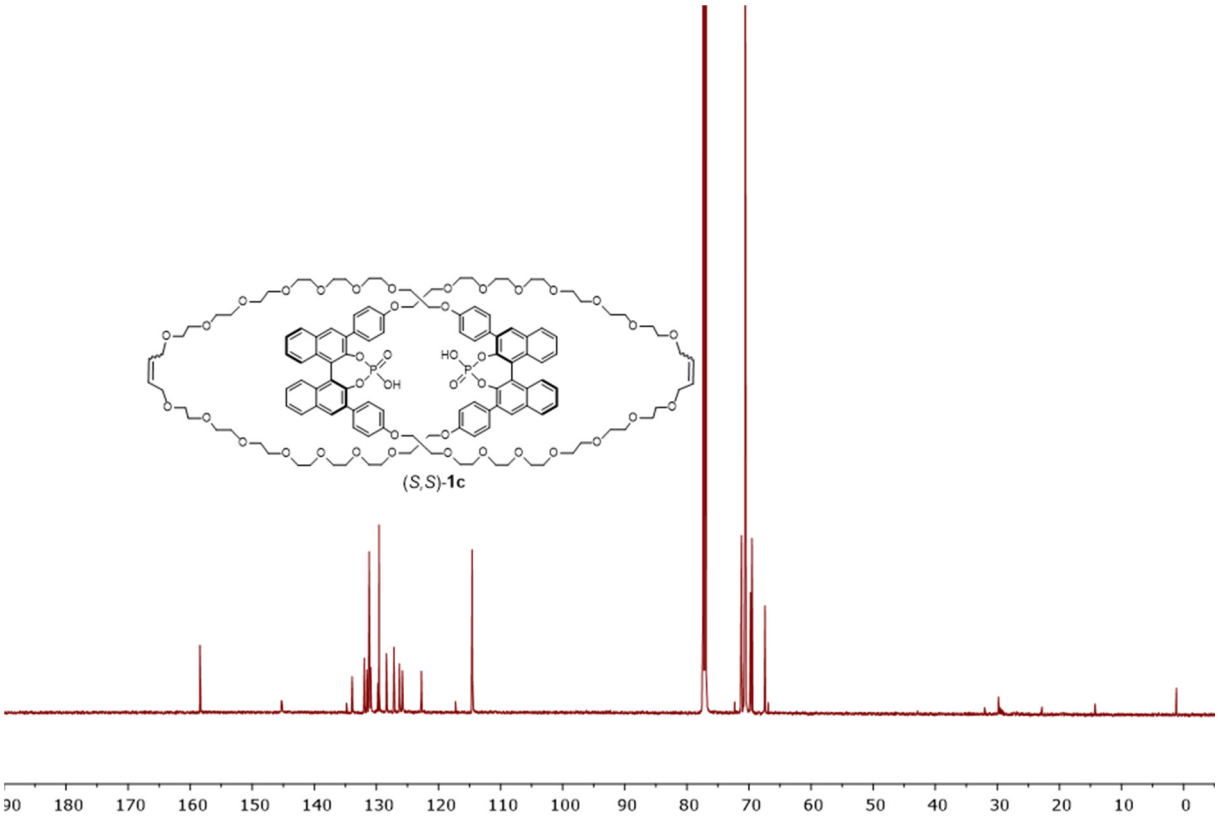

Figure S65: ^{13}C-NMR spectrum of (*S,S*)-**1c** (298 K, 150 MHz, [D$_1$]-chloroform).

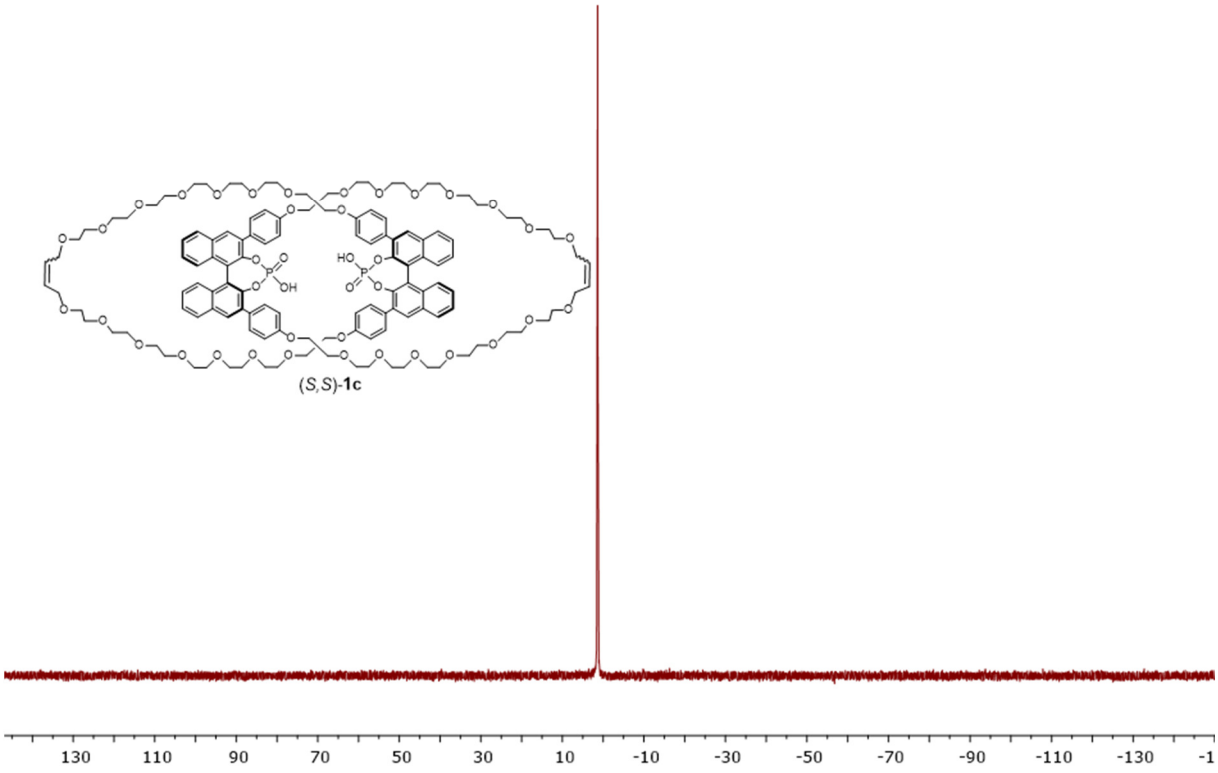

Figure S66: ^{31}P-NMR spectrum of (*S,S*)-**1c** (298 K, 243 MHz, [D$_1$]-chloroform).

8.2. MS/MS-spectra

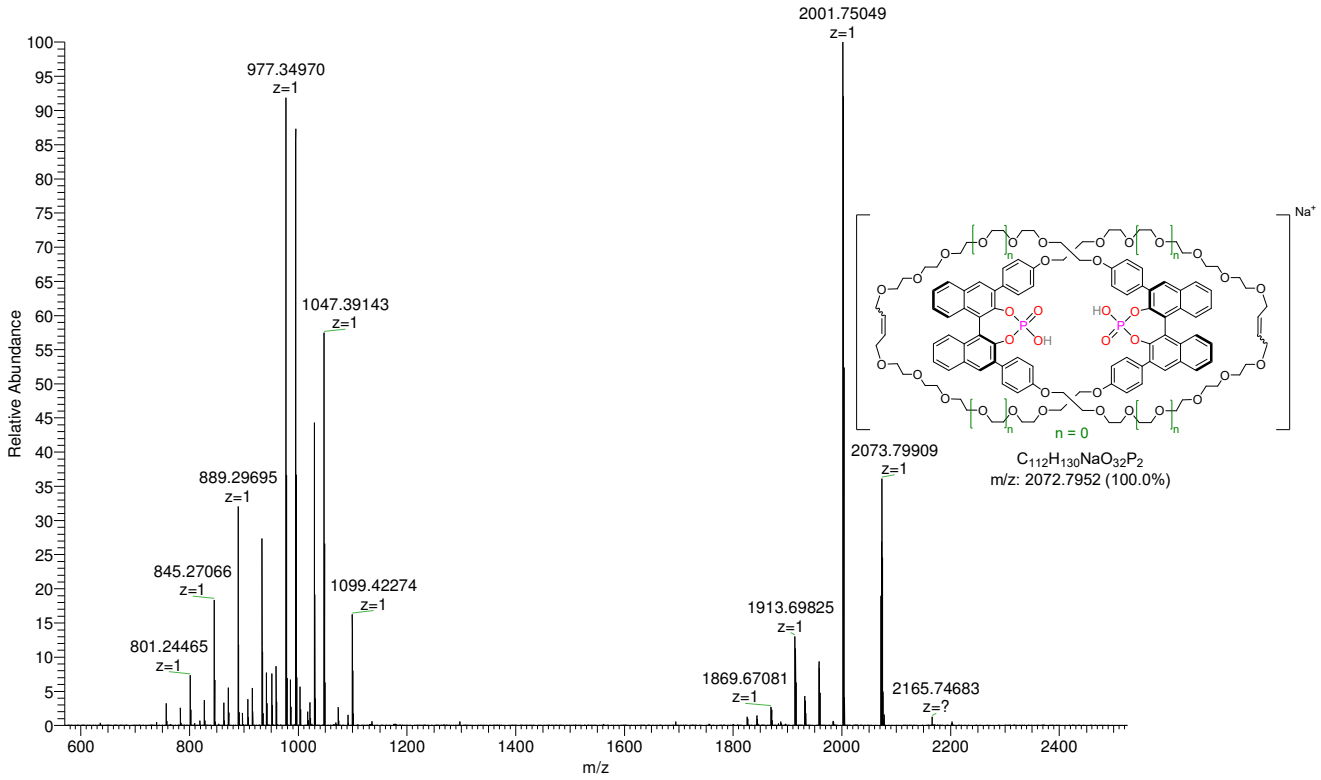

Figure S67: ESI-positive HCD-MS/MS spectrum of catenane **1a** (*m/z* = 2072.7952 @ 50 eV; range: *m/z* = 500-2500

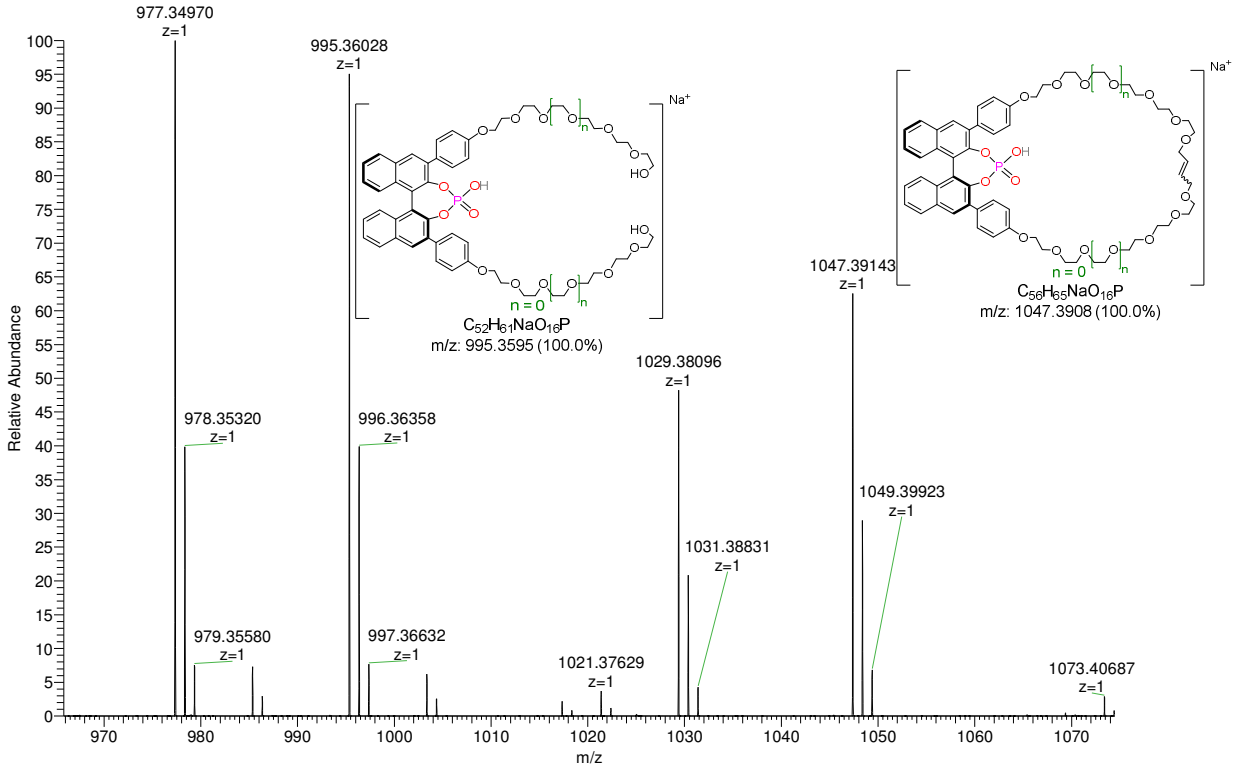

Figure S68: ESI-positive HCD-MS/MS spectrum of catenane **1-a** (*m/z* = 2072.7952 @ 50 eV). Zoom into region containing the intact macrocycle (*m/z* = 1047.3908) and the fragmented macrocycle (*m/z* = 995.3595)

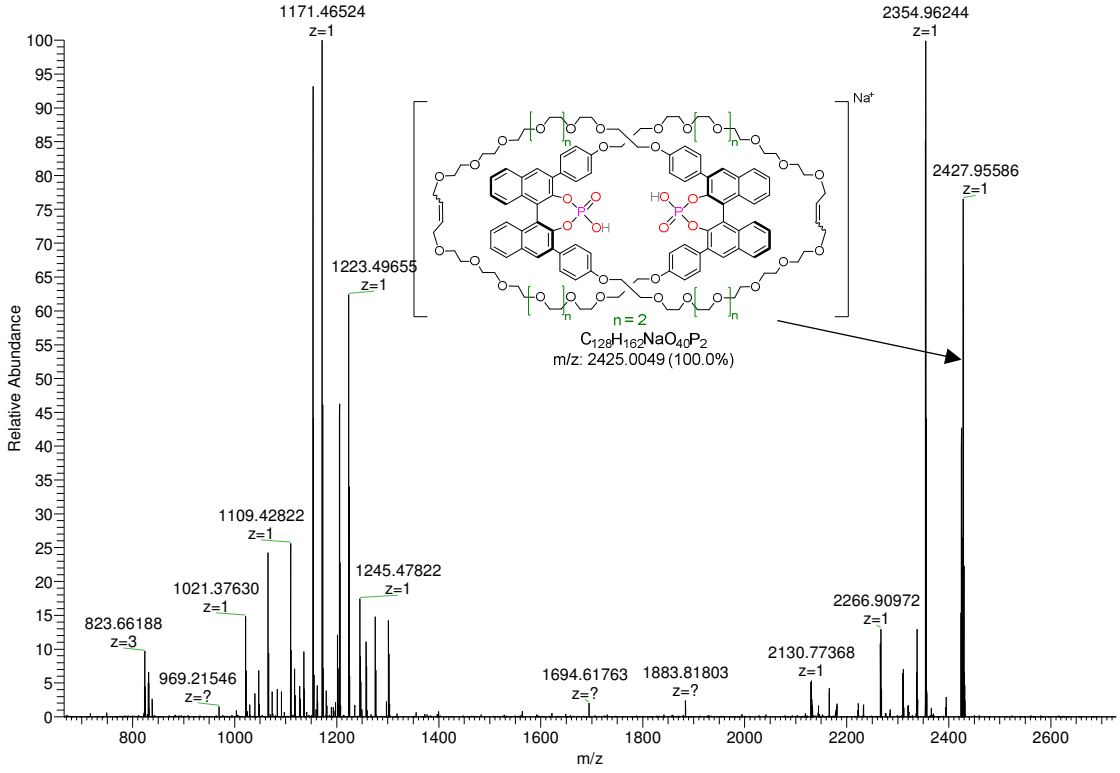

Figure S69: ESI-positive HCD-MS/MS spectrum of catenane **1-c** (*m/z* = 2425.0049 @ 50 eV; range: *m/z* = 500-2500).

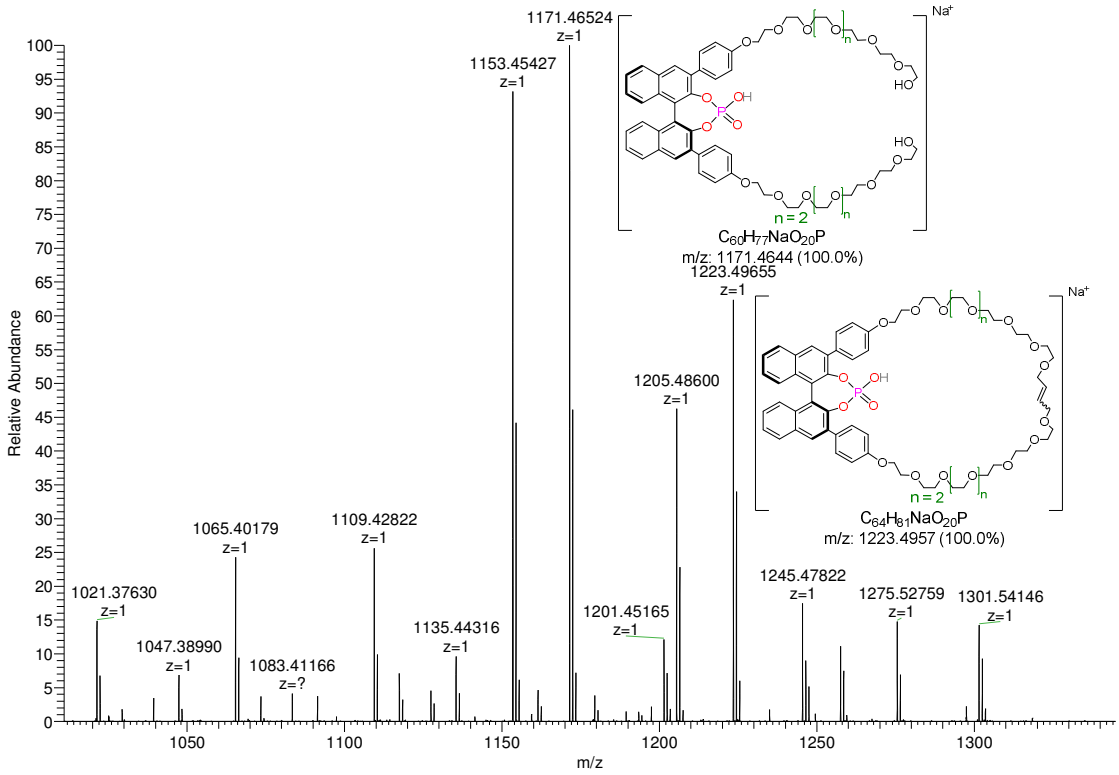

Figure S70: ESI-positive HCD-MS/MS spectrum of catenane **1-a** (*m/z* = 2072.7952 @ 50 eV). Zoom into region containing the intact macrocycle (*m/z* = 1223.4957) and the fragmented macrocycle (*m/z* = 1171.4644).

9. Appendix B: Kinetic investigations

9.1. Concentration vs. time data for catenanes 1a/b/c

a) b)

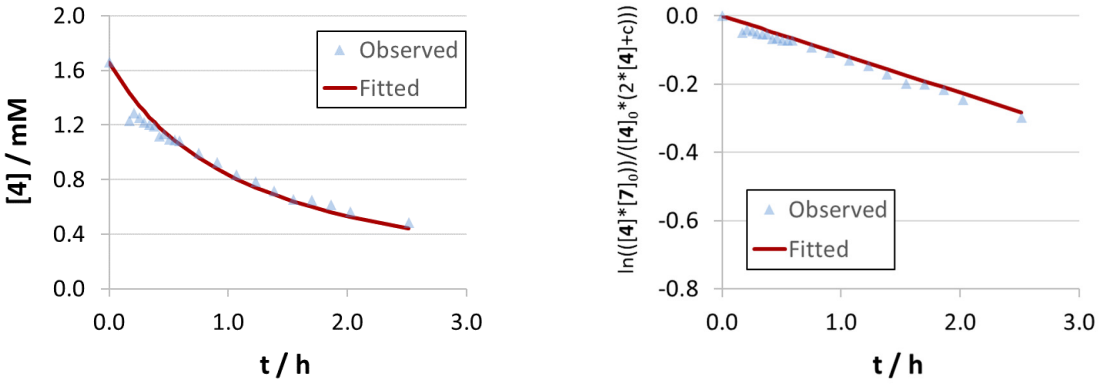

Figure S71: a) Curve of conversion and nonlinear fit. **b)** Linearization and linear fit of concentration vs. time data. Positive slope because of too less $[\mathbf{7}]_0$. Both: $[\mathbf{4}]_0$ = 1.66 mM, $[\mathbf{7}]_0$ = 3.87 mM, **1c** = 9.68 mol%.

Table S15: Concentration vs. time data for the catalytic reaction using catenane **1c** (9.68 mol%) as catalyst.

Time (h)	[**4**] (mM)	Nonlinear fit (mM)	$\ln(([\mathbf{4}]*[\mathbf{7}]_0))/([\mathbf{4}]_0*(2*[\mathbf{4}]+c))$
0.000	1.660	1.660	0.000
0.167	1.232	1.436	-0.048
0.209	1.285	1.387	-0.041
0.251	1.255	1.342	-0.045
0.294	1.218	1.299	-0.050
0.336	1.202	1.259	-0.053
0.378	1.190	1.221	-0.055
0.421	1.118	1.185	-0.067
0.463	1.133	1.150	-0.064
0.506	1.096	1.118	-0.071
0.548	1.092	1.087	-0.072
0.590	1.085	1.058	-0.073
0.749	0.993	0.959	-0.091
0.908	0.925	0.876	-0.107
1.067	0.837	0.805	-0.131
1.226	0.786	0.743	-0.147
1.385	0.717	0.689	-0.172
1.544	0.655	0.641	-0.198
1.703	0.648	0.599	-0.201
1.863	0.615	0.561	-0.217
2.022	0.563	0.527	-0.245
2.514	0.482	0.441	-0.299

a)

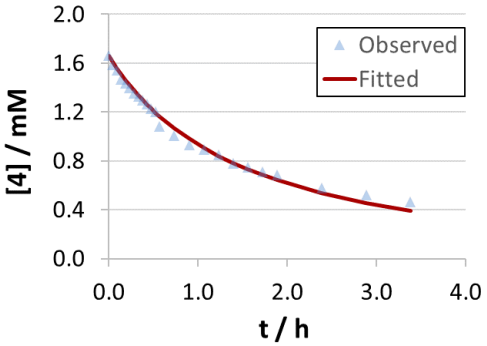

b)

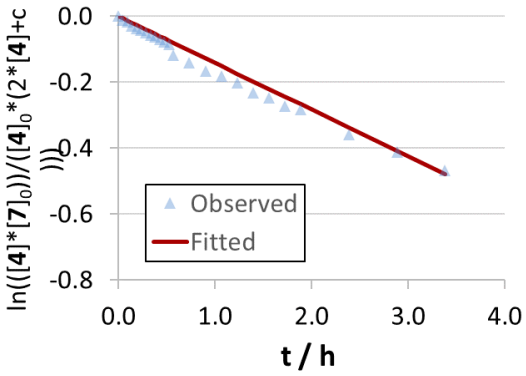

Figure S72: a) Curve of conversion and nonlinear fit. **b)** Linearization and linear fit of concentration vs. time data. Positive slope because of too less $[\mathbf{7}]_0$. Both: $[\mathbf{4}]_0$ = 1.66 mM, $[\mathbf{7}]_0$ = 4.32 mM, **1c** = 11.79 mol%.

Table S16: Concentration vs. time data for the catalytic reaction using catenane **1c** (11.79 mol%) as catalyst.

Time (h)	[**4**] (mM)	Nonlinear fit (mM)	$\ln(([\mathbf{4}]*[\mathbf{7}]_0))/([\mathbf{4}]_0*(2*[\mathbf{4}]+c)))$
0.000	1.660	1.660	0.000
0.042	1.585	1.612	-0.011
0.090	1.545	1.559	-0.017
0.138	1.465	1.510	-0.030
0.185	1.433	1.463	-0.036
0.233	1.396	1.419	-0.043
0.281	1.355	1.377	-0.051
0.329	1.329	1.337	-0.056
0.377	1.295	1.299	-0.063
0.425	1.266	1.263	-0.070
0.473	1.227	1.228	-0.079
0.521	1.199	1.195	-0.085
0.569	1.080	1.164	-0.117
0.733	1.003	1.066	-0.141
0.898	0.932	0.981	-0.166
1.063	0.891	0.907	-0.182
1.227	0.846	0.842	-0.201
1.392	0.780	0.784	-0.232
1.556	0.750	0.732	-0.248
1.721	0.707	0.685	-0.272
1.885	0.687	0.643	-0.284
2.383	0.579	0.538	-0.359
2.881	0.519	0.456	-0.412
3.379	0.464	0.392	-0.468

a) b)

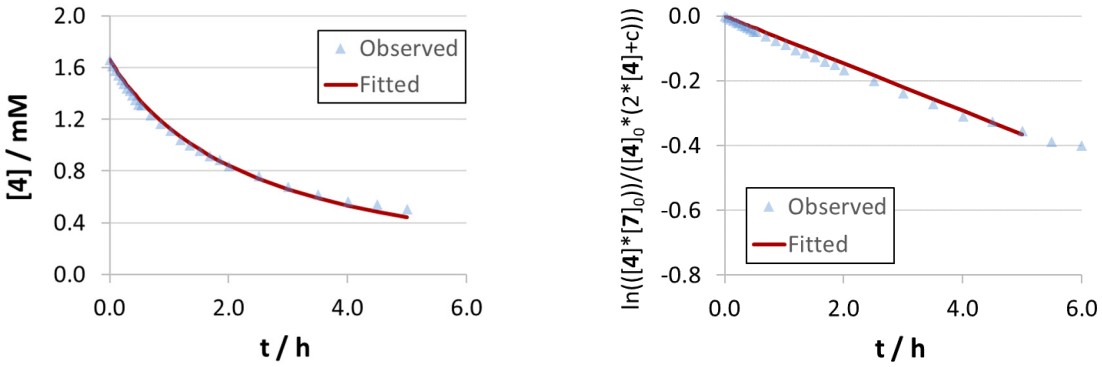

Figure S73: a) Curve of conversion and nonlinear fit. **b)** Linearization and linear fit of concentration vs. time data. Positive slope because of too less $[\mathbf{7}]_0$. Both: $[\mathbf{4}]_0$ = 1.66 mM, $[\mathbf{7}]_0$ = 4.08 mM, **1c** = 9.53 mol%.

Table S17*:* Concentration vs. time data for the catalytic reaction using catenane **1c** (9.53 mol%) as catalyst.

Time (h)	[**4**] (mM)	Nonlinear fit (mM)	ln(([4]*[7]0))/([4]0*(2*[4]+c)))
0.000	1.660	1.660	0.000
0.050	1.614	1.624	-0.005
0.098	1.578	1.590	-0.010
0.146	1.538	1.558	-0.015
0.194	1.504	1.527	-0.019
0.242	1.475	1.497	-0.023
0.290	1.438	1.468	-0.028
0.338	1.420	1.440	-0.031
0.385	1.385	1.413	-0.036
0.433	1.352	1.387	-0.042
0.481	1.313	1.362	-0.048
0.529	1.308	1.338	-0.049
0.694	1.230	1.259	-0.063
0.858	1.166	1.189	-0.076
1.023	1.112	1.125	-0.088
1.188	1.040	1.067	-0.105
1.352	1.001	1.014	-0.115
1.517	0.958	0.965	-0.128
1.681	0.918	0.920	-0.140
1.846	0.886	0.879	-0.150
2.010	0.839	0.841	-0.167
2.508	0.758	0.740	-0.200
3.006	0.678	0.658	-0.238
3.504	0.621	0.590	-0.271
4.002	0.563	0.533	-0.309
4.500	0.540	0.484	-0.326
4.998	0.505	0.442	-0.355

9.2. Concentration vs. time data for catenane 1c

9.2.1. *Substrate orders*

a) b)

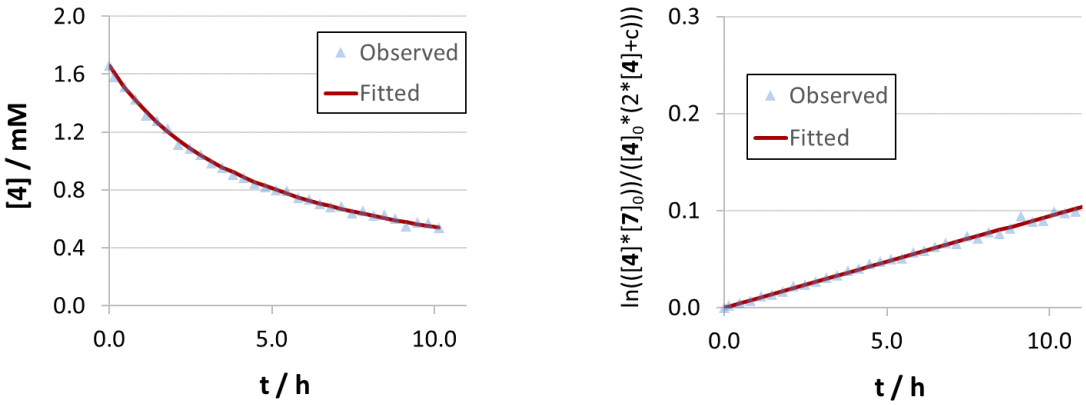

Figure S74: a) Curve of conversion and nonlinear fit. **b)** Linearization and linear fit of concentration vs. time data. Positive slope because of too less $[\mathbf{7}]_0$. Both: $[\mathbf{4}]_0$ = 1.66 mM, $[\mathbf{7}]_0$ = 3.18 mM, **1c** = 4.12 mol%.

Table S18*:* Concentration vs. time data for the catalytic reaction using catenane **1c** (4.12 mol%) as catalyst.

Time (h)	[**4**] (mM)	Nonlinear fit (mM)	ln(([4]*[7]0))/([4]0*(2*[4]+c)))
0.000	1.660	1.660	0.000
0.144	1.582	1.610	0.002
0.470	1.513	1.508	0.004
0.802	1.426	1.417	0.007
1.135	1.314	1.336	0.012
1.473	1.277	1.264	0.014
1.802	1.222	1.200	0.016
2.136	1.112	1.142	0.022
2.470	1.089	1.090	0.024
2.802	1.046	1.042	0.027
3.136	0.987	0.998	0.031
3.468	0.956	0.959	0.034
3.805	0.908	0.922	0.038
4.137	0.886	0.888	0.040
4.466	0.840	0.857	0.045
4.800	0.818	0.827	0.047
5.134	0.798	0.800	0.050
5.469	0.791	0.775	0.051
5.804	0.745	0.751	0.057
6.136	0.734	0.729	0.058
6.468	0.704	0.708	0.063
6.801	0.681	0.688	0.067

7.134	0.685	0.670	0.066
7.468	0.642	0.652	0.074
7.801	0.655	0.636	0.071
8.134	0.622	0.620	0.078
8.469	0.630	0.605	0.076
8.801	0.604	0.591	0.082
9.134	0.551	0.577	0.095
9.470	0.574	0.564	0.089
9.803	0.572	0.552	0.089
10.134	0.537	0.540	0.099

a) b)

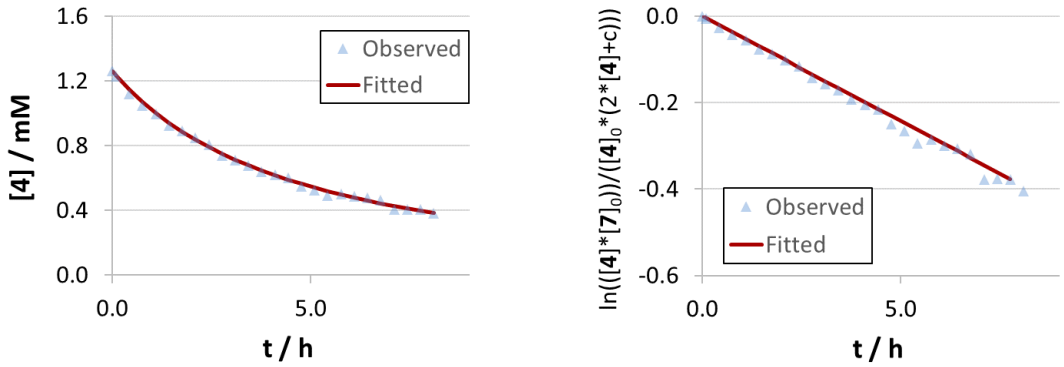

Figure S75: a) Curve of conversion and nonlinear fit. **b)** Linearization and linear fit of concentration vs. time data. Both: $[\mathbf{4}]_0$ = 1.26 mM, $[\mathbf{7}]_0$ = 3.22 mM, **1c** = 5.93 mol%.

Table S19: Concentration vs. time data for the catalytic reaction using catenane **1c** (5.93 mol%) as catalyst.

Time (h)	[**4**] (mM)	Nonlinear fit (mM)	ln(([4]*[7]0))/([4]0*(2*[4]+c)))
0.000	1.260	1.260	0.000
0.094	1.227	1.233	-0.006
0.427	1.121	1.146	-0.027
0.760	1.047	1.070	-0.043
1.094	0.997	1.002	-0.056
1.427	0.922	0.941	-0.077
1.760	0.890	0.886	-0.087
2.094	0.846	0.836	-0.101
2.427	0.804	0.791	-0.117
2.760	0.741	0.750	-0.142
3.094	0.708	0.713	-0.157
3.427	0.679	0.678	-0.171
3.760	0.638	0.646	-0.193
4.094	0.617	0.617	-0.204
4.427	0.599	0.590	-0.215
4.760	0.547	0.564	-0.250
5.094	0.526	0.540	-0.266
5.427	0.491	0.518	-0.294
5.760	0.501	0.498	-0.285
6.094	0.484	0.478	-0.299
6.427	0.476	0.460	-0.307
6.760	0.463	0.443	-0.319
7.094	0.405	0.427	-0.378
7.427	0.406	0.411	-0.377
7.760	0.406	0.397	-0.377
8.094	0.383	0.383	-0.405
0.000	1.260	1.260	0.000
0.094	1.227	1.233	-0.006

0.427	1.121	1.146	-0.027
0.760	1.047	1.070	-0.043
1.094	0.997	1.002	-0.056
1.427	0.922	0.941	-0.077

a) b)

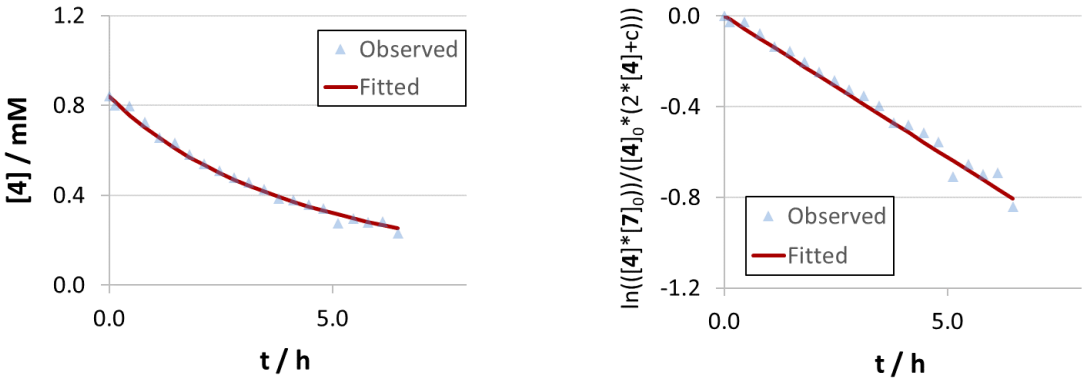

Figure S76: a) Curve of conversion and nonlinear fit. **b)** Linearization and linear fit of concentration vs. time data. Both: [**4**]$_0$ = 0.84 mM, [**7**]$_0$ = 3.40 mM, **1c** = 9.50 mol%.

Table S20: Concentration vs. time data for the catalytic reaction using catenane **1c** (9.50 mol%) as catalyst.

Time (s)	[**4**] (mM)	Nonlinear fit (mM)	ln(([4]*[7]0))/([4]0*(2*[4]+c)))
0.000	0.840	0.840	0.000
0.127	0.799	0.815	-0.025
0.461	0.798	0.755	-0.026
0.794	0.725	0.702	-0.077
1.127	0.655	0.653	-0.133
1.461	0.632	0.609	-0.154
1.794	0.581	0.570	-0.203
2.127	0.540	0.534	-0.247
2.461	0.509	0.501	-0.284
2.794	0.477	0.470	-0.325
3.127	0.457	0.442	-0.353
3.461	0.428	0.417	-0.397
3.794	0.384	0.393	-0.470
4.127	0.378	0.371	-0.482
4.461	0.359	0.350	-0.516
4.794	0.340	0.331	-0.556
5.127	0.276	0.314	-0.709
5.461	0.297	0.297	-0.655
5.794	0.279	0.282	-0.700
6.127	0.282	0.267	-0.693
6.461	0.232	0.254	-0.842

a) b)

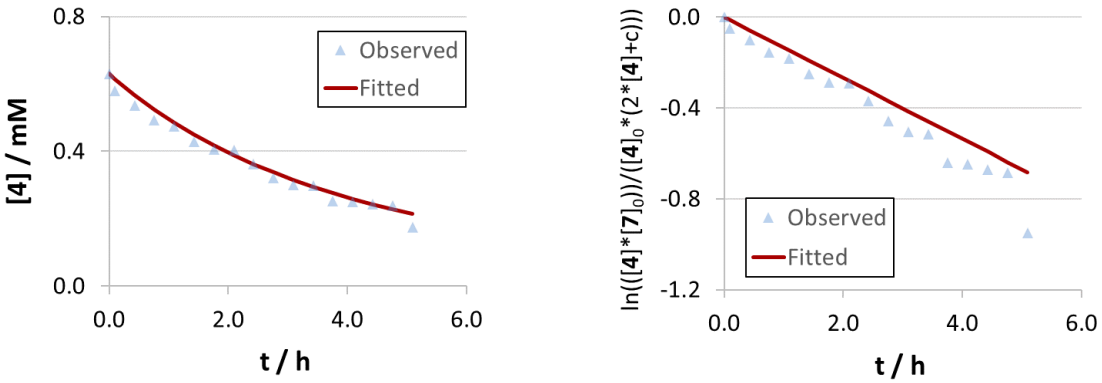

Figure S77: a) Curve of conversion and nonlinear fit. **b)** Linearization and linear fit of concentration vs. time data. Both: $[\mathbf{4}]_0$ = 0.63 mM, $[\mathbf{7}]_0$ = 3.17 mM, **1c** = 11.93 mol%.

Table S21: Concentration vs. time data for the catalytic reaction using catenane **1c** (11.93 mol%) as catalyst.

Time (h)	[**4**] (mM)	Nonlinear fit (mM)	ln(([4]*[7]0))/([4]0*(2*[4]+c)))
0.000	0.630	0.630	0.000
0.091	0.579	0.616	-0.052
0.424	0.536	0.567	-0.100
0.758	0.494	0.524	-0.154
1.091	0.473	0.485	-0.182
1.424	0.429	0.450	-0.249
1.758	0.405	0.418	-0.289
2.091	0.404	0.389	-0.290
2.424	0.362	0.362	-0.369
2.758	0.320	0.338	-0.459
3.091	0.301	0.316	-0.506
3.424	0.297	0.295	-0.516
3.758	0.253	0.276	-0.641
4.091	0.251	0.259	-0.648
4.424	0.243	0.243	-0.671
4.758	0.239	0.228	-0.686
5.091	0.174	0.214	-0.949

a) b)

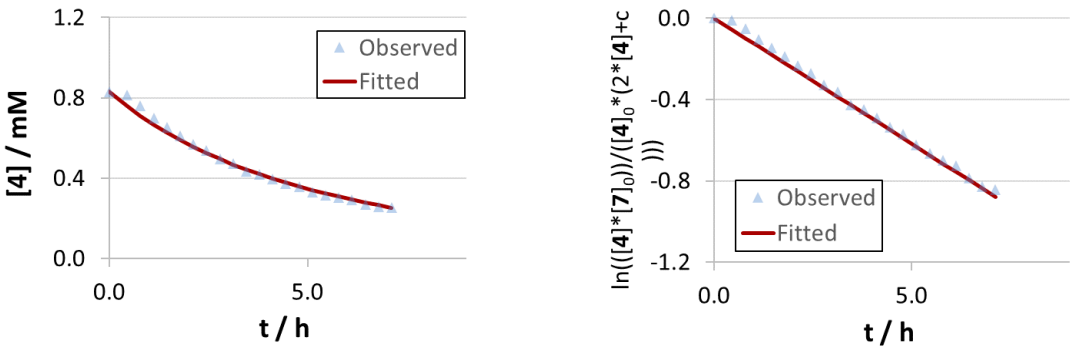

Figure S78: a) Curve of conversion and nonlinear fit. **b)** Linearization and linear fit of concentration vs. time data. Both: $[\mathbf{4}]_0$ = 0.83 mM, $[\mathbf{7}]_0$ = 3.94 mM, **1c** = 4.33 mol%.

Table S22: Concentration vs. time data for the catalytic reaction using catenane **1c** (4.33 mol%) as catalyst.

Time (h)	[**4**] (mM)	Nonlinear fit (mM)	ln(([4]*[7]0))/([4]0*(2*[4]+c)))
0.000	0.830	0.830	0.000
0.456	0.816	0.758	-0.010
0.789	0.760	0.710	-0.052
1.122	0.698	0.667	-0.104
1.456	0.653	0.627	-0.146
1.789	0.611	0.590	-0.189
2.122	0.569	0.556	-0.235
2.456	0.540	0.525	-0.271
2.789	0.496	0.496	-0.329
3.122	0.474	0.469	-0.361
3.456	0.433	0.443	-0.426
3.789	0.420	0.420	-0.449
4.122	0.395	0.398	-0.493
4.456	0.373	0.378	-0.535
4.789	0.356	0.358	-0.570
5.122	0.332	0.340	-0.624
5.456	0.316	0.324	-0.664
5.789	0.302	0.308	-0.698
6.122	0.292	0.293	-0.725
6.456	0.270	0.279	-0.787
6.789	0.257	0.265	-0.829
7.122	0.253	0.253	-0.843

a) b)

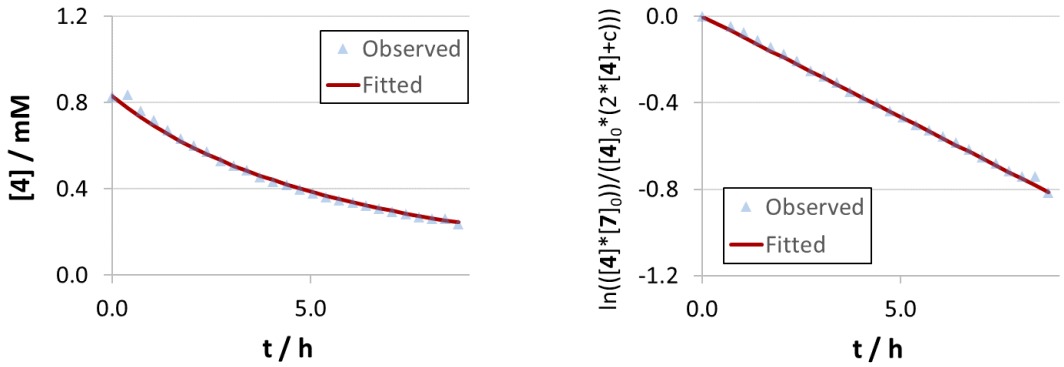

Figure S79: a) Curve of conversion and nonlinear fit. **b)** Linearization and linear fit of concentration vs. time data. Both: $[\mathbf{4}]_0$ = 0.83 mM, $[\mathbf{7}]_0$ = 3.34 mM, **1c** = 4.32 mol%.

Table S23: Concentration vs. time data for the catalytic reaction using catenane **1c** (4.32 mol%) as catalyst.

Time (h)	[**4**] (mM)	Nonlinear fit (mM)	ln(([4]*[7]0))/([4]0*(2*[4]+c)))
0.000	0.830	0.830	0.000
0.389	0.835	0.775	0.003
0.722	0.760	0.732	-0.045
1.056	0.717	0.692	-0.076
1.389	0.673	0.655	-0.111
1.722	0.635	0.621	-0.144
2.056	0.601	0.590	-0.175
2.389	0.572	0.561	-0.205
2.722	0.529	0.533	-0.252
3.056	0.508	0.508	-0.277
3.389	0.486	0.484	-0.305
3.722	0.454	0.462	-0.348
4.056	0.434	0.441	-0.378
4.389	0.417	0.421	-0.404
4.722	0.397	0.402	-0.437
5.056	0.381	0.385	-0.465
5.389	0.361	0.369	-0.503
5.722	0.349	0.353	-0.527
6.056	0.335	0.338	-0.555
6.389	0.322	0.324	-0.583
6.722	0.308	0.311	-0.616
7.056	0.293	0.298	-0.653
7.389	0.282	0.287	-0.682
7.722	0.269	0.275	-0.717
8.056	0.261	0.264	-0.741
8.389	0.261	0.254	-0.742
8.722	0.237	0.244	-0.815

a) b)

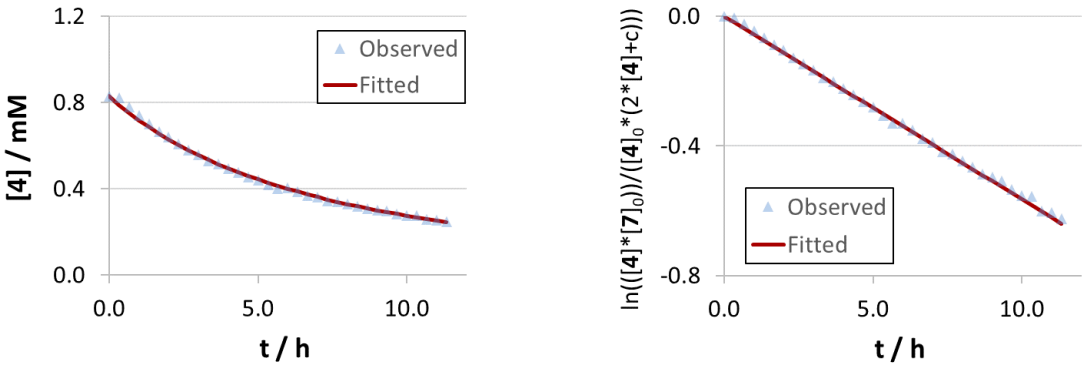

Figure S80: a) Curve of conversion and nonlinear fit. **b)** Linearization and linear fit of concentration vs. time data. Both: [**4**]$_0$ = 0.83 mM, [**7**]$_0$ = 2.63 mM, **1c** = 4.37 mol%.

Table S24*:* Concentration vs. time data for the catalytic reaction using catenane **1c** (4.37 mol%) as catalyst.

Time (h)	[**4**] (mM)	Nonlinear Fit (mM)	ln(([4]*[7]0))/([4]0*(2*[4]+c)))
0.000	0.830	0.830	0.000
0.333	0.790	0.822	-0.004
0.667	0.753	0.778	-0.024
1.000	0.719	0.739	-0.045
1.333	0.687	0.700	-0.066
1.667	0.657	0.665	-0.087
2.000	0.629	0.639	-0.104
2.333	0.603	0.606	-0.127
2.667	0.579	0.579	-0.148
3.000	0.556	0.557	-0.166
3.333	0.535	0.531	-0.189
3.667	0.514	0.517	-0.202
4.000	0.495	0.495	-0.222
4.333	0.477	0.475	-0.243
4.667	0.460	0.456	-0.264
5.000	0.444	0.442	-0.280
5.333	0.429	0.420	-0.307
5.667	0.414	0.402	-0.331
6.000	0.400	0.403	-0.330
6.333	0.387	0.387	-0.352
6.667	0.374	0.370	-0.377
7.000	0.362	0.361	-0.391
7.333	0.351	0.345	-0.418
7.667	0.340	0.340	-0.426
8.000	0.329	0.328	-0.447
8.333	0.319	0.318	-0.465
8.667	0.310	0.307	-0.488

9.000	0.301	0.302	-0.497
9.333	0.292	0.297	-0.508
9.667	0.283	0.284	-0.536
10.000	0.275	0.276	-0.554

a) b)

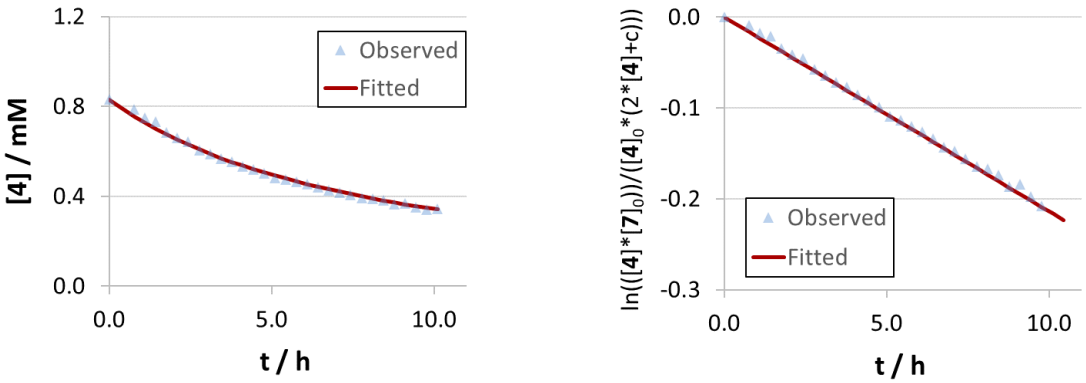

Figure S81: a) Curve of conversion and nonlinear fit. **b)** Linearization and linear fit of concentration vs. time data. Both: [**4**]$_0$ = 0.83 mM, [**7**]$_0$ = 1.98 mM, **1c** = 4.26 mol%.

Table S25: Concentration vs. time data for the catalytic reaction using catenane **1c** (4.26 mol%) as catalyst.

Time (h)	[**4**] (mM)	Nonlinear fit (mM)	ln(([4]*[7]0))/([4]0*(2*[4]+c)))
0.000	0.830	0.830	0.000
0.767	0.786	0.755	-0.009
1.100	0.748	0.727	-0.018
1.433	0.733	0.700	-0.021
1.767	0.683	0.675	-0.034
2.100	0.659	0.651	-0.041
2.433	0.644	0.629	-0.046
2.767	0.606	0.608	-0.058
3.100	0.588	0.589	-0.064
3.433	0.567	0.570	-0.072
3.767	0.555	0.553	-0.077
4.100	0.534	0.536	-0.086
4.433	0.520	0.521	-0.092
4.767	0.504	0.506	-0.099
5.100	0.483	0.492	-0.110
5.433	0.476	0.478	-0.113
5.767	0.463	0.465	-0.120
6.100	0.452	0.453	-0.126
6.433	0.440	0.442	-0.134
6.767	0.425	0.430	-0.143
7.100	0.418	0.420	-0.148
7.433	0.405	0.409	-0.156
7.767	0.393	0.400	-0.165
8.100	0.390	0.390	-0.167
8.433	0.382	0.381	-0.173

8.767	0.366	0.372	-0.186
9.100	0.369	0.364	-0.184
9.433	0.352	0.356	-0.198
9.767	0.341	0.348	-0.208
10.100	0.343	0.341	-0.206

9.2.2. *Catalyst orders*

a) b)

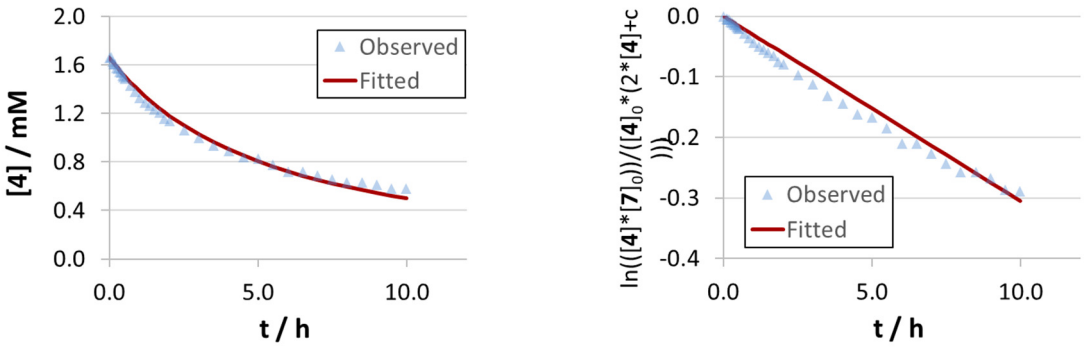

Figure S82: a) Curve of conversion and nonlinear fit. **b)** Linearization and linear fit of concentration vs. time data. Both: $[\mathbf{4}]_0$ = 1.66 mM, $[\mathbf{7}]_0$ = 4.05 mM, **1c** = 3.98 mol%.

Table S26*:* Concentration vs. time data for the catalytic reaction using catenane **1c** (3.98 mol%) as catalyst.

Time (h)	[**4**] (mM)	Nonlinear Fft (mM)	ln(([4]*[7]0))/([4]0*(2*[4]+c)))
0.000	1.660	1.660	0.000
0.050	1.667	1.644	0.001
0.098	1.626	1.629	-0.004
0.146	1.608	1.614	-0.006
0.194	1.606	1.600	-0.006
0.242	1.574	1.585	-0.010
0.290	1.568	1.571	-0.010
0.338	1.545	1.557	-0.013
0.385	1.540	1.544	-0.014
0.433	1.511	1.530	-0.018
0.481	1.498	1.517	-0.019
0.529	1.486	1.504	-0.021
0.694	1.430	1.461	-0.028
0.858	1.379	1.420	-0.036
1.023	1.331	1.381	-0.043
1.188	1.289	1.344	-0.050
1.352	1.265	1.309	-0.055
1.517	1.236	1.275	-0.060
1.681	1.207	1.243	-0.065
1.846	1.157	1.212	-0.075
2.010	1.136	1.182	-0.080
2.508	1.059	1.100	-0.097
3.006	0.998	1.028	-0.112
3.504	0.933	0.963	-0.131
4.002	0.890	0.906	-0.145
4.500	0.838	0.853	-0.162

4.998	0.825	0.806	-0.167
5.496	0.778	0.763	-0.185
5.994	0.721	0.724	-0.210
6.492	0.720	0.688	-0.211
6.990	0.687	0.655	-0.227
7.488	0.655	0.624	-0.244
7.985	0.630	0.596	-0.257
8.483	0.630	0.570	-0.257
8.981	0.612	0.545	-0.268
9.479	0.582	0.522	-0.287
9.977	0.580	0.501	-0.289

a) b)

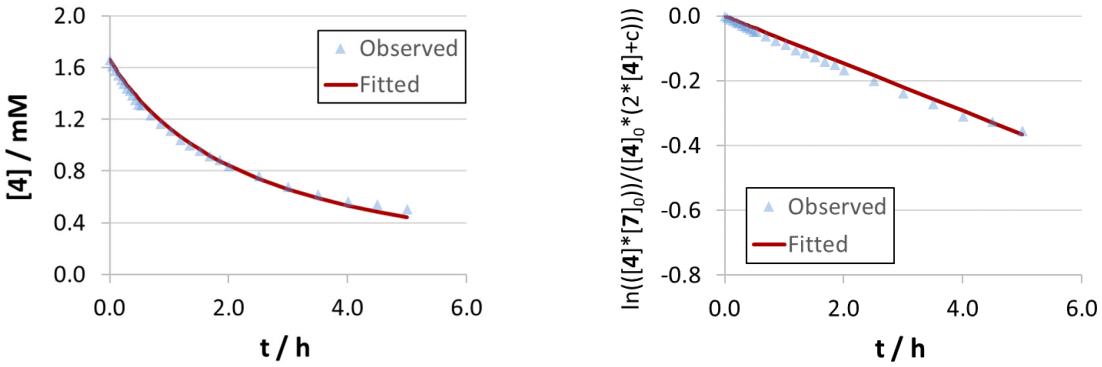

Figure S83: a) Curve of conversion and nonlinear fit. **b)** Linearization and linear fit of concentration vs. time data. Both: $[\mathbf{4}]_0$ = 1.66 mM, $[\mathbf{7}]_0$ = 4.08 mM, **1c** = 9.53 mol%.

Table S27*:* Concentration vs. time data for the catalytic reaction using catenane **1c** (9.53 mol%) as catalyst.

Time (h)	[**4**] (mM)	Nonlinear fit (mM)	ln(([4]*[7]0))/([4]0*(2*[4]+c)))
0.000	1.660	1.660	0.000
0.050	1.614	1.624	-0.005
0.098	1.578	1.590	-0.010
0.146	1.538	1.558	-0.015
0.194	1.504	1.527	-0.019
0.242	1.475	1.497	-0.023
0.290	1.438	1.468	-0.028
0.338	1.420	1.440	-0.031
0.385	1.385	1.413	-0.036
0.433	1.352	1.387	-0.042
0.481	1.313	1.362	-0.048
0.529	1.308	1.338	-0.049
0.694	1.230	1.259	-0.063
0.858	1.166	1.189	-0.076
1.023	1.112	1.125	-0.088
1.188	1.040	1.067	-0.105
1.352	1.001	1.014	-0.115
1.517	0.958	0.965	-0.128
1.681	0.918	0.920	-0.140
1.846	0.886	0.879	-0.150
2.010	0.839	0.841	-0.167
2.508	0.758	0.740	-0.200
3.006	0.678	0.658	-0.238
3.504	0.621	0.590	-0.271
4.002	0.563	0.533	-0.309
4.500	0.540	0.484	-0.326
4.998	0.505	0.442	-0.355

a) b)

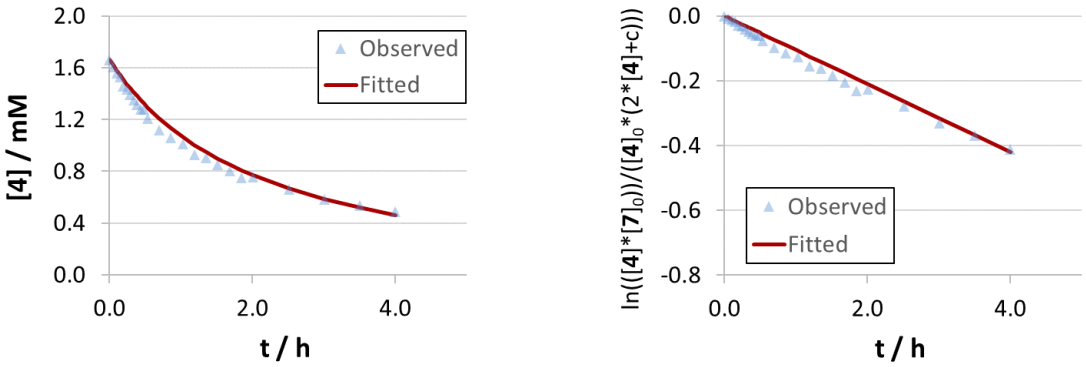

Figure S84: a) Curve of conversion and nonlinear fit. **b)** Linearization and linear fit of concentration vs. time data. Both: $[\mathbf{4}]_0$ = 1.66 mM, $[\mathbf{7}]_0$ = 4.21 mM, **1c** = 15.13 mol%.

Table S28*:* Concentration vs. time data for the catalytic reaction using catenane **1c** (15.13 mol%) as catalyst.

Time (h)	[**4**] (mM)	Nonlinear fit (mM)	ln(([4]*[7]0))/([4]0*(2*[4]+c)))
0.000	1.660	1.660	0.000
0.050	1.603	1.618	-0.007
0.098	1.558	1.580	-0.014
0.146	1.527	1.543	-0.018
0.194	1.457	1.508	-0.029
0.242	1.435	1.474	-0.033
0.290	1.389	1.441	-0.040
0.338	1.350	1.410	-0.047
0.385	1.312	1.380	-0.055
0.433	1.280	1.351	-0.061
0.481	1.280	1.323	-0.061
0.529	1.205	1.296	-0.077
0.694	1.116	1.210	-0.098
0.858	1.058	1.134	-0.114
1.023	1.011	1.065	-0.127
1.188	0.926	1.004	-0.155
1.352	0.903	0.948	-0.163
1.517	0.849	0.897	-0.184
1.681	0.801	0.851	-0.204
1.846	0.746	0.808	-0.230
2.010	0.753	0.769	-0.227
2.508	0.658	0.667	-0.279
3.006	0.582	0.586	-0.330
3.504	0.534	0.519	-0.369
4.002	0.486	0.463	-0.412

a) b)

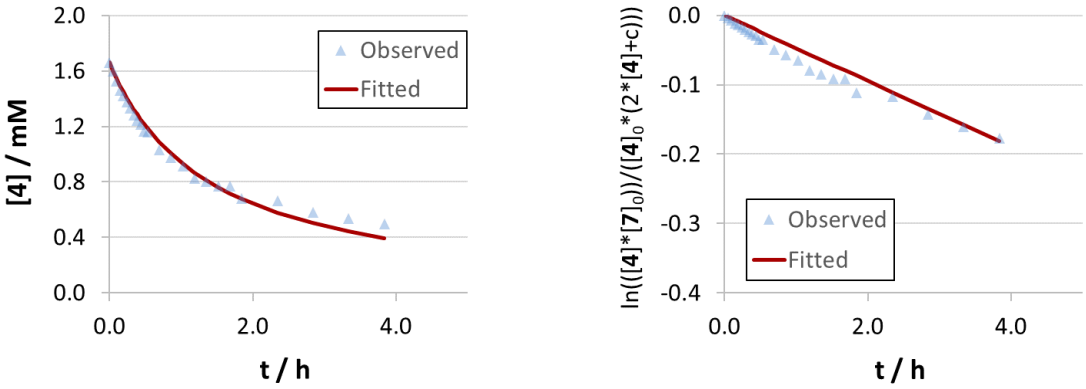

Figure S85: a) Curve of conversion and nonlinear fit. **b)** Linearization and linear fit of concentration vs. time data. Both: [**4**]$_0$ = 1.66 mM, [**7**]$_0$ = 3.62 mM, **1c** = 21.19 mol%.

Table S29: Concentration vs. time data for the catalytic reaction using catenane **1c** (21.19 mol%) as catalyst.

Time (h)	[**4**] (mM)	Nonlinear fit (mM)	ln(([4]*[7]0))/([4]0*(2*[4]+c)))
0.000	1.660	1.660	0.000
0.050	1.597	1.601	-0.003
0.098	1.525	1.547	-0.007
0.146	1.457	1.497	-0.011
0.194	1.422	1.450	-0.014
0.242	1.378	1.406	-0.017
0.290	1.332	1.364	-0.020
0.338	1.281	1.325	-0.024
0.385	1.244	1.287	-0.027
0.433	1.213	1.252	-0.030
0.481	1.163	1.218	-0.035
0.529	1.158	1.186	-0.035
0.694	1.029	1.088	-0.049
0.858	0.972	1.004	-0.057
1.023	0.915	0.931	-0.065
1.188	0.827	0.867	-0.080
1.352	0.800	0.811	-0.085
1.517	0.766	0.762	-0.092
1.681	0.769	0.717	-0.091
1.846	0.683	0.677	-0.112
2.344	0.662	0.578	-0.117
2.842	0.580	0.502	-0.143
3.340	0.533	0.443	-0.161
3.838	0.495	0.394	-0.177

a) b)

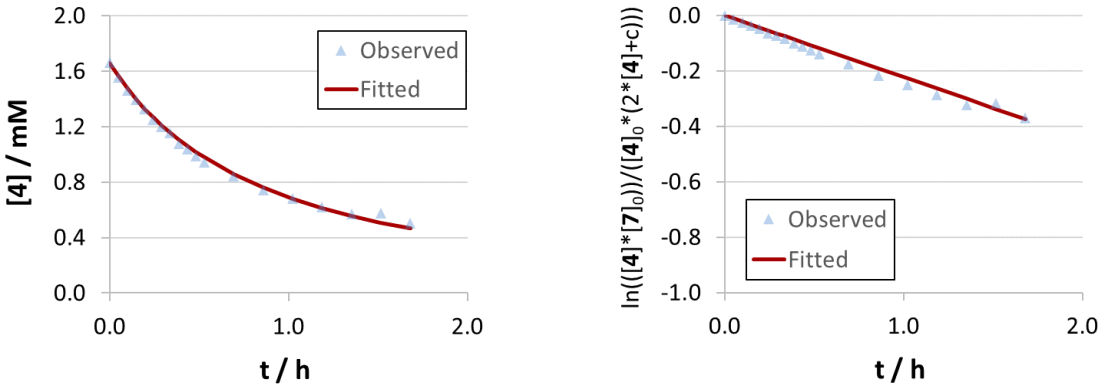

Figure S86: a) Curve of conversion and nonlinear fit. **b)** Linearization and linear fit of concentration vs. time data. Both: $[\mathbf{4}]_0$ = 1.66 mM, $[\mathbf{7}]_0$ = 4.13 mM, **1c** = 34.65 mol%.

Table S30: Concentration vs. time data for the catalytic reaction using catenane **1c** (34.65 mol%) as catalyst.

Time (h)	[**4**] (mM)	Nonlinear fit (mM)	ln(([4]*[7]0))/([4]0*(2*[4]+c)))
0.000	1.660	1.660	0.000
0.050	1.554	1.563	-0.013
0.098	1.463	1.479	-0.026
0.146	1.395	1.402	-0.037
0.194	1.327	1.333	-0.048
0.242	1.248	1.269	-0.063
0.290	1.201	1.210	-0.073
0.338	1.153	1.156	-0.083
0.385	1.079	1.106	-0.101
0.433	1.038	1.060	-0.112
0.481	0.988	1.017	-0.126
0.529	0.943	0.977	-0.139
0.694	0.841	0.857	-0.175
0.858	0.743	0.761	-0.217
1.023	0.680	0.681	-0.250
1.188	0.618	0.614	-0.287
1.352	0.567	0.556	-0.321
1.517	0.575	0.507	-0.316
1.681	0.506	0.465	-0.371

a) b)

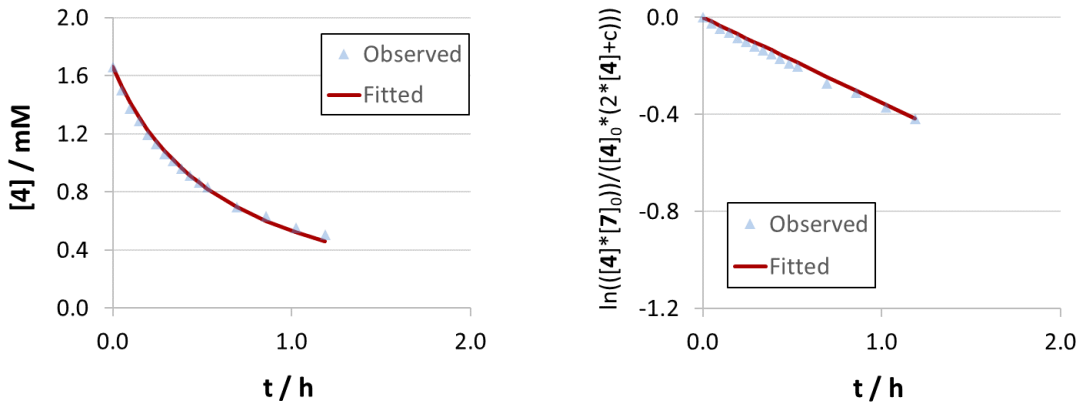

Figure S87: a) Curve of conversion and nonlinear fit. **b)** Linearization and linear fit of concentration vs. time data. Both: [**4**]$_0$ = 1.66 mM, [**7**]$_0$ = 4.29 mM, **1c** = 45.06 mol%.

Table S31*:* Concentration vs. time data for the catalytic reaction using catenane **1c** (45.06 mol%) as catalyst.

Time (h)	[**4**] (mM)	Nonlinear fit (mM)	ln(([4]*[7]0))/([4]0*(2*[4]+c)))
0.000	1.660	1.660	0.000
0.050	1.501	1.526	-0.024
0.098	1.377	1.415	-0.045
0.146	1.287	1.317	-0.063
0.194	1.195	1.231	-0.084
0.242	1.131	1.153	-0.100
0.290	1.063	1.084	-0.119
0.338	1.013	1.021	-0.135
0.385	0.960	0.964	-0.152
0.433	0.913	0.913	-0.169
0.481	0.866	0.865	-0.188
0.529	0.833	0.822	-0.202
0.694	0.696	0.697	-0.272
0.858	0.634	0.600	-0.311
1.023	0.555	0.522	-0.371
1.188	0.504	0.459	-0.417

9.2.3. *Product inhibition*

a) b)

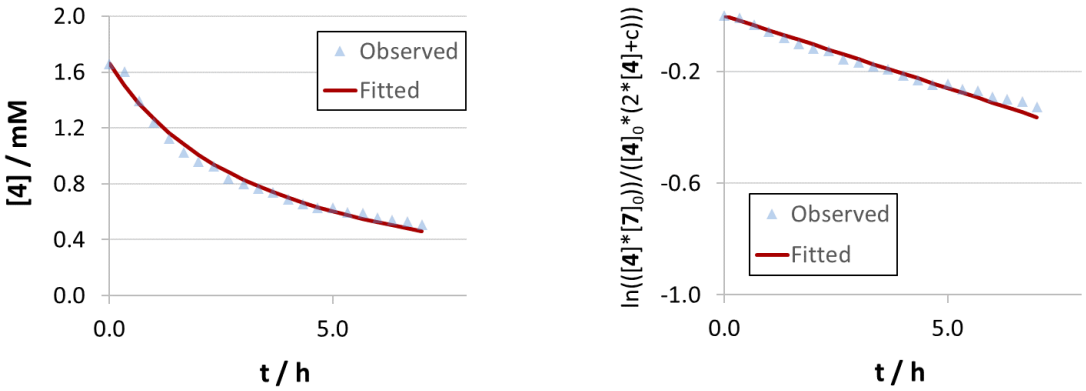

Figure S88: a) Curve of conversion and nonlinear fit. **b)** Linearization and linear fit of concentration vs. time data. Both: $[\mathbf{4}]_0$ = 1.26 mM, $[\mathbf{7}]_0$ = 3.12 mM, $[\mathbf{8}]_0$ = 0.90 mM, **1c** = 9.33 mol%.

Table S32*:* Concentration vs. time data for the catalytic reaction using catenane **1c** (9.33 mol%) as catalyst.

Time (h)	[**4**] (mM)	Nonlinear fit (mM)	ln(([4]*[7]0))/([4]0*(2*[4]+c)))
0.000	1.660	1.660	0.000
0.333	1.601	1.504	-0.006
0.667	1.394	1.374	-0.032
1.000	1.237	1.262	-0.056
1.333	1.121	1.165	-0.078
1.667	1.025	1.081	-0.100
2.000	0.958	1.007	-0.117
2.333	0.927	0.942	-0.126
2.667	0.836	0.883	-0.155
3.000	0.801	0.831	-0.167
3.333	0.765	0.783	-0.181
3.667	0.740	0.740	-0.192
4.000	0.691	0.701	-0.213
4.333	0.658	0.665	-0.230
4.667	0.629	0.632	-0.246
5.000	0.631	0.602	-0.245
5.333	0.597	0.574	-0.264
5.667	0.588	0.548	-0.270
6.000	0.554	0.524	-0.292
6.333	0.543	0.502	-0.300
6.667	0.530	0.481	-0.309
7.000	0.505	0.461	-0.328

9.3. Concentration vs. time data for macrocycle 2c

9.3.1. *Substrate orders*

a) b)

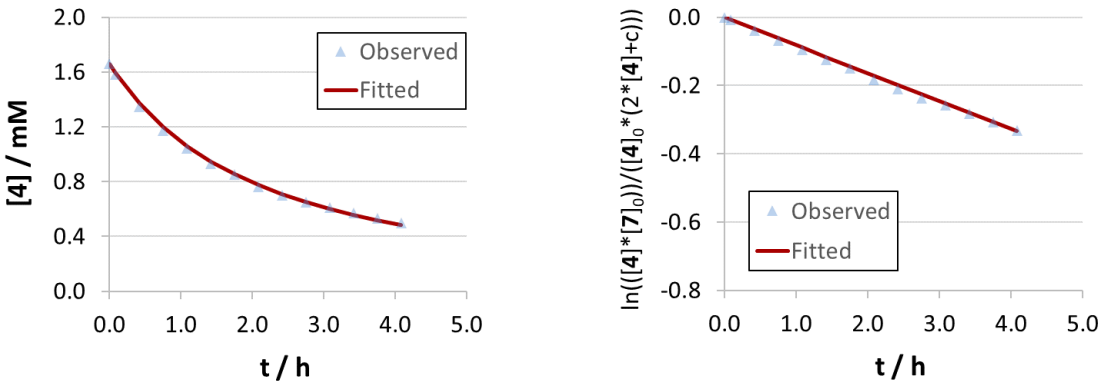

Figure S89: a) Curve of conversion and nonlinear fit. **b)** Linearization and linear fit of concentration vs. time data. Both: [**4**]$_0$ = 1.66 mM, [**7**]$_0$ = 4.00 mM, **2c** = 4.62 mol%.

Table S33: Concentration vs. time data for the catalytic reaction using catenane **2c** (4.62 mol%) as catalyst.

Time (h)	[**4**] (mM)	Nonlinear fit (mM)	ln(([4]*[7]0))/([4]0*(2*[4]+c)))
0.000	1.660	1.660	0.000
0.083	1.583	1.593	-0.008
0.417	1.347	1.369	-0.039
0.750	1.175	1.196	-0.068
1.083	1.046	1.058	-0.095
1.417	0.933	0.946	-0.125
1.750	0.850	0.853	-0.150
2.083	0.764	0.775	-0.182
2.417	0.698	0.708	-0.211
2.750	0.647	0.650	-0.236
3.083	0.608	0.600	-0.258
3.417	0.571	0.556	-0.281
3.750	0.534	0.516	-0.307
4.083	0.501	0.481	-0.333

a) b)

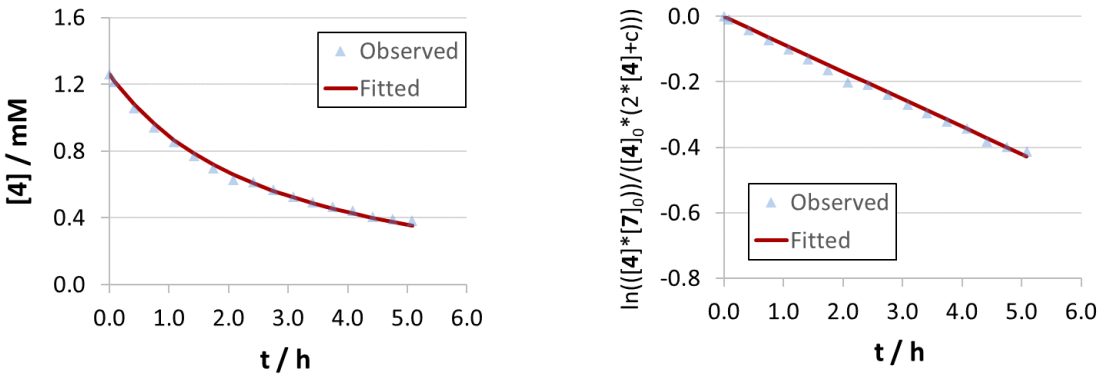

Figure S90: a) Curve of conversion and nonlinear fit. **b)** Linearization and linear fit of concentration vs. time data. Both: $[\mathbf{4}]_0$ = 1.26 mM, $[\mathbf{7}]_0$ = 3.24 mM, **2c** = 6.23 mol%.

Table S34: Concentration vs. time data for the catalytic reaction using catenane **2c** (6.23 mol%) as catalyst.

Time (h)	[**4**] (mM)	Nonlinear fit (mM)	ln(([4]*[7]0))/([4]0*(2*[4]+c)))
0.000	1.260	1.260	0.000
0.083	1.213	1.219	-0.009
0.417	1.059	1.078	-0.041
0.750	0.943	0.963	-0.072
1.083	0.852	0.867	-0.101
1.417	0.773	0.787	-0.131
1.750	0.699	0.718	-0.163
2.083	0.629	0.659	-0.201
2.417	0.614	0.608	-0.209
2.750	0.567	0.563	-0.240
3.083	0.526	0.522	-0.269
3.417	0.493	0.487	-0.296
3.750	0.466	0.455	-0.320
4.083	0.444	0.426	-0.341
4.417	0.406	0.400	-0.382
4.750	0.393	0.376	-0.397
5.083	0.381	0.354	-0.412

a) b)

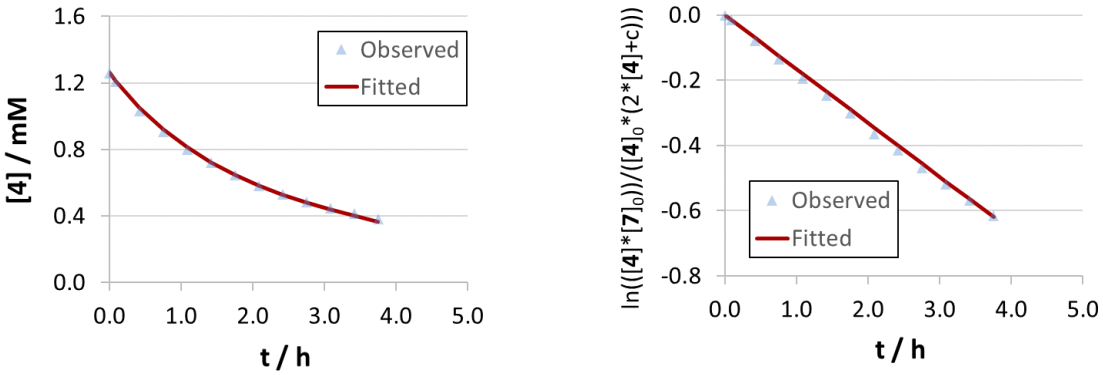

Figure S91: a) Curve of conversion and nonlinear fit. **b)** Linearization and linear fit of concentration vs. time data. Both: $[\mathbf{4}]_0$ = 1.26 mM, $[\mathbf{7}]_0$ = 4.02 mM, **2c** = 6.21 mol%.

Table S35: Concentration vs. time data for the catalytic reaction using catenane **2c** (6.21 mol%) as catalyst.

Time (h)	[**4**] (mM)	Nonlinear fit (mM)	ln(([4]*[7]0))/([4]0*(2*[4]+c)))
0.000	1.260	1.260	0.000
0.083	1.209	1.213	-0.016
0.417	1.033	1.051	-0.079
0.750	0.906	0.920	-0.136
1.083	0.801	0.813	-0.194
1.417	0.721	0.724	-0.246
1.750	0.648	0.649	-0.302
2.083	0.579	0.584	-0.364
2.417	0.529	0.529	-0.416
2.750	0.483	0.480	-0.470
3.083	0.446	0.438	-0.520
3.417	0.413	0.400	-0.568
3.750	0.384	0.367	-0.616

9.3.2. *Catalyst orders*

a) b)

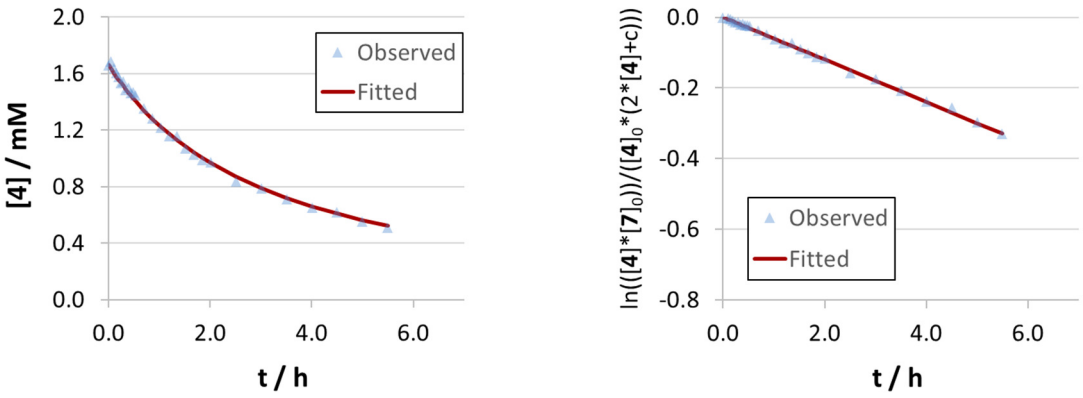

Figure S92: a) Curve of conversion and nonlinear fit. **b)** Linearization and linear fit of concentration vs. time data. Both: $[\mathbf{4}]_0$ = 1.66 mM, $[\mathbf{7}]_0$ = 4.02 mM, **2c** = 4.22 mol%.

Table S36: Concentration vs. time data for the catalytic reaction using catenane **2c** (4.22 mol%) as catalyst.

Time (h)	[**4**] (mM)	Nonlinear fit (mM)	ln(([4]*[7]0))/([4]0*(2*[4]+c)))
0.000	1.660	1.660	0.000
0.050	1.685	1.633	0.003
0.098	1.639	1.607	-0.002
0.146	1.605	1.582	-0.006
0.194	1.579	1.558	-0.009
0.242	1.533	1.535	-0.014
0.290	1.542	1.512	-0.013
0.338	1.485	1.490	-0.020
0.385	1.499	1.468	-0.018
0.433	1.464	1.447	-0.023
0.481	1.470	1.426	-0.022
0.529	1.445	1.406	-0.025
0.694	1.356	1.341	-0.038
0.858	1.281	1.281	-0.050
1.023	1.217	1.226	-0.061
1.188	1.160	1.175	-0.072
1.352	1.159	1.128	-0.072
1.517	1.073	1.083	-0.091
1.681	1.027	1.042	-0.102
1.846	0.990	1.004	-0.111
2.010	0.972	0.967	-0.116
2.508	0.834	0.871	-0.159
3.006	0.790	0.789	-0.175
3.504	0.711	0.720	-0.208
4.002	0.649	0.661	-0.239

4.500	0.618	0.609	-0.257
4.998	0.555	0.563	-0.297
5.496	0.511	0.523	-0.329

a) b)

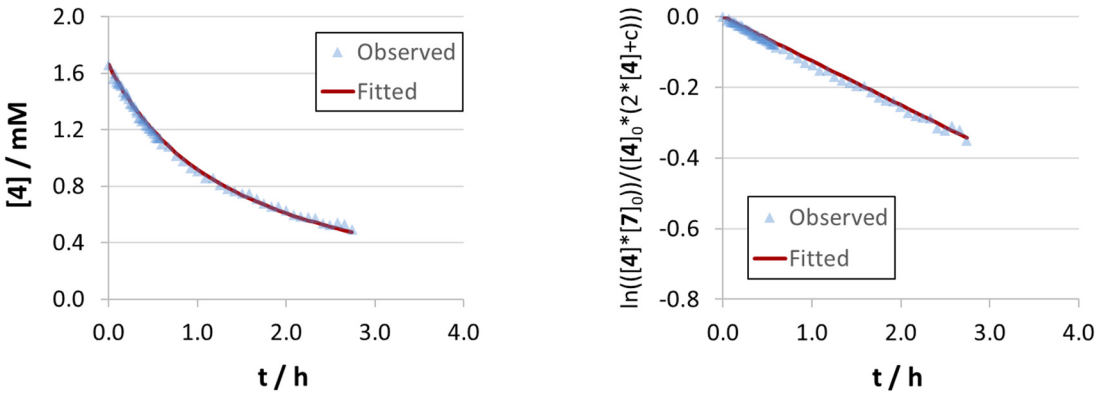

Figure S93: a) Curve of conversion and nonlinear fit. **b)** Linearization and linear fit of concentration vs. time data. Both: [**4**]$_0$ = 1.66 mM, [**7**]$_0$ = 4.03 mM, **2c** = 8.12 mol%.

Table S37: Concentration vs. time data for the catalytic reaction using catenane **2c** (8.12 mol%) as catalyst.

Time (h)	[**4**] (mM)	Nonlinear fit (mM)	ln(([4]*[7]0))/([4]0*(2*[4]+c)))
0.000	1.660	1.660	0.000
0.050	1.562	1.599	-0.011
0.066	1.599	1.581	-0.007
0.082	1.536	1.563	-0.014
0.098	1.526	1.545	-0.015
0.114	1.527	1.528	-0.015
0.130	1.517	1.511	-0.016
0.146	1.510	1.494	-0.017
0.162	1.469	1.477	-0.023
0.178	1.440	1.461	-0.027
0.194	1.460	1.446	-0.024
0.210	1.451	1.430	-0.025
0.226	1.421	1.415	-0.029
0.242	1.387	1.400	-0.034
0.258	1.379	1.386	-0.035
0.274	1.366	1.371	-0.037
0.290	1.361	1.357	-0.038
0.306	1.338	1.344	-0.042
0.322	1.319	1.330	-0.045
0.338	1.282	1.317	-0.051
0.353	1.281	1.304	-0.051
0.369	1.258	1.291	-0.055
0.385	1.278	1.278	-0.051
0.401	1.265	1.266	-0.054
0.417	1.231	1.254	-0.060
0.433	1.228	1.242	-0.060

0.449	1.211	1.230	-0.063
0.465	1.208	1.218	-0.064
0.481	1.191	1.207	-0.067
0.497	1.193	1.196	-0.067
0.513	1.172	1.185	-0.071
0.529	1.147	1.174	-0.076
0.545	1.138	1.163	-0.078
0.561	1.141	1.153	-0.077
0.577	1.139	1.142	-0.078
0.593	1.098	1.132	-0.087
0.676	1.080	1.082	-0.091
0.758	1.017	1.036	-0.106
0.841	0.976	0.993	-0.117
0.924	0.928	0.953	-0.130
1.006	0.906	0.915	-0.137
1.089	0.859	0.881	-0.153
1.172	0.860	0.848	-0.152
1.254	0.809	0.817	-0.171
1.337	0.780	0.789	-0.182
1.419	0.765	0.761	-0.188
1.502	0.748	0.736	-0.195
1.585	0.747	0.712	-0.196
1.667	0.709	0.689	-0.212
1.750	0.678	0.667	-0.228
1.833	0.658	0.646	-0.238
1.915	0.656	0.627	-0.239
1.998	0.629	0.608	-0.254
2.081	0.598	0.591	-0.273
2.163	0.585	0.574	-0.281
2.246	0.578	0.558	-0.286
2.328	0.575	0.542	-0.287
2.411	0.536	0.527	-0.315
2.494	0.528	0.513	-0.321
2.576	0.543	0.500	-0.310
2.659	0.530	0.487	-0.320
2.742	0.491	0.474	-0.351

a) b)

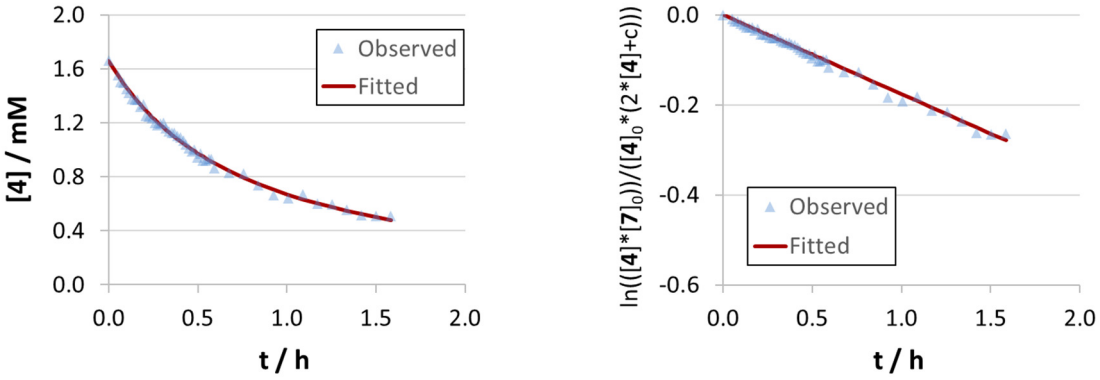

Figure S94: a) Curve of conversion and nonlinear fit. **b)** Linearization and linear fit of concentration vs. time data. Both: [**4**]$_0$ = 1.66 mM, [**7**]$_0$ = 3.83 mM, **2c** = 16.16 mol%.

Table S38*:* Concentration vs. time data for the catalytic reaction using catenane **2c** (16.16 mol%) as catalyst.

Time (h)	[**4**] (mM)	Nonlinear fit (mM)	ln(([4]*[7]0))/([4]0*(2*[4]+c)))
0.000	1.660	1.660	0.000
0.050	1.555	1.555	-0.009
0.066	1.501	1.524	-0.014
0.082	1.495	1.494	-0.015
0.098	1.449	1.465	-0.019
0.114	1.420	1.437	-0.022
0.130	1.376	1.410	-0.027
0.146	1.368	1.384	-0.028
0.162	1.371	1.359	-0.028
0.178	1.319	1.335	-0.034
0.194	1.338	1.311	-0.032
0.210	1.252	1.288	-0.043
0.226	1.247	1.266	-0.043
0.242	1.237	1.245	-0.045
0.258	1.201	1.224	-0.050
0.274	1.185	1.204	-0.052
0.290	1.193	1.185	-0.051
0.306	1.198	1.166	-0.050
0.322	1.159	1.147	-0.056
0.338	1.135	1.129	-0.060
0.353	1.125	1.112	-0.062
0.369	1.126	1.095	-0.061
0.385	1.103	1.079	-0.065
0.401	1.090	1.063	-0.068
0.417	1.066	1.047	-0.072
0.433	1.040	1.032	-0.077

0.449	1.013	1.017	-0.082
0.465	0.991	1.003	-0.086
0.481	0.997	0.989	-0.085
0.497	0.944	0.975	-0.097
0.513	0.974	0.962	-0.090
0.529	0.917	0.949	-0.103
0.545	0.918	0.936	-0.103
0.561	0.933	0.924	-0.099
0.577	0.933	0.912	-0.099
0.593	0.861	0.900	-0.117
0.676	0.827	0.843	-0.126
0.758	0.823	0.792	-0.127
0.841	0.737	0.746	-0.155
0.924	0.665	0.704	-0.183
1.006	0.642	0.667	-0.192
1.089	0.669	0.633	-0.181
1.172	0.599	0.601	-0.213
1.254	0.593	0.572	-0.216
1.337	0.555	0.546	-0.236
1.419	0.513	0.521	-0.262
1.502	0.507	0.499	-0.266
1.585	0.509	0.477	-0.264

a) b)

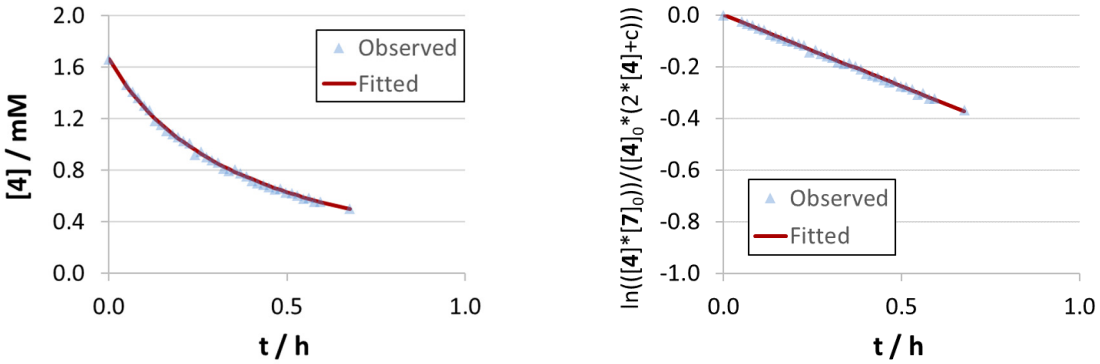

Figure S95: a) Curve of conversion and nonlinear fit. **b)** Linearization and linear fit of concentration vs. time data. Both: [**4**]$_0$ = 1.66 mM, [**7**]$_0$ = 4.11 mM, **2c** = 26.80 mol%.

Table S39: Concentration vs. time data for the catalytic reaction using catenane **2c** (26.80 mol%) as catalyst.

Time (h)	[**4**] (mM)	Nonlinear fit (mM)	ln(([4]*[7]0))/([4]0*(2*[4]+c)))
0.000	1.660	1.660	0.000
0.050	1.460	1.450	-0.026
0.066	1.410	1.393	-0.033
0.082	1.360	1.340	-0.041
0.098	1.301	1.290	-0.052
0.114	1.265	1.243	-0.058
0.130	1.183	1.200	-0.075
0.146	1.154	1.159	-0.081
0.162	1.106	1.120	-0.092
0.178	1.078	1.083	-0.099
0.194	1.058	1.049	-0.104
0.210	1.027	1.016	-0.112
0.226	1.009	0.985	-0.117
0.242	0.921	0.956	-0.144
0.258	0.944	0.928	-0.136
0.274	0.903	0.901	-0.149
0.290	0.877	0.876	-0.158
0.306	0.859	0.852	-0.165
0.322	0.814	0.829	-0.182
0.338	0.796	0.807	-0.189
0.353	0.806	0.786	-0.185
0.369	0.776	0.766	-0.198
0.385	0.752	0.747	-0.209
0.401	0.713	0.728	-0.227
0.417	0.701	0.710	-0.233
0.433	0.688	0.693	-0.240
0.449	0.665	0.677	-0.252

0.465	0.650	0.661	-0.261
0.481	0.657	0.646	-0.257
0.497	0.625	0.631	-0.276
0.513	0.622	0.617	-0.278
0.529	0.605	0.604	-0.289
0.545	0.576	0.591	-0.309
0.561	0.584	0.578	-0.303
0.577	0.556	0.566	-0.323
0.593	0.555	0.554	-0.324
0.676	0.502	0.498	-0.367

a) b)

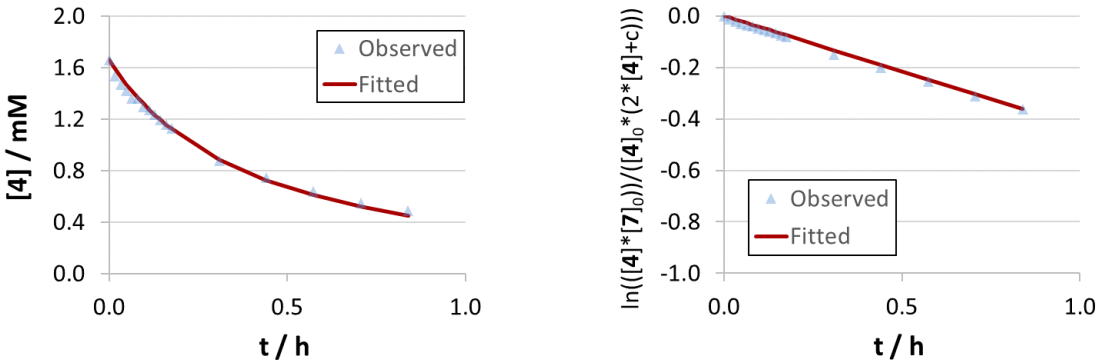

Figure S96: a) Curve of conversion and nonlinear fit. **b)** Linearization and linear fit of concentration vs. time data. Both: $[\mathbf{4}]_0$ = 1.66 mM, $[\mathbf{7}]_0$ = 4.05 mM, **2c** = 32.02 mol%.

Table S40: Concentration vs. time data for the catalytic reaction using catenane **2c** (32.02 mol%) as catalyst.

Time (h)	[**4**] (mM)	Nonlinear fit (mM)	ln(([4]*[7]0))/([4]0*(2*[4]+c)))
0.000	1.660	1.660	0.000
0.016	1.535	1.593	-0.015
0.032	1.470	1.531	-0.023
0.048	1.420	1.473	-0.030
0.064	1.363	1.419	-0.039
0.080	1.361	1.369	-0.039
0.096	1.295	1.321	-0.050
0.112	1.272	1.277	-0.054
0.128	1.233	1.235	-0.061
0.144	1.195	1.195	-0.068
0.160	1.158	1.158	-0.075
0.176	1.126	1.122	-0.082
0.308	0.875	0.888	-0.150
0.441	0.746	0.727	-0.200
0.574	0.636	0.609	-0.256
0.706	0.548	0.520	-0.313
0.839	0.486	0.449	-0.362

a) b)

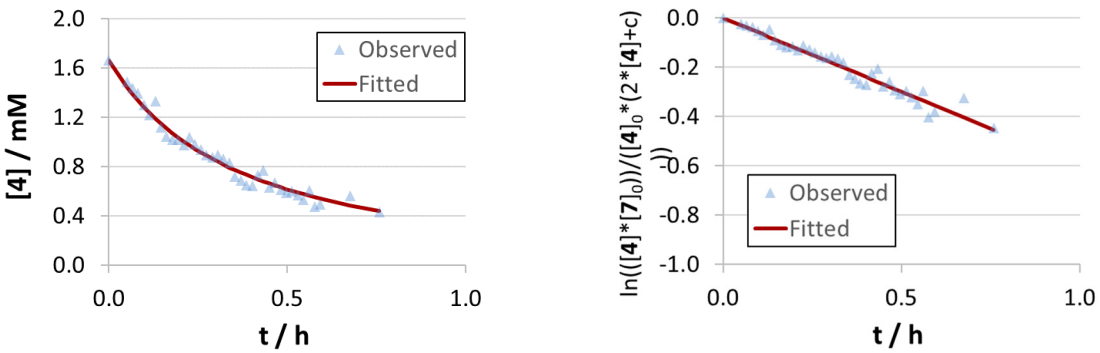

Figure S97: a) Curve of conversion and nonlinear fit. **b)** Linearization and linear fit of concentration vs. time data. Both: $[\mathbf{4}]_0$ = 1.66 mM, $[\mathbf{7}]_0$ = 4.13 mM, **2c** = 36.68 mol%.

Table S41: Concentration vs. time data for the catalytic reaction using catenane **2c** (36.68 mol%) as catalyst.

Time (h)	[**4**] (mM)	Nonlinear fit (mM)	ln(([4]*[7]0))/([4]0*(2*[4]+c)))
0.000	1.660	1.660	0.000
0.050	1.484	1.445	-0.023
0.066	1.436	1.386	-0.030
0.082	1.390	1.332	-0.037
0.098	1.299	1.281	-0.053
0.114	1.221	1.233	-0.068
0.130	1.333	1.189	-0.047
0.146	1.115	1.147	-0.092
0.162	1.043	1.108	-0.110
0.178	1.018	1.071	-0.117
0.194	1.019	1.036	-0.117
0.210	0.974	1.003	-0.130
0.226	1.034	0.971	-0.112
0.242	0.983	0.942	-0.127
0.258	0.938	0.914	-0.141
0.274	0.895	0.887	-0.155
0.290	0.872	0.862	-0.163
0.306	0.892	0.837	-0.156
0.322	0.864	0.814	-0.166
0.338	0.828	0.792	-0.180
0.353	0.715	0.771	-0.231
0.369	0.686	0.751	-0.246
0.385	0.649	0.732	-0.267
0.401	0.641	0.713	-0.272
0.417	0.730	0.695	-0.223
0.433	0.770	0.678	-0.205
0.449	0.630	0.662	-0.278
0.465	0.665	0.646	-0.258

0.481	0.608	0.631	-0.292
0.497	0.583	0.616	-0.309
0.513	0.600	0.602	-0.298
0.529	0.568	0.589	-0.320
0.545	0.529	0.576	-0.351
0.561	0.604	0.563	-0.295
0.577	0.471	0.551	-0.403
0.593	0.495	0.539	-0.380
0.676	0.562	0.484	-0.325
0.758	0.430	0.437	-0.446

a) b)

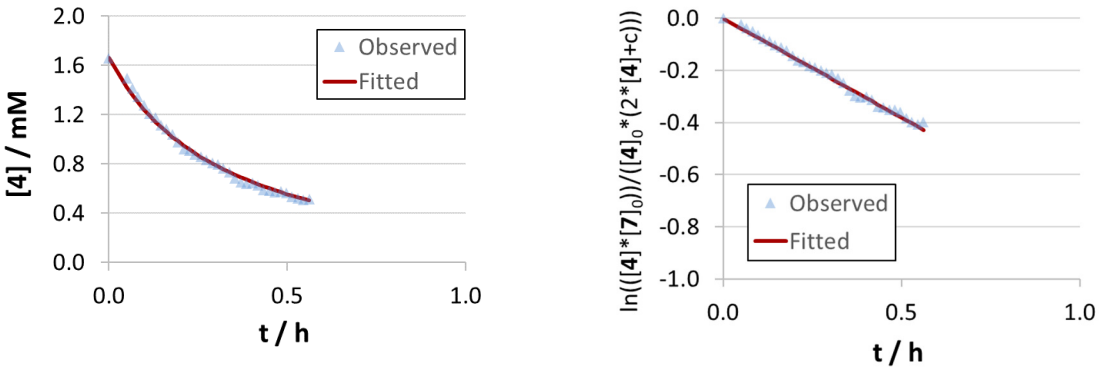

Figure S98: a) Curve of conversion and nonlinear fit. **b)** Linearization and linear fit of concentration vs. time data. Both: $[\mathbf{4}]_0$ = 1.66 mM, $[\mathbf{7}]_0$ = 4.27 mM, **2c** = 39.57 mol%.

Table S42: Concentration vs. time data for the catalytic reaction using catenane **2c** (39.57 mol%) as catalyst.

Time (h)	[**4**] (mM)	Nonlinear fit (mM)	ln(([4]*[7]0))/([4]0*(2*[4]+c)))
0.000	1.660	1.660	0.000
0.050	1.493	1.421	-0.024
0.066	1.414	1.357	-0.038
0.082	1.346	1.298	-0.050
0.098	1.275	1.243	-0.065
0.114	1.206	1.192	-0.080
0.130	1.177	1.145	-0.087
0.146	1.114	1.100	-0.103
0.162	1.084	1.059	-0.111
0.178	1.041	1.020	-0.124
0.194	0.976	0.983	-0.145
0.210	0.922	0.949	-0.163
0.226	0.910	0.917	-0.168
0.242	0.874	0.886	-0.182
0.258	0.857	0.857	-0.189
0.274	0.831	0.830	-0.200
0.290	0.807	0.803	-0.211
0.306	0.797	0.779	-0.215
0.322	0.764	0.755	-0.231
0.338	0.734	0.733	-0.246
0.353	0.681	0.711	-0.277
0.369	0.649	0.691	-0.297
0.385	0.639	0.672	-0.303
0.401	0.643	0.653	-0.300
0.417	0.625	0.635	-0.313
0.433	0.589	0.618	-0.339
0.449	0.586	0.602	-0.341
0.465	0.572	0.586	-0.352

0.481	0.574	0.571	-0.351
0.497	0.563	0.557	-0.359
0.513	0.534	0.543	-0.384
0.529	0.519	0.529	-0.397
0.545	0.507	0.516	-0.408
0.561	0.517	0.504	-0.399

a) b)

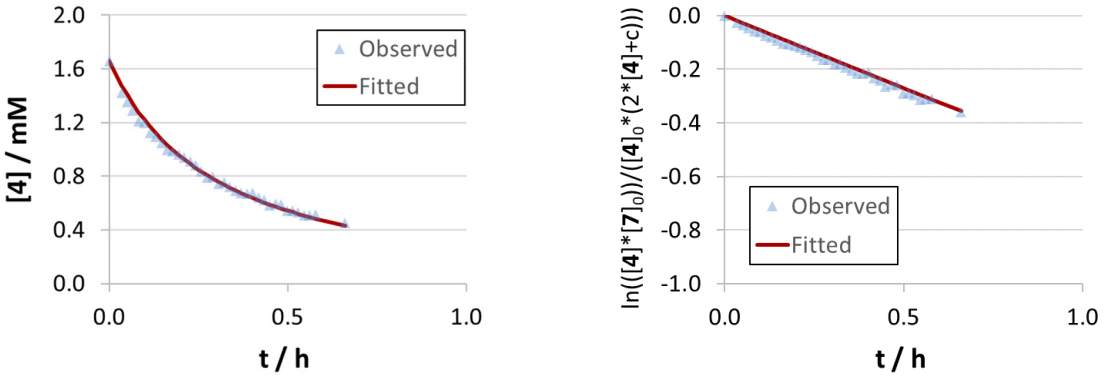

Figure S99: a) Curve of conversion and nonlinear fit. **b)** Linearization and linear fit of concentration vs. time data. Both: $[\mathbf{4}]_0$ = 1.66 mM, $[\mathbf{7}]_0$ = 4.08 mM, **2c** = 42.91 mol%.

Table S43: Concentration vs. time data for the catalytic reaction using catenane **2c** (42.91 mol%) as catalyst.

Time (h)	[**4**] (mM)	Nonlinear fit (mM)	ln(([4]*[7]0))/([4]0*(2*[4]+c)))
0.000	1.660	1.660	0.000
0.034	1.422	1.478	-0.027
0.050	1.353	1.405	-0.036
0.066	1.290	1.338	-0.046
0.082	1.209	1.278	-0.059
0.098	1.199	1.221	-0.061
0.114	1.121	1.170	-0.075
0.130	1.095	1.121	-0.081
0.146	1.046	1.077	-0.091
0.162	0.999	1.035	-0.102
0.178	0.986	0.996	-0.106
0.194	0.965	0.960	-0.111
0.210	0.941	0.926	-0.117
0.226	0.908	0.894	-0.127
0.242	0.880	0.864	-0.135
0.258	0.834	0.835	-0.150
0.274	0.790	0.808	-0.165
0.290	0.794	0.783	-0.164
0.306	0.745	0.759	-0.182
0.322	0.754	0.736	-0.179
0.338	0.723	0.714	-0.192
0.354	0.694	0.693	-0.205
0.370	0.673	0.674	-0.214
0.386	0.668	0.655	-0.217
0.402	0.676	0.637	-0.213
0.418	0.638	0.620	-0.232
0.434	0.621	0.604	-0.241
0.450	0.581	0.588	-0.265

0.466	0.594	0.573	-0.256
0.482	0.589	0.559	-0.260
0.498	0.541	0.545	-0.291
0.514	0.546	0.532	-0.287
0.530	0.532	0.519	-0.297
0.546	0.510	0.507	-0.313
0.562	0.511	0.495	-0.312
0.578	0.515	0.483	-0.309
0.660	0.453	0.431	-0.360

a) b)

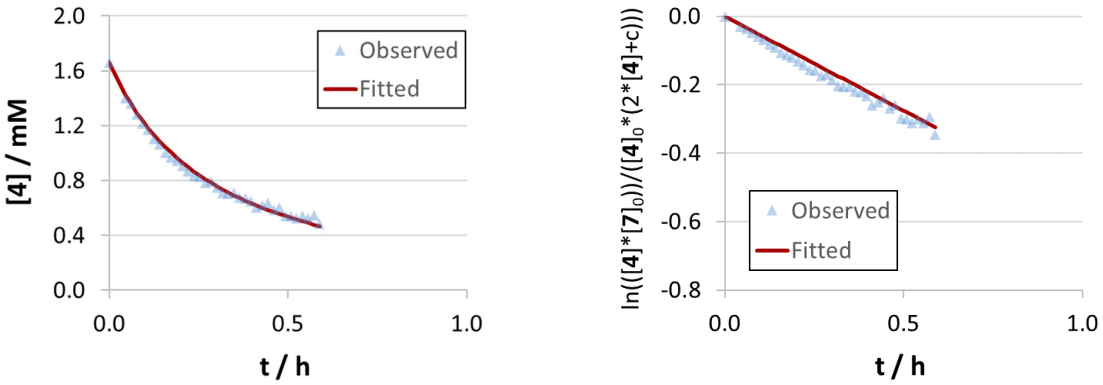

Figure S100: a) Curve of conversion and nonlinear fit. **b)** Linearization and linear fit of concentration vs. time data. Both: [**4**]$_0$ = 1.66 mM, [**7**]$_0$ = 4.00 mM, **2c** = 49.47 mol%.

Table S44: Concentration vs. time data for the catalytic reaction using catenane **2c** (49.47 mol%) as catalyst.

Time (h)	[**4**] (mM)	Nonlinear fit (mM)	ln(([4]*[7]0))/([4]0*(2*[4]+c)))
0.000	1.660	1.660	0.000
0.045	1.402	1.426	-0.031
0.061	1.361	1.357	-0.037
0.077	1.281	1.294	-0.049
0.093	1.214	1.235	-0.060
0.109	1.170	1.182	-0.068
0.125	1.105	1.132	-0.082
0.141	1.063	1.086	-0.091
0.157	1.000	1.043	-0.106
0.173	0.971	1.003	-0.114
0.189	0.947	0.966	-0.120
0.205	0.909	0.931	-0.131
0.221	0.870	0.898	-0.143
0.237	0.831	0.867	-0.156
0.253	0.826	0.838	-0.158
0.269	0.781	0.810	-0.174
0.285	0.794	0.784	-0.169
0.301	0.752	0.760	-0.186
0.317	0.712	0.736	-0.203
0.333	0.706	0.714	-0.206
0.348	0.708	0.693	-0.205
0.364	0.678	0.673	-0.219
0.380	0.672	0.654	-0.222
0.396	0.649	0.636	-0.234
0.412	0.604	0.618	-0.259
0.428	0.619	0.602	-0.251
0.444	0.639	0.586	-0.239

0.460	0.587	0.571	-0.270
0.476	0.604	0.556	-0.259
0.492	0.543	0.542	-0.299
0.508	0.540	0.529	-0.301
0.524	0.524	0.516	-0.313
0.540	0.539	0.503	-0.301
0.556	0.524	0.491	-0.313
0.572	0.549	0.480	-0.294
0.588	0.484	0.469	-0.345

a) b)

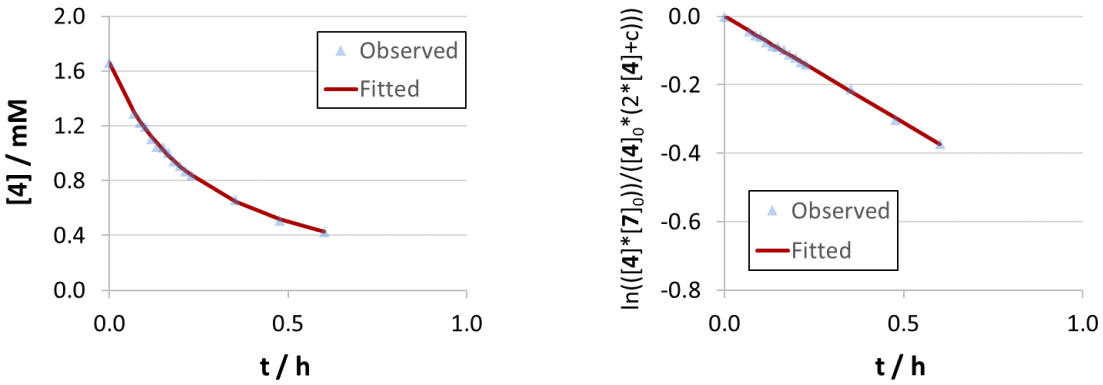

Figure S101: a) Curve of conversion and nonlinear fit. **b)** Linearization and linear fit of concentration vs. time data. Both: [**4**]$_0$ = 1.66 mM, [**7**]$_0$ = 3.93 mM, **2c** = 51.31 mol%.

Table S45: Concentration vs. time data for the catalytic reaction using catenane **2c** (51.31 mol%) as catalyst.

Time (h)	[**4**] (mM)	Nonlinear fit (mM)	ln(([4]*[7]0))/([4]0*(2*[4]+c)))
0.000	1.660	1.660	0.000
0.069	1.291	1.298	-0.044
0.085	1.224	1.234	-0.054
0.101	1.192	1.175	-0.059
0.117	1.104	1.122	-0.076
0.133	1.050	1.072	-0.087
0.149	1.042	1.026	-0.089
0.165	1.006	0.984	-0.097
0.181	0.944	0.944	-0.112
0.197	0.909	0.908	-0.121
0.213	0.870	0.873	-0.133
0.229	0.842	0.841	-0.141
0.353	0.659	0.648	-0.213
0.477	0.507	0.519	-0.303
0.602	0.427	0.427	-0.372

9.3.3. *Product inhibition*

a) b)

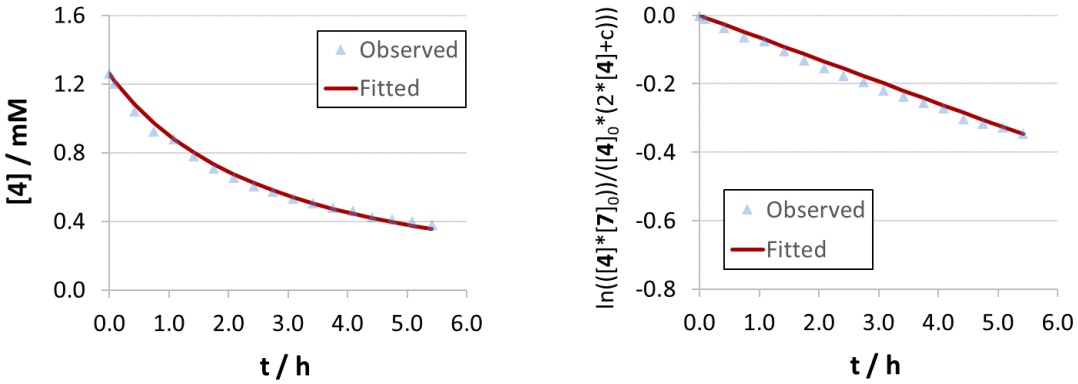

Figure S102: a) Curve of conversion and nonlinear fit. **b)** Linearization and linear fit of concentration vs. time data. Both: [**4**]$_0$ = 1.26 mM, [**7**]$_0$ = 3.07 mM, **2c** = 6.43 mol%.

Table S46: Concentration vs. time data for the catalytic reaction using catenane **2c** (6.43 mol%) as catalyst.

Time (h)	[**4**] (mM)	Nonlinear fit (mM)	ln(([4]*[7]0))/([4]0*(2*[4]+c)))
0.000	1.260	1.260	0.000
0.083	1.201	1.201	-0.009
0.417	1.042	1.042	-0.037
0.750	0.925	0.925	-0.063
1.083	0.879	0.879	-0.075
1.417	0.778	0.778	-0.105
1.750	0.710	0.710	-0.130
2.083	0.653	0.653	-0.154
2.417	0.606	0.606	-0.177
2.750	0.575	0.575	-0.194
3.083	0.534	0.534	-0.219
3.417	0.506	0.506	-0.237
3.750	0.481	0.481	-0.256
4.083	0.462	0.462	-0.270
4.417	0.425	0.425	-0.302
4.750	0.410	0.410	-0.317
5.083	0.399	0.399	-0.328
5.417	0.382	0.382	-0.346

9.4. Concentration vs. time data for acyclic catalyst 3

9.4.1. *Substrate orders*

a) b)

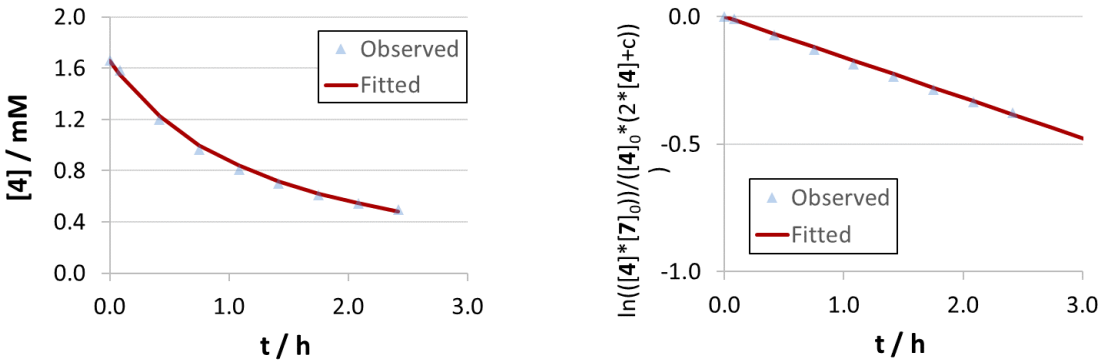

Figure S103: a) Curve of conversion and nonlinear fit. **b)** Linearization and linear fit of concentration vs. time data. Both: $[\mathbf{4}]_0$ = 1.66 mM, $[\mathbf{7}]_0$ = 4.12 mM, **3** = 1.53 mol%.

Table S47: Concentration vs. time data for the catalytic reaction using catenane **3** (1.53 mol%) as catalyst.

Time (h)	[**4**] (mM)	Nonlinear fit (mM)	ln(([4]*[7]0))/([4]0*(2*[4]+c)))
0.000	1.660	1.660	0.000
0.083	1.585	1.552	-0.009
0.417	1.197	1.223	-0.072
0.750	0.966	1.000	-0.131
1.083	0.811	0.838	-0.185
1.417	0.700	0.716	-0.236
1.750	0.613	0.621	-0.286
2.083	0.545	0.544	-0.335
2.417	0.494	0.482	-0.377

a) b)

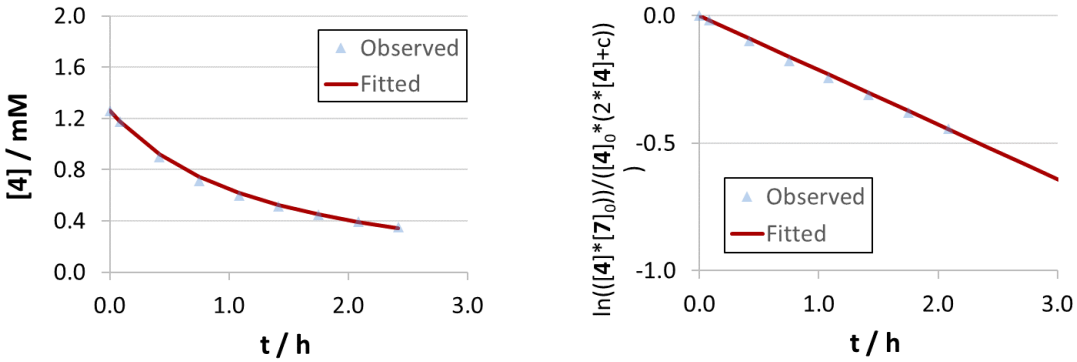

Figure S104: a) Curve of conversion and nonlinear fit. **b)** Linearization and linear fit of concentration vs. time data. Both: $[\mathbf{4}]_0$ = 1.26 mM, $[\mathbf{7}]_0$ = 3.37 mM, **3** = 1.30 mol%.

Table S48: Concentration vs. time data for the catalytic reaction using catenane **3** (1.30 mol%) as catalyst.

Time (h)	[**4**] (mM)	Nonlinear fit (mM)	ln(([4]*[7]0))/([4]0*(2*[4]+c)))
0.083	1.260	1.260	0.000
0.417	1.173	1.177	-0.019
0.750	0.897	0.921	-0.098
1.083	0.714	0.747	-0.177
1.417	0.600	0.621	-0.245
1.750	0.517	0.526	-0.311
2.083	0.446	0.452	-0.380
0.083	0.393	0.392	-0.443

a) b)

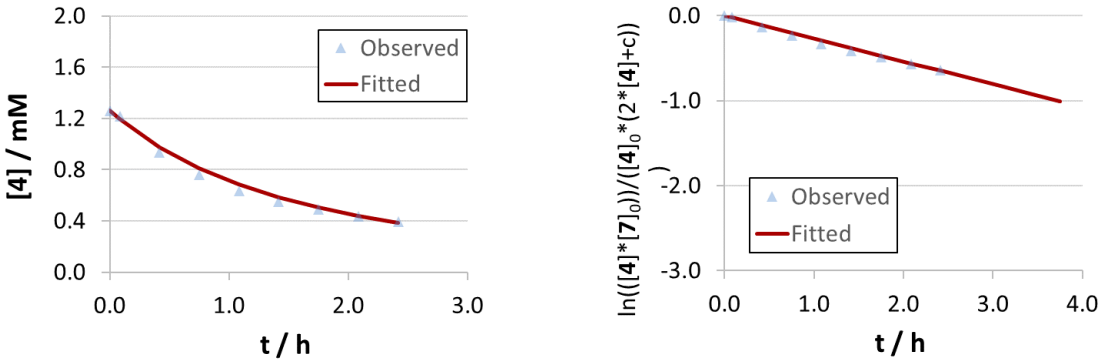

Figure S105: a) Curve of conversion and nonlinear fit. **b)** Linearization and linear fit of concentration vs. time data. Both: $[\mathbf{4}]_0$ = 1.26 mM, $[\mathbf{7}]_0$ = 4.24 mM, **3** = 1.70 mol%.

Table S49: Concentration vs. time data for the catalytic reaction using catenane **3** (1.70 mol%) as catalyst.

Time (h)	[**4**] (mM)	Nonlinear fit (mM)	ln(([4]*[7]0))/([4]0*(2*[4]+c)))
0.000	1.260	1.260	0.000
0.083	1.214	1.193	-0.015
0.417	0.935	0.973	-0.132
0.750	0.761	0.810	-0.236
1.083	0.637	0.685	-0.334
1.417	0.551	0.585	-0.419
1.750	0.491	0.505	-0.492
2.083	0.435	0.439	-0.570
2.417	0.393	0.385	-0.639

9.4.2. *Catalyst orders*

a) b)

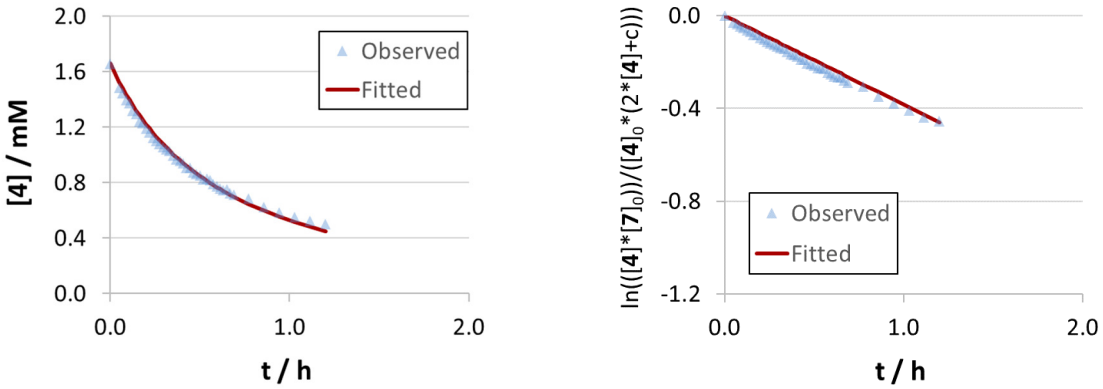

Figure S106: a) Curve of conversion and nonlinear fit. **b)** Linearization and linear fit of concentration vs. time data. Both: [**4**]$_0$ = 1.66 mM, [**7**]$_0$ = 4.44 mM, **3** = 2.48 mol%.

Table S50: Concentration vs. time data for the catalytic reaction using catenane **3** (2.48 mol%) as catalyst.

Time (h)	[**4**] (mM)	Nonlinear fit (mM)	ln(([4]*[7]0))/([4]0*(2*[4]+c)))
0.000	1.660	1.660	0.000
0.050	1.486	1.528	-0.029
0.069	1.446	1.483	-0.037
0.088	1.398	1.440	-0.046
0.106	1.373	1.399	-0.051
0.125	1.319	1.360	-0.063
0.144	1.297	1.323	-0.068
0.163	1.240	1.288	-0.082
0.181	1.232	1.254	-0.084
0.200	1.191	1.222	-0.095
0.219	1.164	1.191	-0.102
0.238	1.124	1.162	-0.113
0.256	1.102	1.133	-0.120
0.275	1.077	1.106	-0.128
0.294	1.058	1.080	-0.134
0.313	1.042	1.055	-0.139
0.331	1.031	1.031	-0.143
0.350	0.996	1.007	-0.155
0.369	0.970	0.985	-0.165
0.388	0.955	0.963	-0.170
0.406	0.943	0.942	-0.175
0.425	0.909	0.922	-0.189
0.444	0.910	0.903	-0.188
0.463	0.872	0.884	-0.205
0.481	0.861	0.866	-0.210

0.500	0.851	0.848	-0.215
0.519	0.827	0.831	-0.226
0.538	0.830	0.815	-0.225
0.556	0.819	0.799	-0.230
0.575	0.791	0.783	-0.244
0.594	0.777	0.768	-0.252
0.613	0.759	0.754	-0.261
0.631	0.749	0.740	-0.267
0.650	0.752	0.726	-0.265
0.669	0.727	0.713	-0.280
0.688	0.714	0.700	-0.288
0.773	0.686	0.645	-0.306
0.858	0.625	0.597	-0.348
0.944	0.588	0.554	-0.378
1.029	0.552	0.515	-0.409
1.115	0.522	0.481	-0.437
1.200	0.504	0.449	-0.456

a) b)

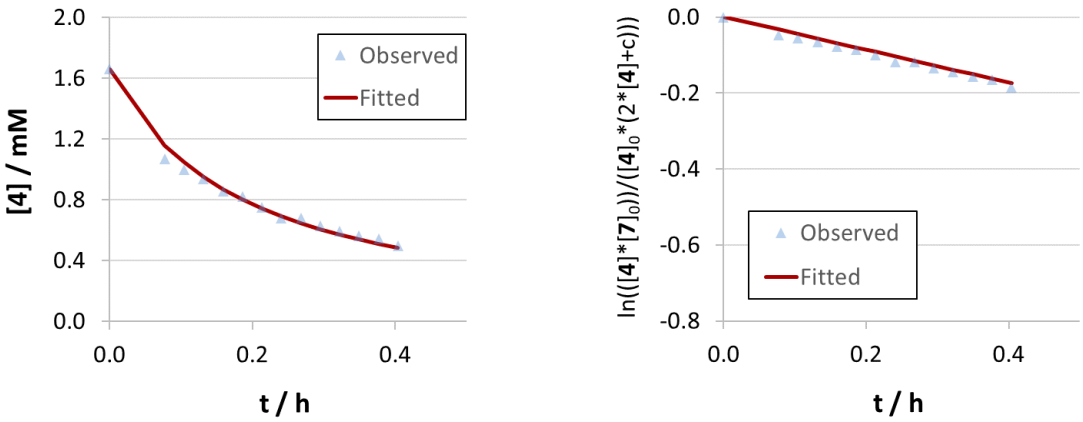

Figure S107: a) Curve of conversion and nonlinear fit. **b)** Linearization and linear fit of concentration vs. time data. Both: $[\mathbf{4}]_0$ = 1.66 mM, $[\mathbf{7}]_0$ = 3.64 mM, **3** = 4.44 mol%.

Table S51: Concentration vs. time data for the catalytic reaction using catenane **3** (4.44 mol%) as catalyst.

Time (h)	[**4**] (mM)	Nonlinear fit (mM)	ln(([4]*[7]0))/([4]0*(2*[4]+c)))
0.000	1.660	1.660	0.000
0.077	1.068	1.159	-0.047
0.104	0.999	1.045	-0.056
0.132	0.936	0.950	-0.065
0.159	0.856	0.870	-0.078
0.186	0.819	0.802	-0.085
0.213	0.747	0.743	-0.101
0.241	0.680	0.691	-0.118
0.268	0.678	0.646	-0.118
0.295	0.626	0.605	-0.134
0.322	0.592	0.569	-0.145
0.349	0.560	0.537	-0.157
0.377	0.539	0.508	-0.166
0.404	0.496	0.481	-0.185

a) b)

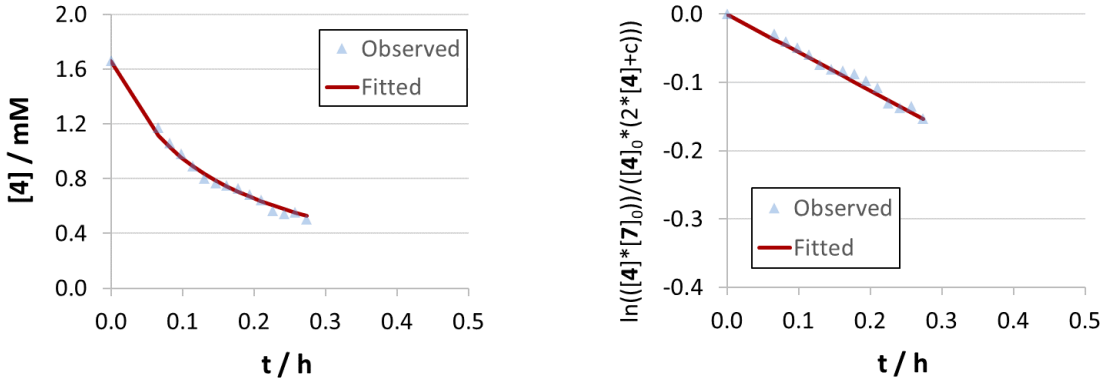

Figure S108: a) Curve of conversion and nonlinear fit. **b)** Linearization and linear fit of concentration vs. time data. Both: [**4**]$_0$ = 1.66 mM, [**7**]$_0$ = 3.58 mM, **3** = 6.91 mol%.

Table S52: Concentration vs. time data for the catalytic reaction using catenane **3** (6.91 mol%) as catalyst.

Time (h)	[**4**] (mM)	Nonlinear fit (mM)	ln(([4]*[7]0))/([4]0*(2*[4]+c)))
0.000	1.660	1.660	0.000
0.066	1.175	1.115	-0.029
0.082	1.059	1.031	-0.040
0.098	0.979	0.959	-0.049
0.114	0.893	0.895	-0.060
0.130	0.802	0.839	-0.074
0.146	0.766	0.789	-0.081
0.162	0.753	0.745	-0.083
0.178	0.728	0.704	-0.088
0.194	0.685	0.668	-0.097
0.210	0.644	0.635	-0.107
0.226	0.563	0.605	-0.131
0.242	0.546	0.577	-0.137
0.258	0.551	0.552	-0.135
0.274	0.504	0.528	-0.153

a) b)

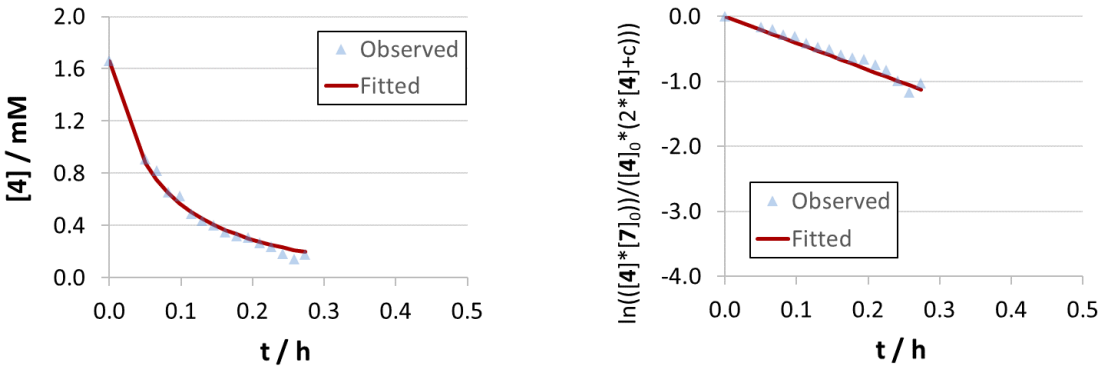

Figure S109: a) Curve of conversion and nonlinear fit. **b)** Linearization and linear fit of concentration vs. time data. Both: $[\mathbf{4}]_0$ = 1.66 mM, $[\mathbf{7}]_0$ = 4.21 mM, **3** = 13.65 mol%.

Table S53: Concentration vs. time data for the catalytic reaction using catenane **3** (13.65 mol%) as catalyst.

Time (h)	[**4**] (mM)	Nonlinear fit (mM)	ln(([4]*[7]0))/([4]0*(2*[4]+c)))
0.000	1.660	1.660	0.000
0.050	0.908	0.878	-0.161
0.066	0.820	0.752	-0.196
0.082	0.655	0.653	-0.281
0.098	0.627	0.573	-0.299
0.114	0.491	0.507	-0.407
0.130	0.437	0.452	-0.464
0.146	0.404	0.406	-0.504
0.162	0.349	0.366	-0.584
0.178	0.318	0.332	-0.637
0.194	0.309	0.302	-0.654
0.210	0.269	0.276	-0.737
0.226	0.236	0.253	-0.822
0.242	0.185	0.232	-0.988
0.258	0.144	0.214	-1.171
0.274	0.176	0.197	-1.021

a) b)

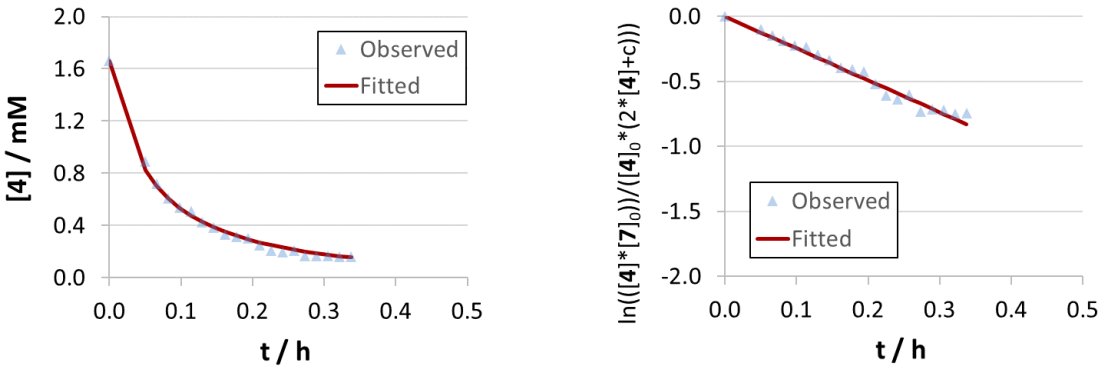

Figure S110: a) Curve of conversion and nonlinear fit. **b)** Linearization and linear fit of concentration vs. time data. Both: $[\mathbf{4}]_0$ = 1.66 mM, $[\mathbf{7}]_0$ = 3.77 mM, **3** = 24.23 mol%.

Table S54: Concentration vs. time data for the catalytic reaction using catenane **3** (24.23 mol%) as catalyst.

Time (h)	[**4**] (mM)	Nonlinear fit (mM)	ln(([4]*[7]0))/([4]0*(2*[4]+c)))
0.000	1.660	1.660	0.000
0.050	0.892	0.825	-0.098
0.066	0.722	0.704	-0.144
0.082	0.610	0.610	-0.186
0.098	0.537	0.536	-0.222
0.114	0.510	0.477	-0.237
0.130	0.426	0.427	-0.296
0.146	0.384	0.386	-0.333
0.162	0.330	0.351	-0.392
0.178	0.316	0.320	-0.409
0.194	0.304	0.294	-0.426
0.210	0.247	0.271	-0.519
0.226	0.207	0.250	-0.606
0.242	0.195	0.232	-0.639
0.258	0.209	0.216	-0.603
0.274	0.164	0.201	-0.735
0.290	0.169	0.188	-0.717
0.306	0.169	0.176	-0.719
0.322	0.160	0.165	-0.748
0.338	0.161	0.155	-0.744

a) b)

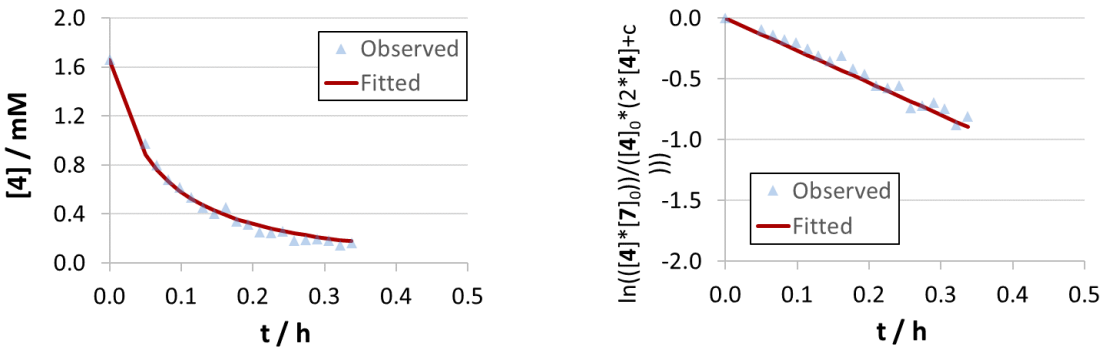

Figure S111: a) Curve of conversion and nonlinear fit. **b)** Linearization and linear fit of concentration vs. time data. Both: $[\mathbf{4}]_0$ = 1.66 mM, $[\mathbf{7}]_0$ = 3.84 mM, **3** = 24.45 mol%.

Table S55: Concentration vs. time data for the catalytic reaction using catenane **3** (24.45 mol%) as catalyst.

Time (h)	[**4**] (mM)	Nonlinear fit (mM)	ln(([**4**]*[**7**]0))/([**4**]0*(2*[**4**]+c)))
0.000	1.660	1.660	0.000
0.050	0.972	0.882	-0.091
0.066	0.800	0.759	-0.135
0.082	0.682	0.664	-0.176
0.098	0.619	0.587	-0.204
0.114	0.534	0.524	-0.249
0.130	0.454	0.472	-0.305
0.146	0.401	0.428	-0.352
0.162	0.451	0.390	-0.307
0.178	0.342	0.357	-0.417
0.194	0.311	0.329	-0.459
0.210	0.254	0.304	-0.555
0.226	0.246	0.281	-0.572
0.242	0.255	0.261	-0.554
0.258	0.182	0.243	-0.737
0.274	0.188	0.227	-0.718
0.290	0.197	0.213	-0.692
0.306	0.179	0.199	-0.746
0.322	0.145	0.187	-0.876
0.338	0.162	0.176	-0.806

a) b)

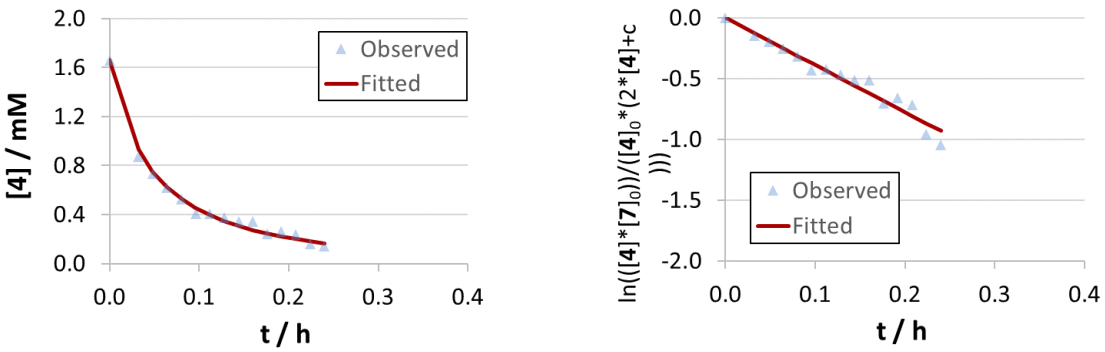

Figure S112: a) Curve of conversion and nonlinear fit. **b)** Linearization and linear fit of concentration vs. time data. Both: $[\mathbf{4}]_0$ = 1.66 mM, $[\mathbf{7}]_0$ = 4.02 mM, **3** = 37.66 mol%.

Table S56: Concentration vs. time data for the catalytic reaction using catenane **3** (37.66 mol%) as catalyst.

Time (h)	[**4**] (mM)	Nonlinear fit (mM)	ln(([4]*[7]0))/([4]0*(2*[4]+c)))
0.000	1.660	1.660	0.000
0.032	0.874	0.932	-0.145
0.048	0.731	0.752	-0.199
0.064	0.622	0.624	-0.254
0.080	0.524	0.528	-0.319
0.096	0.404	0.454	-0.431
0.112	0.408	0.395	-0.426
0.128	0.375	0.347	-0.466
0.144	0.341	0.307	-0.512
0.160	0.341	0.273	-0.513
0.176	0.242	0.245	-0.701
0.192	0.260	0.220	-0.659
0.208	0.236	0.199	-0.716
0.224	0.162	0.181	-0.957
0.240	0.142	0.165	-1.047

a) b)

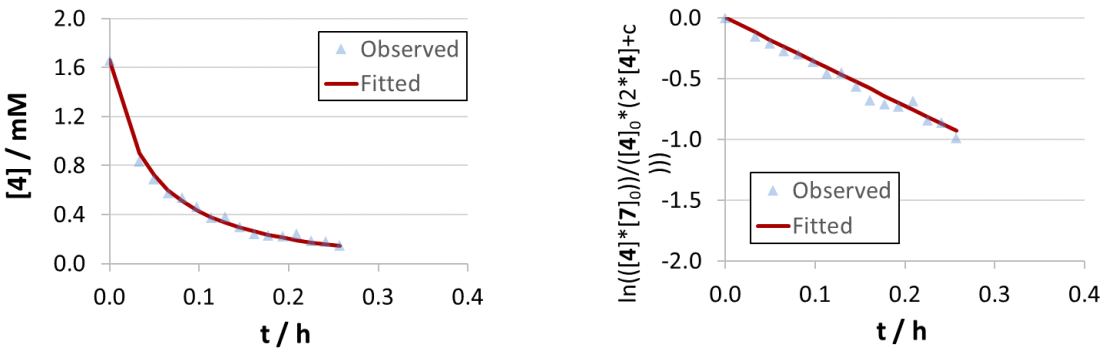

Figure S113: a) Curve of conversion and nonlinear fit. **b)** Linearization and linear fit of concentration vs. time data. Both: $[\mathbf{4}]_0$ = 1.66 mM, $[\mathbf{7}]_0$ = 3.99 mM, **3** = 39.10 mol%.

Table S57: Concentration vs. time data for the catalytic reaction using catenane **3** (39.10 mol%) as catalyst.

Time (h)	[**4**] (mM)	Nonlinear fit (mM)	ln(([4]*[7]0))/([4]0*(2*[4]+c)))
0.000	1.660	1.660	0.000
0.033	0.831	0.900	-0.155
0.049	0.691	0.725	-0.211
0.065	0.574	0.601	-0.276
0.081	0.537	0.508	-0.301
0.097	0.461	0.436	-0.362
0.113	0.375	0.379	-0.455
0.129	0.380	0.332	-0.448
0.145	0.300	0.294	-0.565
0.161	0.245	0.262	-0.678
0.177	0.231	0.235	-0.712
0.193	0.224	0.211	-0.729
0.209	0.241	0.191	-0.687
0.225	0.188	0.173	-0.840
0.241	0.182	0.157	-0.861
0.257	0.150	0.143	-0.988

a) b)

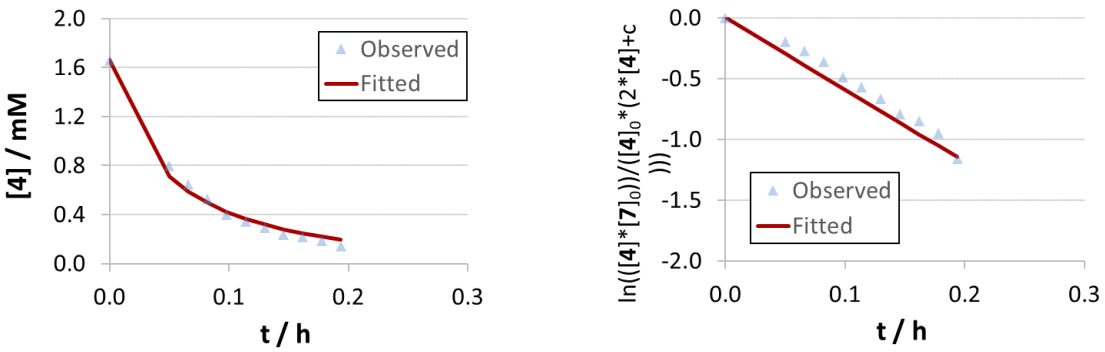

Figure S114: a) Curve of conversion and nonlinear fit. **b)** Linearization and linear fit of concentration vs. time data. Both: $[\mathbf{4}]_0$ = 1.66 mM, $[\mathbf{7}]_0$ = 4.15 mM, **3** = 47.17 mol%.

Table S58: Concentration vs. time data for the catalytic reaction using catenane **3** (47.17 mol%) as catalyst.

Time (h)	[**4**] (mM)	Nonlinear fit (mM)	ln(([4]*[7]0))/([4]0*(2*[4]+c)))
0.000	1.660	1.660	0.000
0.050	0.793	0.713	-0.198
0.066	0.647	0.588	-0.272
0.082	0.523	0.495	-0.361
0.098	0.400	0.422	-0.489
0.114	0.343	0.365	-0.570
0.130	0.291	0.318	-0.663
0.146	0.237	0.280	-0.789
0.162	0.215	0.247	-0.850
0.178	0.186	0.220	-0.949
0.194	0.139	0.196	-1.159

a) b)

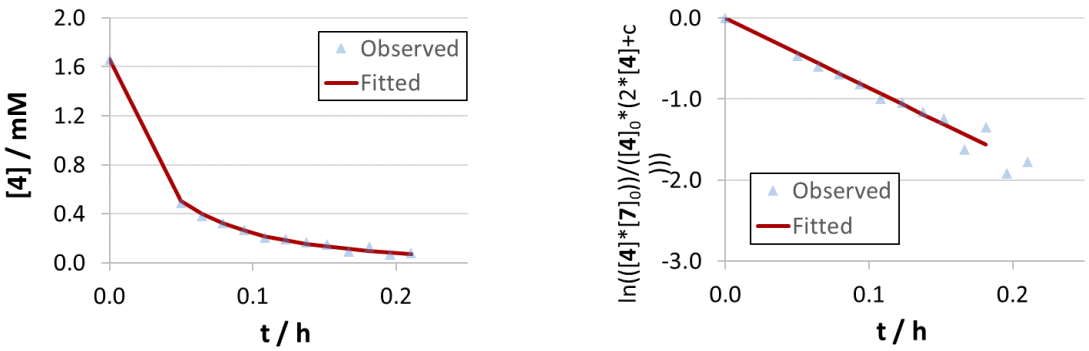

Figure S115: a) Curve of conversion and nonlinear fit. **b)** Linearization and linear fit of concentration vs. time data. Both: $[\mathbf{4}]_0$ = 1.66 mM, $[\mathbf{7}]_0$ = 4.40 mM, **3** = 51.97 mol%.

Table S59: Concentration vs. time data for the catalytic reaction using catenane **3** (51.97 mol%) as catalyst.

Time (h)	[**4**] (mM)	Nonlinear fit (mM)	ln(([4]*[7]0))/([4]0*(2*[4]+c)))
0.000	1.660	1.660	0.000
0.050	0.490	0.506	-0.460
0.065	0.383	0.399	-0.598
0.079	0.328	0.322	-0.691
0.094	0.272	0.264	-0.811
0.108	0.207	0.219	-1.000
0.123	0.196	0.183	-1.041
0.138	0.167	0.155	-1.161
0.152	0.150	0.131	-1.242
0.167	0.095	0.112	-1.619
0.181	0.131	0.096	-1.350
0.196	0.067	0.083	-1.915
0.210	0.080	0.071	-1.769

9.4.3. *Product inhibition*

a) b)

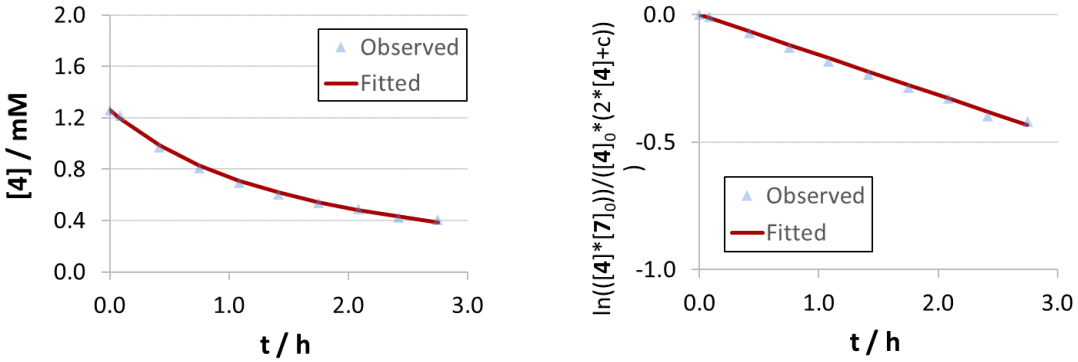

Figure S116: a) Curve of conversion and nonlinear fit. **b)** Linearization and linear fit of concentration vs. time data. Both: $[\mathbf{4}]_0$ = 1.26 mM, $[\mathbf{7}]_0$ = 3.34 mM, **3** = 1.36 mol%.

Table S60: Concentration vs. time data for the catalytic reaction using catenane **3** (1.36 mol%) as catalyst.

Time (h)	[**4**] (mM)	Nonlinear fit (mM)	ln(([4]*[7]0))/([4]0*(2*[4]+c)))
0.000	1.260	1.260	0.000
0.083	1.216	1.195	-0.009
0.417	0.973	0.983	-0.070
0.750	0.807	0.829	-0.130
1.083	0.692	0.711	-0.184
1.417	0.607	0.618	-0.235
1.750	0.536	0.543	-0.287
2.083	0.488	0.481	-0.329
2.417	0.422	0.430	-0.398
2.750	0.404	0.387	-0.420

10. Appendix C: Catalytic reactions

10.1. Results for catenanes 1a/b/c and macrocycles 2a/b/c

Entries 0-5:

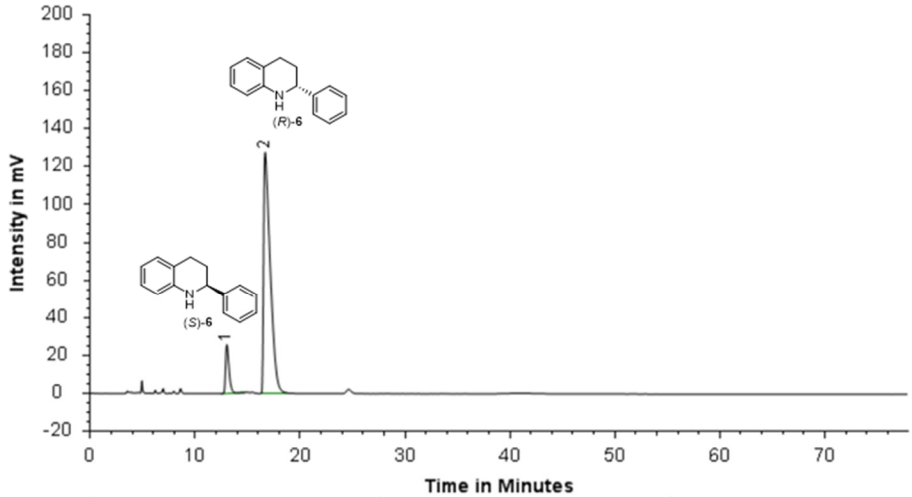

No.	Ret. Time	Height	Area	Percent
1	13.00833	25.71911	588941.6	9.567999
2	16.65833	127.5904	5566385	90.432

Figure S117: Chiral HPLC of **6** using (*S*,*S*)-**1a** as catalyst (Entry 0,Table S1)

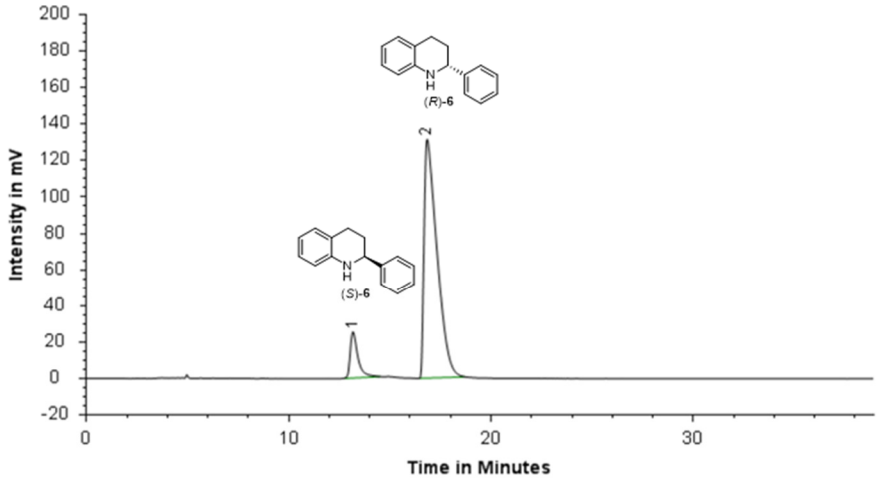

No.	Ret. Time	Height	Area	Percent
1	13.16667	25.31031	670995.4	10.32529
2	16.85	131.3979	5827569	89.67471

Figure S118: Chiral HPLC of **6** using (*S*,*S*)-**1b** as catalyst (Entry 1,Table S1)

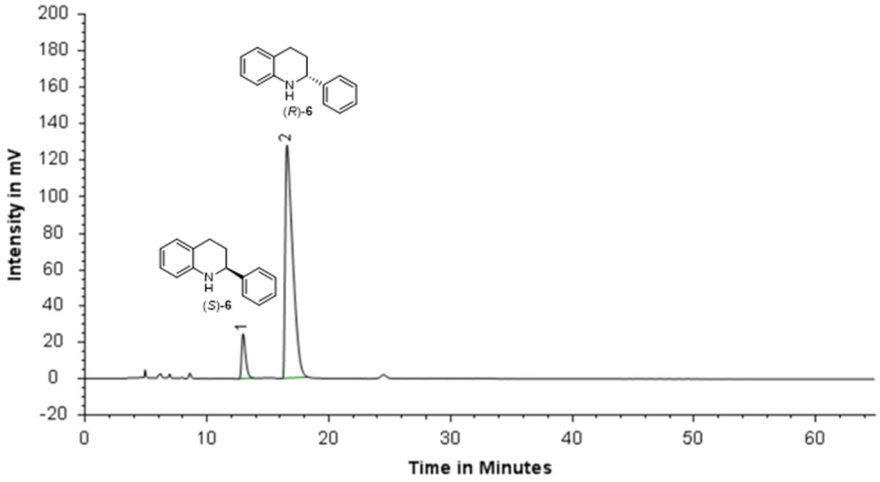

No.	Ret. Time	Height	Area	Percent
1	12.96667	24.43617	550712	9.171595
2	16.575	127.9738	5453828	90.82841

Figure S119: Chiral HPLC of **6** using (*S*,*S*)-**1c** as catalyst (Entry 2,Table S1)

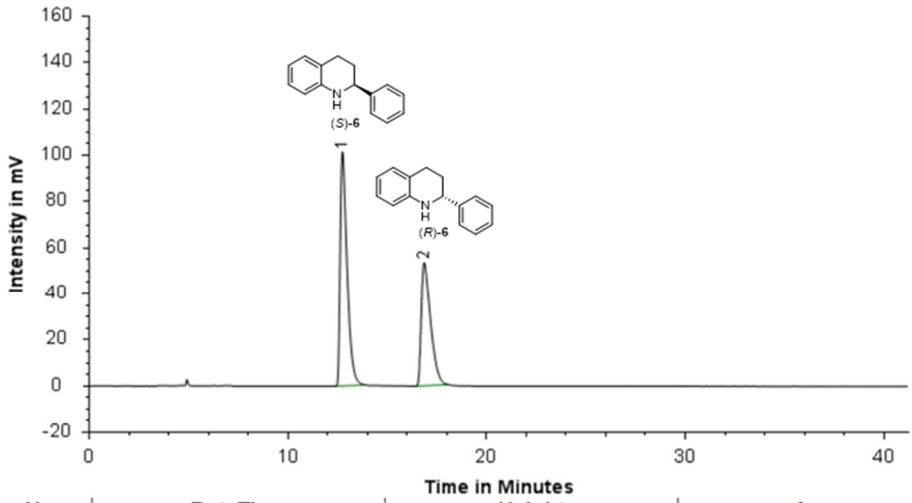

No.	Ret. Time	Height	Area	Percent
1	12.725	101.268	2446670	58.46386
2	16.85833	53.48404	1738258	41.53614

Figure S120: Chiral HPLC of **6** using (*S*)-**2a** as catalyst (Entry 3,Table S1)

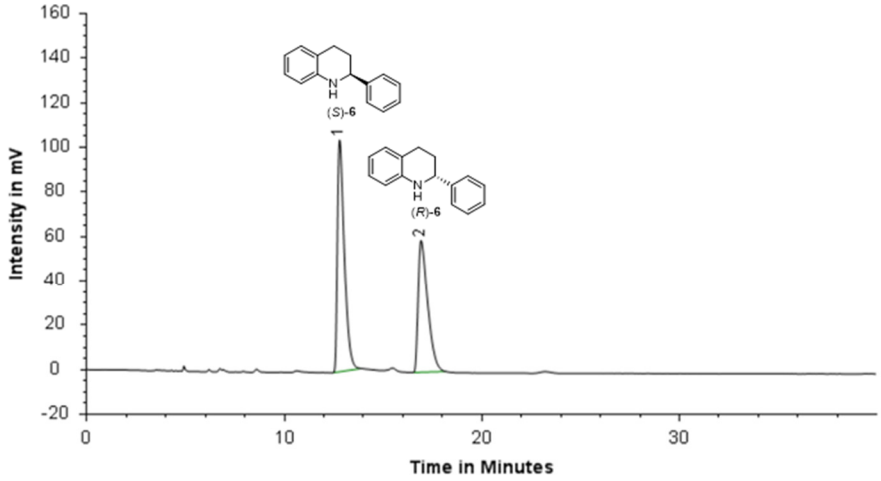

No.	Ret. Time	Height	Area	Percent
1	12.79167	104.1775	2535127	56.08055
2	16.91667	59.3705	1985383	43.91945

Figure S121: Chiral HPLC of **6** using (*S*)-**2b** as catalyst (Entry 4,Table S1)

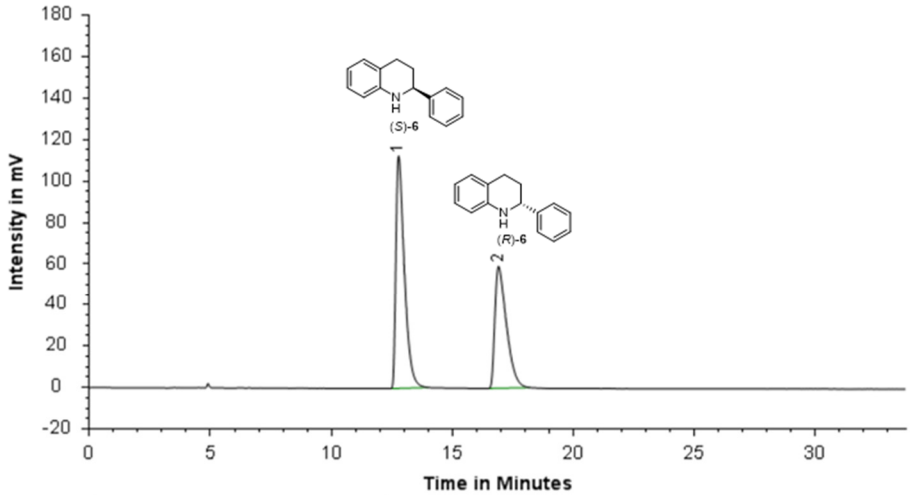

No.	Ret. Time	Height	Area	Percent
1	12.78333	112.4916	2747306	58.32079
2	16.9	59.22459	1963374	41.67921

Figure S122: Chiral HPLC of **6** using (*S*)-**2c** as catalyst (Entry 5,Table S1)

10.2. Results for catalyst 3

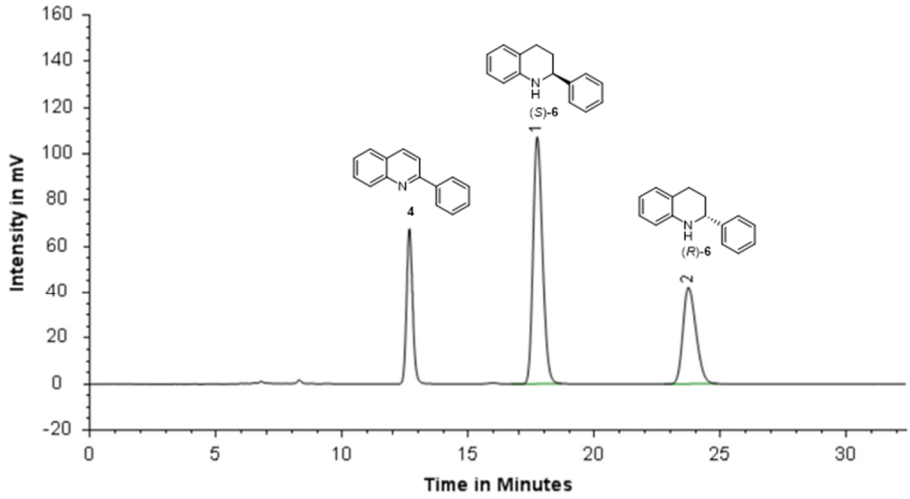

No.	Ret. Time	Height	Area	Percent
1	17.725	107.2213	2780000	64.75316
2	23.73333	42.22018	1513227	35.24684

Figure S123: Chiral HPLC of **6** using (*S*)-**3** as catalyst (Entry 6,Table S1)

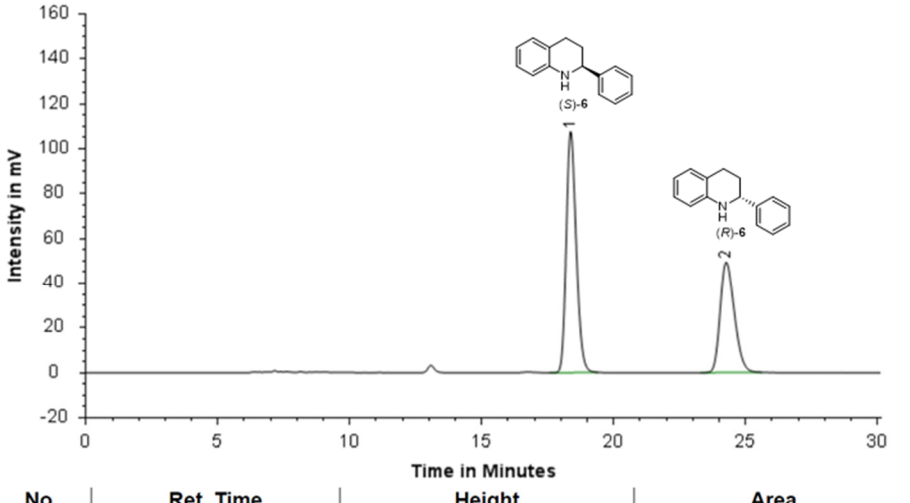

No.	Ret. Time	Height	Area	Percent
1	18.375	107.5309	2814608	60.46938
2	24.275	49.27058	1839992	39.53062

Figure S124: : Chiral HPLC of **6** using (*S*)-**3** as catalyst (Entry 7,Table S1)

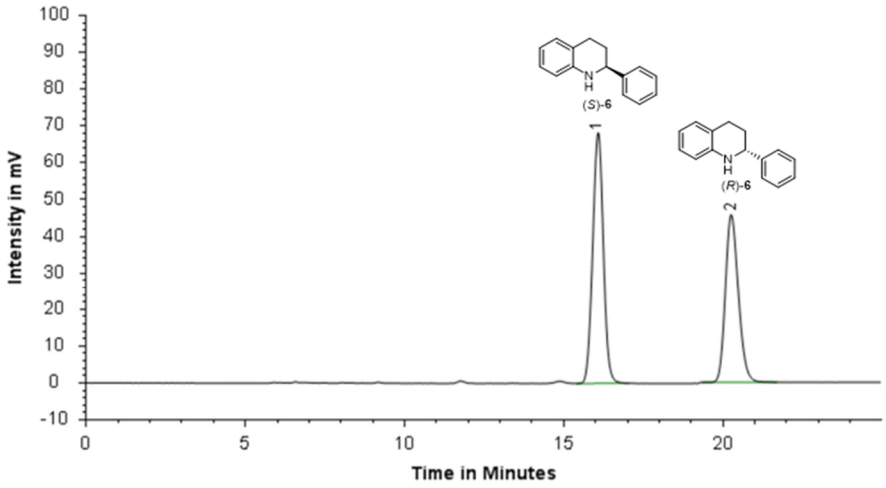

No.	Ret. Time	Height	Area	Percent
1	16.075	68.2239	1584813	55.04815
2	20.26667	45.69062	1294145	44.95185

Figure S125: Chiral HPLC of **6** using (*S*)-**3** as catalyst (Entry 8,Table S1)

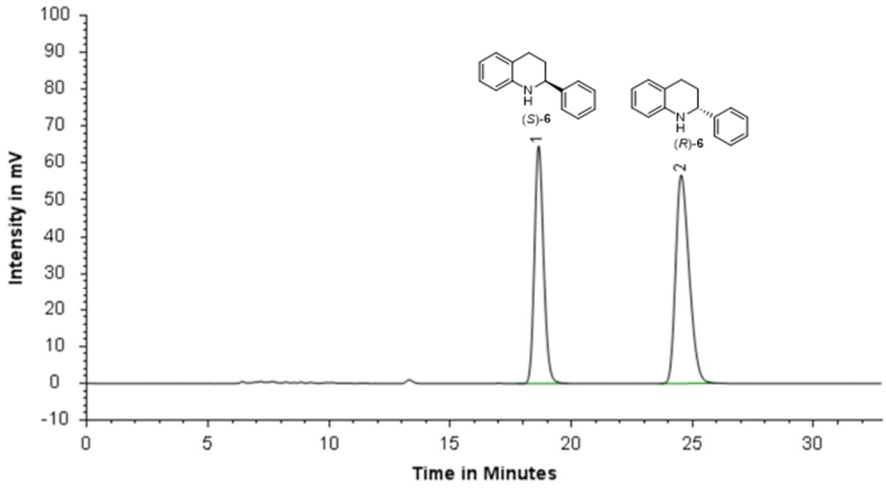

No.	Ret. Time	Height	Area	Percent
1	18.64167	64.62535	1698983	43.57774
2	24.53333	56.76402	2199758	56.42226

Figure S126: Chiral HPLC of **6** using (*S*)-**3** as catalyst (Entry 9,Table S1)

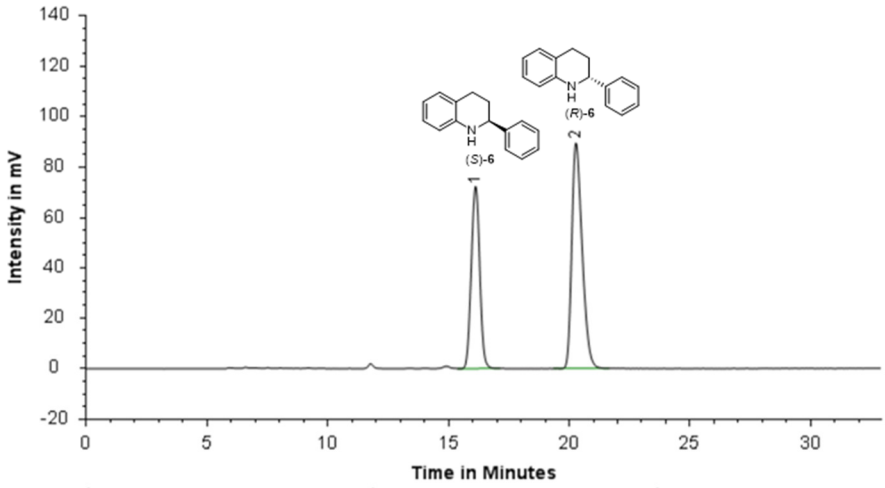

No.	Ret. Time	Height	Area	Percent
1	16.125	72.276	1759421	39.77882
2	20.28333	89.35336	2663588	60.22118

Figure S127: Chiral HPLC of **6** using (*S*)-**3** as catalyst (Entry 10,Table S1)

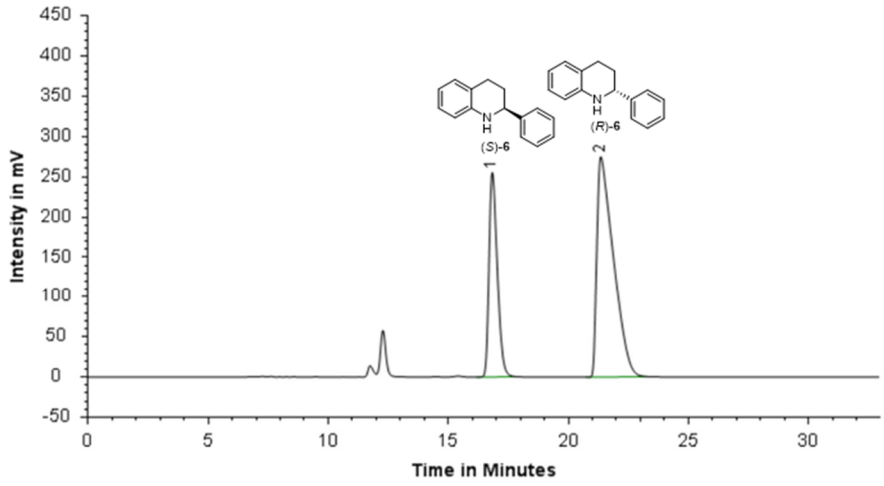

No.	Ret. Time	Height	Area	Percent
1	16.825	255.0939	6124469	31.7409
2	21.35833	274.5272	1.317073E+07	68.2591

Figure S128: Chiral HPLC of **6** using (*S*)-**3** as catalyst (Entry 11,Table S1)

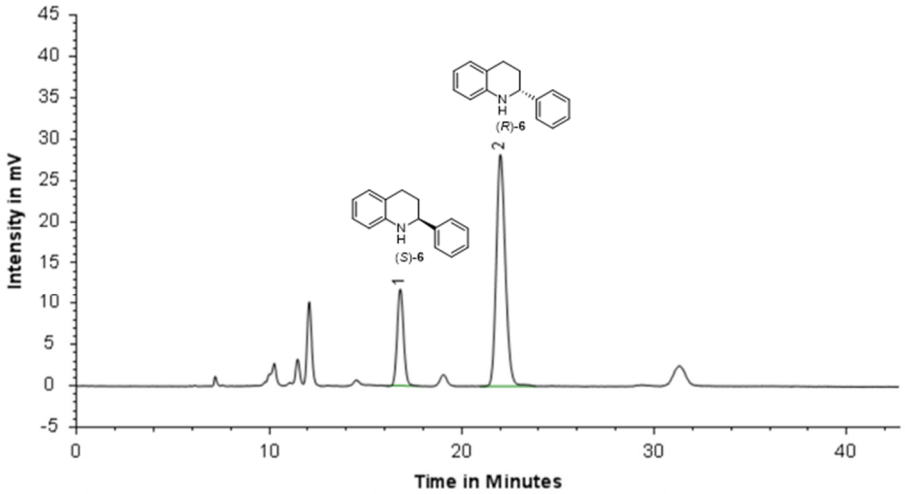

No.	Ret. Time	Height	Area	Percent
1	16.8	11.76157	268443.5	22.63719
2	22.01667	28.13662	917408.2	77.36281

Figure S129: Chiral HPLC of **6** using (*S*)-**3** as catalyst (Entry 12,Table S1)

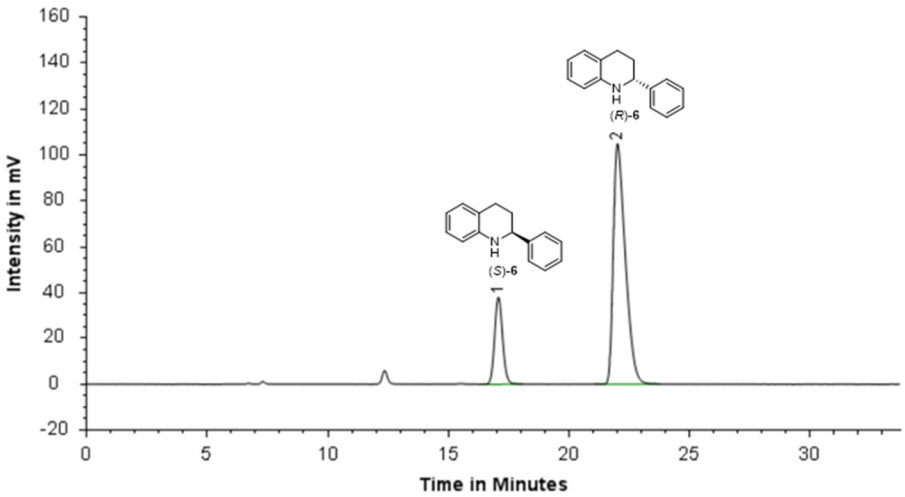

No.	Ret. Time	Height	Area	Percent
1	17.08333	38.21341	872169.1	19.39752
2	22.03333	104.8101	3624123	80.60248

Figure S130: Chiral HPLC of **6** using (*S*)-**3** as catalyst (Entry 13,**Table S1**)

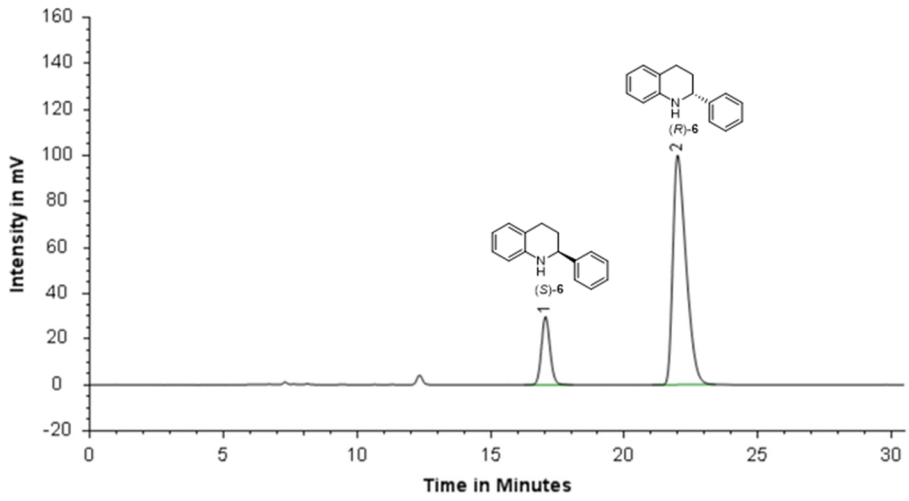

No.	Ret. Time	Height	Area	Percent
1	17.04167	29.54792	664469.5	16.2729
2	21.99167	100.0145	3418820	83.7271

Figure S131*:* Chiral HPLC of **6** using (*S*)-**3** as catalyst (Entry 14,Table S1)

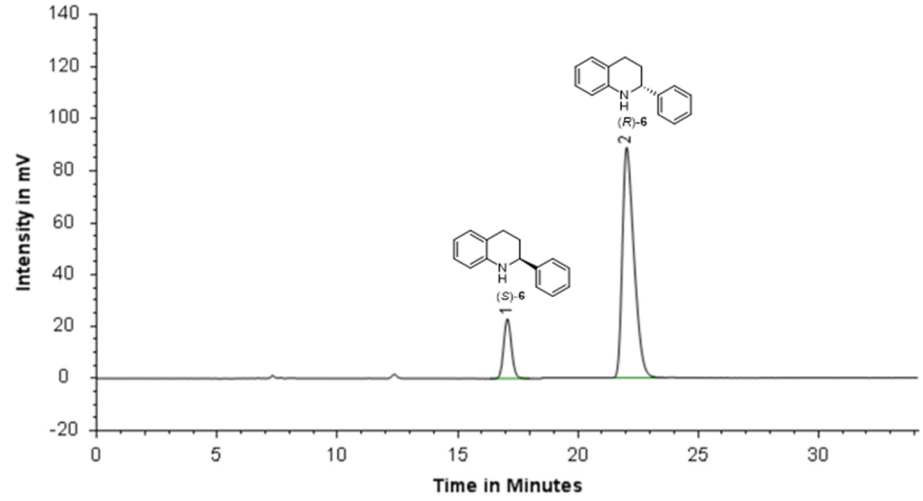

No.	Ret. Time	Height	Area	Percent
1	17.075	22.78235	513200.4	14.71006
2	22.025	88.6094	2975572	85.28994

Figure S132: Chiral HPLC of **6** using (*S*)-**3** as catalyst (Entry 15,Table S1)

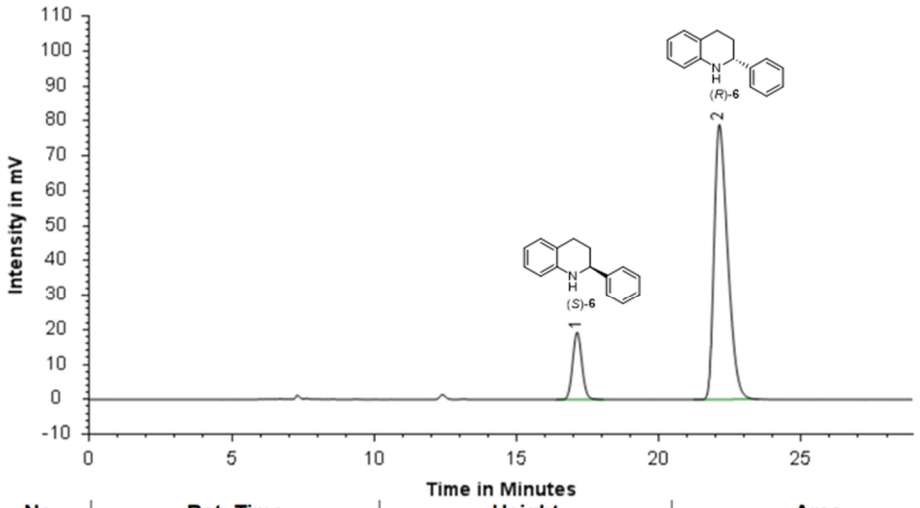

No.	Ret. Time	Height	Area	Percent
1	17.125	19.23234	432094.5	14.20928
2	22.11667	78.88174	2608837	85.79072

Figure S133: Chiral HPLC of **6** using (*S*)-**3** as catalyst (Entry 16,Table S1)

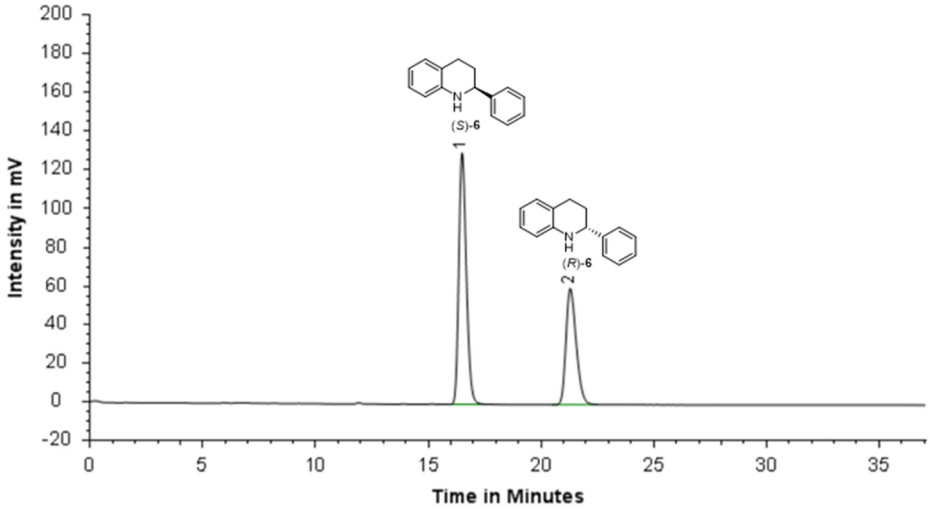

No.	Ret. Time	Height	Area	Percent
1	16.49167	129.9756	3002817	61.37477
2	21.3	60.3768	1889775	38.62523

Figure S134: Chiral HPLC of **6** using (*S*)-**3** as catalyst (Entry 17,Table S1)

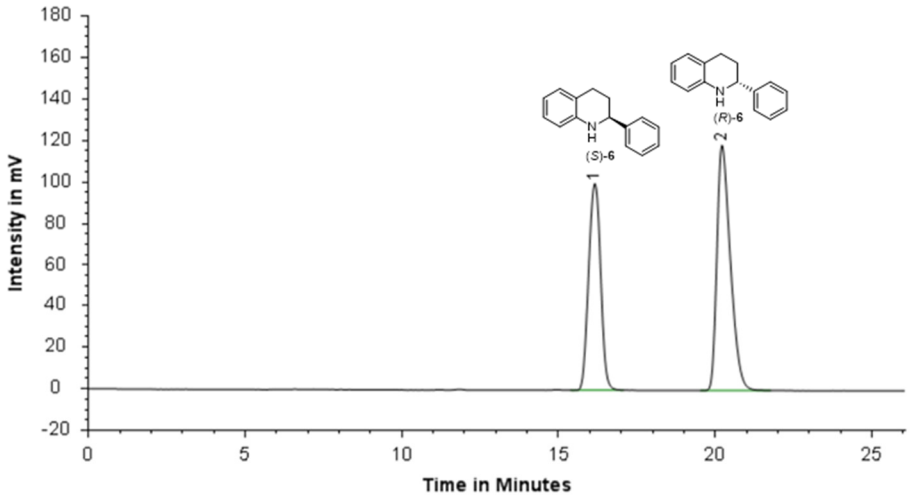

No.	Ret. Time	Height	Area	Percent
1	16.16667	99.8902	2654133	42.84385
2	20.225	118.4804	3540766	57.15615

Figure S135: Chiral HPLC of **6** using (*S*)-**3** as catalyst (Entry 18,Table S1)

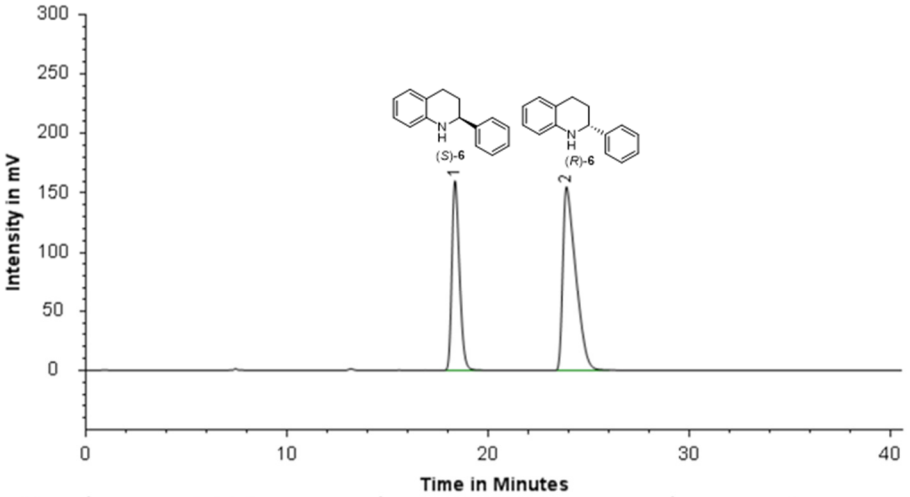

No.	Ret. Time	Height	Area	Percent
1	18.34167	160.2503	4188345	37.75617
2	23.90833	155.1337	6904794	62.24383

Figure S136: Chiral HPLC of **6** using (*S*)-**3** as catalyst (Entry 19,Table S1)

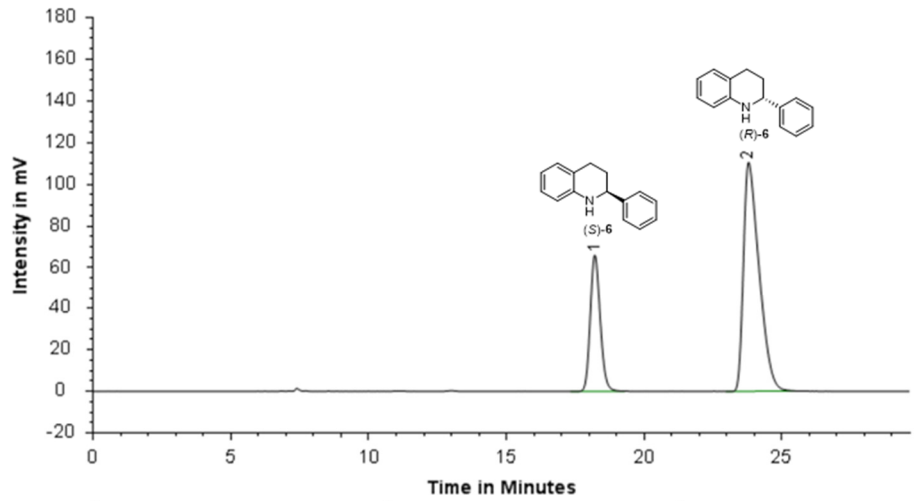

No.	Ret. Time	Height	Area	Percent
1	18.21667	65.88637	1653844	27.51548
2	23.79167	110.4781	4356750	72.48452

Figure S137: Chiral HPLC of **6** using (*S*)-**3** as catalyst (Entry 20,Table S1)

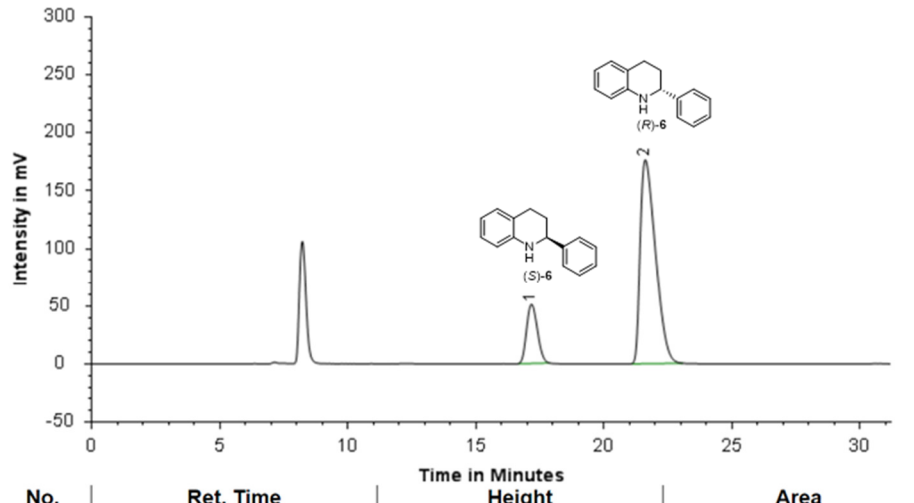

No.	Ret. Time	Height	Area	Percent
1	17.15833	50.81874	1495102	16.97023
2	21.60833	176.5142	7315043	83.02977

Figure S138: Chiral HPLC of **6** using (*S*)-**3** as catalyst (Entry 21,Table S1)

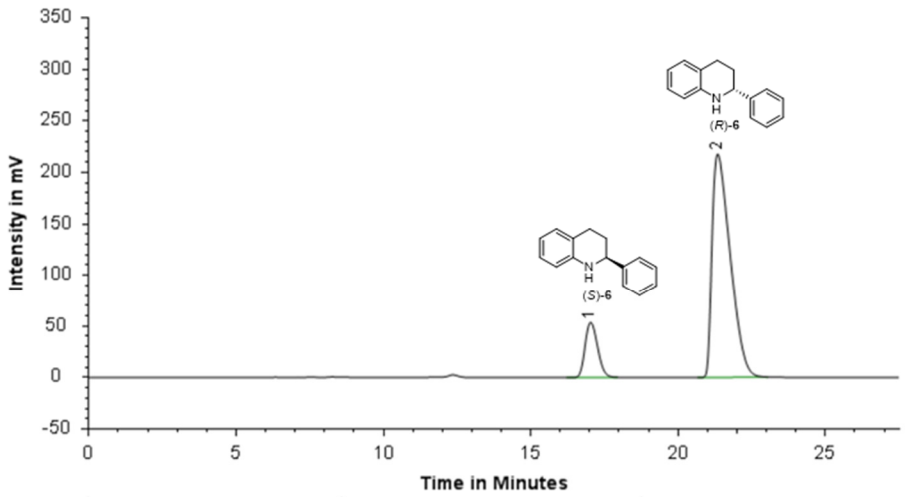

No.	Ret. Time	Height	Area	Percent
1	17.025	53.39006	1576344	14.44667
2	21.35	217.6091	9335125	85.55333

Figure S139: Chiral HPLC of **6** using (*S*)-**3** as catalyst (Entry 22,Table S1)

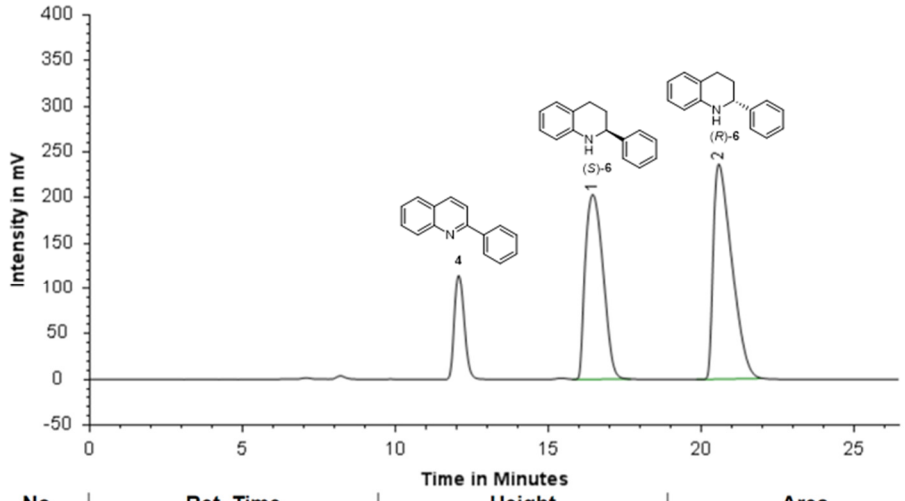

No.	Ret. Time	Height	Area	Percent
1	16.45	203.1863	8231659	45.21163
2	20.58333	236.4389	9975290	54.78837

Figure S140: Chiral HPLC of **6** using (*S*)-**3** as catalyst (Entry 23,Table S1)

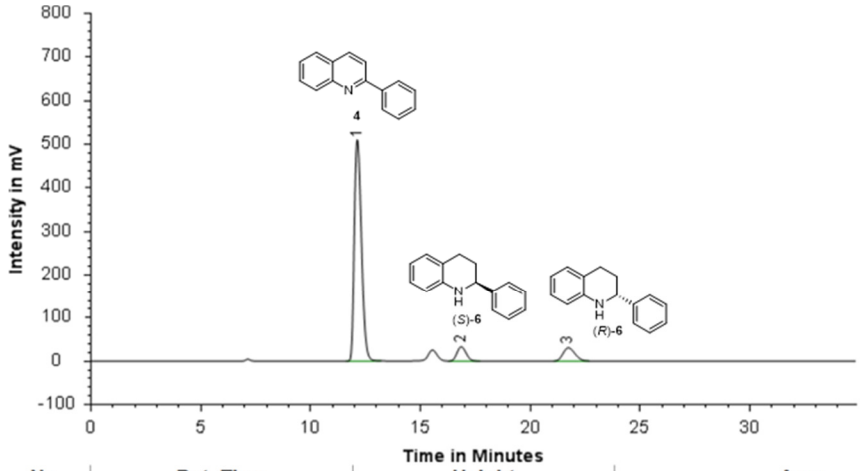

No.	Ret. Time	Height	Area	Percent
1	12.125	510.0208	1.154886E+07	84.49249
2	16.85833	32.95202	960879	7.029877
3	21.725	30.4737	1158766	8.477638

Figure S141: Chiral HPLC of **6** using (*S*)-**3** as catalyst (Entry 1,Table S11)

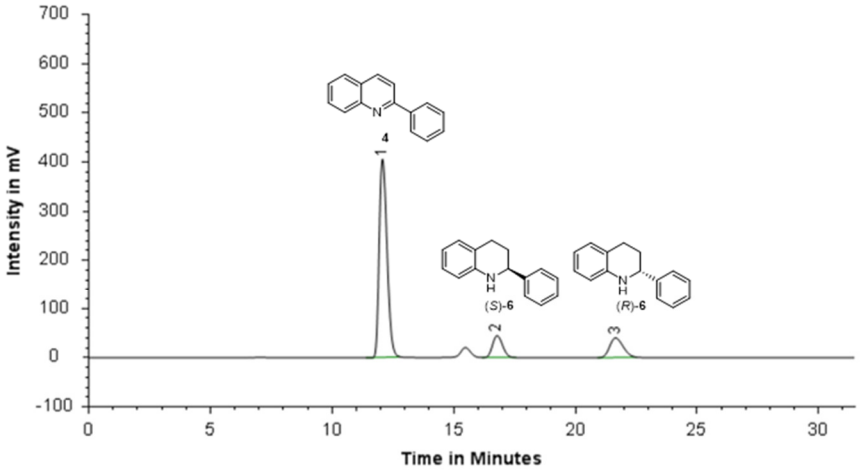

No.	Ret. Time	Height	Area	Percent
1	12.06667	404.6562	9045967	76.32765
2	16.775	44.32379	1281547	10.81338
3	21.65833	39.701	1523980	12.85897

Figure S142: Chiral HPLC of **6** using (*S*)-**3** as catalyst (Entry 2,Table S11)

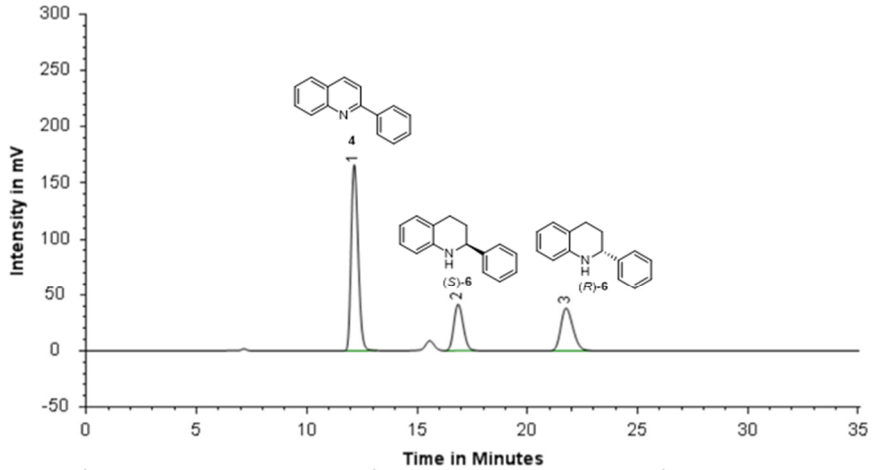

No.	Ret. Time	Height	Area	Percent
1	12.14167	166.2723	3677541	58.07049
2	16.86667	41.09187	1210307	19.11144
3	21.75833	37.83924	1445044	22.81807

Figure S143: Chiral HPLC of **6** using (*S*)-**3** as catalyst (Entry 3,Table S11)

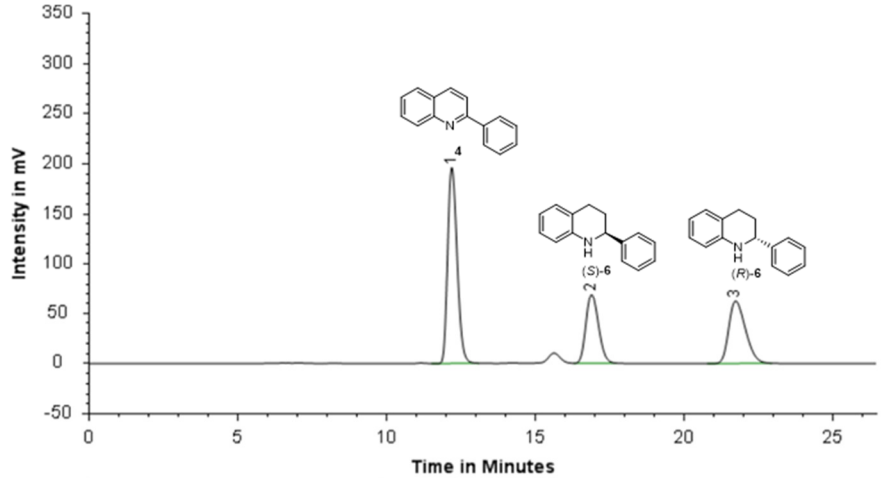

No.	Ret. Time	Height	Area	Percent
1	12.18333	196.0319	4338403	49.39277
2	16.88333	68.90007	2021622	23.0162
3	21.725	61.98493	2423452	27.59103

Figure S144: Chiral HPLC of **6** using (*S*)-**3** as catalyst (Entry 4,Table S11)

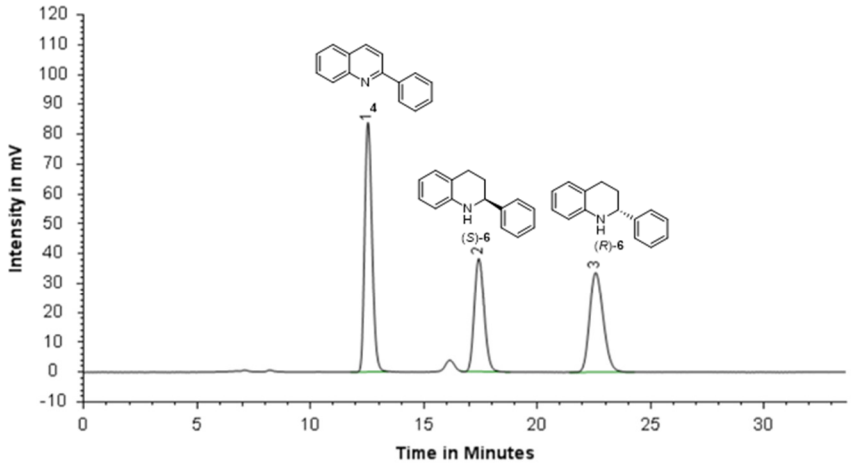

No.	Ret. Time	Height	Area	Percent
1	12.525	83.8101	1896260	42.67086
2	17.425	38.11711	1149674	25.8707
3	22.56667	33.60365	1397989	31.45844

Figure S145: Chiral HPLC of **6** using (*S*)-**3** as catalyst (Entry 5,Table S11)

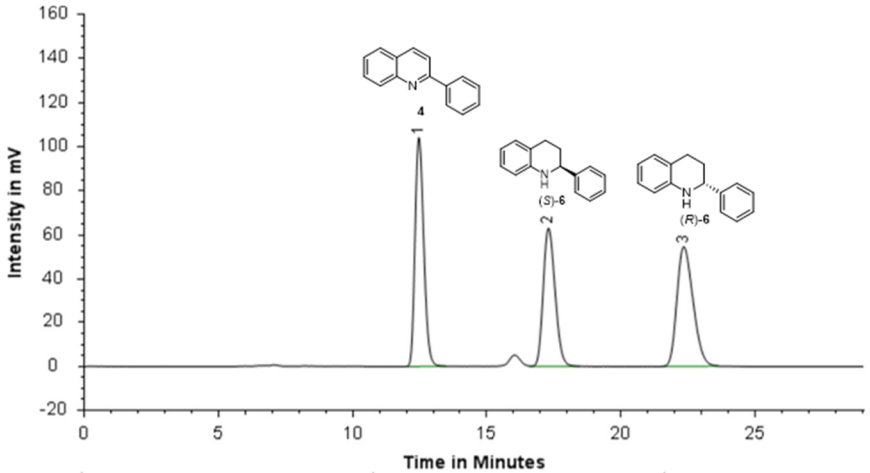

No.	Ret. Time	Height	Area	Percent
1	12.475	104.0633	2359839	35.86658
2	17.30833	63.03045	1934441	29.40105
3	22.35	54.69365	2285214	34.73237

Figure S146: Chiral HPLC of **6** using (*S*)-**3** as catalyst (Entry 6,Table S11)

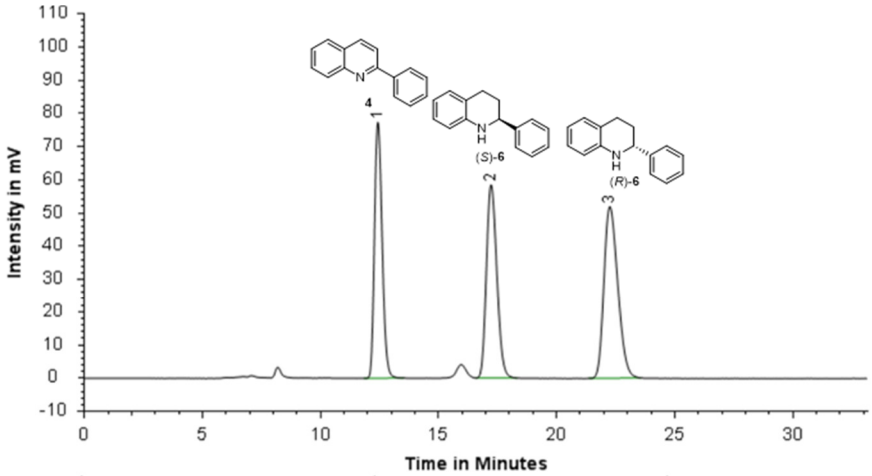

No.	Ret. Time	Height	Area	Percent
1	12.43333	77.22916	1746557	30.87803
2	17.21667	58.34536	1793823	31.71367
3	22.25833	51.95767	2115929	37.40829

Figure S147: Chiral HPLC of **6** using (*S*)-**3** as catalyst (Entry 7,Table S11)

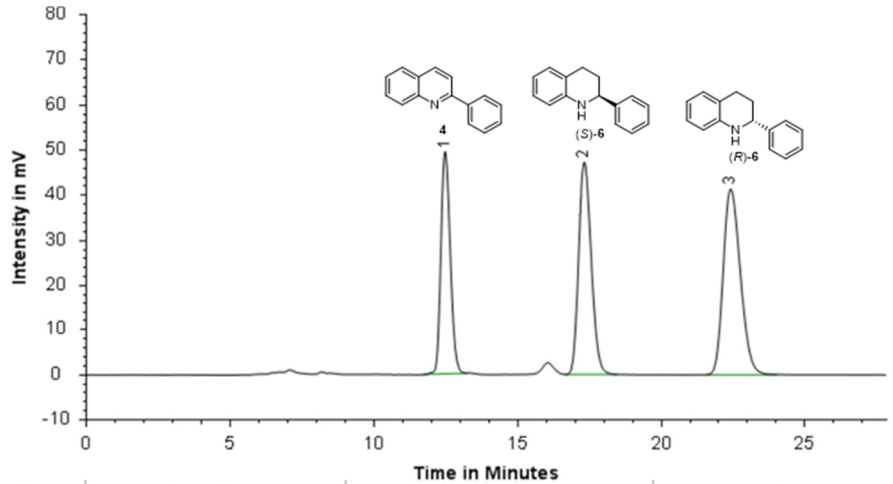

No.	Ret. Time	Height	Area	Percent
1	12.475	49.43974	1121811	26.16131
2	17.325	47.22815	1443340	33.65956
3	22.425	41.38924	1722903	40.17913

Figure S148: Chiral HPLC of **6** using (*S*)-**3** as catalyst (Entry 8,**Table S11**)

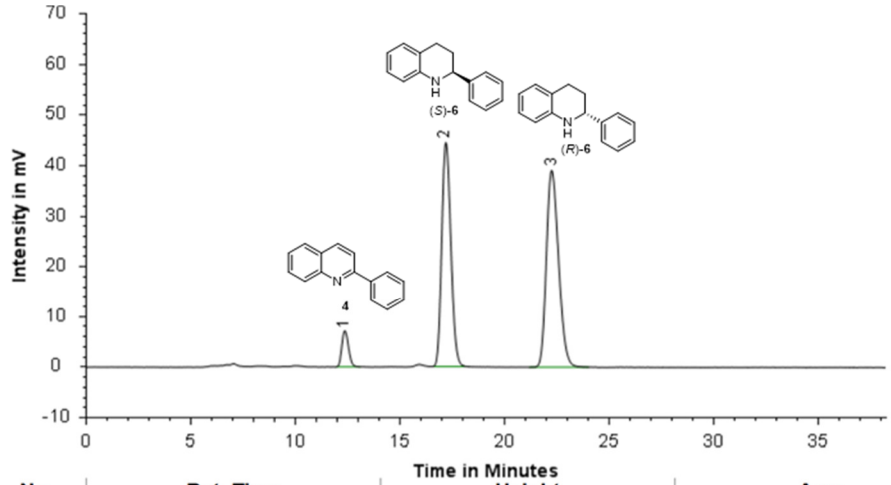

No.	Ret. Time	Height	Area	Percent
1	12.36667	7.109271	156540.4	5.066934
2	17.19167	44.39138	1347339	43.61097
3	22.26667	39.10371	1585570	51.32209

Figure S149: Chiral HPLC of **6** using (*S*)-**3** as catalyst (Entry 9,Table S11)

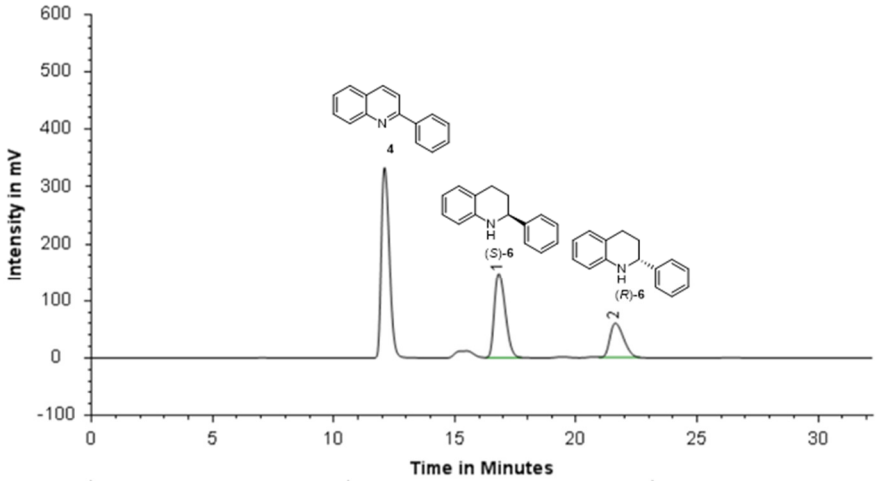

No.	Ret. Time	Height	Area	Percent
1	16.825	147.2991	4624689	66.66691
2	21.625	59.24254	2312319	33.33309

Figure S150: Chiral HPLC of **6** using (*S*)-**3** as catalyst (Entry 1,Table S12)

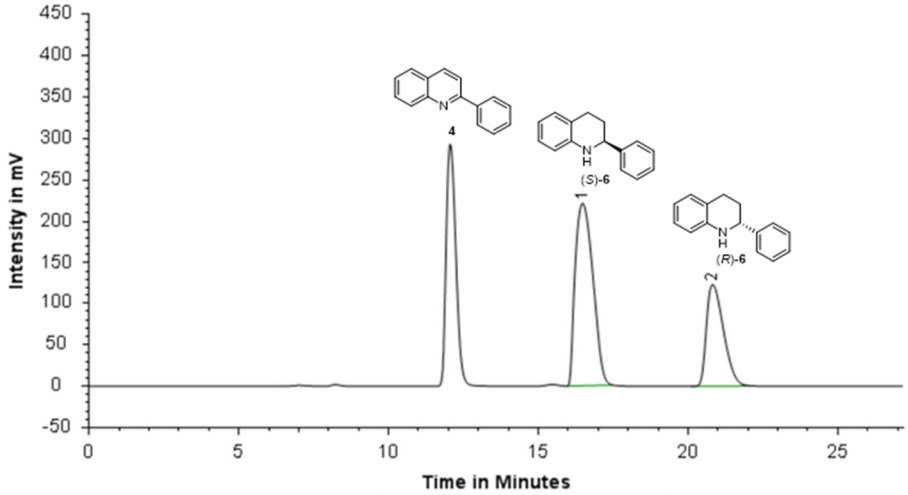

No.	Ret. Time	Height	Area	Percent
1	16.48333	221.1476	9076634	65.13125
2	20.81667	123.6773	4859279	34.86875

Figure S151: Chiral HPLC of **6** using (*S*)-**3** as catalyst (Entry 2,Table S12)

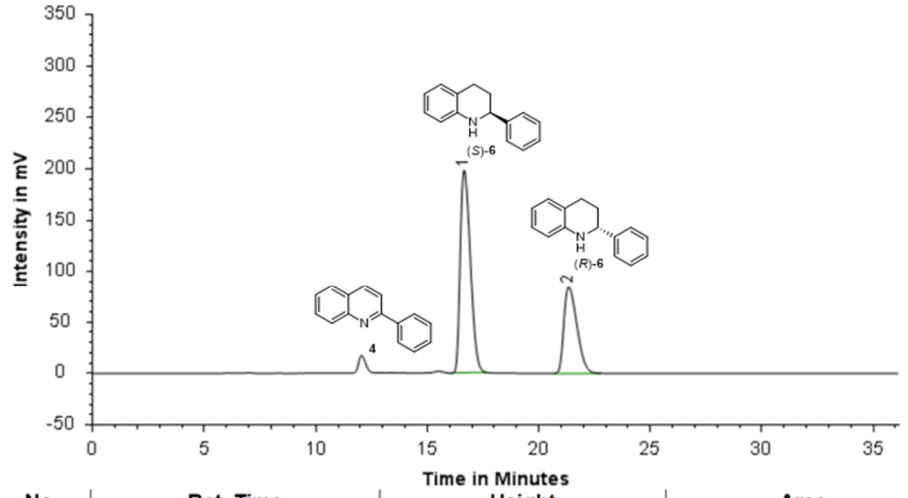

No.	Ret. Time	Height	Area	Percent
1	16.65833	197.7711	6254020	64.56921
2	21.35	84.2336	3431742	35.43079

Figure S152: Chiral HPLC of **6** using (*S*)-**3** as catalyst (Entry 3,Table S12)

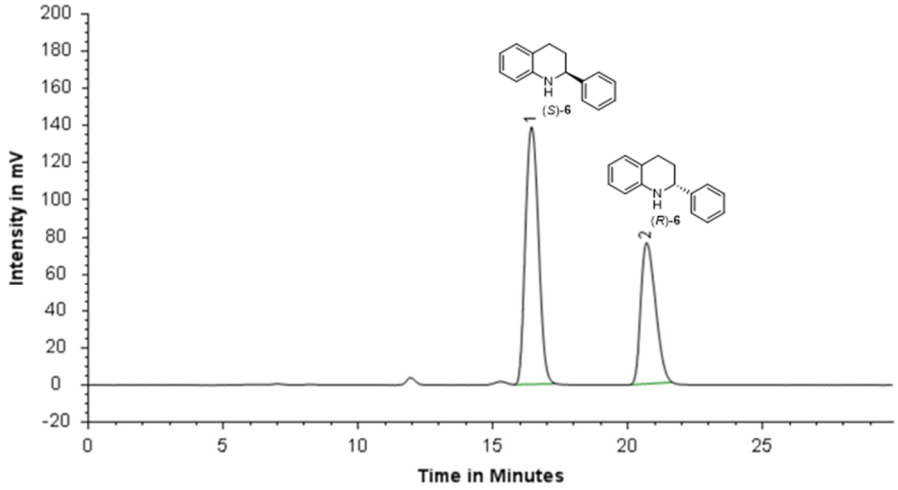

No.	Ret. Time	Height	Area	Percent
1	16.43333	138.8603	4676659	61.78262
2	20.7	76.32972	2892879	38.21738

Figure S153: Chiral HPLC of **6** using (*S*)-**3** as catalyst (Entry 4,Table S12)

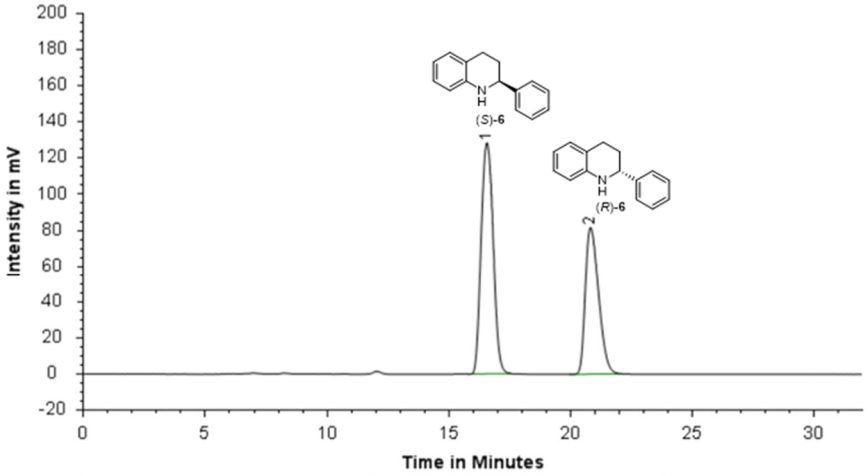

No.	Ret. Time	Height	Area	Percent
1	16.55833	128.4286	4412562	58.86623
2	20.8	81.61079	3083352	41.13377

Figure S154: Chiral HPLC of **6** using (*S*)-**3** as catalyst (Entry 5,Table S12)

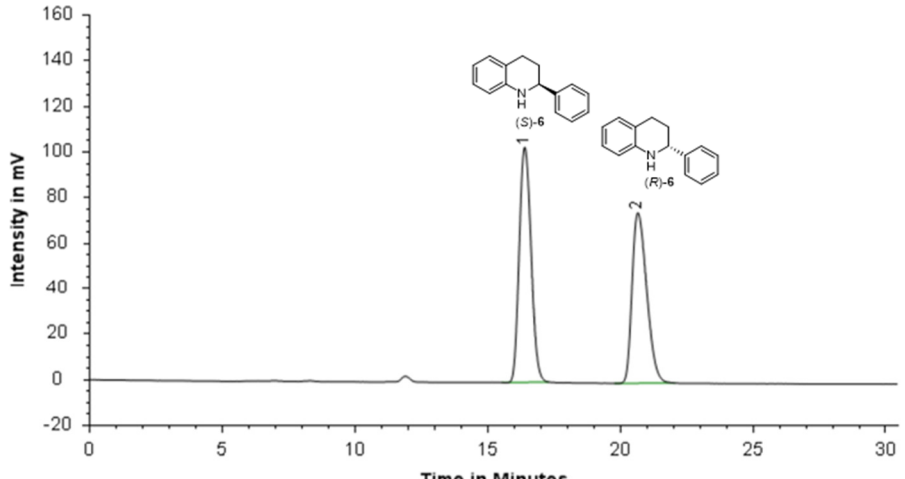

No.	Ret. Time	Height	Area	Percent
1	16.38333	103.1947	3191089	52.66348
2	20.65	74.90418	2868307	47.33652

Figure S155: Chiral HPLC of **6** using (*S*)-**3** as catalyst (Entry 6,Table S12)

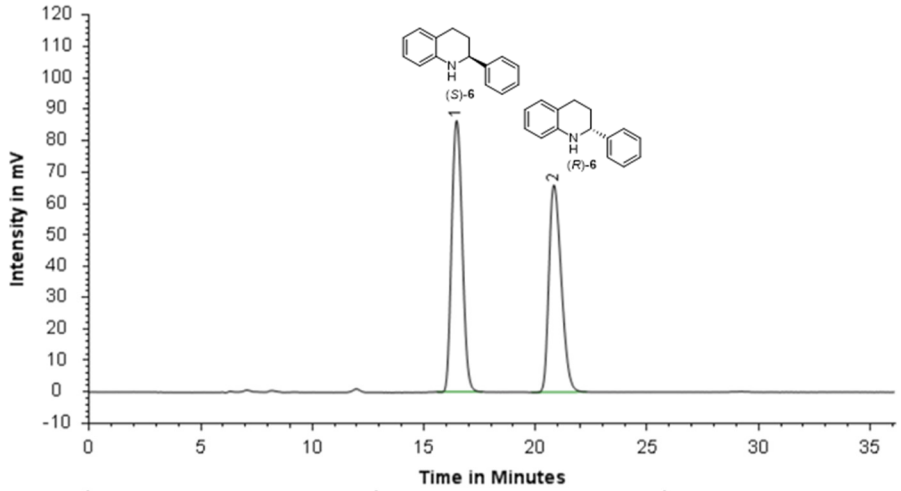

No.	Ret. Time	Height	Area	Percent
1	16.475	86.36382	2850125	53.00689
2	20.83333	65.97689	2526771	46.99311

Figure S156: Chiral HPLC of **6** using (*S*)-**3** as catalyst (Entry 7,Table S12)

11. References

[1] R. Mitra, M. Thiele, F. Octa-Smolin, M. C. Letzel, J. Niemeyer, *Chem. Commun.* **2016**, *52*, 5977-5980.

[2] R. Mitra, H. Zhu, S. Grimme, J. Niemeyer, *Angew. Chem. Int. Ed.* **2017**, 56, 11456–11459.

[3] Tobisu, I. Hyodo, N. Chatani, *J. Am. Chem. Soc.* **2009**, 131, 12070-12071.

[4] A. V. Iosub, S. S. Stahl, *Org Lett*. **2015**, 17, 4404-4407.

[5] J. F. Dellaria, J. F. Denissen, F. A. J. Kerdesky, R. G. Maki, D. J. Hoffman, H. N. Nellans, *J. Label. Compd. Radiopharm.* **1989**, *27*, 1437-1450

[6] E. Delamarche, C. Donzel, F. S. Kamounah, H. Wolf, M. Geissler, R. Stutz, P. Schmidt-Winkel, B. Michel, H. J. Mathieu, K. Schaumburg, *Langmuir* 2003, 19, 8749-8758.

[7] a) J. Burés, *Angew. Chem. Int. Ed.* **2016**, *55*, 16084-16087; b) J. Burés, *Angew. Chem. Int. Ed.* **2016**, *55*, 2028-2031; c) C. D. T. Nielsen, J. Burés, *Chem. Sci.* **2019**, *10*, 348-353.

[8] a) H. Lineweaver, D. Burk, *J. Am. Chem. Soc.* **1934**, *56*, 658-66; b) J. E. Dowd, D. S. Riggs, *J. Biol. Chem.* **1965**, *240*, 863-869.

[9] a) K. Rothermel, M Melikian, J. Hioe, J. Greindl, J. Gramüller, M. Žabka, N. Sorgenfrei, T. Hausler, F. Morana, R.M. Gschwind, *Chem. Sci.* **2019**, DOI: 10.1039/C9SC02342A; b) N. Sorgenfrei, J. Hioe, J. Greindl, K. Rothermel, F. Morana, N. Lokesh, R.M. Gschwind, *J. Am. Chem. Soc.* **2016**, 138, 16345-16354.

[10] a) J. Greindl, J. Hioe, N. Sorgenfrei, F. Morana, R.M. Gschwind, *J. Am. Chem. Soc.* **2016**, 138, 15965-15971; b) M. Melikian, J. Gramueller, J. Hioe, J. Greindl, R.M. Gschwind, *Chem. Sci.* **2019**, 10, 5226-5234; c) N. Lokesh, J. Hioe, J. Gramüller, R. M. Gschwind, *J. Am. Chem. Soc.* **2019**, *141*, 16398-16407.

[11] a) S. Hoffmann, A. M. Seayad, B. List, *Angew. Chem., Int. Ed.* **2005**, *44*, 7424-7427; b) R. I. Storer, D. E. Carrera, Y. Ni, D. W. C. MacMillan, *J. Am. Chem. Soc.* **2006**, *128*, 84-86.

[12] A. Jerschow, N. Müller, *J. Magn. Reson.* **1997**, 125 (2), 372–375.

[13] E. O. Stejskal, J. E. Tanner, *J. Chem. Phys.* **1965**, 42 (1), 288–292.

[14] A. MacChioni, G. Ciancaleoni, C. Zuccaccia, D. Zuccaccia, *Chem. Soc. Rev.* **2008**, 37 (3), 479–489.

[15] H. C. Chen, S. H. Chen, *J. Phys. Chem.* **1984**, 88 (21), 5118–5121.

[16] D. Ben-Amotz, K. G. Willis, *J. Phys. Chem.* **1993**, 97 (29), 7736–7742.

[17] D. Zuccaccia,; A. Macchioni, *Organometallics* **2005**, 24 (14), 3476–3486.

[18] S. Grimme, C. Bannwarth, P. Shushkov, *J. Chem. Theory. Comput*, **2017**, 13, 1989-2009.

[19] S. Grimme, C. Bannwarth, *J. Chem. Phys.* **2016**, *145*, 054103.

[20] P. Shushkov, S. Grimme, unpublished.

[21] TURBOMOLE V7.0 **2015**, a development of University of Karlsruhe and Forschungszentrum Karlsruhe GmbH, 1989-2007, TURBOMOLE GmbH, since 2007; available from http://www.turbomole.com.

[22] J. M. Tao, J. P. Perdew, V. N. Staroverov, G. E. Scuseria, *Phys. Rev. Lett.* **2003**, *91*, 146401.

[23] S. Grimme, J. Antony, S. Ehrlich, H. Krieg, D. *J. Chem. Phys*. **2010**, *132*, 154104.
[24] S. Grimme, L. Goerigk, *J. Comput. Chem*. **2011**, *32*, 1456–1465.
[25] A. Schäfer, H. Horn and R. Ahlrichs, *J. Chem. Phys.* **1992**, *97*, 2571.
[26] F. Weigend, *Phys. Chem. Chem. Phys.* **2006**, *8*, 1057.
[27] S. Sinnecker, A. Rajendran, A. Klamt, M. Diedenhofen, F. Neese, *J. Phys. Chem. A*, **2006**, *110*, 2235–2245.
[28] A. Klamt, G. Schüürmann, *J. Chem. Soc. Perkin Trans.* **1993**, *2*, 799–805.
[29] K. Eichkorn, F. Weigend, O. Treutler, R. Ahlrichs, *Theor. Chem. Acc*. **1997**, *97*, 119–124.
[30] P. Deglmann, K. May, F. Furche, R. Ahlrichs, *Chem. Phys. Lett*. **2004**, *384*, 103–107.
[31] S. Grimme, *Chem. Eur. J.* **2012**, *18*, 9955–9964.
[32] F. Weigend, F. Furche, R. Ahlrichs, *J. Chem. Phys.* 2003, *119*, 12753.
[33] F. Eckert, A. Klamt, *COSMOtherm*, Version C3.0, Release 14.01; COSMOlogic GmbH & Co. KG, Leverkusen, Germany, **2013**;
[34] A. Klamt, *J. Phys. Chem.* **1995,** *99*, 2224–2235;
[35] F. Eckert, A. Klamt, *AIChE Journal*, **2002**, *48*, 369-385.